CHARACTERIZING THE ASSEMBLY OF THE MEMBRANES THAT SEQUESTER PEROXISOMES DURING AUTOPHAGY

By

LAURA A. SCHRODER

A DISSERTATION PRESENTED TO THE GRADUATE SCHOOL
OF THE UNIVERSITY OF FLORIDA IN PARTIAL FULFILLMENT
OF THE REQUIREMENTS FOR THE DEGREE OF
DOCTOR OF PHILOSOPHY

UNIVERSITY OF FLORIDA

2007

This work was completed in remembrance of my dear brother, Glenn Eldon Miller, III, whom I love and miss dearly. You were here when I began this adventure; what would I give that you were here now! I sincerely hope that someday my work and the work of other scientists may curtail the suffering caused by metastic malignant melanoma and other cancers.

This work is dedicated to my daughter, Mya Catalina Schroder, who was born in the second year of the work that cumulated in my doctoral dissertation. Mya is the light around which my universe gravitates: I cannot imagine my life without you. You endow those who are blessed with your presence immense joy. Recently you have asked me what is meant by "hope" and "peace"—both of which are embodied in the gift God gave us when he gave us you.

This work could not have been accomplished without my long-suffering Mom, Lorraine Abate Miller. Your sheer determination to become a botanist inspired me in turn to become a molecular biologist, and your forbearance modeled my stubborn "stick-to-it-ness." Thank you for instilling in me the importance of an education. I truly appreciate all the sacrifices you have made and continue to make for your family. You have found solace in caring for Mya, and your hours are well spent caring for her during my evenings and weekends in the laboratory.

I truly value the support of Glenn Eldon Miller, Jr. and Linda Miller. You love me without limits, you cherish me for being me, and you do not judge.

I am grateful to Jeremiah John Schroder for your loving support. Your patience and forbearance do not go unnoticed; I know you always try your best. Your pride in this dissertation is appreciated. Our genetic experiment is more successful than I could have imagined.

I will not forget the care and patience on the part of Ivonne Ulloa-Ron, Markus Patricio Tellkamp, and Daniela and Domenica Ulloa during Mya's time with you. Mya's sweet, caring and loving personality and her amazing intelligence were formed in her very tender first year and a half in part by all of you.

The emotional and psychological support of Jolene Smith and Donna Tackett have kept me sane. That all friendships were so steadfast! You put things in perspective when times are hard (as they often are), and you always make me laugh.

An extra special thanks to my professor William A. Dunn, Jr., Ph.D. I cannot thank you enough for bestowing a quiet confidence in me with your initial instruction at the bench, your never failing to complement my early work, and your encouragement when science, by definition, is frustrating. You have challenged me to faithfully complete this task. I have learned to think and write scientifically because of you. I value your input, and your honesty astounds me.

ACKNOWLEDGMENTS

I am very grateful to my committee members John Aris, Ph.D., Brian Burke, Ph.D. and David Julian, Ph.D. for their helpful discussions, encouragement and help with editing. I especially thank William Dunn, Jr., Ph.D. for analyzing my writing with a fine-toothed comb. This work was supported by grants from the National Cancer Institute (NIH) CA95552 to W.A.Dunn, Jr., Ph.D.

Specific Acknowledgments

Chapter 2: This work was supported by NSF (MCB-9817002) and NIH (CA95552) grants to W.A. Dunn, Jr. and NIH (GM61156) grant to B. S. Glick.

Chapter 3: This work was supported by grants from the National Science Foundation Grant MCB-9817002 and the National Cancer Institute (NIH) CA95552 to W.A.Dunn, Jr. and a grant from The Norwegian Cancer Society to P. E. Strømhaug. We would like to thank Dr. B.S. Glick (University of Chicago) for generously providing the pREMI-Z, pIB1, and pIB2 vectors. Finally, we would like to thank Mr. Todd Barnash for his help in assembling the figures, and Dr. Michelle Fry and Debbie Akin for helpful discussions and editing.

Chapter 6: This work was supported by grants from the National Cancer Institute (NIH) CA95552 to W.A.Dunn, Jr. We would like to thank Dr. B.S. Glick (University of Chicago) for generously providing the pSar1T34N, pSar1H79G, and pIB2 vectors and Dr. R.Y. Tsein for providing the mRFP gene. Finally, we would like to thank Mr. Todd Barnash for his help in assembling the figures, and Debbie Akin for helpful discussions and editing.

I alone remain responsible for the content of the following, including any errors or omissions which may unwittingly remain.

TABLE OF CONTENTS

page

LIST OF TABLES

LIST OF FIGURES

LIST OF TERMS

Autophagy	Derived from the Latin meaning self-eating. The process by which an organism sequesters and degrades superfluous organelles utilizing the lytic compartment
MIPA	Micropexophagic-specific membrane apparatus which tethers the SM whereby homotypic fusion proceeds. The final expansion step cumulating in completion.
Nucleation	Expansion, completion - sequential steps whereby micropexophagy proceeds phenotypically
PAS	Pre-autophagic structure adjacent to the tips of the sequestering membranes
PC9	Peripheral compartment in which Atg9p resides
Pexophagy	A subset of autophagy specific to methylotropic yeasts whereby the peroxisomes are selectively sequestered and degraded
PVS	Perivacuolar structure present at the base of the sequestering membranes
SM	Sequestering membranes; arm-like extensions of the vacuole characterizing glucose-induced micropexophagy

Abstract of Dissertation Presented to the Graduate School
of the University of Florida in Partial Fulfillment of the
Requirements for the Degree of Doctor of Philosophy

CHARACTERIZING THE ASSEMBLY OF THE MEMBRANES THAT SEQUESTER PEROXISOMES DURING AUTOPHAGY

By

Laura A. Schroder

December 2007

Chair: William A. Dunn, Jr.
Major: Medical Sciences—Moclecular Cell Biology

The methylotropic yeast *Pichia pastoris* efficiently sequesters and degrades peroxisomes by micropexophagy when more easily degraded carbon sources become available. The process by which this degradation occurs during glucose-induced micropexophagy can be phenotypically characterized. Nucleation is the budding of the sequestering membranes (SM) from the vacuole. Expansion follows as the SM surround the peroxisomes. The micropexophagic-specific membrane apparatus (MIPA) bridges the opposing SM. Completion is the final enveloping of the peroxisomes for degradation within the vacuole.

This study has characterized the molecular events of SM expansion mediated by certain Atg proteins. PpAtg9p is an integral membrane protein essential for the events of SM expansion. Upon synthesis, Atg9 transits from the endoplasmic reticulum (ER) to a peripheral Atg9 compartment (PC9). Furthermore, site-directed mutagenesis has identified two domains within Atg9 are essential for ER exit. Specifically, two critical amino acids have been identified that are essential for ER exit. The PC9 is unique exhibiting a density not shared by the ER, the mitochondria, and the vacuole. During glucose-induced micropexophagy, Atg9p transits through perivacuolar structures (PVS) at the base of the sequestering membranes to the SM. The trafficking of Atg9 requires Atg11, Vps15, Atg2, and Atg7. The C-terminal QQHKA motif is

required for exit of Atg9 from the PC9. Next, W607 and Y611 are essential for Atg9 transit to the SM. None of the Atg9 mutants is functional, including the N-terminal deletion that localizes properly to the SM. Thus, a number of amino acid motifs necessary for Atg9p trafficking have been identified and characterized.

The role of Sar1p, a GTPase involved in COPII-mediated ER trafficking, in pexophagy was examined by expressing sar1(T34N) or sar1(H79G) dominant negative mutants. By expressing these mutants, we have demonstrated that the lipidation of Atg8 and the assembly of the micropexophagic-specific membrane apparatus (MIPA) require Sar1.

Sar1 is also required for macropexophagy. Pexophagosomes do not form in the sar1(T34N) mutant. Completion and/or fusion of the pexophagosome with the vacuole is suppressed in the sar1(H79G) mutant. Moreover, sar1(H79G) inhibits the retrograde transport of membranes containing HDEL, which supports the idea that autophagosome membranes originate in the endoplasmic reticulum.

Our data demonstrate that the expansion of the SM during micropexophagy proceeds in two stages, an early Atg9-dependent that requires the PVS to expand the SM and a late Atg8p-dependent that requires Sar1p and the PAS to assemble the MIPA.

CHAPTER 1
INTRODUCTION

Autophagy is the catabolic process by which the cytoplasm and the organelles therewith are sequestered into double-membrane organelles, transported to and degraded within the acidic lysosome or vacuole for possible recycling. Autophagy may be non-selective or selective. An example of selective autophagy is mitophagy, the major route by which the mitochondria are degraded (Abeliovich, 2007). Pexophagy is the selective degradation of the peroxisomes by the vacuole in methylotropic yeasts such as *Pichia pastoris* (Dunn *et al.*, 2005). Membranes of unknown origin condense around individual peroxisomes forming double-membrane bound pexophagosomes which then fuse with the vacuole in the process of macropexophagy (Sakai *et al.*, 2006). Clusters of peroxisomes are incorporated by sequestering membranes derived from the vacuole in the process of micropexophagy (Sakai *et al.*, 2006).

Micropexophagy proceeds by a specific set of phenotypic events characterized by nucleation, expansion and completion. Nucleation, the initial budding of the vacuole to form structures reminiscent of the sequestering membranes (SM), is dependent on signal transduction events and does not require *de novo* protein synthesis or additional membrane sources. Expansion, the exaggeration of the SM to surround the peroxisomes, does require additional membranes and is thought to involve the formation of large cisternal sheets by combining vesicles (Klionsky *et al.*, 2007). Expansion can be divided into early expansion and late expansion in our experimental system. Membrane delivery during the late expansion event in micropexophagy is fulfilled by the micropexophagic-specific membrane apparatus (MIPA), which conjoins the SM (Dunn *et al.*, 2005). Completion occurs as the SM fuse together and the peroxisomes are entirely surrounded by the vacuole for degradation, during which the double membranes are degraded for access to the peroxisomes inside.

Glucose selective autophagy (*GSA*) genes were originally identified based on the inability of *gsa* mutants to degrade the peroxisomes. A more straightforward shotgun approach as compared to a series of tedious yeast mating was desired, cumulating in Restriction Enzyme-Mediated Integration (REMI) which randomly integrates a vector containing the Zeocin cassette into the yeast genome (Schroder *et al.*, 2007). Subsequent screening has enabled the identification of Gsa gene products. A unified yeast nomenclature was developed as some proteins affect more than one autophagic pathway (Klionsky *et al.*, 2003). Thus, the Apg, Aut, Cvt, Gsa, Paz and Pdd prefixes were dropped for the ATG abbreviation meaning autophagy-related genes (Table 1-1).

Pexophagy is best studied in *Pichia pastoris*. *P. pastoris* is easily manipulated genetically (mutations are induced and proteins can be readily upregulated), molecularly (feedback from a dietetic switch results in the rapid degradation of organelles) and biologically (the peroxisome cluster and the vacuole, which is larger than the nucleus, are visible on the light microscope). *P. pastoris* offers a unique perspective for an increasingly understood cellular phenomenon—pexophagy. Micropexophagy is hereby dissected into discrete genetic and morphologic steps. Pexophagy can be described genotypically by defining the ATG gene products required for signaling/recognition, expansion (nucleation, expansion and completion) and degradation (Figure 1-1). Signaling and recognition require Pfk1, Vps15 and Atg11 (Yuan *et al.*, 1997; Kim *et al.*, 2001; Dunn *et al.*, 2005). Nucleation requires Atg1 (Abeliovich *et al.*, 2000), Atg6 (Levine and Klionsky, 2004), Atg18, Vac8, and Vps15 (Stasyk *et al.*, 1999; Guan *et al.*, 2001; Fry *et al.*, 2006). Expansion requires Atg2, Atg7, Atg8, Atg9, and Atg11 (Chang *et al.*, 2005). Completion requires Vac8 (Fry *et al.*, 2006), Atg8, and Atg24 (Ano *et al.*, 2005). Finally, degradation requires Pep4 and Prb1 (Tuttle and Dunn, 1995; Dunn *et al.*, 2005).

The expansion of the sequestering membranes (SM) is classified into early and late events. During the early events, the SM expands from perivacuolar structures (PVS). The late events are characterized by the assembly of the micropexophagy apparatus (MIPA) from the preautophagosome structure (PAS). Atg9 is a transmembrane protein involved in both early and late expansion events. During micropexophagy, Atg9 traffics from a peripheral compartment to the PVS and the SM and to the PAS position at the tips of the SM. Atg11 is found at the PVS and SM, while Atg8 is at the PAS and MIPA (Figure 1-2).

Membrane expansion during pexophagy is a rate-limiting process during pexophagy. Atg9 is the sole transmembrane protein shown to be required for the membrane trafficking events leading to SM formation. We have identified a number of Atg proteins that influence the trafficking of Atg9. This study reveals functional motifs that are essential for to pexophagy. These motifs appear critical to Atg9 trafficking and function. Furthermore, to better understand the diverse role of Atg9, its involvement in autophagy and pexophagy has been explored.

The roles of a number of Sec proteins in autophagy have been reported. These proteins are normally required for vesicular movements between the endoplasmic reticulum and Golgi apparatus in autophagy. The data have shown that ScAtg8 interacts with three v-SNAREs (Legesse-Miller *et al.*, 2000) and eight Sec proteins are required for autophagy (Ishihara *et al.*, 2001; Hamasaki *et al.*, 2003; Reggiori *et al.*, 2004). ScSec12, the guanine-nucleotide exchange factor powered by the COPII GDP-GTP exchange factor Sar1, facilitates formation of the autophagic vacuole from the PAS (Reggiori *et al.*, 2004). ScSec16, ScSec23, and ScSec24 also function in COPII vesicle transport of proteins and have essential roles in autophagy. The functional role of the COPII vesicle pathway in pexophagy has not been examine and forms the basis of my studies. This research highlights a role for Sar1p in pexophagy.

The early membrane events leading to the onset of pexophagy are not known. The means by which the proteins involved in pexophagy are transported to their respective sites of activation and their activation is poorly understood. The way in which the pexophagic proteins interact with one another is not clear. This research will elucidate the functional motifs essential to Atg9, a key transmembrane protein. These studies will also describe the role of the COPII secretory pathway in pexophagy. Finally, this research will broach the implications for the maturation of the sequestering membranes whereby the peroxisomes are engulfed during micropexophagy.

The Role of Atg9 in Glucose-Induced Micropexophagy

The scientific researcher is resourceful. He has multiple overlapping ways to verify his hypotheses. The burgeoning field of micropexophagy has experience basic technique development. The alcohol oxidase assay is a tool to determine whether cells undergoing glucose-induced micropexophagy are functional. Western blot allows us to study cells undergoing ethanol-induced macropexophagy. Pulse-chase proteolysis enables us to examine cells undergoing nitrogen starvation-induced macroautophagy. Using these methods, we have learned that Atg9 is required for multiple autophagic pathways, including glucose-induced micropexophagy, ethanol-induced macropexophagy, and starvation-induced autophagy. The induction of micropexophagy by glucose adaptation reveals the formation of the SM, which nucleates from sites at the vacuole.

Multiple laboratory analyses have enriched our understanding of Atg9. Ultrastructural analyses of *atg9* mutants during glucose-induced micropexophagy show a block at an early event in peroxisome degradation by the vacuole: the vacuole is apposed to the peroxisomes and slightly indents; however, the extension of the SM is not completed (e.g. stunted arm-like protrusions) and the engulfment process by the vacuole stops prematurely. Indeed, examination under the electron microscope has revealed multiple peroxisomes accumulate waiting to be

engulfed in *atg9* cells, halted as if waiting for something; control cells observed at the same timepoints exhibit the remnants of degraded peroxisomes (Chang *et al.*, 2005).

The use of GFP-tagged proteins has revealed much concerning Atg9 cellular localization in *Pichia pastoris*. During glucose-induced micropexophagy, Atg9 trafficks from its peripheral PC9 compartment to the PVS (perivacuolar structure) at the base of the membranes that sequester the peroxisomes to the SM (sequestering membranes) at the vacuole and to the PAS (pre-autophagic structure) adjacent to the tips of the SM for formation of MIPA (micropexophagic-specific membrane apparatus). The localization of Atg9 to the PVS requires Vps15 and Atg11 (Tina Chang, unpublished observations).

The expression of Atg9 changes over time. That is, the cellular levels of Atg9 increase during the first 4 hours of glucose adaptation and then slightly decrease between 4 and 8 hours of glucose adaptation (Chang *et al.*, 2005). Thus, Atg9 appears to be upregulated then possibly degraded during pexophagy. The degradation or recycling of Atg9 in *P. pastoris* is indeterminant.

Atg9 is an integral membrane protein required for an early sequestration event of pexophagy. It localizes to the SM during glucose adaptation. Identifying amino acid domains within Atg9 required for function will reveal structural motifs important to the expansion of the sequestering membranes and the role of membrane-bound Atg9 to this process. Atg9 encodes 885 amino acids of a 102 kDa protein. The C-terminus is asparagine-rich. PpAtg9 shares 77% identity with ScAtg9. The large central region containing the transmembrane domains—residues 190-679—reveal shared homology between the two proteins and 45% identity in that region. There are five to six transmembrane domains with the N and C termini at the cytosolic surface of the membrane (Yen *et al.*, 2007). Some of the conserved regions of Atg9 showed up in a motif

database search as possible functional domains (Figure 1). For example, a region within loop #3 and the C-terminal QQHKA may act as ER exit signals. Furthermore, there exist two putative motifs between amino acids 235-9 and 607-11 that may interact with a peroxisomal membrane protein, Pex14.

Cellular Compartments of Atg9

Under normal growth conditons, PpAtg9 in *P. pastoris* resides in a unique peripheral compartment, PC9 (Chang *et al.*, 2005). This compartment does not contain COXIV-GFP (mitochondria), PpSec13 (intermediate compartment), and PpSec7 (Golgi apparatus). Furthermore, PpAtg2, PpAtg8, and PpAtg11 are absent from these vesicles. Upon glucose-induced micropexophagy, PpAtg9 transits from the PC9 to perivacuolar structures (PVS) that also contain PpAtg11, but not PpAtg2 or PpAtg8. Finally, PpAtg9 is found at the sequestering membranes (SM) that engulf the peroxisomes (Figure 1-2).

The trafficking of ScAtg9 and its organization into discrete puncta are affected in mutant strains in which ER morphology is altered (Mari and Reggiori, 2007), notably trafficking of ScAtg9 to the mitochondria. Peripheral ScAtg9 does not co-localize with peroxisomal and endosomal markers (Chang and Huang, 2007). The co-localization of Atg9 with the mitochondria is a matter of debate. It has been reported that only a small percentage of the protein is found bound to the mitochondria by density gradient fractionation (Mari and Reggiori, 2007); Atg9 did co-fractionate with mitochondrial marker Por1 (Yen *et al.*, 2007). PpAtg9 does not co-localize with the mitochondria (unpublished results).

Mammalian Atg9 is localized to the TGN and late endosomes; starvation causes redistributed from the TGN to more peripheral, endosomal membranes (Young *et al.*, 2006). Studies of mAtg9 have revealed that despite its homology to the yeast protein, its subcellular distribution is distinct. mAtg9 do not have a specialized site for autophagosome biogenesis

(such as the PAS) but have multiple subcellular locations; peripheral, endosomal membranes may be the mammalian counterpart of the PAS (Young *et al.*, 2006). The homology of proteins such as PpAtg9 is greater between *P. pastoris* and *H. sapiens* as opposed to *S. cerevisiae* and *H. sapiens*.

Transport of Atg9 During Micropexophagy Requires Vps15 And Atg11

In *S. cerevisiae,* Atg9 localizes to the PC9 and PAS, the site of SM nucleation and expansion. In P. pastoris, Atg9 can be found at the PC9, PVS, and occasionally at the PAS. The PVS is the site of SM nucleation and expansion, while the membrane assembly of the MIPA occurs at the PAS. Atg9 trafficking requires multiple ATG gene products. ScAtg9 recruits ScAtg2 and ScAtg18 to the PAS (Chang and Huang, 2007). In the absence of ScAtg2 or ScAtg18, ScAtg9 movement is restricted to the PAS (Yen *et al.*, 2007). Anterograde movements of ScAtg9 to the PAS requires ScAtg11, ScAtg23, ScAtg27, and actin (Yen *et al.*, 2007). Recycling back to the PC9 requires the ScAtg1-ScAtg13 complex, ScAtg2, ScAtg18, and the PI3P generated by PI3K which contains ScVps15, ScVps43, and ScAtg14 (Mari and Reggiori, 2007). In mammalian cells, the anterograde movements of HsAtg9 out of the TGN to the limiting membranes of the autophagosome require HsAtg1 and PI3K activity (Young *et al.*, 2006). In *P. pastoris*, Vps15 and Atg11 are required for Atg9 to transit from the PC9 to the PVS, while Atg2 and Atg7 are necessary for the movements of Atg9 from the PVS to the SM during micropexophagy (Chang *et al.*, 2005). The data suggest that Vps15, Atg11, actin, Atg1, Atg23, and Atg27 have major roles in the trafficking of Atg9 into an out of the PAS/PVS.

Vps15, A Component of The Phosphatidyl Inositol-3 Kinase (PI3K) Complex Thought To Signal The Start Of Autophagy, Is Required For Atg9 Trafficking

Vps15 is a protein kinase that functions as the regulatory subunit of the PI3K complex (Kihara *et al.*, 2001; Budovskaya *et al.*, 2002). Vps15 is required for nucleation of the vacuole

during micropexophagy and is involved in early expansion by affecting the trafficking of Atg9 (Stasyk *et al.*, 1999; Chang *et al.*, 2005). Atg9 transit to the PVS requires Vps15 during glucose-induced micropexophagy. Atg9 and Vps15 are not thought to directly interact. Instead, Vps15 is thought to act upstream of Atg9 in a regulatory fashion. Vps15 is also required for Vacuolar Protein Sorting (by definition) and for delivery of hydrolases to the lysosome-like organelle (e.g. vacuole; equivalent to the mammalian lysosome) in yeast.

Deleting or mutating Vps15 can have considerable implications. A vacuolar missorting phenotype is exhibited by *vps15Δ*, in which all transport of vacuolar proteins is inhibited, and cellular growth is slow at 28 °C and arrested at 37 °C (Kihara *et al.*, 2001). Other phenotypic defects associated with *vps15Δ* include defects in osmoregulation and disturbed vacuolar segregation (Stasyk *et al.*, 1999).

Vps15 is composed of 1340 amino acids with a predicted molecular weight of 166 kDa; it runs at about 170 kDa on denaturing gels. It has four functional domains conserved amongst species important to signal transduction, protein trafficking and protein-protein interactions: the myristoylation site, the kinase domain, the HEAT repeats and the WD repeats. These domains are important for the function of Vps15 and for its interaction with other proteins.

The second amino acid from the N-terminus, glycine, is myristoylated for peripheral membrane association (Panaretou *et al.*, 1997). Subcellular fractionation and protease protection assays indicate that ScVps15p is associated with the cytoplasmic face of an intracellular membrane. ScVps15 is myristoylated *in vivo* (Herman *et al.*, 1991a; Herman *et al.*, 1991b). Non-myristoylated Vps15 proteins are 35-50% phosphorylated *in vivo* compared to the wild-type protein and possess near wild-type levels of biological activity. Non-myristoylated Vps15 still seems to be biologically and exhibits near wild-type growth rates.

Amino acids 147-152 (DIKSEN) in ScVps15 is the six amino acid sequence characteristic to the serine/threonine (S/T) kinase family; the lysine residue is absolutely conserved in S/T kinases. D147 and D165 are the aspartate residues thought to bind the ATP phosphate groups through an intermediate Mg^{2+} ion. The glutamate residue occurring at residue 199 is highly conserved among protein kinases. Its mutation abolishes ScVps15's autophosphorylation (Kihara *et al.*, 2001) and confers temperature sensitivity and causes carboxypeptidase Y missorting (Bryant and Stevens, 1998).

HEAT repeats (for Huntington, elongation factor 3, alpha regulatory subunit of protein phosphatase 2A, and TOR1) form pairs of α-antiparallel rod-like (hairpin) helices and function as protein-protein interacting surfaces. The HEAT repeat is a tandemly repeated module occuring in cytoplasmic proteins involved in intracellular transport processes. Structural analyses reveal that the motif could provide a platform for protein-protein interactions. The HEAT repeat motif occurs three times in Vps15, between amino acids 424-462, 562-600, and 601-639. Mutations that disrupt the integrity of the HEAT repeats result in the inactivation of ScVps15 (Budovskaya *et al.*, 2002).

The last 400 amino acids of Vps15 are within the WD repeat region. WD motifs have a conserved core of approximately 40 amino acids with a GH dipeptide 11-24 residues from the C-terminus and a WD dipeptide at the C-terminus; thus, WD40 specifies the motif type and the number of residues present in this motif. All WD-repeat proteins are thought to form circularized β-propeller structures. The β-propellers serve as specialized docking platforms for other proteins and require at least four repeats for functional relevance. Two or three motifs present in single polypeptides may dimerize to form a four- or six-bladed propeller.

ScVps15 CΔ214 was not phosphorylated *in vivo*, suggesting that these amino acids contain the site of phosphorylation; deletions of this domain result in a temperature-conditional vacuolar protein sorting defect which is reversed when mutant cells are shifted back to a permissive temperature. Deleting a short portion of the C-terminus in addition to mutating the kinase domain results in a more severe sorting phenotype; in addition, *ScVps15*^{ts} alleles have equally severe CPY sorting defects, and if the C-terminus is truncated, an even greater exaggeration of the sorting defect results. It is unclear whether the CΔ214 phenotype is due solely to partial deletion of the WD40 domain, or if the last 214 amino acids harbor amino acids of particular importance.

ScVps15p, the regulatory subunit for the PI3K complex, and ScVps34p, the catalytic subunit for the PI3K complex, interact. Vps34 is known to be a major player in signal transduction. The gene product of VPS34 is required for endocytosis and for sorting to the vacuole (Stasyk *et al.*, 1999) in *Saccharomyces cerevisiae*. The phosphatidyl inositol (PtdIns) 3-kinase (PI3K) activity of ScVps34p must be activated by the kinase activity of ScVps15p (Stasyk *et al.*, 1999). An intact Vps15p protein kinase domain is necessary for the association with and activation of Vps34p (Stack *et al.*, 1995). Yeast Two-Hybrid mapping experiments identified all three HEAT repeats to be required for binding of ScVps15 to ScVps34 (Vps15 fusions retaining one HEAT repeat exhibited intermediary binding) (Budovskaya *et al.*, 2002). The HEAT repeats are required but not sufficient for binding of Vps15 to Vps34. Once ScVps34p is activated by ScVps15, PtdIns molecules in the lipid bilayer (of an as yet unidentified intracellular membrane) are phosphorylated; localized patches of these PtdIns(3)P then activate effector molecules, which may include Atg18, Atg20, Atg21, Atg24 or Gsa13, that bind to these glycolipids (Stasyk *et al.*,

1999). The interactions of membrane-bound ScVps15p and ScVps34p are critical to the targeting of acid hydrolases to the yeast vacuole.

Identifying the localization of Vps15 and determining the motifs required for this localization are basic to elucidating the role of Vps15 in early pexophagy. Its interactions with other proteins and its potential as a gatekeeper to pexophagic sequestration will help explain autophagy in systems besides just methylotropic yeasts.

Atg11 Is a Membrane-Associated Protein Required For Pexophagy But Not Autophagy

Atg11 has been shown to interact directly with Atg9, although the exact mechanism by which these interactions occur and the implications of these interactions may not be fully realized. Different avenues of investigation of Atg9 and Atg11 have revealed the regions necessary for these proteins to interact with one another.

Immunofluorescent studies in *S. cerevisiae* have shown that ScAtg9 and ScAtg11 co-localize. ScAtg9 and ScAtg11 do not co-fractionate with any other known resident organelle marker proteins (Kim *et al.*, 2002). It has been suggested that the presence of ScAtg11 at the PAS recruits additional ScAtg9 to the same place (Kim *et al.*, 2002). Studies in *S. cerevisiae* provide evidence that Atg11 interacts with other proteins (namely Atg9) as a gatekeeper for sequestration by the vacuole. Atg9 and Atg11 are known to be present at the PVS in *P. pastoris.* Atg9 requires Atg11 to localize to the PVS. Thus, PpAtg11 may regulate protein trafficking to the PVS. Such transport may be mediated by actin, since Reggiori and coworkers have shown that ScAtg11 interacts with actin and both are required for anterograde transport of ScAtg9 from the PC9 to the PAS during autophagy (Monastyrska *et al.*, 2006).

Even though the localization of ScAtg9 is dependent on ScAtg11, the reverse is not true. Localization of GFP-ScAtg11 to the PAS is not significantly affected in *Scatg9Δ* cells (Chang

and Huang, 2007). Thus, ScAtg11 appears to affect PAS function independently of its interaction with ScAtg9 (Chang and Huang, 2007).

PpAtg11 is a peripheral membrane protein that contains 1313 amino acids and has a predicted molecular weight of 151,077 Daltons. The primary putative structural motif in Atg11 is its coiled-coil domain. The coiled-coil domain is a scaffold for protein interactions. Atg11 contains four coiled-coil domains (Chang and Huang, 2007), of which the first 2 coiled-coil regions of ScAtg11 are required for interaction with ScAtg9 (Chang and Huang, 2007). Deletion of residues 272-325 of Atg11ΔCC1 was important to Atg9-Atg11 interactions (Chang and Huang, 2007), contrary to Klionsky's earlier findings regarding the deletion of residues 272-321. The interaction of ScAtg11 with ScAtg9 via the coiled-coil domains is essential for the recruitment of ScAtg9 to the PAS by ScAtg11.

The region within Atg9 that is required for its interaction with Atg11 has been narrowed down as well. Deletion of the first 152 residues of the N-terminus did not affect the interaction of Atg9 with Atg11 (Chang and Huang, 2007). Deletion of the first 201 residues of the N-terminus of ScAtg9, however, did obliterate its interaction with Atg11. (Chang and Huang, 2007). Two hybrid analyses narrowed this region to amino acids 154-200. Based on the fact that Atg9Δ154N and Atg9Δ201N both migrated faster than Atg9Δ200C, there appears to a post-translational protein modification at the N-terminus of Atg9 which inhibits the migration of Atg9 even when the last 200 amino acids of Atg9 are deleted (Chang and Huang, 2007).

The Atg11 coiled-coil domains may not be the only regions that interact with Atg9. The transport of Atg9 after knocking out Atg1 (TAKA assay) in *S. cerevisiae* examines the localization of Atg9 to the PAS in mutant Atg1 background as control. A double knockout background determines whether Atg9 localization changes when another protein in addition to

Atg1 is knocked out. If Atg9 is restricted to the PAS, the gene product that is knocked out in addition to Atg1 acts after Atg1 in Atg9 trafficking. If Atg9 does not localize to the PAS and is present in cytosolic dots, the gene product that is knocked out in addition to Atg1 acts prior to Atg1 in Atg9 trafficking.

The TAKA assay has been applied to determine whether the coiled-coil domains are the means by which Atg11 interacts with Atg9 prior to Atg1 involvement. Atg11ΔCC1 or Atg11ΔCC2 did not restore the GFP-Atg9 restriction to the PAS during starvation in *atg1*Δ-*atg11*Δ double knockout cells (Chang and Huang, 2007). Thus, it appears that the coiled-coil domains of Atg11 are not the only region that interact with Atg9.

Deletion and insertion mutations of the PpAtg11 gene product have enabled researchers to pinpoint the step at which PpAtg11 participates in micropexophagy. Both *Ppatg11* (identified by the REMI mutant approach (Schroder *et al.*, 2007)) and *Ppatg11*Δ exhibit defects in micropexophagy at an early stage of the engulfment process, characterized by the vacuolar extensions only partially surrounding the peroxisome—perhaps a checkpoint stop in the sequestration process (Kim *et al.*, 2001). PpAtg11 also requires PpVac8 for its proper localization; *Ppvac8*Δ exhibits a completely round vacuole characteristic of a very early micropexophagy mutant.

Atg11 has a specific role in autophagy. Atg11 is the only protein known to function exclusively in micropexophagy in *Pichia pastoris* (Kim *et al.*, 2001). ScAtg11, which shares significant coiled-coil domain sequence homology to PpAtg11, is specific to the pexophagy pathway but not the macroautophagy pathway (Kim *et al.*, 2001).

PpAtg11 has an important role in pexophagy. It distributes around the peroxisomes early in sequestration, possibly "tagging" them for vacuolar recognition during pexophagy. Upon

induction of pexophagy, localization of PpAtg11 to the point of contact between the vacuolar and the peroxisomal membranes occurs (Kim *et al.*, 2001). PpAtg11 is concentrated in the PVS adjacent to the vacuole membrane, and it has been hypothesized that this protein mediates interactions between the vacuole and the peroxisome during microautophagy (Kim *et al.*, 2001).

Based on the existence of multiple bands by Western blot, PpAtg9 is thought at least to dimerize (unpublished observations). Atg11, as well, is thought to dimerize, at least in *S. cerevisiae*. ScAtg11p forms detergent-resistant homodimeric complexes (or homooligomers) (Kim *et al.*, 2001). The presence of multimeric Atg11 complexes has not been confirmed in *P. pastoris*, but their formation via the coiled-coil domain may be important to PpAtg11's association with itself and other proteins during micropexophagy. Another motif present in PpAtg11 that may be important to its function is the WKSYY sequence (amino acids 241-5), a WXXXF/Y motif shared by Pex5, Pex14 and Atg9. This domain may enable PpAtg11 to interact with Pex and other Atg proteins. Once Pex14 or another protein attracted to the PpAtg11 WXXXF/Y motif, the coiled-coil domain of PpAtg11 may promote and enhance this interaction, possibly resulting in multimeric complex formation.

Actin Is Required For Efficient Autophagy

It is possible that Atg11 directs the trafficking of Atg9 to the PVS via actin cables (Monastyrska *et al.*, 2006). A role for actin has been implicated in autophagy. Atg9 and Atg11 trafficking is altered and the formation of the PAS is aberrant when toxins or mutant strains inhibit actin polymerization (Reggiori *et al.*, 2003; Reggiori and Klionsky, 2006; Mari and Reggiori, 2007; Yen *et al.*, 2007). Lantrunculin A destroys the actin cytoskeleton by interfering with polymerization. ScAtg9 does not accumulate at the PAS in $atg1^{ts}$ strain treated with lantrunculin A (Yen *et al.*, 2007). In the absence of Atg11 and actin filaments, ScAtg9

anterograde transport from the PC9 to the PAS is blocked [Mari Reggiori Atg9 trafficking in S. cerevisiae Autophagy 2007]. However, Atg11 and actin filaments are not required for Atg9 transport to the PAS during starvation-induced autophagy (Mari and Reggiori, 2007). Thus, actin is required for Atg9 movement during normal growth and pexophagy but not starvation-induced autophagy. Moreover, a toxin or a mutant strain that blocks actin filament formation severely impairs Atg9 transport from the PC9 locations (Mari and Reggiori, 2007), suggesting that the initial activation of Atg9 is impaired.

Another requirement for actin has been described in regards to Atg11. ScAtg11 is mislocalized from the PAS to several dispersed fluorescent dots throughout the cytoplasm in VFT (Vps53, VPS Fifty-three) mutants (Reggiori *et al.*, 2003). The VFT complex, named for Vps53, the first protein discovered in the complex, functions as a tethering factor for retrograde traffic from the early endosome back to the late Golgi and is required specifically for degradation processes during normal growth in *S. cerevisiae*. Nitrogen starvation-induced autophagy elicits the correct re-localization of ScAtg11—and the block in VFT mutants is bypassed. Further investigation showed that Vps51, Vps52, Vps53 and Vps54 are required for actin organization (Reggiori and Klionsky, 2006).

The Atg1 Protein Kinase Is Required For Pexophagy And Autophagy

Atg1 is required for late expansion during micropexophagy. Atg9 localization late in autophagy requires Atg1 in *S. cerevisiae*. Whether Atg1 acts after Atg11 is no longer a matter of debate. GFP-Atg9 is restricted to the PAS in growing or starved cells in *atg1Δ* cells (Chang and Huang, 2007). The transport of Atg9 after knocking out Atg1 (TAKA assay) in *S. cerevisiae* examines the localization of Atg9 to the PAS in mutant Atg1 background as control.

Deletion of full-length Atg11 and Atg1 together provide further insight regarding Atg9 trafficking. In *atg1Δ-atg11Δ* background, GFP-Atg9 localized to the PC9, not the PAS. Similar results were obtained in *atg1Δ-atg23Δ* and *atg1Δ-atg27Δ* cells. For example, in *atg27Δ* and *atg27Δ-atg1Δ* cells, Atg9 localized to multiple punctate dots—none of which corresponded to the PAS—and some of which were restricted to the mitochondria (Yen *et al.*, 2007). Atg27 may be required for movement of Atg9 from the mitochondria to the PAS and is thought to function before Atg1 in the cycling of Atg9 (Yen *et al.*, 2007). Thus, different null Atg proteins were substituted and the *atg1Δ* deletion was constant during the TAKA assay, and the action of Atg23 and Atg27 in regards to Atg9 trafficking was determined. Taken together, this would suggest that Atg11, Atg23, and Atg27 are required for anterograde transport from the PC9 to the PAS, and that Atg1 is the only protein known to be required for retrograde transport

The majority of Atg27 is restricted to the PAS in *atg1Δ* cells (Yen *et al.*, 2007). In *atg9*Δ and *atg1*Δ-*atg9*Δ cells, Atg27 localized to multiple punctate structures similar to wild-type localization except that none of the dots localized to the PAS. In this case, Atg9 and Atg1 were deleted and the localization of Atg27 to the PAS was studied—a modified TAKA assay with an aim to determine Atg27 trafficking. Atg9 is required for anterograde movement of Atg27 to the PAS (Yen *et al.*, 2007). Retrograde movement of Atg27 to the PC9 is dependent on the Atg1-Atg13 complex (Yen *et al.*, 2007), however Atg1 kinase activity was not required. The region for Atg27 and Atg9 interactions is being whittled down: the anterograde movement of Atg9 to the PAS does not require the cytosolic C-terminus of Atg27 (Yen *et al.*, 2007).

Atg9 dots co-localize with Atg8 and Atg5, which are known to be involved in autophagosome nucleation. Thus, the multiple GFP-Atg9 dots induced by starvation treatment of *atg1Δ-ape1Δ* cells is thought to represent nucleated sites of autophagosome assembly (Chang

and Huang, 2007). GFP-atg9Δ154-201 behaved the same as GFP-Atg9 during growth or starvation in *atg1Δ-ape1Δ* background (Chang and Huang, 2007).

Atg9 Retrograde Trafficking Requires Atg23 And Atg27

Atg27, Atg23 and Atg11 are essential for Atg9 retrograde trafficking (Yen *et al.*, 2007). Atg9 and Atg23 show similar distribution to Atg27 localization, with non-PAS cytosolic dots. Atg23 is a cytosolic protein required for the Cvt pathway and autophagy but not pexophagy (Yen *et al.*, 2007). Because there is no equivalent Cvt pathway in *P. pastoris* and the role of Atg23 in *P. pastoris* is unclear, for our purposes Atg23 is neglected. PpAtg27 is an integral membrane protein required for efficient pexophagy, which may be related to its Atg9 trafficking role.

In addition, Atg27 is required for starvation-induced autophagy. *atg27*Δ cells exhibited partial induction of *Pho8Δ60* activity (a biochemical measure of normal autophagy), suggesting that starvation-induced autophagy did occur but not as efficiently as in wild-type cells (Yen *et al.*, 2007). With further investigation, *atg27*Δ was shown to have reduced autophagosome number (a defect in nucleation) or reduced autophagosome size (a defect in expansion) (Yen *et al.*, 2007). Thus, Atg27 is required for nucleation and expansion during macroautophagy.

Structure precludes function; thus, the structure of Atg27 is described in detail. Atg27 (also known as Etf1) is a Type I transmembrane protein (Yen *et al.*, 2007). Atg27 topology indicates that it could be present within the intermembrane space between the autophagosome inner and outer vesicle membrane or in the lumenal space during autophagosome formation (Yen *et al.*, 2007). The C-terminus of Atg27 is cytosolic (Yen *et al.*, 2007). Atg27 harbors an N-terminal signal sequence and the N-terminus may therefore also face the cytoplasm (Yen *et al.*, 2007).

Atg27 cellular localization has been examined fluorescently. Atg27-GFP distributes to several subcellular punctate structures. None of these was found to co-localize with the ER or with the peroxisomes (Yen *et al.*, 2007). ScAtg27 does co-localize with the PAS marker Ape1 (Yen *et al.*, 2007), with MitoFluor red (which labels the mitochondria) and with the Golgi marker Vrg4-GFP (Yen *et al.*, 2007). Atg27 cellular localization is similar to Atg9 localization except that Atg9 has not been observed at the Golgi.

To verify the fluorescence data, Atg27 vesicles were separated by sucrose density gradient fractionation (Yen *et al.*, 2007) and co-fractionated with Por1 and the Mnn1 marker for the Golgi complex (Yen *et al.*, 2007). Multiple membrane sources are thought to supply the lipids required for autophagosome formation; these lipids may originate in the Golgi. Atg27 is a putative PI3P binding protein downstream of Vps34 (Yen *et al.*, 2007). The Vps34 kinase complex I generates PtdIns(3)P at the PAS and is essential for autophagy (Yen *et al.*, 2007), specifically MIPA formation. Thus, Atg27 may regulate lipids essential to MIPA formation.

Atg27 is required for Atg9 cycling between the PAS, mitochondria and Golgi (Yen *et al.*, 2007). The localization and transit pattern of Atg27 is similar to that of Atg9 (Yen *et al.*, 2007). Atg9 was predicted to interact with Atg27 by yeast two hybrid analysis. Affinity isolation showed that Atg9 and Atg27 interact with one another (Yen *et al.*, 2007).

Components Of The COPII Secretory Pathway Are Required For Autophagy

A number of Sec proteins have been shown to be required for macroautophagy (Table 1-2). Notably, Klionsky showed that Sec12, which is the guanine nucleotide exchange factor (GEF) for Sar1p recruiting this protein to the ER membrane, is required for the formation of the autophagic vacuole (Ishihara *et al.*, 2001; Reggiori *et al.*, 2004). Sec18 and Vti1 are required for fusion of the autophagic vacuole with the yeast vacuole. Finally, Sec7, Sec17, and three COPII vesicle coat proteins (Sec16, Sec23, and Sec24) are necessary for autophagy, but their

roles have not been defined (Ishihara *et al.*, 2001; Hamasaki *et al.*, 2003). Sec12, Sar1, Sec23 and Sec24 are required for assembling the cargo to be packaged by the COPII vesicle (Sato and Nakano, 2007). Interestingly, Sec13 and Sec31 essential for polymerization of the COPII coat were not required for autophagy (Ishihara *et al.*, 2001). The data suggest that components of COPII assembly, but not COPII vesicles, are essential for autophagy. However, the roles of COPII vesicles and of Sar1, a major player in the assembly of the COPII vesicles, in autophagy and pexophagy have not been investigated. We have shown that that Sar1 is required for pexophagy and autophagy suggesting a direct link between the secretory pathway and these degradative pathways.

Sar1 and Protein Transport

COPII vesicles organize the delivery of proteins from the ER to the Golgi apparatus. Mutants that disrupt ER to Golgi transport can be categorized into two categories, phenotypically defined as those defective in fusion of ER-derived vesicles with the Golgi complex (that accumulate 50 nm vesicles but do not fuse with the Golgi) and those defective in vesicle formation (that accumulate in ER membranes). Sar1 is the GTPase responsible for incorporating cargo into COPII vesicles. Upon accepting GTP from Sec12, active Sar1 interacts with Sec23 and Sec24 at the ER and the COPII complex assembles. The COPII complex assembles cargo and then polymerizes and buds from the ER. The hydrolysis of the GTP by the Sar1 results in COPII complex disassembly and uncoating the COPII vesicles which then fuse with the Golgi apparatus delivering their contents.

Sar1p-guanosine 5'-*O*-(3-thiotriphosphate), a non-hydrolyzable form of GTP, is unable to promote targeting of ER vesicles to the Golgi at all (Oka and Nakano, 1994). In other words, GTP hydrolysis by Sar1 is not required for vesicle formation but is required for subsequent

transport from the ER to the Golgi. Cells expressing sar1(T39N) (equivalent to T34N in *P. pastoris*) has an extensive ER and are defective in COPII vesicle formation. Cells expressing sar1(H79G) form an exaggerated Golgi apparatus and are defective in retrograde transport to the ER. The sar1(T39N) mutant has a high affinity for GDP and blocks COPII vesicle formation from the ER. The sar1(H79G) mutant is unable to hydrolyze GTP and prevents disassembly of COPII vesicle coats thereby inhibiting retrieval of proteins to the ER (Ward *et al.*, 2001).

Sar1 controls COPII budding and that it was hypothesized that Sar1 is the means by which coat assembly and cargo selection are integrated (Barlowe, 2002). Membrane-bound Sar1-GTP links vesicle cargo to pre-budding complexes and to the COPII coat. At that time it was not understood how coat polymerization leads to membrane deformation, how the variety of cargo to be included in COPII vesicles is recognized by coat subunits, and how Sar1 regulates the coat assembly/disassembly stages to execute these tasks (Barlowe, 2002).

The recycling of proteins from the Golgi complex is not the principle means by which sorting is achieved: rather, the separation of proteins destined for transport (as opposed to proteins that remain in the ER) occurs primarily at the moment of transport vesicle budding from the ER. Thus, Sar1 is critical to protein dispersion throughout the cell.

Sar1 was reported in yeast to be detected in a diffuse, perinuclar and reticular localization (overlapping with Kar2 and Sec62) as well as in punctuate structures that did not overlap with ER or Golgi markers (Kuge *et al.*, 1994). These structures may be a small population of Sar1 that labels transport vesicles so that they might eventually be recycled back to the ER. Sar1 serves as a discriminating molecule that transports key proteins throughout the cell and imparts a unique signal to a membrane certifying proper travel throughout the secretory pathway be it to the Golgi apparatus or degradation by the ubiquitin-proteasome system (Sato and Nakano, 2007).

Thus, a role for Sar1 could be to provide regulatory control to sort and concentrate cargo to ensure efficient export from the ER (Kuge *et al.*, 1994).

Sar1 And Lipid Transport

Ceramide is synthesized in the ER and is sorted to other organelles in a non-vesicular fashion by at least two pathways: an ATP- and cytosol-dependent major pathway and an ATP- and cytosol independent minor pathway (Hanada *et al.*, 2003). CERT, for example, interacts specifically with the ER membranes and specifically extracts ceramide. This may suggest that another lipid-transfer-catalyzing enzyme specifically extracts PtdEtn. The importance of PtdEtn trafficking is that during autophagy Atg8 becomes covalently bound to this lipid at the expanding autophagic vacuole. Sar1 may decrease the propensity of PtdEtn to traffick properly to the forming autophagic vacuole. However, in cells expressing sar1(T39N) the conversion of ceramide to sphingomyelin was not affected. This would suggest that PtdEtn trafficking would not be affected but is by no means definitive. The ATP dependence of ceramide transport could be relevant to PI4-P metabolism at the Golgi (Hanada *et al.*, 2003).

A specific subdomain of the ER is thought to be closely associated with the Golgi stacks (Hanada *et al.*, 2003). If PtdEtn trafficks via a non-vesicular mechanism, the integrity and the close association of the ER and the Golgi may be essential to PtdEtn trafficking; the alteration of this association by mutant Sar1 would alter PtdEtn trafficking or posttranslational modification of PtdEtn and conversion of PtdEtn to another compound, such as PI4-P, that is crucial for Atg8 trafficking and MIPA formation.

Summation

Glucose signals and peroxisome recognition initiates the sequestration of peroxisomes by micropexophagy. During sequestration, the SM nucleate from the vacuole, then expand from the PVS and PAS (Figure 1-1). Completion occurs when the peroxisomes are engulfed and

incorporated into the vacuole where they are degraded. The sequestration of peroxisomes begins by nucleation of the sequestering membranes (SM) from the vacuole. During expansion, two unique membranes surround the peroxisomes: the SM that expands from the PVS and the MIPA that assembles from the PAS. SM expansion from the PVS is Atg9 dependent, while the formation of the MIPA from the PAS is dependent upon Atg8 and Sar1. The MIPA is situated between opposing membranes thereby promoting membrane fusion of the SM and MIPA resulting in the completion of the sequestration of the peroxisomes. Once inside the vacuole the peroxisomes are degraded by the hyrdrolytic enzymes and the amino acids, sugars, and lipids recycled. In this thesis, I will characterize the roles of Atg9 and Sar1 in SM expansion during micropexophagy.

Table 1-1: Autophagy-related Genes

Gene Name	*Pichia pastoris*[2]	Function[3]	Characteristics	References
ATG1[1]	*GSA10 PAZ1*	P,A	Serine/threonine-kinase that complexes with Atg11 and Vac8	(Stromhaug *et al.*, 2001; Mukaiyama *et al.*, 2002)
ATG2	*GSA11 PAZ7*	P,A	Peripheral membrane protein that interacts with Atg9	(Stromhaug *et al.*, 2001; Mukaiyama *et al.*, 2002)
ATG3	*GSA20*	P,A	E2-like enzyme responsible for the conjugation of Atg8 to lipids	
ATG4	*PAZ8*	P,A	Cysteine proteinase	(Mukaiyama *et al.*, 2002)
ATG7	*GSA7 PAZ12*	P,A	E1-like enzyme responsible for the conjugation of Atg12 to Atg5 and Atg8 to lipids	(Yuan *et al.*, 1999; Mukaiyama *et al.*, 2002)
ATG8	*PAZ2*	P,A	Soluble protein that becomes conjugated to lipids	(Mukaiyama *et al.*, 2004; Monastyrska *et al.*, 2005)
ATG9	*GSA14 PAZ9*	P,A	Integral membrane protein associated with structures juxtaposed to the vacuole and essential for expansion of the sequestering membranes	This Study
ATG11	*GSA9 PAZ6*	P	Coiled-coil domain found at vacuole surface	(Kim *et al.*, 2001; Klionsky *et al.*, 2003)
ATG18	*GSA12*	P,A	WD40 protein	(Guan *et al.*, 2001)
ATG24	*PAZ16*	P,A	Sorting nexin with PX domain	(Ano *et al.*, 2005)
ATG26	*PAZ4*	P	UDP-glucose:sterol glucosyl-transferase	(Mukaiyama *et al.*, 2002)
ATG28	*PpATG28*	P	Coiled-coil protein	(Dunn *et al.*, 2005)
PFK1	*GSA1*	P	α-subunit of phosphofructokinase	(Yuan *et al.*, 1997)
PEP4	*GSA15 PAZ14*	P,A	Endopeptidase	(Mukaiyama *et al.*, 2002)
VPS15	*GSA19 PAZ13*	P,A	Membrane-anchored Serine/threonine-kinase with WD40 domains	(Stromhaug *et al.*, 2001; Mukaiyama *et al.*, 2002)
Vac8	*PpVac8*	P	Armadillo-repeat protein	(Fry *et al.*, 2006)

[1] A unified gene nomenclature of autophagy and autophagy-related processes such as pexophagy has been standardized across species to be ATG for the gene name.
[2] GSA, glucose-induced selective autophagy; PAZ, pexophagy zeocin-resistance.
[3] P, required for pexophagy; A, required for autophagy; nd, not determined.

Table 1-2: Secretory-related Genes

Gene Name	Function[1]	Characteristics	References
SEC7	A	Guanine nucleotide exchange factor (GEF) for ADP ribosylation factors involved ER-to-Golgi transport	(Reggiori *et al.*, 2004)
SEC12	AV formation	Guanine nucleotide exchange factor (GEF) for Sar1p involved in ER-to-Golgi transport	(Ishihara *et al.*, 2001; Reggiori *et al.*, 2004)
SEC16	A formation	COPII vesicle coat protein	(Ishihara *et al.*, 2001; Hamasaki *et al.*, 2003)
SEC17	A	Peripheral membrane protein required for ER-to-Golgi transport	(Ishihara *et al.*, 2001)
SEC18	AV fusion with vacuole	N-ethylmaleimide-sensitive fusion protein, NSF	(Ishihara *et al.*, 2001)
SEC23	A formation	COPII vesicle coat protein	(Ishihara *et al.*, 2001; Hamasaki *et al.*, 2003)
SEC24	A	COPII vesicle coat protein	(Ishihara *et al.*, 2001)
SAR1	P,A	GTP-binding protein of the ARF family, component of COPII coat of vesicles; required for ER-to-Golgi transport	This Study
VTI1	AV fusion with vacuole	N-ethylmalemide-sensitive fusion protein attachment protein, SNARE	(Ishihara *et al.*, 2001)

[1] P, required for pexophagy; A, required for autophagy; AV, autophagic vacuole.

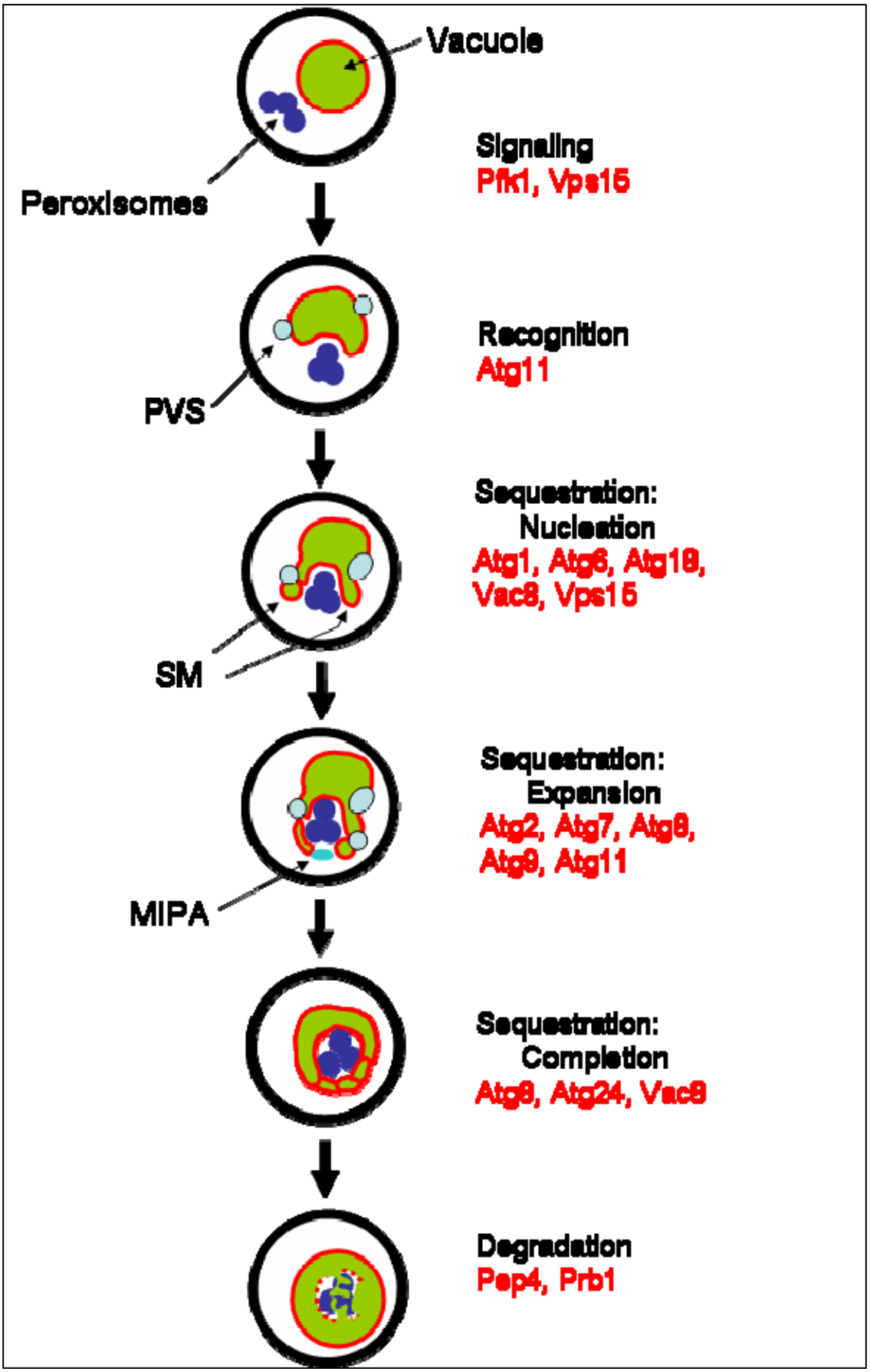
Vacuole
Peroxisomes
Signaling
Pfk1, Vps15
PVS
Recognition
Atg11
Sequestration:
Nucleation
Atg1, Atg6, Atg18,
Vac8, Vps15
SM
Sequestration:
Expansion
Atg2, Atg7, Atg8,
Atg9, Atg11
MIPA
Sequestration:
Completion
Atg8, Atg24, Vac8
Degradation
Pep4, Prb1

Figure 1-1. Peroxisome engulfment by glucose-induced micropexophagy. Micropexophagy occurs by specific events defined phenotypically and genetically. These events are dependent upon autophagy-related (Atg) and other proteins. Upon glucose signaling and peroxisome recognition, the sequestering membranes (SM) nucleate from the vacuole. The SM then expands from perivacuolar structures (PVS) and the micropexophagy apparatus (MIPA). Sequestration is complete when the peroxisomes are incorporated into the vacuole for degradation.

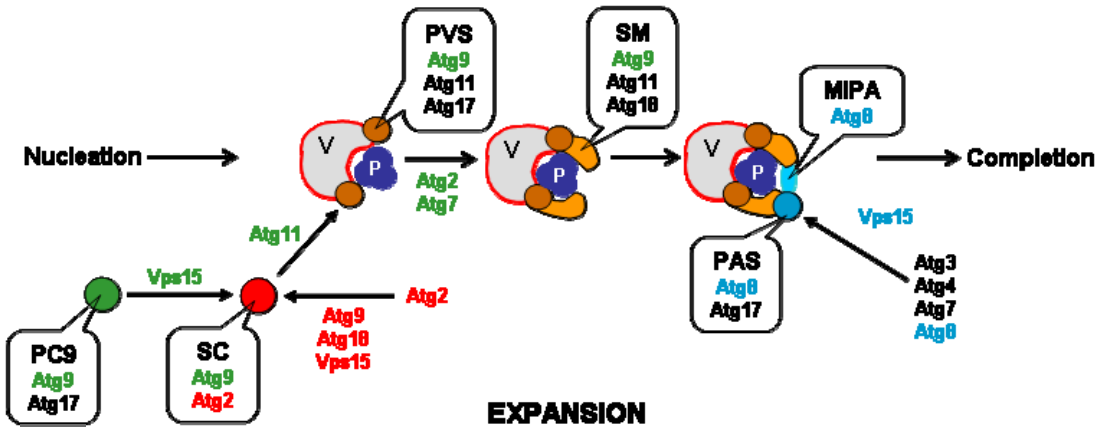

Figure 1-2. Molecular events of the expansion of the sequestering membranes that engulf peroxisomes during micropexophagy. There exist multiple molecular events that regulate the expansion of the sequestering membranes to engulf the peroxisomes (P). Upon glucose adaptation, nucleation of the sequestering membranes proceeds from the vacuole (V). We have subdivided the expansion events into two categories: early Atg9 dependent and late Atg8 dependent. The early events involve the association of Atg2 with a unique sorting compartment (SC), which requires Atg9, Atg18 and Vps15. At this time, Atg9 transits from a peripheral compartment (PC9) to perivacuolar structures (PVS) and the sequestering membranes (SM). The trafficking of Atg9 requires Vps15, Atg11, Atg2 and Atg7. During late expansion, the SM are tethered for fusion by the micropexophagy apparatus (MIPA). The assembly of the MIPA from the pre-autophagosomal structure (PAS) requires Atg8. The membrane anchoring of Atg8 by lipidation is mediated by Atg3, Atg4, and Atg7, which in turn is regulated by Vps15. Upon fusion of the SM with the MIPA, the peroxisomes are incorporated into the vacuole where they are degraded.

CHAPTER 2
IDENTIFICATION OF PEXOPHAGY GENES BY RESTRICTION ENZYME-MEDIATED INTEGRATION (REMI)[1]

Introduction

The methylotropic yeast, *Pichia pastoris*, can grow on methanol by synthesizing peroxisomal (e.g., alcohol oxidase and dihydroxyacetone synthase) and cytosolic (e.g., formate dehydrogenase) enzymes necessary to metabolize and assimilate this carbon source. Upon adapting these cells from growth on methanol to a medium containing glucose, the peroxisomes are rapidly and selectively degraded by a process called micropexophagy (Sakai *et al.*, 1998; Stromhaug *et al.*, 2001; Mukaiyama *et al.*, 2002; Habibzadegah-Tari and Dunn, 2003). During glucose adaptation, clusters of peroxisomes are surrounded by arm-like extensions from the vacuole. Upon homotypic membrane fusion of the arms, the peroxisome cluster is incorporated into the vacuolar lumen where it is subsequently degraded.

The highly regulated degradation of these large peroxisomes combined with classical yeast genetics makes *P. pastoris* an ideal model to characterize the molecular events of pexophagy. In order to identify those genes essential for pexophagy, we developed a direct colony assay by which to screen thousands of nitrosoguanidine-generated mutants that were unable to degrade peroxisomal alcohol oxidase. Once the mutant was verified, we would identify the mutated gene by complementation with a genomic library. This approach was quite time consuming and false positives were inevitable. Therefore, we set out to design a new approach to identify those genes essential for glucose-induced pexophagy.

[1] Article reprinted with permission from publisher: Schroder, L.A., B.S. Glick, and W.A. Dunn, Jr. (2007) Identification of pexophagy genes by restriction enzyme-mediated integration (REMI). In Methods in Molecular Biology (Vol 389): Pichia Protocols, Second Edition. J.M. Cregg, editor. Humana Press. pp. 203-218

We have utilized restriction enzyme-mediated integration (REMI) to facilitate a random disruption of genes in the *P. pastoris* genome by the incorporation of a Zeocin resistance gene. *P. pastoris* was transformed with a pREMI-Z vector that had been linearized with BamHI in the presence of BamHI or DpnII that would randomly cleave genomic DNA leaving four base overhangs compatible with the linearized vector. Transformed cells were selected by growth on Zeocin plates. Those transformed cells unable to degrade peroxisomes during glucose adaptation were identified by direct colony assays and the interrupted genes (*GSA*, glucose-induced selective autophagy) sequenced. REMI mutagenesis provides a novel approach to identifying key genes involved in autophagic processes and straightforward assays estimate the impact of the interrupted gene on pexophagy.

Materials

Pichia Pastoris and E. coli Strains

1. GS115 (*his4*)
2. PPF1 (*his4 arg4*)
3. DH5α

Culture Media

1. YPD: 1% Bacto yeast extract, 2% Bacto peptone, and 2% dextrose.
2. YND: 0.67 % yeast nitrogen base, 0.4 mg/l biotin, and 2% glucose.
3. YNDH: 0.67 % yeast nitrogen base, 0.4 mg/l biotin, 40 μg/l histidine, and 2% glucose.
4. YPD+Z: 1% Bacto yeast extract, 2% Bacto peptone, and 2% dextrose plus 100 μg/ml Zeocin.
5. YNM: 0.67 % yeast nitrogen base, 0.4 mg/l biotin, and 0.5% methanol.
6. YNMH: 0.67 % yeast nitrogen base, 0.4 mg/l biotin, 0.5% methanol, and 40 μg/l histidine.
7. LB+Z: 0.5% Bacto yeast extract, 1% Bacto tryptone, and 0.5% NaCl plus 25 μg/ml Zeocin.

8. YETM: 0.5% Bacto yeast extract, 1% Bacto tryptone, and 5% $MgSO_4 \cdot 7H_2O$, pH to 7.5 with KOH.

Vector

1. pREMI-Z (NCBI accession number AF282723)

Transformation of *Pichia Pastoris*

1. YPD
2. 1M NaHEPES, pH 8
3. 1M dithiothreitol
4. 1M Sorbitol

Qualitative Assessment of Alcohol Oxidase Degradation by Direct Colony Assay

1. P5 Filter Paper, 9 cm circle
2. NitroBind, nitrocellulose 0.45μm, 85mm circle
3. AOX Detection Solution: 3.4 U/mL horseradish peroxidase, 0.56 mg/mL 2,2'-azinobis (3-ethylbenzthazoline-6-sulfonic acid), 33 mM potassium phosphate buffer pH 7.5, 0.13% MeOH.
4. Liquid Nitrogen

Quantitative Assessment of AOX Degradation by Liquid Medium Assay

1. Cell Lysis Buffer: 20 mM Tris pH 7.5, 50 mM NaCl, 1 mM EDTA, 1 mM phenylmethylsulfonyl fluoride, 1 μg/mL pepstatin A, 0.5 ug/mL leupeptin.
2. 425-600 μm glass beads (Sigma G-8772)
3. AOX Assay Solution: 3.4 U/mL horseradish peroxidase, 0.56 mg/mL 2,2'-azinobis (3-ethylbenzthazoline-6-sulfonic acid), 33 mM potassium phosphate buffer pH 7.5.
4. MeOH

5. 4N HCl

Isolation of Yeast Genomic DNA

1. DNA Extraction Buffer :10 mM Tris pH 8.0, 2% Triton X-100, 1% SDS, 100 mM NaCl, 1 mM Na_2EDTA.

2. Phenol:chloroform:isoamyl alcohol (25:24:1 v/v)

3. Tris EDTA (10 mM Tris pH 7.5, 1 mM Na_2EDTA)

4. 10 mg/ml RNase A

5. Chloroform:isoamyl alcohol (24:1 v/v)

6. 3M NaOAc

7. 425-600 μm glass beads (Sigma G-8772)

8. Ethanol (ice cold)

Methods

We have developed a protocol to rapidly identify genes essential for glucose-induced micropexophagy (see Figure 2-1). This method utilizes a random integration assisted by restriction enzymes of a Zeocin resistance cassette vector into the genomic DNA thereby disrupting gene expression. The Zeocin-resistant yeast defective in peroxisome degradation are then identified by direct colony assays. Afterwards, the site of insertion of the REMI-Z is determined by first digesting the genomic DNA with restriction enzymes and then isolating the pREMI-Z with flanking genomic DNA by amplifying in *E. coli*. Once this vector is isolated, the flanking genomic DNA can be sequenced and the gene identified by BLAST searches of the NCBI databases. The methods described below outline: 1. vector construction, 2. yeast transformation with the pREMI-Z vector, 3. identification and isolation of pexophagy mutants, 4. isolation of the pREMI-Z vector with flanking genomic DNA, and 5. identification of mutated genes.

1.0. Vector Construction

A pREMI-Z vector containing the Zeocin-resistance gene behind the *S. cerevisiae* TEF and bacterial EM7 promoters to facilitate expression in yeast and bacteria (*E. coli*) was constructed. This includes (a) construction of vector and (b) amplification of vector.

Two 68 base oligos were annealed to yield the adapter that contains multiple stop codons in all 6 frames and the M13 reverse and M13 (-20) sequencing primers pointed in towards the central BamHI site:

The parent vector pPICZ-A (Invitrogen, San Diego) was cut at unique *BamHI* and *BglII* sites. The above adapter was then ligated into the pPICZ-A fragment at the *BamHI* and *BglII* sites to create pREMI-Z (see Figure 2-1). The vector was amplified by transforming Rb-competent DH5α and growing the transformants on LB+Z.

2.0 Yeast Transformation

The next step in this process involves the transformation of yeast and genomic integration of the pREMI-Z vector. This section includes (a) preparation of electro-competent yeast, (b) transformation yeast by electroporation, (c) selection on minimal medium and (d) verification of vector integration.

2.1 Electro-Competent Yeast

1. GS115 of PPF1 cells are grown in 250mls YPD to an OD_{600} of 1.0 – 1.5.
2. Cells are harvested at 4 °C in sterile 250 mL Nalgene centrifuge bottles at 4000xg for 20 minutes.

3. Cells are then resuspended in 50mls YPD containing 1ml 1M HEPES pH 8. 1.25 mls of 1M DTT is added dropwise while swirling the cells and the cells are incubated at 30 °C for 15 minutes with gentle shaking.
4. Bring to 250mls with sterile cold water and harvest the cells as above.
5. Wash cells two times with 250mls of sterile cold water.
6. Resuspend cells in 25mls sterile cold 1M sorbitol, transfer to 50ml conical tube and harvest cells at 2000xg for 10 minutes.
7. Resuspend cells into 0.5mls sterile cold 1M sorbitol.

Electro-competent *P. pastoris* are more effective when used immediately, but can be frozen at -80°C for later use.

2.2 Transformation of Yeast by Electroporation

1. pREMI-Z is linearized by digestion with BamHI.
2. 50 µL of competent yeast cells are mixed with 1-2 µg of linearized pREMI-Z and 0.5-1.0 units of BamHI or DpnII.
3. The solution is then transferred to a 0.2 cm gap cuvette for electroporation (1.5 kV, 25 µF, 400 Ohms).
4. Immediately after electroporation the cells are suspended in 1 mL of cold 1M sorbitol.

2.3 Selection of Transformants

1. The entire sample of electroporated cells is transferred to multiple YPD+Z plates (200-250 µL per plate).
2. Plates are then incubated for 2-4 days at 30°C until colonies appear.

2.4 Verifying Vector Integration

1. Pexophagy mutants are grown to stationary growth in 2 mL of YPD

2. Cells are lysed and genomic DNA isolated as described in Section 3.4.1
3. 10 μL of genomic DNA is digested with EcoRI
4. The genomic DNA fragments are then separated on an agarose gel and transferred to nylon membranes.
5. The DNA probe was made from BamHI-linearized pREMI-Z following instructions included in the North2South Biotin Random Primer Kit (Pierce, Rockford, IL)
6. pREMI-Z vectors containing DNA fragments on the nylon membranes were detected following instruction included in the North2South Chemiluminescent Hybridization and Detection Kit (Pierce, Rockford, IL).
7. The visualized bands demonstrate pREMI-Z insertions (Fig. 2-2). Virtually all the Zeocin-resistant clones have a single band suggesting a single insertion site. However, it appears that some clones have pREMI-Z inserted into two genes (see R23, Fig. 2-2).

3.0. Identification and Isolation of Glucose-induced Pexophagy Mutants

After isolating hundreds to thousands of Zeocin-resistant clones, the next step is to screen for pexophagy mutants. This is done by direct colony assay to identify those clones that do not degrade AOX when adapted from methanol to glucose. Those pexophagy mutants identified by direct colony assay are then isolated and verified by a liquid medium assay. This section includes (a) identification of pexophagy mutants by direct colony assay and (b) quantification of the pexophagy defect by liquid medium assay.

3.1 Direct Colony Assay

1. Colonies are grown on YPD+Z selection plates overnight 2-3 days at 30 °C.
2. Colonies are replica-plated from the YPD+Z plates to YNM plates (with appropriate amino acid supplements) and grown for 3-4 days at 30 °C.

3. Colonies are then replica-plated from the YNM plates to nitrocellulose which is placed onto YND plates colonies up and grown for 16-18 hours at 30 °C.
4. The colonies on nitrocellulose are removed from the YND plates and the cells lysed by freezing in liquid nitrogen for 20 seconds, taking care not to break the paper into shards.
5. The frozen nitrocellulose is carefully placed on Whatman paper soaked with AOX Detection Solution (33 mM potassium phosphate buffer (pH 7.5) with 0.13% MeOH, 3.4 U/mL HRP, and 0.53 mg/mL ABTS).
6. The nitrocellulose is incubated for 60-90 minutes at room temperature.
7. AOX activity is visualized with the appearance of periwinkle (purple) dots (Figure 2-3). When grown on YNM plates, all colonies have AOX activity. However, only those pexophagy mutants unable to degrade AOX will have AOX activity when transferred from YNM to YND.

3.2 AOX Degradation by Liquid Medium Assay

1. Pexophagy mutants identified by direct colony assay are isolated either from the original YPD-Z or the YNM plates and grown in YPD medium.
2. Cells (0.6 mL of saturated YPD culture) are grown in 20 mL YNM with appropriate amino acid supplements.
3. After 36-38 hours growth on YNM, 0.4 g glucose is added.
4. Two mL aliquots of cells at 0 and 6 hours of glucose adaptation are harvested by centrifugation.
5. The pellets are resuspended in 1 mL of cell lysis buffer (20 mM Tris pH 7.5, containing 50 mM NaCl, 1 mM EDTA, 1 mM PMSF, 1 μg/mL pepstatin A, and 0.5 μg/mL leupeptin).

6. The cells are then lysed by vortexing in the presence of 0.5 g of 425-600 μm glass beads.
7. The glass beads and cellular debris are removed by centrifugation.
8. Alcohol oxidase is measured by adding 50 μL of this extract to 3 mL of AOX Assay Solution (3.4 U/mL HRP and 0.53 mg/mL ABTS in 33 mM potassium phosphate buffer, pH 7.5).
9. The reaction is started by adding 10 μL MeOH and continued at room temperature for 15-30 minutes until the appearance of a teal color.
10. The reaction is stopped by addition of 200 μL 4N HCl.
11. The developed teal color is measured at 410 nm.

A representation of AOX degradation measured by liquid medium can be seen in Figure 2-4. Parental GS115 cells degrade over 90% of the AOX after six hours of glucose adaptation compared to 10% in gsa7 and pep4/prb1 mutants. In comparison, 30-60% of the AOX is degraded by eight unique REMI mutants.

4.0 Identification of the Disrupted Gene caused by the Insertion of pREMI-Z

After isolating the pexophagy mutants and verifying on Southerns (see Section 3.2.4) that the pREMI-Z inserted into a single site, the next step is to identify the site of insertion and the disrupted GSA/PAX gene. This is done by isolating the genomic DNA, digesting the DNA with selected restriction enzymes, ligating the pREMI-Z and its flanking DNA into a circular vector, and amplifying the vector in *E. coli* for DNA sequencing. This section will cover (a) the isolation of gDNA in yeast cells, (b) the isolation of the pREMI-Z vector, and (c) sequencing the genomic DNA that flanks the pREMI-Z.

4.1 Genomic DNA Isolation

1. *P. pastoris* is grown to stationary phase in 1 mL YPD at 30 °C.

2. Harvest the cells by centrifugation (14,000xg; 2 minutes).
3. To the cell pellets add 0.2 mL of DNA extraction buffer (2% Triton X-100, 1% SDS, 100 mM NaCl, 10 mM Tris-HCl pH 8, and 1 mM Na_2EDTA), 0.2 mL of phenol:chloroform:isoamyl alcohol (25:24:1), and 0.3 g 425-600 μm glass beads.
4. Vortex on high setting for 3-4 minutes.
5. Add 0.2 mL of Tris-EDTA pH 8.
6. Microfuge (14,000xg; 2 minutes).
7. Transfer the top, aqueous layer to a fresh 1.5 mL microfuge tube and add a 2:1 volume of 100% ethanol (about 1 mL) and gently mix by inversion.
8. Microfuge (14,000xg; 2 minutes) and decant supernatant.
9. Resuspend the pellet in 0.4 mL Tris-EDTA pH 8 and 3 μL 10 mg/mL RNase A.
10. Incubate 5 minutes at 37 °C.
11. Add 10 μL 4M ammonium acetate and 1 mL 100% cold EtOH and gently mix by inversion.
12. Microfuge (14,000xg; 2 minutes) and decant supernatant.
13. Air-dry the pellet (approximately 20 minutes; do not allow the pellet to dry completely).
14. Resuspend the pellet in 50 μL Tris-EDTA pH 8 or in 50 μL water.

4.2 Amplification of pREMI-Z Isolated From Pexophagy Mutants

1. Genomic DNA (5-10 μL) is digested in a total volume of 20 μL with EcoRI, HindIII, XbaI, SacI, or BglII (enzymes that do not cut pREMI-Z) for 20-24 hours at 37˚C.
2. Add 180 μL ddH_2O and 200 μL Phenol/Chloroform/Isoamyl alcohol (25:24:1).
3. Vortex the solution for 30 seconds, then microfuge (14,000xg; 2 minutes).

4. Remove the majority of the aqueous top phase and discard, avoiding the proteins at the aqueous:phenol interface.
5. To the aqueous phase add half a volume (200 μL) of chloroform/isoamyl alcohol.
6. Again vortex the solution for 30 seconds, then microfuge (14,000xg; 2 minutes).
7. Remove 180 μL of the top phase (aqueous layer) and transfer to a clean tube.
8. Add 20 μL of 3M sodium acetate (NaOAc) and 400 μL 100% Ethanol.
9. Place the vial for 20 minutes in the -80 ˚C freezer or in dry ice.
10. Microfuge (14,000xg; 2 minutes) and decant supernatant.
11. Wash the pellet with 0.5 mL cold 70% EtOH.
12. Microfuge (14,000xg; 2 minutes) and decant supernatant.
13. Air-dry the pellet (approximately 20 minutes; do not allow the pellet to dry completely).
14. Resuspend the pellet in 20 μL water.
15. Incubate 5 μL of digested genomic DNA in a total volume of 10 μL with T4 DNA ligase.
16. Incubate 20-24 hours at 16˚C.
17. Add 5 μL of the ligation reaction to 100 μL Rb-competent DH5α cells.
18. Place the solution on ice for 2 minutes, then 42 ˚C for 90 seconds, then ice for 2 minutes.
19. Add 0.5 mL YETM and incubate for 1 hour at 37 ˚C with gentle shaking.
20. Plate onto LB+Z.
21. Colonies are picked up and grown in liquid LB+Z
22. The pREMI-Z vector with flanking DNA is isolated using Qiagen miniprep spin columns.

4.3 Sequencing Flanking Genomic DNA

1. The Big Dye sequencing reaction is done following routine procedures (Applied Biosystems) using M13 reverse and M13 (-20) primers.
2. Sequencing is done on an Applied Biosystems (ABI) 310 Prism Capillary Electrophoresis DNA Sequencer.
3. The disrupted gene is then identified by BLAST analysis on the NCBI and *S. cerevisiae* databases.

Notes

1. In some studies, the linearized pREMI-Z is dephosphorylated with calf intestinal phosphatase prior to electroporation (Mukaiyama *et al.*, 2002).

2. The addition of a restriction enzyme during electroporation with the linearized pREMI-Z is believed to generate free chromosomal ends in the yeast genome for incorporation of the REMI-Z plasmid. However, the number of transformations was only increased two-fold when investigated in *H. polymorpha* (van Dijk *et al.*, 2001). Furthermore, doses of BamHI higher than 2 units had a detrimental affect on the efficiency of transformation. Interestingly, only thirty percent of the integrations had occurred at a BamHI site and in many cases the BamHI site was not conserved because of nucleotide loss from the pREMI-Z vector (van Dijk *et al.*, 2001). However, REMI mutagenesis reported for *C. albicans* and *S. cerevisiae* do require the addition of restriction enzymes (Schiestl and Petes, 1991; Brown *et al.*, 1996).

3. The integration of the pREMI-Z vector is stable for several generations of growth in non-selective YPD medium (van Dijk *et al.*, 2001). A majority of the integrations occur at a single site within an open reading frame that can be easily characterized. However, there are some genomic integrations that could complicate the characterization of the mutant as well as the identification of the disrupted gene. First, the pREMI-Z could insert into more than one gene.

Although we have found that this is a rare event, each disrupted gene would have to be characterized individually. Van Dijk, et al. have observed only two out of forty *H. polymorpha* transformants contained insertions into two genomic loci (van Dijk *et al.*, 2001). Second, there could be multiple insertions of the pREMI-Z vector into the same site. Although a single gene would be disrupted, the tandem insertion of pREMI-Z vectors would make it difficult to obtain any meaningful sequence data. Studies in *H. polymorpha* have shown that single copy integration occurred in 50% of the transformants, double copy integration occurred in 25% of the transformants, and 3 or more copies of pREMI-Z occurred in 25% of the transformants (van Dijk *et al.*, 2001). It appears that the pREMI-Z cassette formed multimers prior to integration since it occurred independent of the addition of restriction enzymes. Finally, the insertion could cause a genomic deletion. These can be identified by sequencing the flanking DNA isolated with the pREMI-Z vector and noting that the sequence on both sides of the pREMI-Z is not continuous. Finally, intergenic insertions are also difficult to interpret.

4. The REMI protocol has been used successfully in both *P. pastoris* and *H. polymorpha* to isolate genes (GSA, glucose-induced selective autophagy; PAZ, pexophagy zeocin-resistance; PDD, peroxisome degradation-deficient) essential for peroxisome degradation (see Table 1). The quantification of AOX activity has been the screen of choice for pexophagy mutants in *P. pastoris*. A more detailed characterization of these mutants can be done by observing the vacuole morphology labeled with FM4-64 relative to the peroxisomes labeled with BFP-SKL or GFP-SKL (Kim *et al.*, 2001; Stromhaug *et al.*, 2001; Mukaiyama *et al.*, 2002). However, a second screen has been used to identify pexophagy mutants in *H. polymorpha* (van Dijk *et al.*, 2001). This qualitative screen requires the microscopic observation of the prolonged presence of eGFP-SKL (eGFP protein which is C-terminally extended with a peroxisomal targeting signal of

serine-lysine-leucine-COOH) in cells after the shift from YNM to YND medium. The REMI protocol has also been utilized to identify mutants defective in peroxisome biogenesis (van Dijk *et al.*, 2001). In general, these mutants fail to thrive when grown on YNM plates. However, a more detailed characterization of the mutant regarding protein sorting or aberrant number or size of peroxisomes can be done by microscopic visualization of eGFP-SKL (van Dijk *et al.*, 2001).

5. Efficient lysing of the yeast is critical for accurate measurements of AOX activity. For the direct colony assay, cells were originally lysed by digestion of the cell wall with Zymolase 20T (0.25 mg/mL). However, this procedure yielded variable results and we found that liquid nitrogen freezing and thawing was more efficient. For cells in liquid suspension, the cells are lysed by vortexing in the presence of glass beads.

6. It is possible that some genomic fragments containing the pREMI-Z vector may be too large to be amplified in *E. coli*. However, we have been able to amplify vectors that are 10-12 kb. If the vectors are too large, then we suggest using a different restriction enzyme to digest the genomic DNA for recovery of the pREMI-Z. In principal, any enzyme that does not cut pREMI-Z would be appropriate.

7. The Zeocin antibiotic is sensitive to high salt concentrations. Normally, the selection of yeast that had been electroporated consists of growth on minimal medium plates (0.67% yeast nitrogen base without amino acids, 2% dextrose, 1M sorbitol, 0.4 mg/L biotin, 2% agar). However, we have found that Zeocin does not appear to be active in such medium. Therefore, we have utilized YPD plates with Zeocin. Furthermore, the selection of Zeocin-resistant *E. coli* is done in medium containing only 0.5% NaCl.

8. Restriction enzyme-mediated integration has been utilized successfully to generate mutants and identify genes essential for a number of cellular pathways in many different

organisms including: *Saccharomyces cerevisiae* (Schiestl and Petes, 1991), *Candida albicans* (Brown *et al.*, 1996), *Coprinus cinereus* (Granado *et al.*, 1997), *Lentinus edodes* (Sato *et al.*, 1998), *Gibberella fujikuroi* (Linnemannstons *et al.*, 1999), and *Aspergillus fumigatus* (Brown *et al.*, 1998)

Table 2-1: Pexophagy genes identify by REMI.

Pichia pastoris[1]	Hansenula polymorpha[2]		Characteristics	References
GSA10 PAZ1	PDD7	ATG1[3]	Serine/threonine-kinase that complexes with Atg11 and Vac8	(Stromhaug et al., 2001; Mukaiyama et al., 2002; Komduur et al., 2003)
PAZ2	HpAtg8	ATG8	Soluble protein that becomes conjugated to lipids	(Mukaiyama et al., 2004; Monastyrska et al., 2005)
PAZ3		ATG16	Component of Atg12-Atg5 complex	(Mukaiyama et al., 2002)
PAZ4		ATG26	UDP-glucose:sterol glucosyl-transferase	(Mukaiyama et al., 2002)
PAZ5		GCN3	Translation initiation factor	(Mukaiyama et al., 2002)
GSA9 PAZ6	PDD18	ATG11	Coiled-coil domain found at vacuole surface	(Kim et al., 2001; Klionsky et al., 2003)
GSA11 PAZ7		ATG2	Peripheral membrane protein that interacts with Atg9	(Stromhaug et al., 2001; Mukaiyama et al., 2002)
PAZ8		ATG4	Cysteine proteinase	(Mukaiyama et al., 2002)
GSA14 PAZ9		ATG9	Integral membrane protein associated with organelles juxtaposed to the vacuole	(Stromhaug et al., 2001; Mukaiyama et al., 2002)
PAZ10		GCN1	Regulates translation elongation	(Mukaiyama et al., 2002)
PAZ11		GCN2	Regulates translation initiation	(Mukaiyama et al., 2002)
PAZ12		ATG7	E1-like enzyme responsible for the conjugation of Atg12 to Atg5 and Atg8 to lipids	(Mukaiyama et al., 2002)
GSA19 PAZ13	PDD19	VPS15	Membrane-anchored Serine/threonine-kinase with WD40 domains	(Stromhaug et al., 2001; Mukaiyama et al., 2002)
GSA15 PAZ14		PEP4	Endopeptidase	(Mukaiyama et al., 2002)
PAZ16		ATG24	Sorting nexin with PX domain	(Ano et al., 2005)
PAZ19		GCN4	Transcriptional activator	
GSA12		ATG18	WD40 protein	(Guan et al., 2001)
GSA20		ATG3	E2-like enzyme responsible for the conjugation of Atg8 to lipids	
	PDD13	MPP1	$Zn(II)_2Cys_6$ Transcription Factor	(Leao-Helder et al., 2003)
	PDD15	ATG21	WD40 protein	(Leao-Helder et al., 2004)
	PDD20	VAM3	Vacuolar t-SNARE	

[1] GSA, glucose-induced selective autophagy; PAZ, pexophagy zeocin-resistance.
[2] PDD, peroxisome degradation-deficient.
[3] A unified gene nomenclature of autophagy and autophagy-related processes such as pexophagy has been standardized across species to be ATG (autophagy-related) for the gene names (Klionsky *et al.*, 2003).

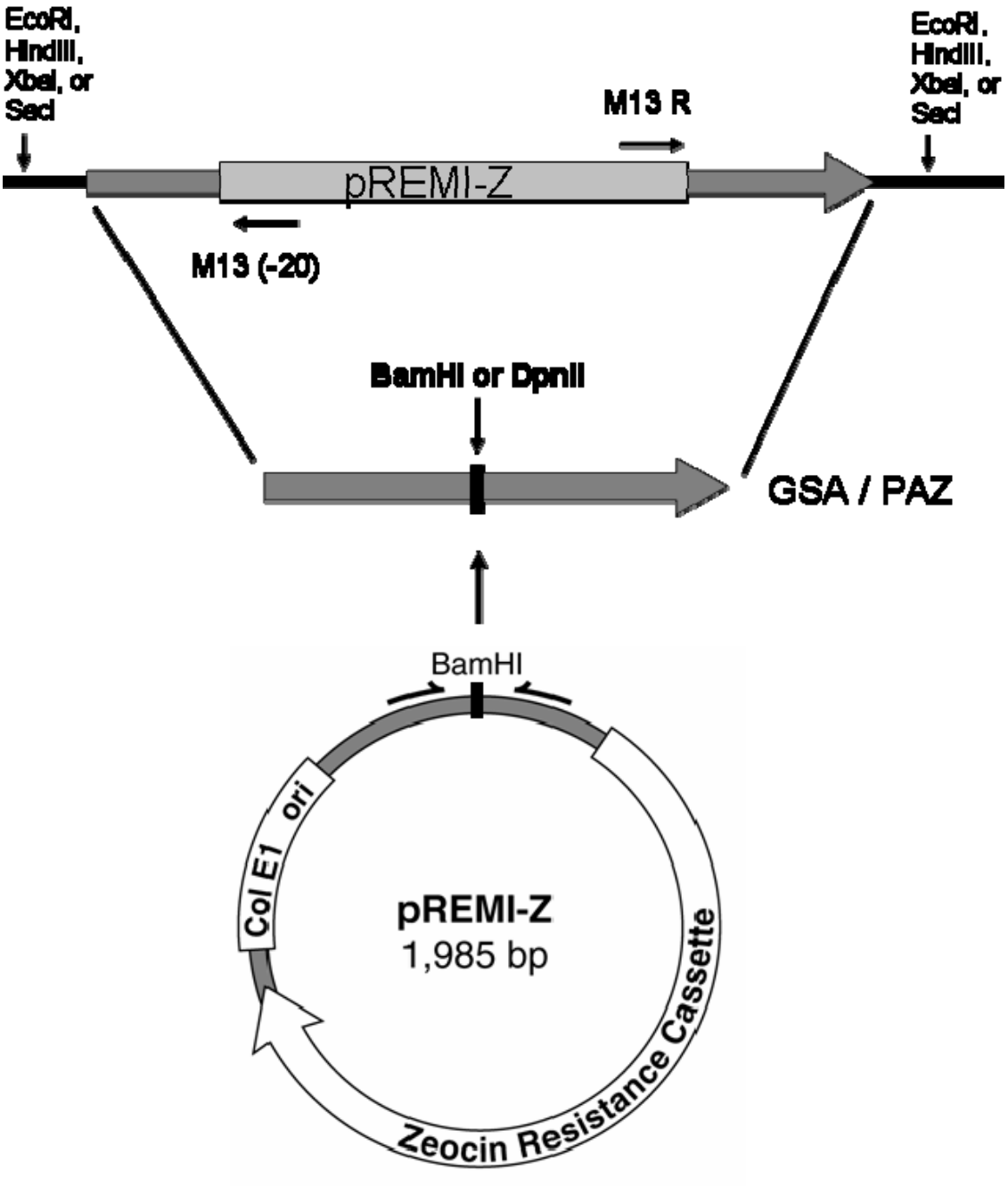

Figure 2-1: Insertional mutagenesis by restriction enzyme-mediated integration of linearized pREMI-Z. GS115 cells are transformed by the insertion of linearized pREMI-Z (NCBI accession number AF282723) into the BamHI or DpnII site of a putative GSA gene. Zeocin-resistant cells that are defective in pexophagy are isolated and the GSA/PAZ gene identified by excising the pREMI-Z and flanking genomic DNA by restriction digest.

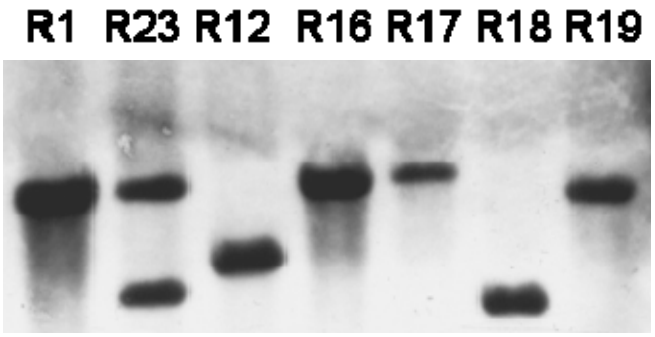

Figure 2-2: Insertion of pREMI-Z into the genomic DNA of REMI mutants as visualized on Southern blots. Genomic DNA isolated from REMI mutants was digested with EcoRI, the resulting DNA fragments separated on agarose gels, and those DNA fragments containing pREMI detected on Southern blots using biotinylated probes prepared from pREMI-Z.

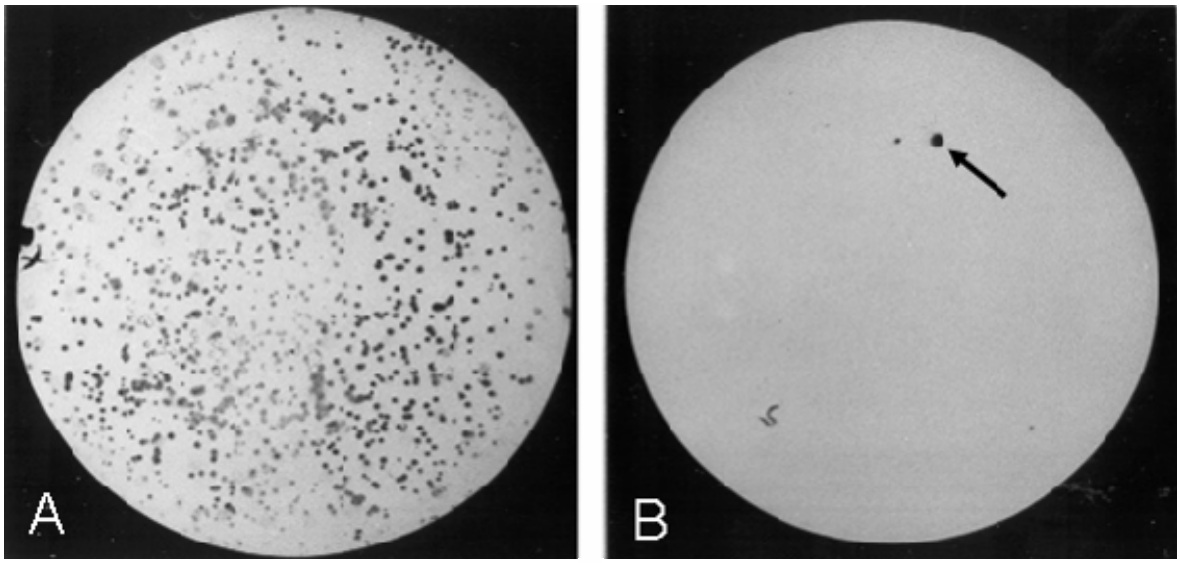

Figure 2-3: The direct colony assay of AOX activity in REMI-mutated cells grown on YNM (A) or adapted from YNM to YND (B). The arrow indicates a colony defective in degrading AOX.

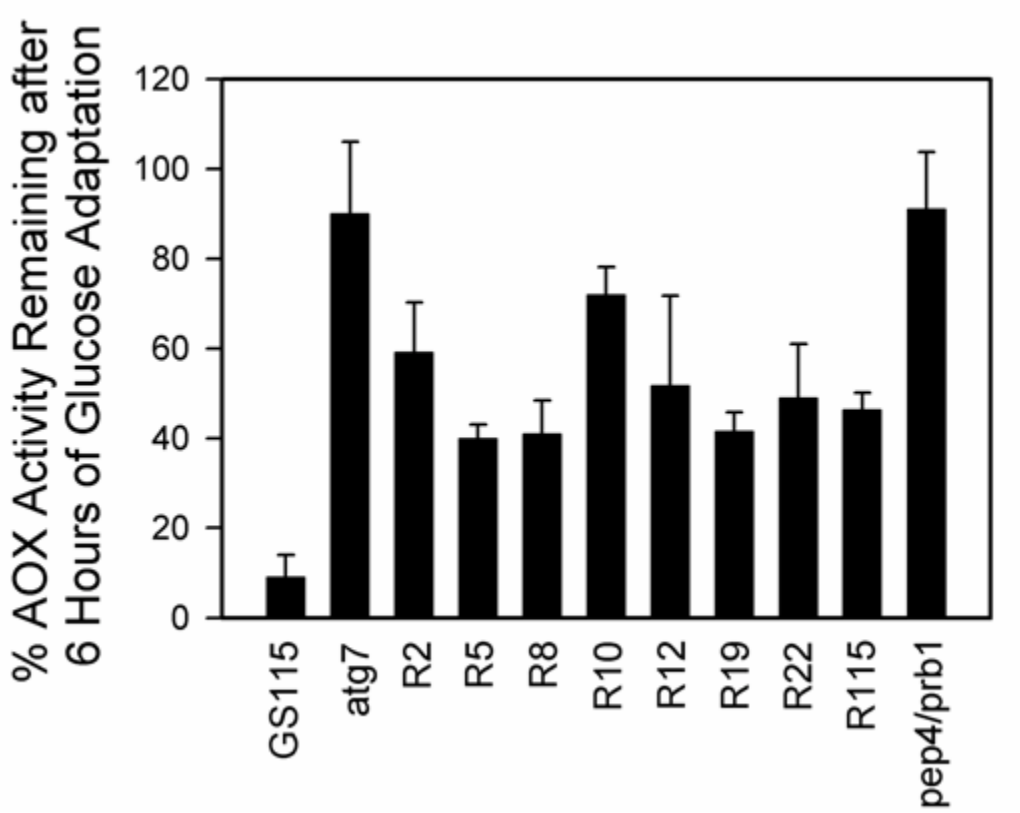

Figure 2-4: Glucose-induced degradation of AOX in REMI mutants. Parental GS115, autophagy-defective atg7 mutants, vacuole-defective pep4/prb1 mutants, and REMI mutants (R2, R5, R8, R10, R12, R19, R22, and R115), were grown in YNM medium and then switched to YND medium. At 0h and 6h, the cells were lysed and AOX activity determined. Only 10% of the AOX remained at 6h of glucose adaptation in GS115, while 90% was present in atg7 and pep4/prb1 mutants. The pexophagy defect in the REMI mutants was not as severe as that observed in the atg7 mutants with 40-70% of the AOX activity remaining.

CHAPTER 3
PPATG9 TRAFFICKING DURING PEXOPHAGY[2]

Introduction

Cellular activities are regulated and maintained as a well-controlled balance between protein synthesis and degradation of essential proteins and enzymes. Protein lifetimes can last from minutes to days with a majority of the cellular proteins being degraded in a lytic compartment such as the lysosome or vacuole. Autophagy is the primary pathway for the delivery of endogenous proteins and organelles to this compartment (Levine and Klionsky, 2004; Klionsky, 2005). There exist a number of autophagic pathways in yeast: micro- and macro-autophagy, micro- and macro-pexophagy, cytoplasm-to-vacuole targeting pathway (CVT)[3], and vacuole import and degradation pathway. The CVT pathway is constitutive while the other pathways are regulated by environmental signals. For example, autophagy is enhanced when cells are deprived of nutrients such as amino acids and glucose while pexophagy is activated when methylotrophic yeasts adapt from growth on methanol medium to growth on glucose or ethanol medium. Autophagy sequesters cytosolic proteins and organelles nonselectively while pexophagy is responsible for the selective degradation of peroxisomes. Despite their differences, these pathways share a number of common molecular events. For example, Atg7/Gsa7/Apg7, Atg1/Gsa10/Apg1/Aut3, Atg2/Gsa11/Apg2, Atg18/Gsa12/Cvt18, and Vps15 are required for

[2] Article reprinted with permission from publisher: Chang, T., L.A. Schroder, J.M. Thomson, A.S. Klocman, A.J. Tomasini, P.E. Strømhaug, and W.A. Dunn, Jr. (2005) PpATG9 encodes a novel membrane protein that traffics to vacuolar membranes which sequester peroxisomes during pexophagy in Pichia pastoris. Mol Biol Cell.16(10):4941-53.

[3] The abbreviations used are: AOX, alcohol oxidase; FM 4-64, N-(triethlyammoniumpropyl)-4-(p-diethylaminophenylhexatrienyl) pyridinium dibromide; TCA, trichloroacetic acid; GFP, green fluorescent protein; BFP, blue fluorescent protein; mRFP, monomeric red fluorescent protein; GSA, glucose-induced selective autophagy; REMI, restriction enzyme-mediated integration; CVT, cytoplasm-to-vacuole targeting; Atg9-PC, Atg9 peripheral compartment; PVS, perivacuolar structure; MIPA, micropexophagy-specific membrane apparatus; PAS, pre-autophagosome structure.

pexophagy, autophagy and CVT pathways, while Atg11/Gsa9/Cvt9 and Vac8 are essential for pexophagy and CVT pathways, but not autophagy (Stasyk *et al.*, 1999; Yuan *et al.*, 1999; Scott *et al.*, 2000; Guan *et al.*, 2001; Kim *et al.*, 2001; Stromhaug *et al.*, 2001; Stromhaug and Klionsky, 2001; Wang *et al.*, 2001; Huang and Klionsky, 2002; Abeliovich *et al.*, 2003). Since many autophagy genes and their orthologues have been identified using different yeast models, the nomenclature for these genes had become confusing. Therefore, we will utilize the ATG[4] nomenclature for those genes uniquely essential for autophagy (Klionsky *et al.*, 2003).

Pichia pastoris is able to synthesize enzymes to assimilate methanol for energy and growth. These enzymes such as alcohol oxidase (AOX) are housed primarily in the peroxisomes (Tuttle *et al.*, 1993). When these cells adapt from methanol to ethanol or glucose, the now superfluous peroxisomes are rapidly degraded by autophagic events. During ethanol adaptation, peroxisomes are individually and selectively sequestered into autophagosomes that then fuse with the vacuole. This process is called macropexophagy. A second venue for selective peroxisome degradation occurs during glucose adaptation. Micropexophagy proceeds by a mechanism whereby the vacuolar membrane invaginates, resulting in protrusions that surround and engulf the entire cluster of peroxisomes (Tuttle *et al.*, 1993; Sakai *et al.*, 1998). Both pathways result in the degradation of peroxisomes within the vacuole by proteolytic enzymes.

Pichia pastoris is a particularly good genetic model for the study of pexophagy because of its ability to rapidly and selectively degrade peroxisomes (i.e., AOX) when adapting from methanol to glucose medium. The sequestration and degradation of peroxisomes during glucose adaptation is completed within 6 h (Tuttle and Dunn, 1995). Based on the movements of the vacuole that can be easily observed by fluorescence and electron microscopy, glucose-induced

[4] We will conform to the ATG nomenclature; all the autophagy-related (ATG) genes will contain a genus and species prefix (e.g., PpAtg for the P. pastoris and ScAtg for the S. cerevisiae homologues).

micropexophagy has been described as a multistage process that includes: signaling events (vacuole round), early sequestration events (vacuole indented), intermediate sequestration events (vacuole indented with short arm-like processes), late sequestration events (vacuole indented with long arm-like processes), and vacuole degradation (vacuole with autophagic bodies) (Sakai *et al.*, 1998; Stromhaug *et al.*, 2001; Mukaiyama *et al.*, 2002). We and others have utilized genetic screens to identify a number of unique proteins required for peroxisome degradation in *Pichia pastoris* (Tuttle and Dunn, 1995; Sakai *et al.*, 1998; Stromhaug *et al.*, 2001). In order to better understand the functions of these proteins, we examined the vacuole morphology upon glucose-induced pexophagy. For example, PpVps15 (Paz13), PpAtg11 (Gsa9), and PpAtg18 (Gsa12) appear to act at early sequestration events (Stasyk *et al.*, 1999; Guan *et al.*, 2001; Mukaiyama *et al.*, 2002), PpAtg2 (Gsa11) and PpAtg7 (Gsa7/Paz12) at intermediate sequestration events (Yuan *et al.*, 1999; Stromhaug *et al.*, 2001), and PpAtg1 (Paz1/Gsa10) at late sequestration events (Mukaiyama *et al.*, 2002). Many of these proteins are structurally and functionally homologous to those proteins essential for autophagy and CVT pathways in *S. cerevisiae* (Habibzadegah-Tari and Dunn, 2003; Klionsky *et al.*, 2003). Furthermore, structural homologues of these proteins can be found in various invertebrates and vertebrates including humans (Klionsky *et al.*, 2003).

In this study, we have sequenced and characterized a unique membrane protein that is required for both pexophagy and autophagy in *P. pastoris*. Based on vacuole morphology during glucose adaptation, we project that PpAtg9 is required for an early sequestration event. In growing cells, this protein localizes to unique foci near the cell periphery. During glucose-induced pexophagy, PpAtg9 traffics from these vesicles to perivacuolar structures that appear to adjoin the vacuole and then to the sequestering membranes that arise from the vacuole. The

trafficking of PpAtg9 requires PpAtg7, PpAtg11, PpAtg2, and PpVps15, but not PpAtg1, PpAtg18, or PpVac8. Furthermore, our data suggest that the transfer of PpAtg9 to the vacuole is a prerequisite for the formation of those sequestering membranes that engulf the peroxisome for incorporation into the vacuole for degradation.

Experimental Procedures

Yeast Strains And Media

The yeast strains used in this study are listed in Table 1 and were routinely cultured at 30°C in YPD (1% Bacto yeast extract, 2% Bacto peptone, and 2% dextrose). *P. pastoris* was grown in YNM (0.67 % yeast nitrogen base, 0.4 mg/l biotin, and 0.5% methanol) to induce peroxisome biogenesis. The degradation of peroxisomes was induced when cells grown in YNM were transferred to YND (0.67 % yeast nitrogen base, 0.4 mg/L biotin, and 2% glucose) or YNE (0.67 % yeast nitrogen base, 0.4 mg/L biotin, and 0.5% ethanol). Nitrogen starvation medium contained 0.17 % yeast nitrogen base (without amino acids and NH_4SO_4) and 2% glucose. All media contained 2% agar when made as plates. Histidine or arginine or both were added at 40 μg/ml when needed. Vector amplification was done in E. coli (DH5α) cultured at 37°C in LB (0.5% Bacto yeast extract, 1% Bacto tryptone, and 1% NaCl) with ampicillin (100 μg/ml). Zeocin was added at 25 μg/ml when culturing DH5α and 100 μg/ml when culturing *P. pastoris*.

Yeast Transformation

Cells grown overnight in YPD to an optical density (OD_{600}) of 1.0 were harvested and treated with 10 mM DTT in YPD containing 25 mM HEPES, pH 8, for 15 min at 30°C. The cells were washed twice in ice-cold water and once in 1 M sorbitol and then resuspended into 1 M sorbitol. Cells (40 μl) were mixed with 0.2-1 μg of linearized vector and transferred to a 0.2 cm gap cuvette (Bio-Rad, Hercules, CA), and the DNA was introduced by electroporation at 1.5 kV,

25 μF, 400Ω (Gene Pulser, Bio-Rad Corp.). The cells transformed with vectors containing the His4 gene were transferred to plates containing 0.67% yeast nitrogen base without amino acids, 2% glucose, 1M sorbitol, 0.4 mg/L biotin, and 2% agar and incubated at 30°C for 3 - 5 d before colonies appeared. Cells transformed with vectors containing the zeocin resistance gene (zeo^R) were grown on YPD with 100 μg/ml Zeocin.

Isolation of GSA Mutants and Cloning of GSA Genes By Restriction Enzyme Mediated Integration (REMI) Mutagenesis

Mutagenesis was performed by randomly inserting the pREMI-Z vector (provided by Dr. Ben Glick, Univ. of Chicago) that contained the Zeocin resistance gene into the genome of *P. pastoris* as previously described (Stromhaug *et al.*, 2001). Those *gsa* mutants caused by disruption of gene expression were identified by direct colony assays (Stromhaug *et al.*, 2001). The site of insertion of the pREMI-Z and identification of the disrupted gene was done as described (Stromhaug *et al.*, 2001). Based on the genomic sequences around the pREMI-Z insertion site that was isolated along with the pREMI-Z vector from the R19 mutant, *GSA14* was cloned and sequenced from genomic DNA using a linker-mediated PCR method previously described (van Der Wel *et al.*, 2001). We were able to completely assemble the *GSA14* gene (NCBI accession number AY075105) and show it encodes a protein homologous to ScAtg9 of *Saccharomyces cerevisiae*, using the adapted ATG nomenclature for those genes uniquely essential for autophagy (Klionsky *et al.*, 2003). A search of the National Center for Biotechnology Information (NCBI) database revealed structural homologues of PpAtg9 and ScAtg9 in *Schizosaccharomyces pombe* (NP_596247), *Arabidopsis thaliana* (NP_180684), *Neurospora crassa* (XP_331198), *Drosophila melanogaster* (NP_611114), *Caenorhabditis elegans* (NP_503178), and *Homo sapiens* (NP_076990) (Yamada *et al.*, 2005). The alignment of these proteins reveals a large central region (190-679 residues) of homology containing at least

five putative transmembrane domains. The pREMI-Z disruption of PpAtg9 occurred after the first putative transmembrane domain at aspartic acid 245. Using this approach, we have isolated R2, R12, R13 and R22 mutants. The R2 (*his4 Ppatg18-1*::zeo^R) and R13 (*his4 Ppatg11-1*:: zeo^R) mutants have been described elsewhere (Guan *et al.*, 2001; Kim *et al.*, 2001; Stromhaug *et al.*, 2001). The R12 mutants had the pREMI-Z inserted into the *PpATG1* gene loci. The R22 (*his4 Ppatg2-2*:: zeo^R) and WDK011 (*his4 Ppatg2Δ*:: zeo^R) mutants have been characterized previously (Stromhaug *et al.*, 2001). The *Ppatg7/gsa7* mutants have been previously described (Yuan *et al.*, 1999). The null mutant of PpVps15 was provided by Dr. J. Cregg (Keck Graduate Institute) (Stasyk *et al.*, 1999). *PpVAC8* was cloned from genomic DNA using degenerate primers combined with linker-mediated PCR (van Der Wel *et al.*, 2001). The entire gene was sequenced and assembled (NCBI accession number AY886543). A *Ppvac8* null mutant was constructed by replacing the entire gene (–7 bp through 1669 bp) with the zeo^R gene driven by the TEF1 promoter. The null mutants were selected on YPD plates containing 100 μg/ml Zeocin and replica-plated to YNM plates. Null mutants were identified by direct colony assay (see below) and verified by PCR using primers flanking *PpVAC8* and within the zeo^R gene (data not shown).

Measurements Of Alcohol Oxidase (AOX) And Endogenous Protein Degradation

The direct colony and liquid medium assays to detect and measure the degradation of peroxisomal AOX was performed as previously described (Stromhaug *et al.*, 2001). Briefly, cells were grown in YNM for 40 h. At which time, glucose (2%) or ethanol (0.5%) was added. Aliquots of cells (2 ml of OD_{600} = 1.4) at 0 and 6 hours of glucose or ethanol adaptation were pelleted and resuspended in 1 ml 20 mM Tris, pH 7.5, containing 50 mM NaCl, 1 mM EDTA, 1 mM PMSF, 1 μg/ml pepstatin A, and 0.5 μg/ml leupeptin. The cells were then lysed by

vortexing in the presence of glass beads (425-600 microns). The glass beads and cellular debris were removed by centrifugation and AOX measured (Tuttle and Dunn, 1995; Yuan *et al.*, 1999). The degradation of endogenous proteins during nitrogen starvation was performed as described previously (Stromhaug *et al.*, 2001). Briefly, cellular proteins were radiolabeled with ^{14}C-valine for 16 h and the cells switched to nitrogen starvation medium containing 0.17 % yeast nitrogen base (without amino acids and NH_4SO_4) and 2% glucose and supplemented with 10 mM valine. The rates of protein degradation were calculated from the slopes of the linear plots of TCA-soluble radioactivity over 2-24 h of chase.

Western Blot Analysis

Cells (2 mls) from cultures grown to an optical density (OD_{600}) of 1.4 were collected by centrifugation and prepared for SDS-PAGE as previously described (Tuttle and Dunn, 1995). The cells were lysed in 67 mM Tris, pH 6.8, 2% SDS, 10% glycerol, 0.1% bromophenol blue, 1.5% DTT solution and 2 µl of a proteinase inhibitor cocktail (200 mM phenylmethylsulfonyl fluoride, 14.5 mM pepstatin A, 10.5 mM leupeptin in DMSO) by vortexing with glass beads. The proteins were separated by SDS-PAGE and then transferred to nitrocellulose by Trans-Blot Semi-Dry Transfer Cell (Bio-Rad Laboratories, Hercules, CA) for 1 h. The blots were blocked in 5% nonfat dried milk in PBS and then incubated with mouse anti-AOX or rabbit anti-HA antibody (Covance Inc., Princeton, NJ). Following incubation with secondary goat anti-mouse antibody conjugated with HRP (Covance Inc., Princeton, NJ), the blots were washed and HRP detected using ECL-plus (Amersham, Piscataway, NJ) and quantified using the Typhoon 9400 laser scanner (Molecular Dynamics, Sunnyvale, CA).

Construction of PpAtg Expression Vectors

The gene for the green fluorescent protein (GFP) was inserted behind the glyceraldehyde 3-phosphate dehyrogenase (GAPDH) promoter into the EcoRI site of pIB2 (Sears *et al.*, 1998).

The resulting expression vector, pPS55, was then used to construct the GFP fusion protein of PpAtg9 being expressed by the constitutive and glucose-inducible GAPDH promoter. *PpATG9* was amplified from genomic DNA by PCR with EnzyPlus™ polymerase (Enzypol, Ltd., Boulder, CO) using a forward primer of 5'-CTCTCACATTGTCGGTACCATGCATAAGAATAACACGAC-3' that contained a KpnI site. The reverse primer 5'-GTTTTGGACTCGAGGGTACTAATGCTTCATT-3' contained a XhoI site. *PpATG9* was inserted behind the *GFP* gene in pPS55. A second expression vector called pTC2 was created by inserting *PpATG9* with its endogenous promoter in front of *GFP* in pWD3 whereby *GFP* had been inserted into the SphI site of pIB1 (Sears *et al.*, 1998). *PpATG9* was amplified from genomic DNA by PCR using a forward primer 5'-GCAGGCTAGGGTACCGGTACTGGCACATT-3' that contained KpnI site and a reverse primer 5'-CAAGATCTATGCTCGAGAACAAAT AATGCCTTATGCTGTTGACTAA-3' with a XhoI site. This product was then inserted into the KpnI and XhoI sites of pWD3, the resulting fusion construct verified by sequencing, and the vector used to transform R19 (*his4 atg9*:: zeo^R) cells. pTC3 was made using *PpATG9* with a GAPDH promoter in place of the *PpATG9* endogenous promoter by amplifying it from genomic DNA using a forward primer 5'-CTCTCACATTGTCGGTACCATGCATAAGAATAACACGAC-3' containing a KpnI site and a reverse primer 5'-CAAGATCTATGCTCGAGAACAAATAATGCCTTAT GCTGTTGACTAA-3' with a XhoI site. It was inserted in front of the *GFP* gene of pWD4, which had been inserted into the SphI site of pIB2 (Sears *et al.*, 1998). Two additional expression vectors were made by inserting the *PpATG9* gene behind the *GFP* and *mRFP* genes that were inserted into the EcoRI site of pGAPZ (Invitrogen, San Diego). The gene for *mRFP* was kindly provided by Dr. R.Y. Tsein (University of California at San Diego) (Campbell *et al.*,

2002). *PpATG9* was amplified from genomic DNA using a forward primer 5'-CTCTCACATTGTCGGTACCATGCATAAGAATAACACGAC-3' containing a KpnI site and a reverse primer 5'-CATTATTATTCAAGACCGCGGAATGAAAA-3' with a SacII site. The PCR product was then cut with KpnI and SacII and inserted into pGAPz-GFP and pGAPz-RFP resulting in pWD17 and pAJM6 vectors, respectively. GFP-*Ppatg9*(ΔN) lacking the N-terminus upstream of the first transmembrane region and GFP-*Ppatg9*(ΔL3) lacking a highly conserved third loop between the 3rd and 4th transmembrane regions was constructed by PCR. A *Ppatg9* gene product lacking M1 through Y211 was amplified from genomic DNA by PCR using a forward primer 5'-CGACTATGGTACCGGAAATGGATTCAA-3' with a KpnI site and a reverse primer 5'-GTTTTGGACTCGAGGGTACTAATGCTTCATT-3' with a XhoI site. The resulting gene was inserted into the KpnI and XhoI sites of pPS55. A second *Ppatg9* gene product lacking T471 through A523 was constructed by independently amplifying the gene fragments upstream and downstream of the deletion. The upstream region of the *PpATG9* gene was amplified using a forward primer of 5'-CTCTCACATTGTCGGTACCATGCATAAGAATAACACGAC-3' that contained a KpnI site and a reverse primer of 5'-CCGCAGGATTAAGCTTAAAATCGTAAAAAA-3' containing a unique HindIII site. The dowstream region of the *PpATG9* gene was amplified using a forward primer of 5'-CTACAACGAAGCTTCTGAAGTTCATCATGT-3' containing a HindIII site and a reverse primer 5'-GTTTTGGACTCGAGGGTACTAATGCTTCATT-3' containing a XhoI site. These two fragments were digested with the appropriate restriction enzymes and ligated into the KpnI and XhoI sites of pPS55. The expression vector, pWD21, contained PpAtg8 with a GFP at its N-terminus. PpAtg8 was amplified from genomic DNA by PCR using a forward primer of 5'-CCATGAATCCATGCGATCGCAATTTAAAGACGAACA-3' containing an

EcoRI site and a reverse primer of 5'-GGCACTACTCGAGTTATTATTCAATCTCCTCAACACCTGGAA-3' containing a XhoI site. PpAtg8 was inserted behind the *GFP* gene in pPS55. The final expression vector, pASK1, contained PpAtg9 with an HA tag at its N-terminus driven by the endogenous promoter of *PpATG9*. This construct was made by PCR of the *PpATG9* promoter and open reading frame separately, which was then followed by a PCR amplification of the entire gene including promoter. The promoter was amplified using a forward primer of 5'-GCAGGCTAGGGTACCGGTACTGGCACATT-3' containing a KpnI site and a reverse primer of 5'-GCGTAATCTGGAACATCGTATGGATACATTCAATCGAC AATGTGAGAGATTCAGTGAAG-3' containing the HA tag. The open reading frame was amplified using a forward primer of 5'-TGTATCCATACGATGTTCCAGATTACGCGATGCATAAGAATAACACGACATTTTTATCC-3' containing an HA tag (MYPYDVPDYA) insertion in front of the PpAtg9 start codon and a reverse primer of 5'-GTCAGACTCCAAACTCGAGTTCATTTTCAA-3' containing a XhoI site. Finally, the entire gene with promoter was amplified from the above products by PCR using forward 5'-GCAGGCTAGGGTACCGGTACTGGCACATT-3' and reverse 5'-GTCAGACTCCAAACTCGAGTTCATTTTCAA-3' primers. The resulting product was cut with KpnI and XhoI and inserted into pIB1. The CoxIV signal sequence plus the upstream ADH1 promoter was excised from pCC4 by cutting with EcoRV and XbaI (Campbell and Thorsness, 1998). The fragment was then inserted into the SmaI and SpeI sites upstream of the *GFP* gene of pWD3, which had been constructed by inserting the *GFP* gene into the SphI site of pIB3 (Sears *et al.*, 1998). The resulting expression vector, pAJM3, produced a GFP protein that was targeted to the mitochondria. The construction of pPS55-G12, pPS64, and pPS69 vectors

have been previously described (Guan *et al.*, 2001; Kim *et al.*, 2001; Stromhaug *et al.*, 2001) and pPOP-S7-GFPX3, pPOP-SEC13-GFP, and pIB2-DsRED-HDEL were provided by Dr. Ben Glick (Univ. of Chicago) (Bevis *et al.*, 2002). For transformation, these vectors were first linearized by cutting either within the HIS4 gene with StuI or SalI or within the *PpATG9* gene with SacI.

Fluorescence Microscopy And FM 4-64 Labeling

Cells expressing GFP or RFP fusion proteins were grown in either YPD for 24 h or YNM for 20 h. Cells grown on YNM medium were then transferred to YND or YNE for 1 to 4 h. FM 4-64 (Molecular Probes, Eugene, OR) was added to a final concentration of 20 μg/ml and the cells incubated for 2-12 h. The cells were washed of unbound FM 4-64 and examined immediately using a Zeiss Axiophot fluorescence microscope. Image capture was done using SPOT camera (Diagnostics Instruments, Inc., Sterling Heights, MI) interfaced with IP Lab software.

Electron Microscopy

The cellular ultrastructure of *Ppatg9* mutants was examined as previously described (Tuttle and Dunn, 1995). Briefly, cells grown in YNM or grown in YNM and adapted to YND or YNE were harvested by centrifugation, washed in water, and fixed in 1.5% $KMnO_4$ in veronal-acetate buffer (28 mM sodium acetate, 28 mM sodium barbital, pH 7.6) for 20 min at 22° C (Veenhuis *et al.*, 1983). The specimens were dehydrated with increasing concentrations of ethanol and infiltrated with POLY/BED 812 (Polysciences, Inc., Warrington, PA) with accelerator 2,4,6-Tri(dimethylaminomethyl) phenol (DMP-30, Polysciences, Inc.) for 2 d at 22° C under vacuum. After polymerization of the resin, the samples were sectioned and examined using a JEOL 100CX transmission electron microscope.

Results

Ppatg9 Mutants Are Defective In Glucose-Induced Pexophagy And Starvation-Induced Autophagy

Pichia pastoris can assimilate methanol for growth by synthesizing peroxisomal enzymes such as alcohol oxidase (AOX). When these cells are switched from a medium containing methanol to one containing glucose, the peroxisomes are selectively sequestered by the vacuole for degradation by a process called micropexophagy (Tuttle and Dunn, 1995). In order to identify the molecular components of this degradative process, we developed a novel approach whereby genes can be randomly mutagenized *in vivo* by the integration of a vector containing a zeo^R gene, pREMI-Z. Those Zeocin resistant cells that were unable to degrade AOX during glucose adaptation were identified by direct colony assay and verified by liquid medium assay (see Materials and Methods). Using this approach, we have isolated a number of mutant strains based on their poor ability to degrade AOX during glucose adaptation. The gene mutated by the insertion of the pREMI-Z was sequenced and identified in each of our mutants (see Table 3-1). We then compared the inability of these mutants to degrade peroxisomes to parental GS115 and to vacuole defective mutants that lack proteinases A (pep4) and B (prb1) (Figure 3-1A). Within 6 h of glucose adaptation, over 90% of the AOX was degraded by the GS115 cells. In comparison, only 10% of the AOX was degraded in mutants lacking proteinases A and B. Less than 60% of the AOX was degraded in R19 cells that contained a pREMI-Z insertion within the open reading frame of the *PpATG9* gene. AOX degradation in these R19 cells was comparable to that observed for *Ppatg1*, *Ppatg2*, and *Ppatg11* mutants, but higher than the 10-30% degraded by *Ppatg7*, *Ppatg18*, *Ppvps15* or *Ppvac8* mutants. Next, we examined the ability of R19 cells to degrade AOX during ethanol adaptation (Figure 3-1B). We observed on Western blots a substantial loss of AOX protein when GS115 cells adapt from methanol to ethanol medium.

However, no loss of AOX was detected in R19 cells over 24 h suggesting that macropexophagy was suppressed in the cells lacking PpAtg9.

Our previous studies have shown that a number of those REMI mutants defective in pexophagy were also defective in nitrogen starvation-enhanced proteolysis (Yuan *et al.*, 1999; Guan *et al.*, 2001; Stromhaug *et al.*, 2001). Therefore, we next quantified protein degradation in R19 starved for amino acids (Figure 3-1C). When GS115 parental cells are starved for nitrogen and amino acids, the cellular protein was degraded at a rate of 0.36 percent per hour. The rate of protein degradation in starved cells was significantly lower in cells lacking proteinases A and B consistent with this degradation being mediated by the vacuole. In cells lacking PpAtg11 or Vac8, cellular protein degradation was 70-90% of control suggesting these proteins have a minimal role in starvation-induced autophagy. To the contrary, we determined that the degradation of cellular proteins was reduced by 60% in *Ppatg9* cells starved for amino acids and nitrogen. This value was comparable to the rates of degradation observed in *Ppatg1*, *Ppatg2*, *Ppatg7*, *Ppatg18* and *Ppvps15* mutants.

Ppatg9 Is Essential For A Sequestration Event In Pexophagy

We have shown that during glucose-induced micropexophagy the vacuole indents while sequestering membranes encircle multiple peroxisomes (Tuttle and Dunn, 1995). The sequestering membranes are labeled with FM 4-64, a dye that selectively labels vacuole membranes, suggesting that they likely form from the vacuole. A micropexophagic membrane apparatus (MIPA) containing PpAtg8 forms near the tips of the sequestering membranes. The MIPA is thought to assist in the fusion of the sequestering membranes, thereby incorporating the peroxisomes into the vacuole for degradation. During ethanol-induced macropexophagy, individual peroxisomes are selectively incorporated into pexophagosomes whose membranes contain PpAtg8. The pexophagosome then fuses with the vacuole and its contents degraded. In

order to better assess the site of blockage of pexophagy in the R19 cells, we examined the formation of the sequestering membranes and the MIPA during micropexophagy and of the pexophagosome during macropexophagy. GS115 (Figure 3-2, A,C) and R19 (Figure 2, E, G, I, K) cells were grown in methanol-enriched YNM medium and then adapted to glucose-enriched YND (Figure 3-2, E, I) or ethanol-enriched YNE (Figure 3-2, G, K) medium. Cells were harvested at 3 h, fixed in potassium permanganate, and prepared for electron microscopy. During glucose adaptation, profiles of peroxisomes engulfed by the vacuole were routinely observed in GS115 cells (Figure 2A). However, when R19 cells were adapted to glucose, the sequestering membranes appear to be absent, but instead the vacuole appeared only slightly indented (Figure 3-2E) with an occasional short arm-like projection (Figure 3-2I). Similar vacuole morphology has been reported for *Ppatg11*, *Ppatg18* and *Ppvps15* mutants (Stasyk *et al.*, 1999; Guan *et al.*, 2001; Kim *et al.*, 2001)]. Next, we examined whether the MIPA was forming in R19 cells. WDY70 cells expressing BFP-SKL and GFP-PpAtg8 were adapted from YNM to YND for 2 h. At this time, PpAtg8 was localized to the MIPA and foci adjacent to the peroxisomes (Figure 3-2B). In the absence of PpAtg9, the MIPA was absent and PpAtg8 localized solely to foci (Figure 3-2, F, J). During ethanol adaptation, peroxisomes within pexophagosomes were observed by electron (Figure 3-2C) and fluorescence (Figure 3-2D) microscopy. In WDY70 cells, the PpAtg8 was localized almost exclusively to pexophagosomes (Figure 3-2D). Pexophagosomes were absent in cells lacking PpAtg9 (Figure 3-2, G, H, K, L), and PpAtg8 was localized to multiple foci that appear within and about the peroxisome cluster (Figure 3-2, H, L). The data demonstrate that PpAtg9 is essential for the formation of sequestering membranes that arise from the vacuole and the assembly of the MIPA during micropexophagy and of the pexophagosome during macropexophagy.

Cellular Localization Of Ppatg9 In Growing Cells

Next, we examined the cellular distribution of PpAtg9 in cells grown in glucose medium. This was done by constructing the following expression vectors: GFP-PpAtg9 behind the GAPDH promoter in pIB2 (pTC1), PpAtg9-GFP behind the endogenous PpAtg9 promoter (pTC2), GFP-PpAtg9 behind the GAPDH promoter in pGAPz (pWD17), and mRFP-PpAtg9 behind the GAPDH promoter in pGAPz (pAJM6). PpAtg9-GFP (data not shown), GFP-PpAtg9 (see Figure 3-8) and mRFP-PpAtg9 (see Figure 3-8) were functional as determined by their ability to rescue R19 cells. When these cells were grown in YPD, GFP-PpAtg9 (Figure 3-3A) localized to one or more foci or structures distributed about the cell periphery. In order to better define the nature of these structures, we co-expressed GFP-PpAtg9 with DsRed-HDEL and mRFP-PpAtg9 with CoxIV-GFP in GS115 cells. Some structures containing GFP-PpAtg9 appeared to be in close association with endoplasmic reticulum identified by DsRed-HDEL (Figure 3-3C, arrow) and mitochondria identified by CoxIV-GFP (Figure 3-3D arrow). We next examined whether these structures contained Sec13 (intermediate compartment) or Sec7 (Golgi apparatus) by co-expressing mRFP-PpAtg9 with Sec13-GFP and Sec7-GFPx3. The results demonstrate that PpAtg9 does not co-localize with either Sec13 (Figure 3-3E) or Sec7 (Figure 3-3F). In *S. cerevisiae*, the peripheral vesicles containing ScAtg9 do not colocalize with any defined organelle markers for the Golgi apparatus, endosomes, or the endoplasmic reticulum (Noda *et al.*, 2000; Kim *et al.*, 2002; Reggiori *et al.*, 2004). Therefore, we will refer to these unique peripheral structures collectively as the Atg9 peripheral compartment (Atg9-PC).

Cellular Trafficking Of Ppatg9 During Glucose-Induced Pexophagy

The trafficking of PpAtg9 during glucose-induced pexophagy was visualized in TC3 cells expressing BFP-SKL behind the AOX promoter and GFP-PpAtg9 behind the GAPDH promoter (Figure 3-4). When TC3 cells were grown in YNM, GFP-PpAtg9 localized to one or more

structures, described above as the Atg9-PC (Figure 3-4A). Upon adapting these cells from YNM to YND for 3 h, GFP-PpAtg9 localized to multiple structures of differing sizes and shapes that were positioned at the vacuole surface labeled with FM 4-64 and to the sequestering membranes that could be seen flanking the peroxisomes labeled with BFP-SKL (Figure 3-4). We refer these structures that appear as dots and patches as perivacuolar structures (PVS). The PVS were routinely observed near those sites where the sequestering membranes joined the vacuole suggesting they may function in the formation of these membranes from the vacuole. Indeed, the sequestering membranes contained both PpAtg11 and PpAtg18 present at the vacuole membrane and stain with FM 4-64 suggesting that they originated from the vacuole (Guan *et al.*, 2001; Kim *et al.*, 2001). These results were not due to overexpression of GFP-PpAtg9 that may be caused by the GAPDH promoter, since PpAtg9-GFP whose expression is regulated by the endogenous PpAtg9 promoter in TC14 cells showed a similar distribution but weaker signal (data not shown). In a given population of cells, the onset of micropexophagy is variable resulting in cells at differing stages of micropexophagy. Nevertheless, we have presented a time course based on images obtained from 0-2h of glucose adaptation that best illustrates our understanding of PpAtg9 trafficking (Figure 3-4C). We show that during glucose-induced pexophagy, PpAtg9 traffics from the Atg9-PC (arrowheads) to the PVS (arrows) and then to the vacuole membrane and those sequestering membranes (double arrowheads) that engulf the peroxisomes for degradation within the vacuole.

We next examined the expression of PpAtg9 in cells during glucose-induced micropexophagy. This was done by constructing a PpAtg9 protein tagged at the N-terminus with an HA epitope. This construct along with the PpAtg9 promoter of about 400 bp upstream of the start codon was inserted into the pIB1 vector (Sears *et al.*, 1998). The resulting vector was used

to transform GS115 cells and the expression evaluated on Western blots using antibodies that recognized the HA tag. A single protein around 100 kDa was detected in cells expressing HA-PpAtg9. This protein was absent in extracts of GS115 cells that were not transformed (data not shown). At 4-6 h of glucose-induced pexophagy, the cellular levels of HA-PpAtg9 increased over two-fold relative to zero hour (Figure3- 4D). Over the next 2 h, the cellular levels of HA-PpAtg9 diminished. Similar results were observed when HA-PpAtg9 was expressed in R19 cells (data not shown).

Cellular Trafficking Of Ppatg9 During Glucose-Induced Pexophagy Requires Other Ppatg Proteins

Many Atg proteins interact with each other, thereby influencing function and trafficking (Wang and Klionsky, 2003; Reggiori *et al.*, 2004). In fact, the trafficking of ScAtg9 appears to be regulated by a number of ScAtg proteins including ScAtg1 and ScAtg18 (Reggiori *et al.*, 2004). Therefore, we investigated whether other PpAtg proteins were required for the trafficking of PpAtg9 from the Atg9-PC to the PVS and sequestering membranes. We examined the trafficking of GFP- PpAtg9 during glucose-induced pexophagy in mutants defective in early (*Ppatg11*, *Ppatg18* and *Ppvps15Δ*), intermediate (*Ppatg2* and *Ppatg7*), and late (*Ppatg1* and *Ppvac8Δ*) sequestration events. These mutants were transformed by electroporation with pTC1 and GFP-PpAtg9 expression verified by Western blotting and fluorescence microscopy. When the resulting transformants were grown in YNM, GFP-PpAtg9 was found almost exclusively at the Atg9-PC (data not shown). After growth in YNM, the mutants expressing GFP-PpAtg9 were then adapted to glucose for 3 h. In *Ppatg11*, *Ppatg18* and *Ppvps15Δ* mutants, the vacuoles were predominantly round with a slight indentation and no arm-like extensions were evident (Figure 5). GFP-PpAtg9 expressed in *Ppatg11* and *Ppvps15Δ* cells was found predominantly at peripheral foci (Figure 5). In addition, the vacuole membrane was void of GFP-PpAtg9 in these

mutants. In *Ppatg18* cells, GFP-PpAtg9 localized to the PVS and to the vacuole membrane (Figure 3-5). The vacuoles in *Ppatg7* and *Ppatg2* mutants were indented with short extensions (Figure 3-6). In these cells, GFP-PpAtg9 was found in peripheral structures (arrowheads) and the PVS (arrows) located either at the vacuole or at the site where the sequestering membranes join the vacuole (Figure 3-6). Although the location of the PVS appeared unaltered, the PVS morphology appeared to be smaller and less diffuse in these mutants than that observed in control TC3 cells (see Figure 3-4). Furthermore, GFP-PpAtg9 was not detected at the sequestering or vacuole membranes. During micropexophagy, the vacuoles in *Ppatg1* and *Ppvac8Δ* mutants contained an extensive segmented array of sequestering membranes that extended from the vacuole to almost completely surround the peroxisome cluster (Figure 3-7). GFP-PpAtg9 was found at the PVS and sequestering membranes (Figure 3-7).

Domains Of Ppatg9 Required For Function And Trafficking

We have demonstrated that PpAtg9 traffics from the Atg9-PC to the PVS where it appears to function in the formation of the sequestering membranes. In order to define those domains that are essential for PpAtg9 function, we have characterized the function and trafficking of PpAtg9 mutants lacking specific peptide regions. We first deleted the N-terminus (M1-Y221), a region of low homology when compared to its *S. cerevisiae* counterpart. Unlike wild-type GFP-PpAtg9, GFP-Ppatg9ΔN only partially rescued R19, suggesting this protein has limited function for glucose-induced micropexophagy (Figure 3-8A). However, during glucose adaptation, GFP-Ppatg9ΔN could be observed at the Atg9-PC (Figure 3-8B, arrowheads), PVS (Figure 3-8B, arrows) and vacuolar membranes suggesting that the N-terminus is not essential for PpAtg9 trafficking. Next, we deleted a highly conserved loop (T471 - A523) between two putative transmembrane domains. As seen for Ppatg9ΔN, Ppatg9ΔL3 was also unable to

efficiently rescue the R19 phenotype (Figure 3-8A). However, unlike Ppatg9ΔN, Ppatg9ΔL3 was not present at the Atg9-PC, PVS or vacuole membrane but to a compartment morphologically similar to the endoplasmic reticulum (Figure 3-8C, large arrows). The data suggest that loop T471 - A523 is essential for trafficking of PpAtg9 to the Atg9-PC.

Perivacuolar Structures Contain Ppatg9 And Ppatg11, But Not Ppatg2

We have previously shown that Atg2 becomes associated with peripheral structures during pexophagy and that this association requires PpAtg9 (Stromhaug *et al.*, 2001). In addition, we have reported that PpAtg11 localizes to the vacuole membrane and to one or more structures associated with either the vacuole or the arm-like extensions that surround the peroxisomes (Kim *et al.*, 2001). In this study, we have shown that the trafficking of PpAtg9 requires PpAtg2 and PpAtg11. Therefore, we compared the localization of mRFP-PpAtg9 with PpAtg2-GFP and PpAtg11-GFP in cells adapting from YNM to YND (Figure 3-9). We first compared the localization of mRFP-PpAtg9 with PpAtg18-GFP, which we have previously shown to be present at the vacuole and sequestering membranes. In cells undergoing micropexophagy, mRFP-PpAtg9 was present in the Atg9-PC and at the PVC localized at sites where the sequestering membranes appear to extend from the vacuole (Figure 9, arrows). Unlike GFP-PpAtg9, mRFP-PpAtg9 was not present at the vacuole membrane, but instead was present within the vacuole that was delineated by PpAtg18-GFP and PpAtg11-GFP. One possible explanation is that the mRFP at the N-terminus of PpAtg9 is exposed to vacuolar enzymes and proteolytically removed from PpAtg9. However, the accumulation of mRFP within the vacuole persisted in cells lacking Pep4 or Prb1 (Tomasini and Dunn, unpublished observations). The data reveal that PpAtg2 does not colocalize with the Atg9-PC nor the PVS. However, some of the PpAtg2 vesicles can be found in close proximity to the PVS (see Fig. 3-9 arrows). PpAtg11

localized to the vacuole membrane and the PVS containing PpAtg9 (Figure 3-9, arrows), but did not colocalize with the peripheral structures of PpAtg9 (Figure 3-9, arrowhead). The data suggest that the Atg9-PC does not contain PpAtg2 and that the peripheral compartment of PpAtg2 may be unique. Furthermore, we have shown that the PVS contains PpAtg9 and PpAtg11 but not PpAtg2 or PpAtg18.

Ppatg9 Does Not Localize To MIPA or The Pexophagosome

Finally, we examined whether mRFP-PpAtg9 colocalized with GFP-PpAtg8 at the MIPA, at the pexophagosomes, or at the perivacuolar foci referred to as pre-autophagosome structures (PAS) in *S. cerevisiae*. During glucose-induced micropexophagy, PpAtg8 was present at perivacuolar foci and at the MIPA (arrowheads) which did not contain PpAtg9 (Figure 3-10A). During ethanol-induced macropexophagy, PpAtg8 was found at perivacuolar foci and at the pexophagosome (arrowheads), while PpAtg9 localized to the Atg9-PC (small arrow) and the PVS (large arrow) (Figure 3-10B). PpAtg9 did not colocalize with PpAtg8 and was absent from the pexophagosome. To the contrary, PpAtg8 was not present at the Atg9-PC (Figure 3-10B, small arrow) or at the PVS (Figure 3-10, large arrows). The data suggest that PpAtg9 is not a component of the MIPA or the pexophagosome and that the PVS lacks PpAtg8.

Discussion

Autophagy is an avenue for the degradation of proteins and organelles. This process is critical for cell survival during times of nutrient deprivation. Twenty-seven autophagy genes (ATG) have been identified using yeast models of autophagy (Klionsky *et al.*, 2003). One such model is *Pichia pastoris* in which we can follow the molecular events required for the selective sequestration and vacuolar degradation of peroxisomes by a process called pexophagy. When cells adapt from growth in methanol to glucose, the cells respond by activating the degradation of peroxisomes by pexophagy. During glucose-induced pexophagy, sequestering arms extend

from the vacuole to engulf multiple peroxisomes. Upon homotypic membrane fusion of the arms, the peroxisomes are incorporated into autophagic bodies within the vacuole where they are degraded. We have previously shown that PpAtg2 (Gsa11), PpAtg7 (Gsa7), PpAtg11 (Gsa9), and PpAtg18 (Gsa12) are required for the sequestration events of micropexophagy (Yuan *et al.*, 1999; Guan *et al.*, 2001; Kim *et al.*, 2001; Stromhaug *et al.*, 2001). In this study, we show that PpAtg9 is required for an early sequestration event in micropexophagy, possibly the initial formation of the sequestration membranes that extend from the vacuole. In addition, the assembly of MIPA during micropexophagy and the formation of the pexophagosome during macropexophagy does not occur in cells lacking PpAtg9. PpAtg9 is an integral membrane protein with five possible transmembrane domains that traffics to the vacuole membrane becoming a component of the sequestration membranes that appear to arise from the vacuole. PpAtg9 is not essential for cell viability, but appears to be structurally conserved throughout a number of plant, fungi, insect, and mammalian species. PpAtg9 is also necessary for starvation-induced nonselective autophagy in *P. pastoris*, *S. cerevisiae*, and *Arabidopsis thaliana*, and for the trafficking of Ape1 to the vacuole in *S. cerevisiae* (Noda *et al.*, 2000; Hanaoka *et al.*, 2002).

In *S. cerevisiae*, ScAtg9 resides in two populations of vesicles, one at the cell periphery and a second found adjacent to the vacuole. These vesicles distribute as a single peak on sucrose gradients which can be resolved from the vacuole (Pho8), plasma membrane (Pma1), Golgi apparatus (Kex2), endoplasmic reticulum (Sec12), and endosomes (Pep12) (Noda *et al.*, 2000). In addition, our results suggest that those vesicles adjacent to the vacuole are not the prevacuolar compartment (Noda *et al.*, 2000). The pre-autophagosome structure (PAS) appears as a single structure located at the vacuolar surface and is composed of a number of proteins such as ScAtg2 (Apg2), ScAtg8 (Aut7), ScAtg9 (Apg9), ScAtg11 (Cvt9), ScAtg17 (Apg17), ScAtg18 (Cvt18),

ScAtg20 (Cvt20), and ScAtg24 (Cvt13) (Suzuki *et al.*, 2001; Huang and Klionsky, 2002; Kim *et al.*, 2002; Nice *et al.*, 2002; Reggiori *et al.*, 2004). The PAS is thought to be responsible for organizing the formation of the autophagosome and transferring ScAtg8 to the autophagosome membrane. However, the appearance of these structures does not change when cells are starved for amino acids, and other components of the PAS such as ScAtg9 do not appear to associate with autophagosomes (Noda *et al.*, 2000; Kim *et al.*, 2002). Those ScAtg9 vesicles not adjacent to the vacuole but more at the cell periphery differ from the PAS in that they do not contain ScAtg8 (Kim *et al.*, 2002; Tucker *et al.*, 2003). In *S. cerevisiae*, ScAtg9 appears to recycle between the peripheral vesicles and the PAS. Furthermore, the movements of ScAtg9 from the PAS to the peripheral vesicles require ScAtg1 independent of its kinase activity, ScAtg2, ScAtg18 and the PtdIns 3-kinase complex I which includes ScVps34, ScVps15, and ScAtg14 (Reggiori *et al.*, 2004).

In Figure 3-11, we have presented a working model for the trafficking of PpAtg9 during glucose-induced pexophagy. In growing cells, PpAtg9 resides in the Atg9 peripheral compartment (Atg9-PC) that consists of one or more structures distributed near the cell periphery. These structures are neither intermediate vesicles nor the Golgi apparatus since they lack PpSec13 and PpSec7, respectively. However, they occasionally contain the endoplasmic reticulum marker, mRFP-HDEL, while others are in close association with the endoplasmic reticulum suggesting these structures may be a subcompartment of the endoplasmic reticulum. Furthermore, Ppatg9ΔL3 is not present at the Atg9-PC, but appears to be associated with the endoplasmic reticulum. However, additional studies are needed to substantiate the relationship between the endoplasmic reticulum and the Atg9-PC. ScAtg9 appears to recycle between the peripheral compartment and the PAS (Reggiori *et al.*, 2004). Such recycling was not detected in

P. pastoris, although we have not analyzed this under the same conditions defined in *S. cerevisiae*. We have also shown that the PpAtg9-PC is sometimes associated with mitochondria. However, the functional significance of this location remains unclear. Nevertheless, based on our findings and those from *S. cerevisiae*, we suggest that the peripheral vesicles containing PpAtg9 are a unique compartment. Upon the onset of glucose-induced pexophagy, PpAtg9 is recruited from the Atg9-PC to two or more perivacuolar structures (PVS) and then to those membranes that sequester the peroxisomes. The PVS is in many ways similar to the PAS defined in *S. cerevisiae*. For example, both contain PpAtg9 and PpAtg11 (see Fig. 3-10). Ano et al. have shown that similar perivacuolar spots contain PpAtg24 (Ano *et al.*, 2005). Both PVS and PAS are located at the vacuole and appear to be essential for organizing the formation of sequestering membranes. However, the PVS does not contain PpAtg2 or PpAtg8 and appears to be structurally different from the PAS. There exist multiple foci of PVS of differing sizes situated about the vacuole and the sequestering membranes while the PAS usually consists of a single, well-defined structure at the vacuole. PpAtg17, a component of the PAS in *S. cerevisiae*, resides in a single structure juxtaposed to the vacuole (Ano *et al.*, 2005). PpAtg24 colocalizes with PpAtg17 but is also found at multiple other perivacuolar structures (Ano *et al.*, 2005). PAS has been implicated in the formation of the autophagosome from membranes of unknown origin, but its function remains unclear (Suzuki *et al.*, 2001). We have demonstrated that the PVS is situated at sites where the sequestering membranes appear to form from the vacuole and that PpAtg9 is transported from the PVS to those sequestering membranes that engulf the peroxisomes. Therefore, we project that PVS may act as the site of assembly in the formation of the sequestering membranes that appear to originate from the vacuole because they stain with FM 4-64. It is unclear how these membranes are formed. Mukaiyama et al., suggest these

membranes form by a "septation" of the vacuole (Mukaiyama *et al.*, 2002). Our data suggest that the formation of these membranes requires protein synthesis and both PpAtg9 and PpAtg18. We have previously shown that these membranes do not form in the presence of cycloheximide (Tuttle and Dunn, 1995). In this study, we show that the cellular levels of PpAtg9 are increased during pexophagy suggesting a role for protein synthesis. In addition, we have demonstrated that when PpAtg9 is absent or does not traffic to the PVS, the vacuole arms are either not present or short. Conversely, when PpAtg9 localizes to the PVS and the vacuole membrane but PpAtg18 is missing, the vacuole arms are absent. Furthermore, we have shown that PpAtg9 lacking its N-terminus is sorted to the PVS, but the peroxisomes are not sequestered or degraded. This suggests that there exists a region within the N-terminus of PpAtg9 that is essential for its function once it arrives at the PVS. This domain and its function have yet to be defined and are currently under investigation.

We have shown that PpAtg11 and PpVps15, but not PpAtg18, PpAtg2, PpAtg7, PpAtg1, or PpVac8, are essential to recruit PpAtg9 to the PVS. In *S. cerevisiae*, the overexpression of ScAtg11 appears to enhance the recruitment of ScAtg9 to the PAS (Kim *et al.*, 2002). In cells lacking ScAtg1, ScAtg2, ScAtg14, or ScAtg18, ScAtg9 is found predominantly at the PAS either because trafficking to the PAS is enhanced or recycling to the peripheral vesicles is suppressed (Reggiori *et al.*, 2004). ScAtg11 and ScAtg18 are present at the PAS and vacuole surface, but the localization of ScVps15 has not yet been determined (Guan *et al.*, 2001; Kim *et al.*, 2001). From the PVS, PpAtg9 is transferred to the membranes of the vacuole and those sequestering membranes that extend from the vacuole. The apparent movement of PpAtg9 from the PVS to the sequestering membranes requires PpAtg2 and PpAtg7, but not PpAtg18, PpAtg1 or PpVac8. We have previously shown that during pexophagy PpAtg2 becomes associated with foci of

unknown origin (Stromhaug *et al.*, 2001). In this study, we show that these structures are situated juxtaposed to the PVS. The homotypic fusion of the sequestering membranes and formation of the autophagic body within the vacuole completes the sequestration of the peroxisomes. A membrane sac called MIPA (micropexophagy-specific membrane apparatus), which contains PpAtg8 and PpAtg26, forms between the tips of the sequestering membranes to presumably direct membrane fusion (Oku *et al.*, 2003; Mukaiyama *et al.*, 2004). In addition to PpAtg8 and PpAtg26, the assembly of MIPA requires the lipidation of PpAtg8, which is mediated by PpAtg3, PpAtg4, and PpAtg7. We show here that the assembly of MIPA also requires PpAtg9. However, it is unclear whether PpAtg9 has a direct role in MIPA formation or if the assembly of MIPA requires the presence of the sequestering membranes. Our data suggest that late sequestration or fusion events require PpAtg1, a serine-threonine protein kinase, and PpVac8, an Armadillo-repeat protein structurally homologous to ScVac8 that when anchored to the vacuole membrane by palmitoylation will promote homotypic vacuole fusion (Wang *et al.*, 1998). PpAtg24 is also essential for homotypic fusion of the sequestering membranes (Ano *et al.*, 2005). PpAtg24 is not required for MIPA formation (Ano *et al.*, 2005), but it is unclear whether PpAtg1 and PpVac8 are essential for the formation of the MIPA.

In summary, we have characterized the functional role of PpAtg9 in glucose-induced micropexophagy. We have shown that PpAtg9 is essential for the formation of the sequestrating membranes that engulf the peroxisomes for degradation within the vacuole. During micropexophagy, PpAtg9 traffics from a unique compartment of the Atg9-PC to the PVS juxtaposed to the vacuole where it then becomes associated with the vacuole and those sequestering membranes that engulf the peroxisomes for degradation (see Fig. 3-11). We have also demonstrated that the trafficking of PpAtg9 requires PpAtg11, PpVps15, PpAtg2, and

PpAtg7, but not PpAtg1, PpAtg18 or PpVac8. We propose that upon the onset of micropexophagy, PpAtg11 recruits PpAtg9 to the PVS, which act as sites of formation of the sequestering membranes presumably by causing segmentation of the vacuole. These membranes then engulf the peroxisomes and eventually fuse with the assistance of PpAtg1 and PpVac8 to incorporate the peroxisomes into the vacuole for degradation.

Table 3-1: *Pichia pastoris* strains

Name	Genotype	Reference
GS115	his4	(Cregg et al., 1985)
PPF1	arg4 his4	(Yuan et al., 1997)
SMD1163	his4 pep4 prb1	(Tuttle and Dunn, 1995)
DMM1	GS115::pDM1 (P_{AOX1}BFP-SKL, zeo^R)	(Kim et al., 2001)
WDY7	his4 Ppatg7	(Yuan et al., 1999)
WDKO7	PPF1 Ppatg7Δ::ARG4	(Yuan et al., 1999)
WDKO11	GS115 Ppatg2Δ:: zeo^R	(Stromhaug et al., 2001)
R2	GS115 Ppatg18-1:: zeo^R	(Stromhaug et al., 2001)
R12	GS115 Ppatg1-1:: zeo^R	(Stromhaug et al., 2001)
R13	GS115 Ppatg11-1:: zeo^R	(Kim et al., 2001)
R19	GS115 Ppatg9-1:: zeo^R	(Stromhaug et al., 2001)
R22	GS115 atg2-1:: zeo^R	(Stromhaug et al., 2001)
Ppvps15Δ	PPF1 his4 Ppvps15Δ::ARG4	(Stasyk et al., 1999)
S7-GFPx3	PPF12 arg4 his4::pPOP-S7-GFPX3 (P_{Sec7} PpSec7-GFPx3)	(Bevis et al., 2002)
Sec13-GFP	PPF12 arg4 his4::pPOP-SEC13-GFP (P_{Sec13} PpSec13-GFP)	(Bevis et al., 2002)
WDY53	arg4 his4 vac8Δ:: zeo^R	This study
WDY70	DMM1 his4::pWD21 (P_{GAPDH} GFP-PpAtg8, HIS4)	This study
WDY71	R19 his4::pWD21 (P_{GAPDH} GFP-PpAtg8, HIS4)	This study
WDY75	AJM26 his4::pWD21 (P_{GAPDH} GFP-PpAtg8, HIS4)	This study
WDY78	R19 his4::pAJM9 (P_{GAPDH} mRFP-PpAtg9, HIS4)	This study
TC1	GS115 his4::pTC1 (P_{GAPDH} GFP-PpATG9, HIS4)	This study
TC3	DMM1 his4::pTC1 (P_{GAPDH} GFP-PpATG9, HIS4)	This study
TC4	WDY7 his4::pTC1 (P_{GAPDH} GFP-PpATG9, HIS4)	This study
TC5	WDKO7 his4::pTC1 (P_{GAPDH} GFP-PpATG9, HIS4)	This study
TC6	R13 his4::pTC1 (P_{GAPDH} GFP-PpATG9, HIS4)	This study
TC7	R12 his4::pTC1 (P_{GAPDH} GFP-PpATG9, HIS4)	This study
TC8	R22 his4::pTC1 (P_{GAPDH} GFP-PpATG9, HIS4)	This study
TC9	R2 his4::pTC1 (P_{GAPDH} GFP-PpATG9, HIS4)	This study
TC10	R19 his4::pTC1 (P_{GAPDH} GFP-PpATG9, HIS4)	This study
TC11	PpVsp15Δ his4::pTC1 (P_{GAPDH} GFP-PpATG9, HIS4)	This study
TC12	WDY53 arg4 his4::pTC1 (P_{GAPDH} GFP-PpATG9, HIS4)	This study
TC14	R19 his4::pTC2 (P_{GSA14} PpATG9-GFP, HIS4)	This study
TC16	R19 his4::pTC3 (P_{GAPDH} PpATG9-GFP, HIS4)	This study
TC19	WDKO11 his4::pTC1 (P_{GAPDH} GFP-PpATG9, HIS4)	This study
ASK2	GS115 his4::pHA-G14 (P_{GSA14} HA-PpATG9, HIS4)	This study
ASK3	R19 his4::pHA-G14 (P_{GSA14} HA-PpATG9, HIS4)	This study
ASK4	R19 his4::pGFP-G14(ΔL3) (P_{GAPDH} GFP-PpAtg9ΔL3, HIS4)	This study
ASK5	R19 his4::pGFP-G14(ΔN) (P_{GAPDH} GFP-PpAtg9ΔN, HIS4)	This study
AJM18	S7-GFPx3 arg4 his4::pAJM6 (P_{GAPDH} mRFP-PpATG9, zeo^R)	This study
AJM19	Sec13-GFP arg4 his4::pAJM6 (P_{GAPDH} mRFP-PpATG9, zeo^R)	This study
AJM22	GS115 his4::pPS69(P_{GAPDH} GFP/HA-PpATG2, HIS4)	This study
AJM24	GS115 his4::pWD17 (P_{GAPDH} GFP-PpATG9, zeo^R)	This study
AJM25	AJM22::pAJM6 (P_{GAPDH} mRFP-PpATG9, zeo^R)	This study

Table 3-1 continued

Name	Genotype	Reference
AJM26	GS115 *his4*::pAJM6 (P_{GAPDH} mRFP-PpATG9, zeo^R)	This study
AJM27	AJM24 *his4*::pIB2-dsRED-HDEL (P_{GAPDH} dsRFP-HDEL, HIS4)	This study
AJM32	AJM26 *his4*:: pPS64 (P_{GAPDH} GFP/HA-PpATG11, HIS4)	This study
AJM33	AJM26 *his4*:: pPS55-G12 (P_{GAPDH} GFP/HA-PpAtg18, HIS4)	This study
AJM44	AJM26 *his4*::pAJM3(P_{ADH} CoxIV-GFP, HIS4)	This study

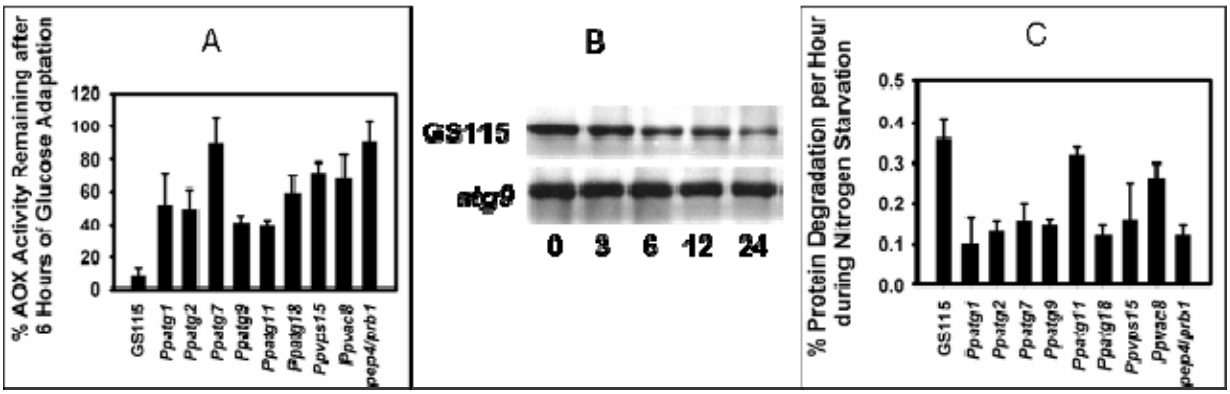

Figure 3-1. Pexophagy and autophagy are defective in Ppatg9 mutants. Panel A: Wild type GS115, R12 (*Ppatg1*), R22 (*Ppatg2-2*), WDY7 (*Ppatg7*), R19 (*Ppatg9*), R13 (*Ppatg11-1*), R9 (*Ppatg18*), Ppvps15Δ (*Ppvps15Δ*), WDY53 (*Ppvac8Δ*), and SMD1163 (*pep4*, *prb1*) cells were grown in YNM for 36 h. At that time, cells were switched to a medium containing 2% glucose. Aliquots were removed at 0 and 6 h of adaptation, the cells lysed, and AOX activities measured as describe in Experimental Procedures. The data is expressed as a percentage of AOX remaining at 6 h relative to 0 h and represents the mean ± SE of 3 - 6 trials. Panel B: Wild type GS115 and R19 (*Ppatg9*) cells were grown in YNM for 36 h and then switched to YNE medium. Aliquots were removed, the cells lysed, and AOX protein visualized by Western blotting as describe in Experimental Procedures. Panel C: Wild type GS115, R12 (*Ppatg1*), R22 (*Ppatg2-2*), WDY7 (*Ppatg7*), R19 (*Ppatg9*), R13 (*Ppatg11-1*), R9 (*Ppatg18*), Ppvps15Δ (*Ppvps15Δ*), WDY53 (*Ppvac8Δ*), and SMD1163 (*pep4*, *prb1*) cells were grown in minimal medium containing ^{14}C-valine for 18 h. The cells were pelleted and resuspended in medium lacking amino acids and nitrogen and containing 10 mM valine. The production of TCA-soluble radioactivity was measured at 2, 5, 8, and 24 h of chase and the rates calculated by linear regression of the slope of the line. The rates represent the mean ± S.E. of 5-7 trials.

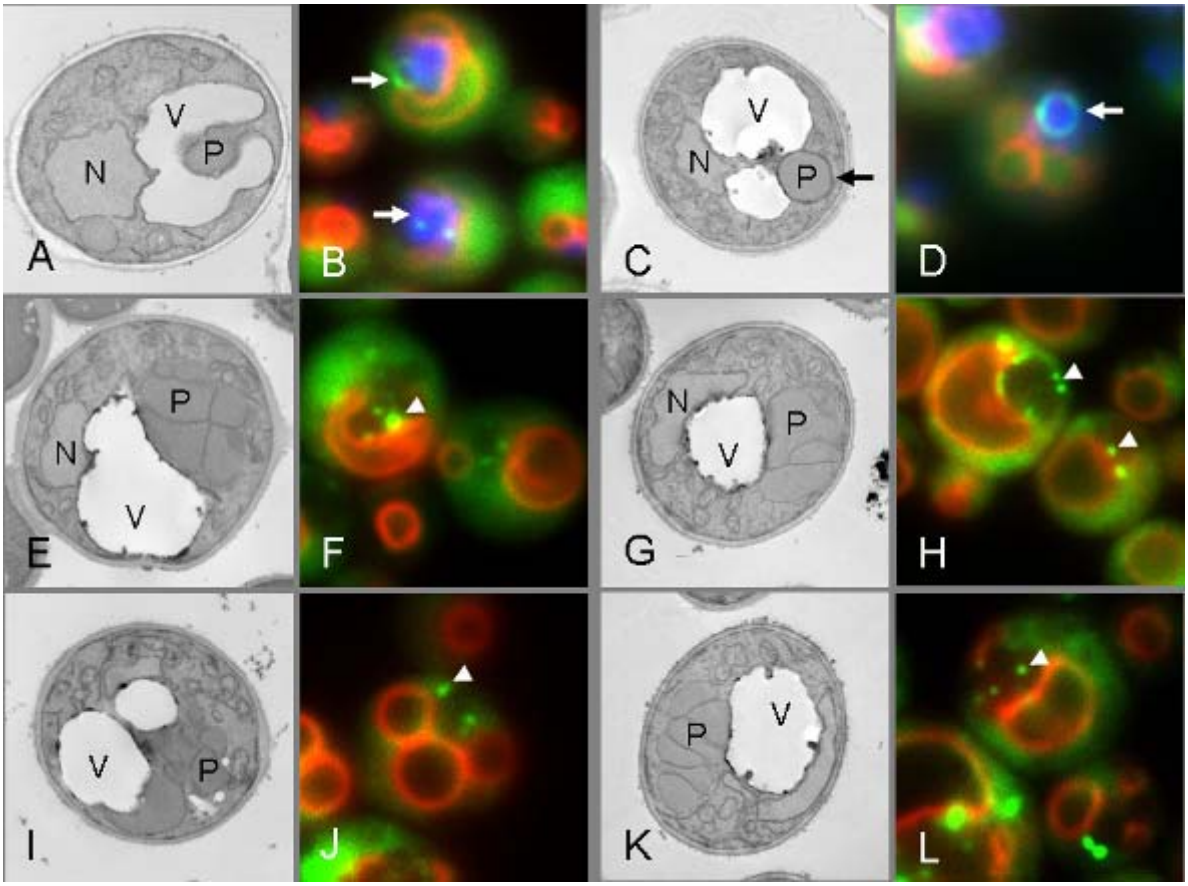

Figure 3-2. Pexophagy is blocked at an early sequestration event in cells lacking PpAtg9. Wild type cells, GS115 (A, C) and WDY70 (B, D) and cells lacking PpAtg9, R19 (E, G, I, K) and WDY71 (F, H, J, L) were grown in YNM for 24-36 h. At that time, cells were switched to medium containing 2% glucose (A, B, E, F, I, J) or 0.5% ethanol (C, D, G, H, K, L) for 3 h. Cells were fixed with potassium permanganate and prepared for viewing on a JEOL 100CX transmission electron microscope (A, C, E, G, I, K) or viewed *in situ* by fluorescence microscopy (B, D, F, H, J, L). When GS115 and WDY70 cells were adapted to glucose for 3 h, many of the cells lacked peroxisomes while in others the vacuole was found to virtually surround the peroxisome cluster (A, B). In R19 and WDY71 cells, peroxisome clusters were evident in virtually all the cells. The vacuole was either oblong with a cup-like depression at the surface adjacent to the peroxisomes (E, F) or round with short arm-like segments (I, J). By fluorescence microscopy, the vacuole was observed by staining with FM 4-64, the peroxisomes by expressing BFP-SKL, and the MIPA and pexophagosomes by expressing GFP-PpAtg8. GFP-PpAtg8 was observed at the MIPA in WDY70 cells (B, arrow), but appeared as foci in WDY71 cells lacking PpAtg9 (F and J, arrowheads). During ethanol adaptation, individual peroxisomes were sequestered into pexophagosomes (C, arrow) that contained PpAtg8 (D, arrow). No pexophagosomes were evident in R19 and WDY71 cells lacking PpAtg9 (G, H, K, L). In the absence of macropexophagy, PpAtg8 resided in numerous foci (H and L, arrowheads). N, nucleus; P, peroxisome; V, vacuole.

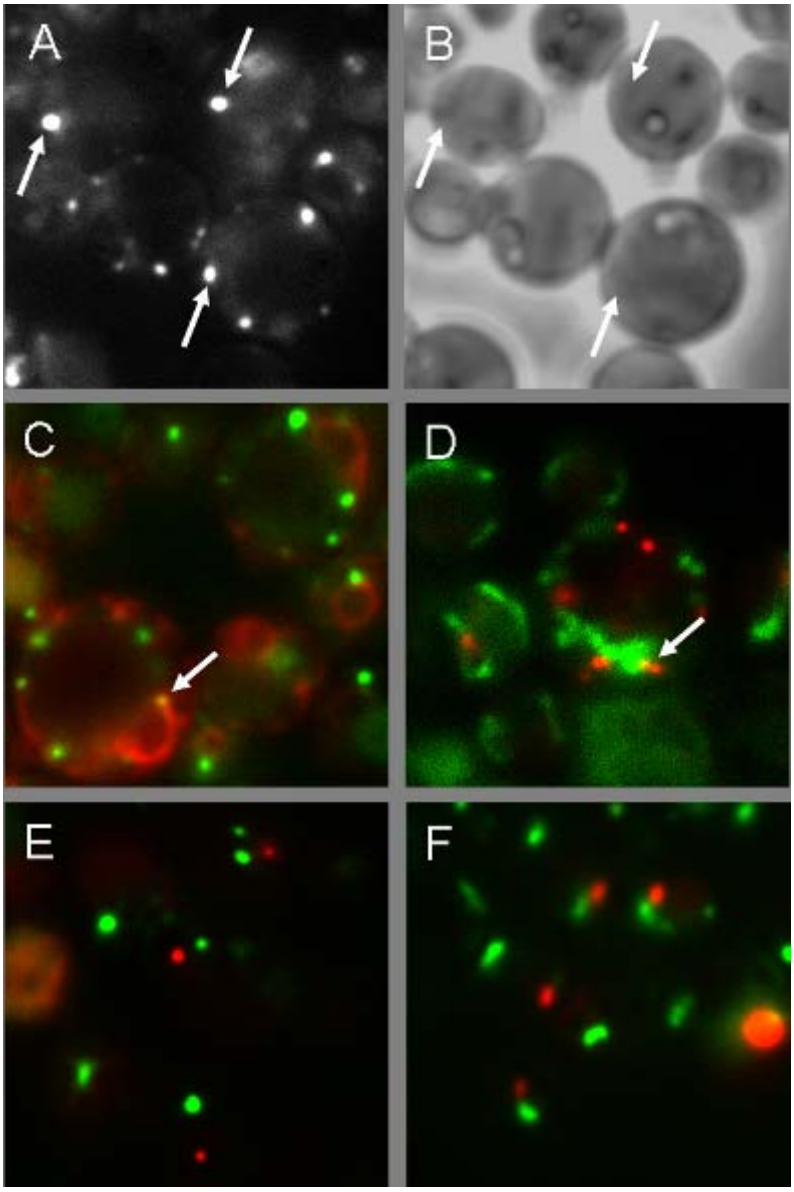

Figure 3-3. Cellular localization of PpAtg9. TC14 expressing PpAtg9-GFP behind the endogenous PpAtg9 promoter (A, B), AJM27 expressing GFP-PpAtg9 behind the GAPDH promoter and dsRFP-HDEL (C), AJM44 expressing mRFP-Atg9 behind the GAPDH promoter and CoxIV-GFP (D), AJM19 expressing mRFP-PpAtg9 behind the GAPDH promoter and Sec13-GFP (E), and AJM18 expressing mRFP-PpAtg9 behind the GAPDH promoter and Sec7-GFP (F) were grown in YPD and the cellular distribution of the GFP and mRFP tagged proteins visualized by *in situ* fluorescence microscopy. In TC14 cells, PpAtg9-GFP was present in foci situated at the cell periphery (arrows). The GFP-PpAtg9 structures appeared to be juxtaposed to the endoplasmic reticulum containing dsRFP-HDEL (C) and mitochondria containing CoxIV-GRP (D), but distinct from intermediate vesicles containing Sec13-GFP (D) and Golgi apparatus containing Sec7-GFP (E).

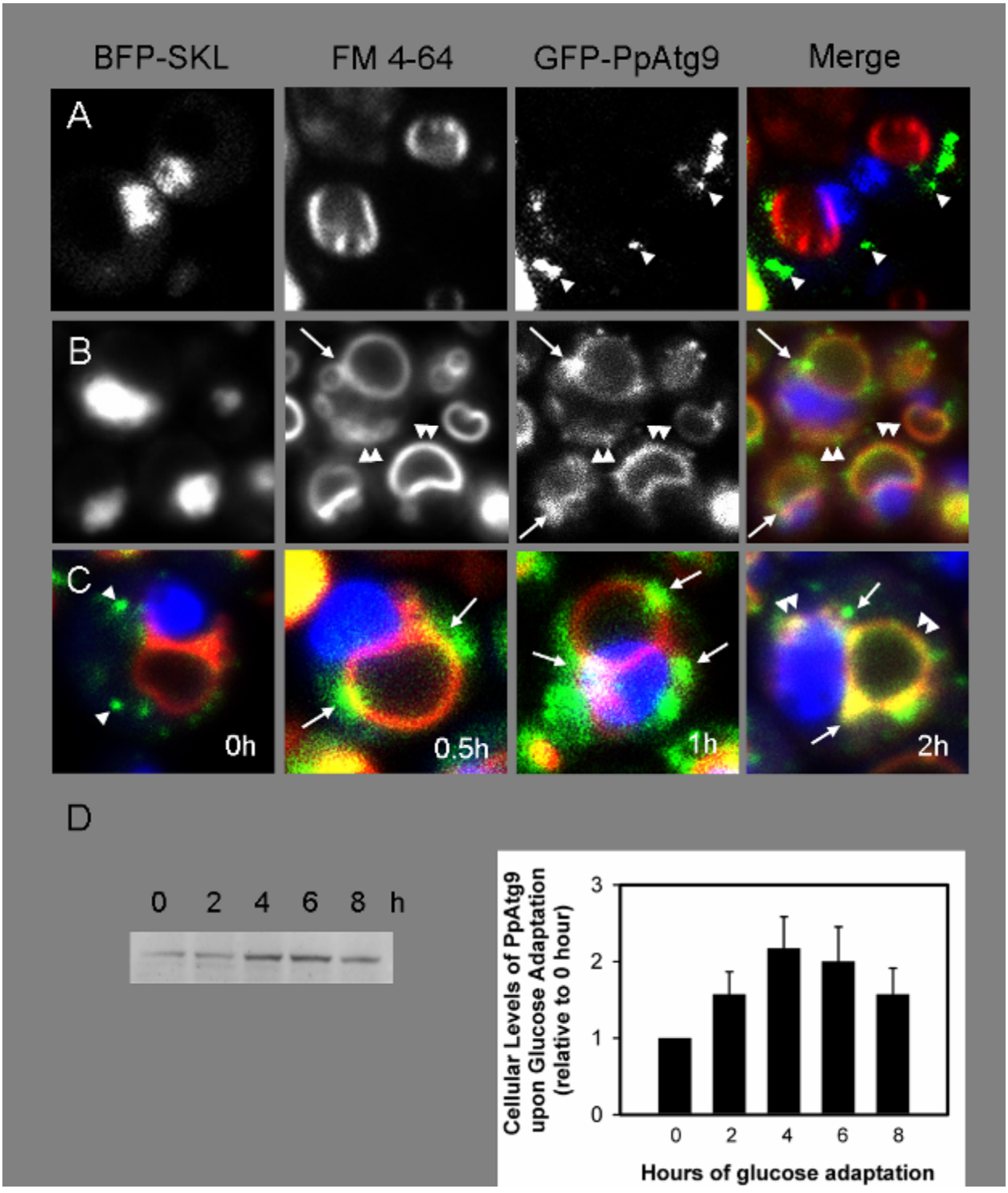

Figure 3-4. PpAtg9 relocates from peripheral structures to the sequestering membranes during glucose-induced pexophagy. TC3 cells expressing both BFP-SKL behind the AOX1 promoter and GFP-PpAtg9 behind the GAPDH promoter were grown in YNM medium in the presence of FM 4-64, adapted to YND medium for 0 h (Panel A) and 3 h (Panel B), and the cellular distribution of GFP-PpAtg9 visualized by *in situ* fluorescence microscopy. Peroxisomes were identified by the presence of BFP, which was targeted by its SKL signal and the vacuole by the

red dye FM 4-64. At 0 h, many cells had BFP-containing peroxisomes and a single round vacuole. GFP-PpAtg9 was localized to foci near the cell periphery (arrowheads). At 3 h of glucose adaptation, numerous profiles of vacuoles with arm-like extensions surrounding the BFP-containing peroxisomes could be observed. GFP-PpAtg9 was present at perivacuolar structures (arrows) and at the vacuole membrane (double arrowhead). In panel C, images from 0-2 h of glucose adaptation depict the movements of GFP-PpAtg9 from peripheral structures (arrowheads) to the perivacuolar structures (arrows) and sequestering and vacuole membranes (double arrowhead). In panel D, ASK2 cells expressing HA-PpAtg9 behind the endogenous PpAtg9 promoter were grown in methanol medium and then adapted to glucose medium. At 0-8 h, equivalent numbers of cells based on the optical density (OD_{600}) of the cultures were solubilized in SDS, and the proteins separated by SDS-PAGE. HA-PpAtg9 was then visualized by Western blotting using anti-HA antibodies and quantified using a Typhoon laser scanner. The values were normalized to 0 h and presented as the mean $\pm$ SE (n = 6).

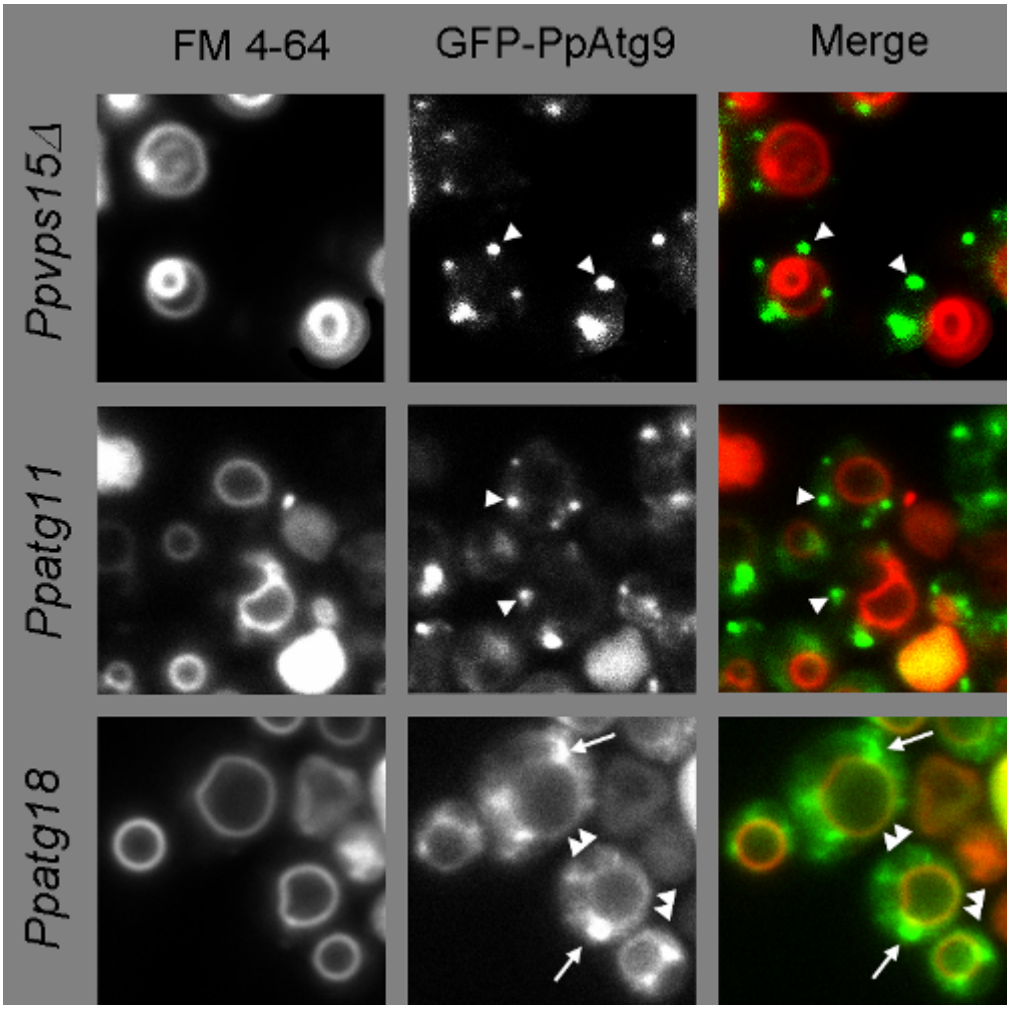

Figure 3-5. Trafficking of PpAtg9 in mutants defective in early sequestration events. TC6 (*Ppatg11*), TC9 (*Ppatg18*), and TC11 (*Ppvps15Δ*) mutants expressing GFP-PpAtg9 behind the GAPDH promoter were grown in YNM medium in the presence of FM 4-64 then adapted to YND medium for 3 h and the cellular distribution of GFP-PpAtg9 visualized by *in situ* fluorescence microscopy. The vacuoles in the *Ppvps15Δ*, *Ppatg11* and *Ppatg18* mutants were either round, flattened, or slightly indented. GFP-PpAtg9 was present in peripheral structures (arrowheads) in the *Ppvps15Δ* and *Ppatg11* mutants. However, in *Ppatg18* mutants, GFP-PpAtg9 was visualized at the large sometimes diffuse perivacuolar structures (arrows) and the vacuole membrane (double arrowheads).

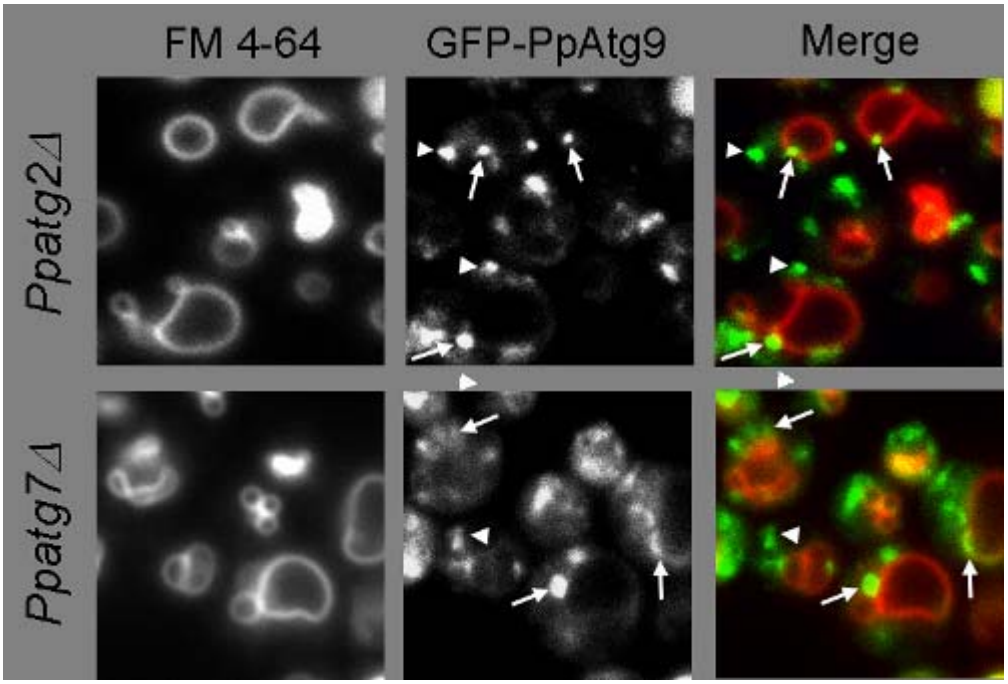

Figure 3-6. Trafficking of PpAtg9 in mutants defective in intermediate sequestration events. TC19 (*Ppatg2Δ*) and TC5 (*Ppatg7Δ*) mutants expressing GFP-PpAtg9 behind the GAPDH promoter were grown in YNM medium in the presence of FM 4-64 then adapted to YND medium for 3 h and the cellular distribution of GFP-PpAtg9 visualized by *in situ* fluorescence microscopy. The vacuoles in *Ppatg2Δ* and *Ppatg7Δ* mutants were indented with an occasional short segmented arm-like extension. In these mutants, GFP-PpAtg9 localized to peripheral structures (arrowheads) and the PVS at the vacuole surface (arrows), but was absent from the vacuolar membrane. Similar results were obtained in TC8 (*Ppatg2*) and TC4 (*Ppatg7*) cells.

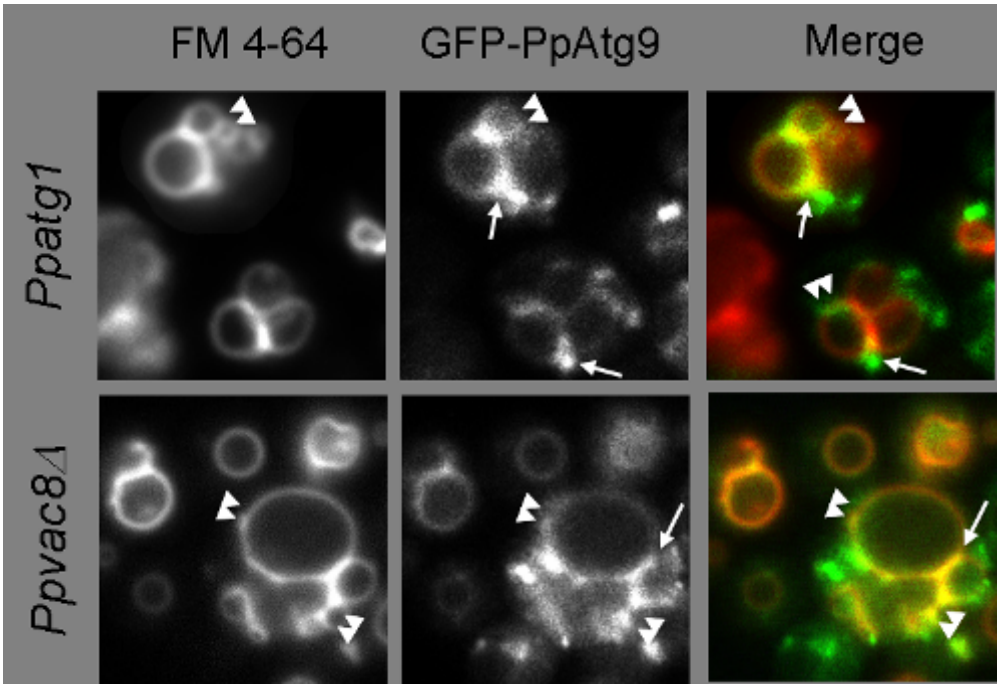

Figure 3-7. Trafficking of PpAtg9 in mutants defective in late sequestration events. TC7 (*Ppatg1*) and TC12 (*Ppvac8Δ*) mutants expressing GFP-PpAtg9 behind the GAPDH promoter were grown in YNM medium in the presence of FM 4-64 then adapted to YND medium for 3 h and the cellular distribution of GFP-PpAtg9 visualized by *in situ* fluorescence microscopy. The vacuoles in *Ppatg1* and *Ppvac8* mutants were indented with multiple "segmented" arm-like extensions that surrounded the peroxisome cluster. GFP-PpAtg9 was visualized at the vacuole membrane but appeared to be more concentrated at the sequestered membrane extensions of the vacuole (double arrowheads). In addition, GFP-PpAtg9 was found at the PVS situated at sites of the vacuole surface adjacent to the arm-like extensions (arrows).

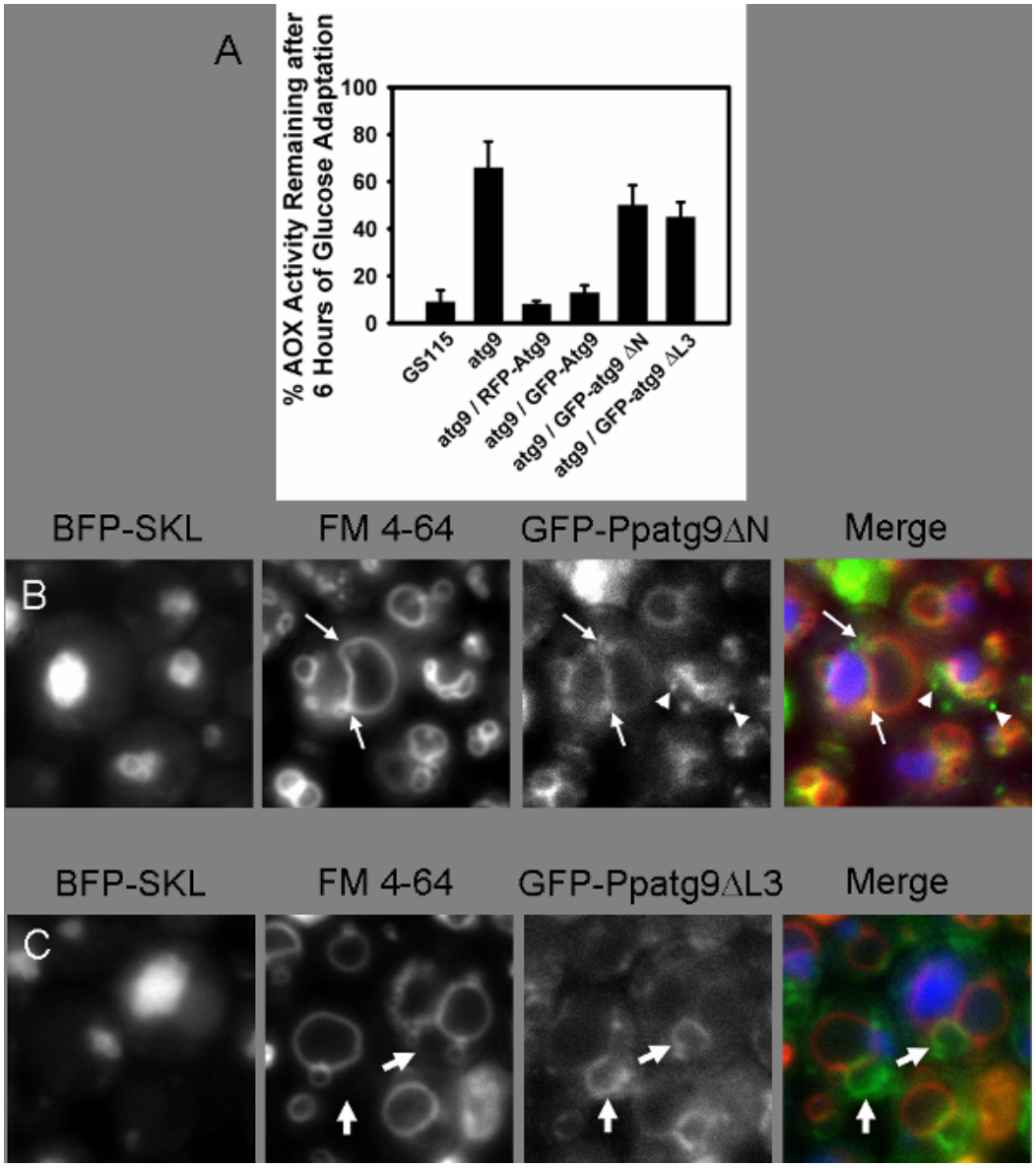

Figure 3-8. PpAtg9 domains required for function and trafficking. In panel A, wild type GS115, R19 (*Ppatg9*), and R19 cells expressing mRFP-PpAtg9, GFP-PpAtg9, GFP-Ppatg9ΔN (ΔM1-Y221), or GFP-Ppatg9ΔL3 (ΔT471 - A523) were grown in YNM medium for 36 h. All proteins were expressed behind the GAPDH promoter. Cells were then switched to glucose medium. Aliquots were removed at 0 and 6 h of adaptation, the cells lysed, and AOX activities measured as described under "Experimental Procedures". The data are expressed as a percentage of AOX remaining at 6 h relative to 0 h and represent the mean ± S.E. of 4-6 trials. ASK5 (B) and ASK4 (C) cells were grown in YNM for 20 h in the presence of FM 4-64. The cells were then transferred to YND medium for 3 h and then visualized by fluorescence microscopy. GFP-Ppatg9ΔN was found at the Atg9-PC (arrowheads), PVS (arrows) and the vacuolar membranes. GFP-Ppatg9ΔL3 was absent from the Atg9-PC and PVS, but found in a compartment that resembled the endoplasmic reticulum (large arrows).

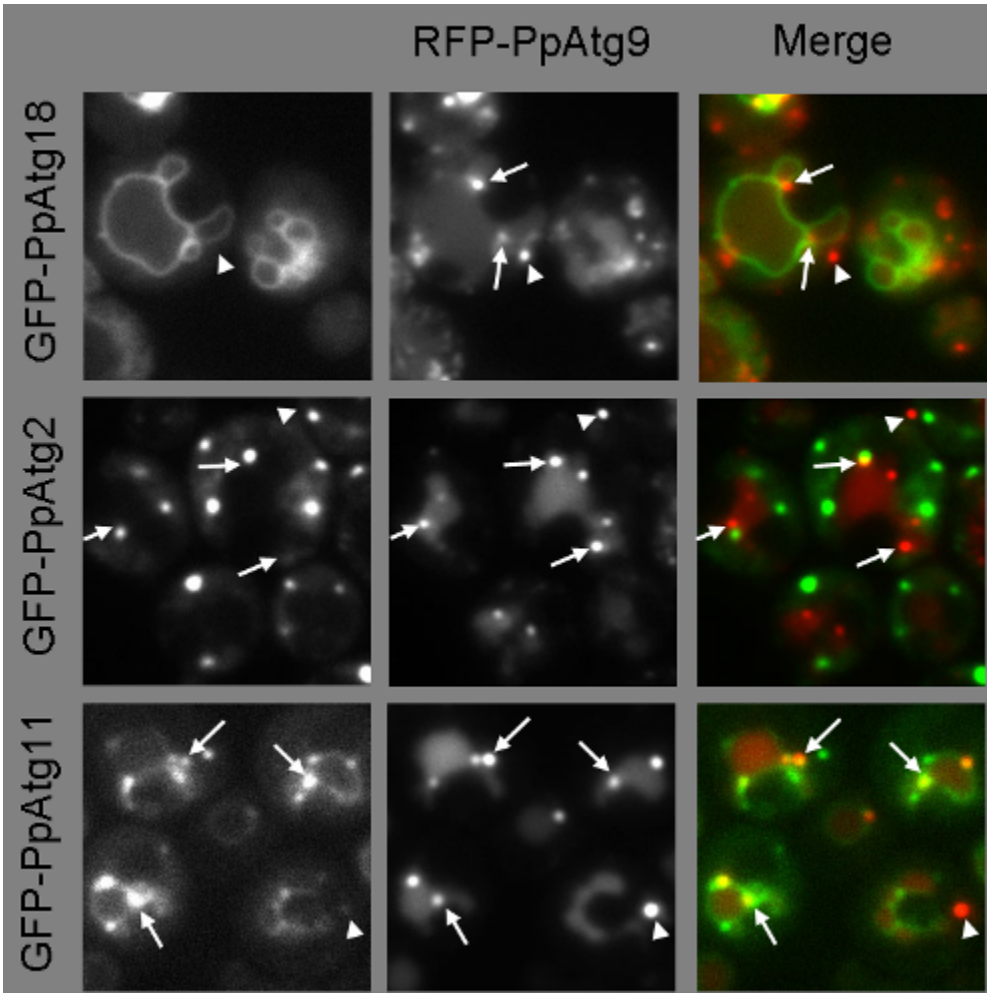

Figure 3-9. Perivacuolar structures contain PpAtg9 and PpAtg11. AJM33 expressing GFP-PpAtg18 and mRFP-PpAtg9, AJM25 expressing GFP-PpAtg2 and mRFP-PpAtg9 and AJM32 expressing GFP-PpAtg11 and mRFP-PpAtg9 were grown in YNM medium then adapted to YND medium for 2 h and the cellular distribution of GFP and RFP tagged proteins visualized by *in situ* fluorescence microscopy. PpAtg9 was found at peripheral structures (arrowheads) and PVS (arrows) and within the vacuole delineated by PpAtg18 and PpAtg11. The Atg9-PC did not contain PpAtg2, PpAtg11 or PpAtg18. GFP-PpAtg2 resided in distinct vesicles of which a few were in close association with the PVS. Meanwhile, virtually all the PVS contained both GFP-PpAtg11 and mRFP-PpAtg9 (arrows).

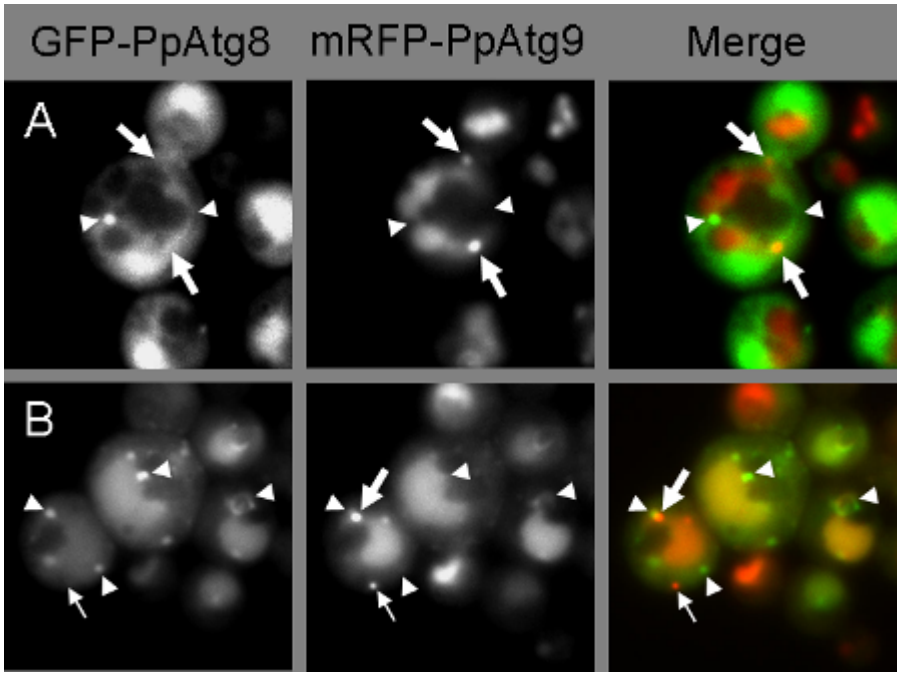

Figure 3-10. PpAtg9 does not colocalize with PpAtg8 structures. WDY75 expressing GFP-PpAtg8 and mRFP-PpAtg9 were grown in YNM then adapted to glucose or ethanol medium for 2 h and the cellular distribution of GFP and RFP tagged proteins visualized by *in situ* fluorescence microscopy. During glucose adaptation (panel A), mRFP-PpAtg9 was found within the vacuole and at the PVS (large arrows), but absent from PpAtg8 foci and MIPA (arrowheads). When cells were transferred from methanol to ethanol medium (panel B), mRFP-PpAtg9 was present within the vacuole and at the peripheral compartment (small arrow) and the PVS (large arrow), but not at the PpAtg8 foci or pexophagosome (arrowheads).

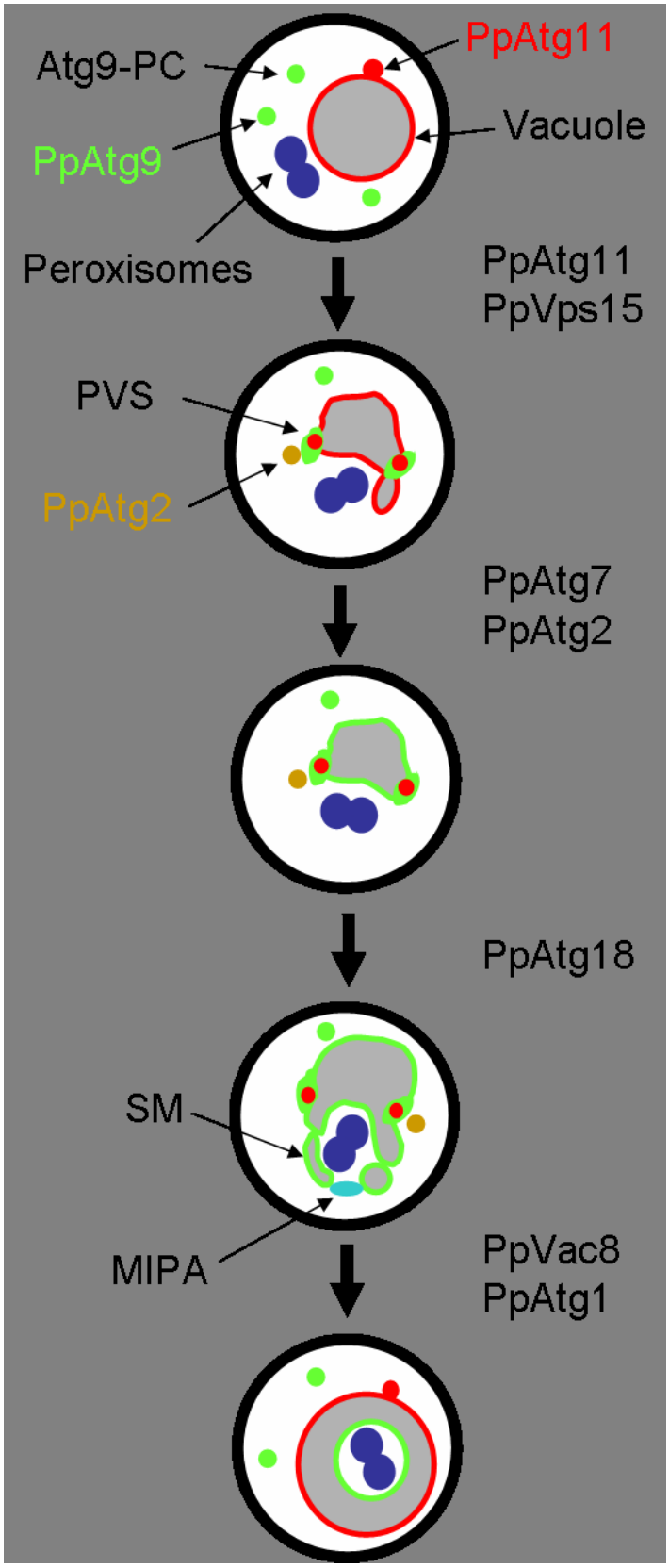
Atg9-PC
PpAtg11
Vacuole
PpAtg9
Peroxisomes
PpAtg11
PpVps15
PVS
PpAtg2
PpAtg7
PpAtg2
PpAtg18
SM
MIPA
PpVac8
PpAtg1

Figure 3-11. Model of PpAtg9 trafficking during pexophagy. During growth in YNM, PpAtg9 (green) is in peripheral compartment (Atg9-PC), PpAtg11 (red) at the vacuole membrane, and PpAtg2 (brown) cytosolic. Upon glucose-induced pexophagy, PpAtg9 is trafficked from the Atg9-PC, to the PVS juxtaposed to the vacuole which also contains PpAtg11, and to the sequestering membranes (SM) that surround the peroxisomes (blue). Also at this time, PpAtg2 becomes associated with unknown structures situated near the PVS. The trafficking of PpAtg9 from the Atg9-PC to the PVS requires PpAtg11 and PpVps15. The movements of PpAtg9 from the PVS to the vacuolar and sequestering membranes require PpAtg7 and PpAtg2. The formation of the sequestering membranes from the vacuole requires PpAtg18, but the movements of PpAtg9 to the vacuolar membrane proceeds normally in the absence of this protein. Finally, the fusion of the sequestering membranes that enable the incorporation of the peroxisomes into the vacuole is guided by the micropexophagy-specific membrane apparatus (MIPA) and requires PpVac8 and PpAtg1.

CHAPTER 4
PPATG9 TRAFFICKING DURING MICROPEXOPHAGY IN *PICHIA PASTORIS*[5]

PpAtg9 encodes a 102 kDa membrane protein with five or more putative membrane spanning domains. Atg9 is structurally conserved throughout eukaryotes with each containing the APG9 domain (Pfam ID, PF04109). Unlike lower eukaryotes, there appears to have evolved two homologues, Atg9L1 and Atg9L2, in vertebrates including fish, amphibians, birds, and mammals.(Yamada *et al.*, 2005) Interestingly, both forms are functional for autophagosome formation.(Yamada *et al.*, 2005) The insertion of Atg9 into the lipid bilayer occurs independent of a recognizable signal peptide. Furthermore, placing GFP at the N- or C-terminus of PpAtg9 has no effect on its function. We have recently described the trafficking of Atg9 during glucose-induced micropexophagy in *Pichia pastoris*.(Chang *et al.*, 2005) Here we will summarize our findings and describe those cellular events responsible for PpAtg9 trafficking.

During exponential growth, we have shown that PpAtg9 resides in peripheral vesicles lacking Sec7 or Sec13 but that sometimes colocalizes with markers of the rough endoplasmic reticulum (dsRFP-HDEL) and the mitochondria (CoxIV-GFP).(Chang *et al.*, 2005) A majority of the ScAtg9 localize with mitochondria or in vesicles situated near mitochondria.(Reggiori *et al.*, 2005) However, these authors have also shown that only a small fraction of the PpAtg9 localize with the mitochondria.(Reggiori *et al.*, 2005) The function of Atg9 at the mitochondria remains unclear, but it may have a role in the selective degradation of damaged mitochondria (e.g., mitophagy). Because of the unique characteristics of the PpAtg9 vesicles, we have classified them as the Atg9 peripheral compartment (Atg9-PC) which likely arises from the endoplasmic reticulum (ER). In fact, we have identified a putative ER exit motif, which upon

[5] Article reprinted with permission from the publisher: Schroder, L.A. and W.A. Dunn, Jr. (2006) PpATG9 trafficking during micropexophagy in Pichia pastoris. Autophagy. 2(1):52-54.

deletion (Atg9-ΔL3) results in the accumulation of PpAtg9 within the ER.(Chang *et al.*, 2005) This di-acidic ER exit motif is positioned within a highly conserved region of Atg9 situated between putative transmembrane domains in *P. pastoris*, *S. cerevisiae*, *D. melanogaster*, *C. elegans*, and *H. sapiens* (Fig. 1). This di-acidic (YxDxE) motif was first identified at the C-terminal tail of VSV-G protein and later shown to be functional in other membrane proteins (Barlowe, 2003). Furthermore, a di-acidic YKDAD motif has been shown to be essential for the exit of the cystic fibrosis transmembrane conductance regulator (CFTR) from the ER.(Wang *et al.*, 2004) In the latter case, this motif is located not at the C-terminus, but at a surface-exposed loop as is likely the case for Atg9. The YKDAD motif is similar to the FNELE sequences in CeAtg9 and HsAtg9L1 and to the FNELD sequence present in DmAtg9. The di-acidic ER exit motifs in PpAtg9 and ScAtg9 have similarities to motifs found in both CFTR and Kir2.1, a potassium channel protein (Fig. 4-1). ScAtg9 has been shown to cycle between a peripheral compartment (e.g., mitochondria) and the pre-autophagosomal structure (PAS).(Reggiori *et al.*, 2004; Reggiori *et al.*, 2005) We suggest that Atg9 transits the Atg9-PC during this cycling (Fig. 2). However, the dynamics of the Atg9-PC and its relationship with the mitochondria and PAS have not yet been defined.

Upon the onset of glucose-induced micropexophagy, a number of events occur prior to the formation of the sequestering membranes (SM), a portion of the vacuole membrane, that surround the peroxisomes (Fig. 4-2). First, PpAtg11 transits from a single site at the vacuole surface presumed to be the PAS to multiple perivacuolar structures (PVS) (Step 1, Fig. 4-2). Next, PpAtg9 is transferred from the Atg9-PC to the PVS (Step 2, Fig. 4-2). The PVS is unique from the PAS in that it does not contain PpAtg8 and is situated at multiple foci at the vacuole surface where it appears to direct the formation of the SM in much the same way that the PAS

organizes the formation of the autophagosome. The trafficking of PpAtg9 to the PVS requires PpAtg11 and PpVps15. It remains unclear whether PpAtg9 transits from the PAS to the PVS or arrives directly from the Atg9-PC. At this time, cytosolic PpAtg2 becomes associated with peripheral foci and the PVS, while cytosolic PpAtg18 becomes bound to the vacuolar membrane.(Guan *et al.*, 2001; Stromhaug *et al.*, 2001) The PpAtg2 foci do not contain PpAtg9, but are distinct from the Atg9-PC. However, the assembly of this Atg2 compartment (Atg2-C) requires PpAtg9 suggesting a transient association. PpAtg9 is then transferred from the PVS to the vacuole membrane and newly forming SM (Step 3, Fig. 4-2). PpAtg2 is required for PpAtg9 trafficking from the PVS to the SM, while PpAtg18 is essential for the formation of the SM. The assembly of the SM is best described by a combination of incomplete and complete septation from the vacuole followed by membrane fusion events to form arm-like structures. Since PpAtg11 is unique to pexophagy and found at the SM, we propose this protein may act to recognize and guide the SM around the peroxisomes. The SM fusion events require PpAtg24 and PpVac8.(Ano *et al.*, 2005; Chang *et al.*, 2005; Wohlgemuth *et al.*, 2007) As the SM is being formed, the PAS assembles a unique micropexophagy-specific membrane apparatus (MIPA) which contains PpAtg8 and PpAtg26 (Step 4, Fig. 4-2). In addition to those enzymes (e.g., PpAtg3, PpAtg4, and PpAtg7) essential for the conjugation of PpAtg8 to phosphatidylethanolamine (Oku *et al.*, 2003; Mukaiyama *et al.*, 2004), the formation of the MIPA requires PpAtg11 (unpublished data) and PpAtg9.(Chang *et al.*, 2005) Although neither PpAtg11 nor PpAtg9 are associated with the MIPA, their role in its formation suggests these proteins may be at least transiently associated with the PAS. Once the MIPA is assembled it directs the final membrane fusion of the SM thereby incorporating the peroxisomes into the vacuole for degradation (Step 5, Fig. 4-2). We suggest that glucose-induced micropexophagy

proceeds through a complex but well-organized sequence of molecular events to ensure the selective and efficient degradation of superfluous peroxisomes.

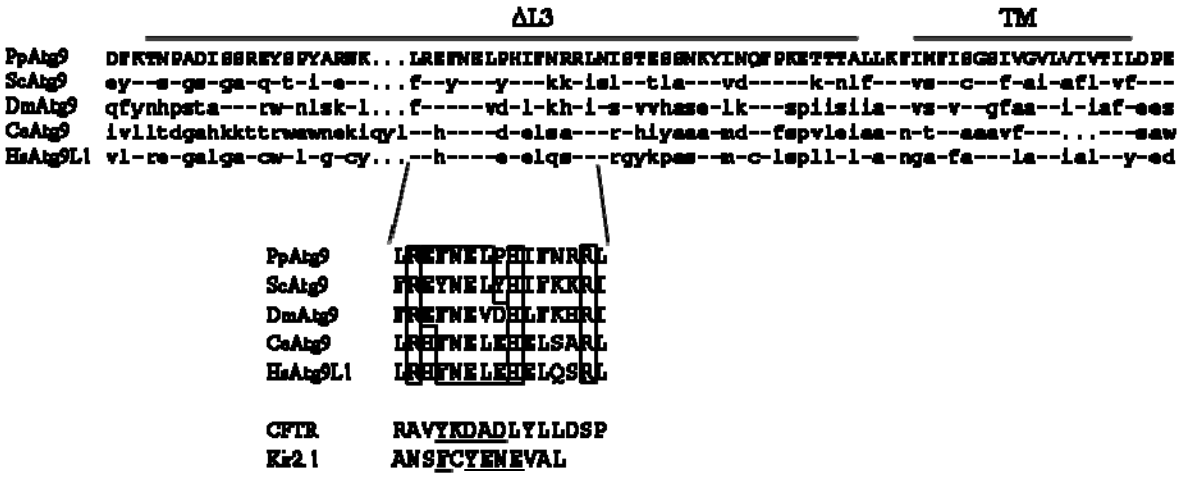

Figure 4-1. Alignment of the putative ER exit motifs of Atg9. The amino acid sequence between putative transmembrane (TM) domains of Atg9 from *P. pastoris*, *S. cerevisiae*, and *H. sapiens* were aligned with structural homologs from *D. melanogaster* and *C. elegans*. Amino acid identities (--) and gaps (…) are indicated and the putative ER exit domain aligned with similar motifs in CFTR and Kir2.1.

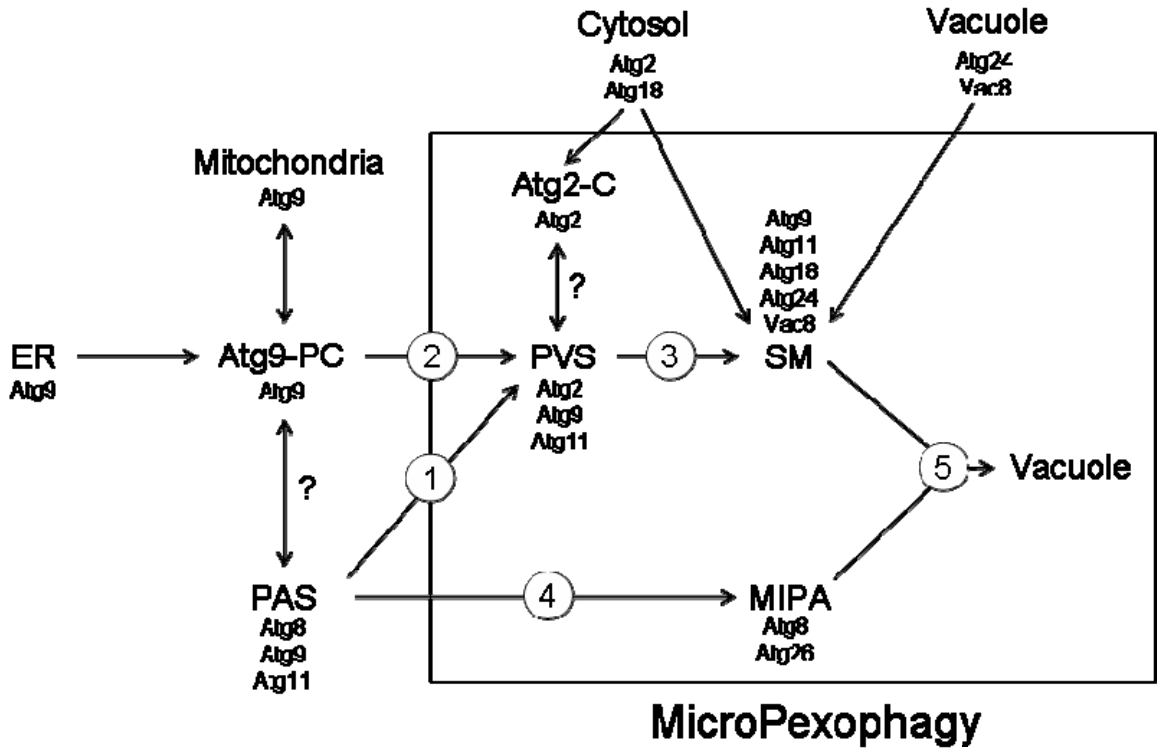

Figure 4-2. Trafficking of PpAtg9 and other Atg proteins during micropexophagy. When *P. pastoris* are grown in methanol medium, PpAtg proteins can be found in a number of compartments (outside the box): endoplasmic reticulum (ER), Atg9 peripheral compartment (Atg9-PC), pre-autophagosomal structure (PAS), mitochondria, cytosol and the vacuole. Upon adaptation to glucose medium and induction of micropexophagy, many of the PpAtg proteins traffic to compartments unique to micropexophagy (inside the box): Atg2 compartment (Atg2-C), perivacuolar structures (PVS), sequestering membranes (SM), and micropexophagy-specific membrane apparatus (MIPA). The trafficking of PpAtg9 and other Atg proteins during micropexophagy is summarized in this diagram and discussed in the text.

CHAPTER 5
TARGETING MOTIFS OF ATG9

Introduction

Protein degradation keeps the cell in constant homeostasis even during times of starvation and stress. Autophagy is the foremost mechanism by which cellular milieu, from proteins to organelles, is delivered in a highly regulated fashion to the lytic compartment—the lysosome or the vacuole—for degradation. Multiple selective and nonselective modes of autophagy exist in yeast, namely autophagy, pexophagy, and mitophagy (Wang and Klionsky, 2003; Dunn *et al.*, 2005). Autophagy is turned on when cells are starved for amino acids. Pexophagy occurs in methylotropic yeasts during adaptation from methanol to ethanol or glucose as peroxisomes are degraded with the media shift (Dunn *et al.*, 2005). When stationary cultures of S. cerevisiae are switched to medium containing lactose, mitochondria are degraded by mitophagy (Abeliovich, 2007).

Pichia pastoris is a methylotropic yeast able to synthesize the enzymes to consume methanol as sole dietetic source. The peroxisomes are synthesized when *P. pastoris* is exposed to methanol to metabolize this carbon source. When the cells are adapted to glucose the peroxisomes are rapidly sequestered and degraded by the vacuole via key micropexophagic events—the superfluous organelle is no longer needed and is consumed and degraded to provide the building blocks for protein synthesis (Dunn *et al.*, 2005). These events include the recognition of the peroxisome by the vacuole and the invagination of the vacuole with the protrusion of vacuolar arms that surround then engulf the collection of peroxisomes as a whole for degradation. If *P. pastoris* is adapted from methanol to ethanol (rather than glucose), the peroxisomes are selectively sequestered individually by pexophagosomes that fuse with the vacuole.

The sequestration events of glucose-induced micropexophagy can be phenotypically characterized as the sequential events nucleation, expansion, completion and degradation. Nucleation of the sequestering membranes occurs with the budding of the sequestering membranes (SM) from the vacuole and requires Atg18. Expansion of the sequestering membranes to surround the peroxisomes follows from perivacuolar structures (PVS), involving Atg2, Atg11 and Atg9. To assist in tethering of the SM, the micropexophagic-specific membrane apparatus (MIPA) forms between the expanding sequestering membranes (Mukaiyama *et al.*, 2004; Ano *et al.*, 2005). The assembly of the MIPA requires Atg7 and Atg8. Completion is the final enveloping of the peroxisomes by the SM, with the participation of Vac8.

Atg9 is a transmembrane protein required for SM expansion during pexophagy and autophagy (Chang *et al.*, 2005). That is, in the absence of Atg9 the SM only partially engulfs the peroxisomes. Upon ER synthesis, Atg9 transits to the Atg9 peripheral compartment (PC9). When cells adapt to glucose, Atg9 moves to the perivacuolar structure (PVS) and to the preautophagosome structures (PAS). From the PVS, Atg9 transits to the sequestering membranes (SM) (Schroder and Dunn, 2006). The PVS is present at the base of the SM while the PAS is localized adjacent to the tips of the SM (Chang *et al.*, 2005). Atg11 recruits Atg9 to the PVS which has been shown to contain Atg9 and Atg11 but not Atg2 in *P. pastoris*. Atg9 is required for early and late sequestration; more specifically, Atg9 is required for MIPA formation during late sequestration. Recent data in *Saccharomyces cerevisae* indicate a direct interaction between ScAtg9 and ScAtg11 at the PAS (Chang and Huang, 2007; Mari and Reggiori, 2007). The interaction between ScAtg11 and ScAtg9 appears to require the first two coiled-coil regions of ScAtg11 as well as amino acids 154-200 of the N-terminus of ScAtg9 but not the last 200

residues of the C-terminus of ScAtg9 (Chang and Huang, 2007). Interestingly, actin is essential for the trafficking of ScAtg9 and ScAtg11 to the PAS (Reggiori *et al.*, 2003; Yen *et al.*, 2007).

In order to better clarify its dynamic role of Atg9 in pexophagy, we have mutated conserved regions of Atg9. Deletion of the N-terminus resulted in a non-functional albeit properly sorted mutant phenotype that localizes to the vacuole and SM. There are two ER exit domains within Atg9. Deletion of the region between the third and fourth transmembrane domains, an Atg9 loop—most importantly amino acids E491 and E494—suggests that this domain is critical for ER exit. Deletion of the region past the last transmembrane domain also resulted in ER localization. The PC9 exit domain encompasses amino acids QQHKA at the extreme C-terminal end of Atg9. Localization to the SM requires amino acids W607 and Y611. All the mutants presented exhibit altered trafficking save atg9ΔN which localizes to the SM along the vacuole but does not function. Indeed, none of the atg9 mutants was functional, revealing that Atg9 trafficking to the SM is essential for micropexophagy.

Materials and Methods

Yeast Strains And Media

Table 1 lists the yeast strains utilized in this study. *Pichia pastoris* was routinely cultured and incubated at 30°C in YPD (1% Bacto yeast extract, 2% Bacto peptone, and 2% dextrose). To induce peroxisome proliferation, *P. pastoris* was grown in YNM (0.67 % yeast nitrogen base, 0.4 mg/l biotin, and 0.5% methanol); to induce peroxisome abiogenesis, cells grown in YNM were transferred to YND (0.67 % yeast nitrogen base, 0.4 mg/l biotin, and 2% glucose) or YNE (0.67 % yeast nitrogen base, 0.4 mg/l biotin, and 0.5% ethanol). For induction of macroautophagy, yeast was grown in nitrogen starvation medium (SD-N) containing 0.17 % yeast nitrogen base (without NH_4SO_4 and amino acids except for auxotrophic amino acids as needed) and 2% glucose. For plates, all media included 2% agar. Auxotrophic strains had

arginine or histidine or both added at 40 μg/l as necessary. Vectors were amplified in the DH5α strain of *E. coli* and cultured with ampicillin (100 μg/ml) in LB broth (0.5% Bacto yeast extract, 1% Bacto tryptone with 1% NaCl) at 37° C. 25μg/mL of Zeocin was added to DH5α and 100μg/ml of Zeocin was added to *P. pastoris*.

Yeast Transformation

Once yeast cultures reached saturation density (A_{600} = 1.0), they were harvested and treated with 10 mM DTT in YPD containing 25 mM HEPES, pH 8, for 15 min, all at 30°C. Afterwards, the cells were washed twice with cold water, washed once with 1 M sorbitol, and resuspended in 1 M sorbitol. Electroporation of linearized vector (40 μl of yeast cells to 0.2-1 μg of linearized vector) occurred in a 0.2 cm gap cuvette (Bio-Rad, Hercules, CA) with electroporation conditions as follows: 1.5 kV, 25 μF, 400Ω (Gene Pulser, Bio-Rad Corp.). Histidine was the remaining auxotrophy for Atg9; cells transformed with vectors containing the His4 gene were screened on plates containing 0.67% yeast nitrogen base without amino acids, 2% glucose, 1M sorbitol, 0.4 mg/l biotin, and 2% agar and checked for colonies after 3-5 d at 30°C. The other screening method utilized was the incorporation of the zeocin resistance gene (zeo^R) , and cells transformed with (zeo^R) vectors were grown on YPD with 100 μg/ml Zeocin.

Isolation Of Gsa Mutants And Cloning Of GSA Genes By Restriction Enzyme Mediated Integration (REMI) Mutagenesis

Mutagenesis by random insertion the pREMI-Z vector (provided by Dr. Ben Glick, Univ. of Chicago) for genomic incorporation of the Zeocin resistance gene into the genome of *P. pastoris* has been described previously (Stromhaug *et al.*, 2001). Direct colony assays verified *gsa* mutants as described before(Stromhaug *et al.*, 2001). The site of insertion of the pREMI-Z and identification of the disrupted has been explained (Stromhaug *et al.*, 2001). The *GSA14* gene (NCBI accession number AY075105) was assembled and is homologous to to following: ScAtg9

of *Saccharomyces cerevisiae*, NP_596247 of *Schizosaccharomyces pombe*, NP_180684 of *Arabidopsis thalian*, XP_331198 of *Neurospora crass*, NP_611114 of *Drosophila melanogaster*, NP_503178 of *Caenorhabditis elegans*, and NP_076990 of *Homo sapiens* (Yamada *et al.*, 2005). Homologous residues 190-679 contain a minimum of 5 putative transmembrane domains. The pREMI-Z disruption of PpAtg9 occurred after the first putative transmembrane domain at aspartic acid 245. The null mutant of Atg9 was made as follows. *ATG9* was cloned and inserted into the pUC19 vector. ScARG4 was amplified from genomic DNA by PCR using a forward primer 5'-CCACGTTCTAGAGGTAGATGT-3' that contained an XbaI site and a reverse primer 5'-GATGAAGTCCGCGGAGTACCA -3' that contained a SacII site. ScARG4 with its endogenous promoter was ligated within the *ATG9* gene that had been cut with SacII and XbaI thereby replacing the entire coding region of *ATG9*. The product was then transformed in PPF1 cells and the resulting mutants screen by direct colony assays. WDY55 was constructed by mating R19 with PPF1 and screening the haploids for double his^- and arg^- auxotrophy. Those double auxotrophs defective in pexophayg were then identified by direct colony assays. WDY100 cells expressing were constructed by transforming PPF1 cells with pWD26 (P_{GAPDH} RFP-Atg17, ARG4).

Construction of Ppatg9 Expression Vectors

The GFP-Atg9 and RFP-Atg9 expression vectors (pTC1 and pAJM6) as well as the pGFP-atg9ΔN and pGFP-atg9ΔL3 have been described previously (Chang *et al.*, 2005). The GFP-atg9ΔQQHKA mutant was made as follows. *Pp*ATG9 minus the ΔQQHKA sequence was amplified from pTC1 with forward primer 298 5'-GCAGGCTAGGGTACCGGTACTGGCACATT-3' that contained the KpnI restriction site and reverse primer 5'-CAAATTATGCCT**CGA**GCTGTTAACTAA-3'. The *ATG9* sequence minus

the last 5 amino acids was then cut with KpnI and XhoI. GFP was excised from pIB2 from the KpnI and the XhoI restriction sites. The *Pp*atg9ΔQQHKA was ligated to GFP at the KpnI and XhoI restriction sites, amplified, verified by sequencing, and the vector used to transform R19 (*his4 atg9*:: zeo^{R}) cells. The GFP-atg9Δ579-668 mutant was composed as follows. First, the coding region between the endogenous promoter upstream of the N-terminus and amino acid 579 of *Pp*ATG9 was amplified from pTC1 with forward primer 298 5'-GCAGGCTAGGGTACCGGTACTGGCACATT-3' that contained the KpnI restriction site and the reverse primer 5'-CAGGAATCGA**AAG**CTTGCAAATAGT-3' that contained the HindIII restriction site. Next, the region between amino acid 669 and the C-terminus of *Pp*ATG9 was amplified from pTC1 with forward primer 5'-GTGTTCATGTTGAT**AAGC**CT**T**GGATATGTA-3' that contained the HindIII restriction site and reverse primer 266 5'-CAAGATCTATGCTCGAGAACAAAT AATGCCTTATGCTGTTGACTAA-3' that contained the XhoI site. The parent vector pPS55 was cut with KpnI and XhoI. The N-terminus of Atg9 including the promoter region through amino acid 579 region and the C-terminus of Atg9 not including the stop codon and pPS55 with GFP upstream of the XhoI site were ligated together, amplified, verified by sequencing, and the vector used to transform R19 (*his4 atg9*:: zeo^{R}) cells. The GFP-atg9Δ489-502 mutant was constructed as follows. The region between the N-terminus and amino acid 489 of ATG9 was amplified from pTC1 with forward primer 298 5'-GCAGGCTAGGGTACCGGTACTGGCACATT-3' with the KpnI restriction site and with reverse primer 5'-AATGCGATCCACCTTCGA**T**TCTCTTAAATTAC-3' with the HindIII restriction site. The region between amino acid 502 and the C-terminus of *ATG9* gene was amplified from pTC1 with forward primer 5'-CATTTTCAACAGAA**A**GCT**T**AACATTTCCA-3' with the HindIII restriction site and with reverse primer 5'-

CATTATTATTCAAGA**CC**G**CG**GAATGAAAA-3' with the SacII restriction site. The digest products were ligated together, amplified, the vector verified by sequencing, and used to transform R19 (*his4 atg9*:: zeo^R) cells.

The GFP-atg9(W607A/Y611A) mutant was generated as follows. *ATG9* gene upstream of the N-terminus and flanking amino acids 607-611 was amplified by PCR from genomic DNA with the forward primer 298 5'-GCAGGCTAGGGTACCGGTACTGGCACATT-3' and with the reverse primer 5'-CTTCCTCTGTGTGGGCTTTCCCTTCCGCTTCTTGAGGAA-3' with a KpnI restriction site. At the same time, Atg9 flanking amino acids 607-611 and through the stop codon at the C-terminus was amplified from genomic DNA with the forward primer 5'-CTTCCTCAAGAAGCGGAAGGGAAAGCCCACACAGAGGAA-3' and with the reverse primer 5'-GTTTTGGACTCGAGGGTACTAATGCTTCATT-3'. The product sizes were first verified by restriction digest, then amplified together with the forward primer 298 5'-GCAGGCTAGGGTACCGGTACTGGCACATT-3' and with the reverse primer 5'-GTTTTGGACTCGAGGGTACTAATGCTTCATT-3'. The size of the amplified product *atg9*(W607A/Y611A) was verified by restriction digest and by sequencing and afterwards digested with the restriction enzymes KpnI and XhoI. The product of the restriction digests from *atg9*(W607A/Y611A) was inserted into the KpnI and XhoI sites of pTC1 and the vector used to transform R19 (*his4 atg9*:: zeo^R) cells.

Qualitative And Quantitative Assessment Of Alcohol Oxidase (AOX) Degradation

The direct colony assay was used to verify and select *atg9* deletion mutant colonies, as described in previous publications (Tuttle and Dunn, 1995; Yuan *et al.*, 1997). For clarification, colonies were replica-plated from Zeocin to YNMH plates and incubated for 3-4 days. Replicas on nitrocellulose were then placed on YNDH plates for 12-15 h. The replica nitrocellulose was dipped in liquid nitrogen with a tweezer for 20 seconds with care not to sheer the nitrocellulose

to lyse the cells. Placing the nitrocellulose on Whatman paper soaked in 33 mM potassium phosphate buffer, pH 7.5, containing 3.4 U/ml horseradish peroxidase, 0.53 mg/ml 2,2'-azino-bis(3-ethylbenz-thazoline-6-sulfonic acid), and 0.13% methanol at room temperature for 60-90 minutes allows visualization of colonies that are unable to degrade AOX. For the liquid medium assay, cells are grown to saturation in 20 mls YNM with methanol as carbon source. After 40 hours' incubation, 0.4 g of powdered glucose or 100 µl of ethanol was added. At 0 and 6 hours of glucose or ethanol adaptation (8.0 OD_{600}), 2 ml aliquots of glucose or ethanol were pelleted and resuspended in 1 ml 20 mM Tris, pH 7.5, containing 50 mM NaCl, 1 mM EDTA, 1 mM PMSF, 1 µg/ml pepstatin A, and 0.5 µg/ml leupeptin. 0.5 ml glass beads (425-600 microns) were used to lyse the cells by vortexing. The glass beads and cellular debris were removed by centrifugation and AOX measured by adding 50 µl of this extract to 3 mls of reaction mix containing 3.4 U/ml horseradish peroxidase and 0.53 mg/ml 2,2'-azino-bis(3-ethylbenz-thazoline-6-sulfonic acid) in 33 mM potassium phosphate buffer, pH 7.5 (Tuttle *et al.*, 1993; Tuttle and Dunn, 1995). The addition of 10 µl methanol initiated the reaction, which was then continued at room temperature for 15-30 minutes. The assay was quenched by addition of 200 µl of 4 N HCl and the absorbance read at 410 nm.

Western Blot Analysis

Cells were grown for 16 hours in 20 ml YNM and then adapted to YND or YNE. Cell aliquots were collected by centrifugation. The cells were pelleted and lysed in 100-150 µL of 67 mM Tris, pH 6.8, 2% SDS, 10% glycerol, 0.1% bromophenol blue, 1.5% DTT solution and 2 µL of PIC (200 mM phenylmethylsulfonyl fluoride (PMSF), 14.5 mM pepstatin A, 105 mM leupeptin in DMSO) by vortexing (four times at one-minute intervals) with glass beads for SDS-PAGE. After the sample preparation, they were heated at 100 °C for 5 minutes and cell debris

was removed by centrifugation. Fifteen to thirty microliters of each sample were loaded onto 10% or 10-15% SDS-PAGE. The proteins were then transferred to nitrocellulose by Trans-Blot SD-Dry Transfer Cell (Bio-Rad Laboratories, Hercules, CA) for 1.15-1.5 h, depending on whether the proteins being transferred were small or large respectively. The blots were blocked in 5% nonfat dried milk in PBS containing 0.1% Tween 20 (PBS-T) for 2 hours at room temperature, incubated with mouse anti-GFP or mouse anti-HA primary antibody (Covance Inc., Princeton, NJ) overnight at 4°C, and then incubated in 2% nonfat dried milk with secondary goat anti-mouse antibody conjugated with HRP (Covance Inc., Princeton, NJ) for 2 h at room temperature. After each step the blots were washed 3 times in PBS-T. HRP was detected using ECL-plus (Amersham, Piscataway, NJ) and quantified using the Typhoon 9400 laser scanner (Molecular Dynamics, Sunnyvale, CA).

Measurements of Protein Degradation

The degradation of cellular proteins during nitrogen starvation was performed as described previously (Tuttle and Dunn, 1995; Yuan *et al.*, 1999). Endogenous proteins were radiolabeled with 1 μCi/ml ^{14}C-valine for 16 h in 0.67 % yeast nitrogen base, 2% glucose, 0.4 mg/l biotin, and 40 μg/l histidine or arginine (if needed). The cells were then washed and switched to nitrogen starvation medium containing 0.17 % yeast nitrogen base (without amino acids and NH_4SO_4) and 2% glucose and supplemented with 10 mM valine. Aliquots were removed at 2 – 24 hours of chase and trichloroacetic acid (TCA) added to a final concentration of 20%. Acid soluble and insoluble radioactivity was separated by centrifugation and the radioactivity present measured by scintillation counting. The rates of protein degradation were calculated from the slopes of the linear plots of TCA-soluble radioactivity versus time of chase.

Fluorescence Microscopy and FM 4-64 Labeling

Cells were grown in either YPD or YNM for 20 hours for visualization of GFP or RFP fusion protein expression. Cells grown on YNM medium were then transferred to YND or YNE for 2 hours. FM 4-64 (Molecular Probes, Eugene, OR) was added to a final concentration of 20 μg/ml and the cells incubated for 2-12 hours prior to nutrient adaptation. The cells were washed of unbound FM 4-64 and examined immediately using a Zeiss Axiophot fluorescence microscope. Image capture was done using a SPOT camera (Diagnostics Instruments, Inc., Sterling Heights, MI) interfaced with IP Lab software.

Results

Atg9 and Atg17 Occasionally Co-localize

Atg9 is known to localize transiently to the PAS in *S. cerevisiae*(Reggiori *et al.*, 2005). We have previously shown that Atg9 did not colocalize with Atg8, but studies have shown that these proteins may transiently interact (Tellkamp, unpublished observations). To determine whether Atg9 is present in a compartment distinct from the PAS, monomeric RFP tagged Atg9 was co-expressed with GFP-Atg17, a marker for the PAS (Oku *et al.*, 2006). mRFP-Atg9 did not completely co-localize with the GFP-Atg17 (Figure 5-1). The GFP-Atg17 localized to a number of dots not containing mRFP-Atg9, but remarkably near dots containing mRFP-Atg9. Meanwhile, GFP-Atg17 did localize with mRFP-Atg9 at the PC9 and PVS. Based on our observations, we propose that the Atg9-containing PVS abuts the Atg17-containing PAS, and that Atg9 may transit to the PAS during glucose-induced micropexophagy.

Ppatg9 Partial Deletion And Site-Specific Mutants Are Defective In Glucose-Induced Pexophagy And Starvation-Induced Autophagy

When the available carbon source is restricted to methanol, *Pichia pastoris* responds to this environmental stress by synthesizing peroxisomal enzymes such as alcohol oxidase (AOX)

for degradation. When this stress is relieved by a media switch from methanol to glucose, the peroxisomes are selectively sequestered and degraded via micropexophagy. A number of ATG gene products have been shown to be required for autophagic induction. We have shown that Atg9 transports from unique peripheral vesicles to the expanding SM where it functions. Our aim was to delete highly conserved regions of Atg9 or sequences identified by motif databases to be important. Thus, the following regions were deleted: the N-terminus prior to the first transmembrane domain (atg9ΔN), the loop between the third and fourth transmembrane domains (atg9ΔL3), the C-terminal region just past the last transmembrane domain (atg9Δ579-668), a motif present in Pex5 and Pex14 (atg9-W607A/Y611A) and recognized by Pex13 and Pex14 for Pex5 binding [the significance of the domain present in Pex14 is not understood], and a motif with high homology to the ER export motif for transmembrane proteins (atg9ΔQQHKA 881-885) (Figure 5-2). Smaller motifs of higher homology of the third loop were subsequently identified and deleted (atg9Δ489-502; atg9ΔE491,4A). The aforementioned mutants were tagged at the N-terminus with GFP.

We have shown previously that Atg9 is essential for glucose-induced micropexophagy specifically SM expansion. We first screened these mutants for functionality: whether they were able to rescue the R19 insertion mutant (Chang *et al.*, 2005; Schroder and Dunn, 2006). Within 6 h of glucose adaptation, more than 80% of AOX was degraded by wild-type GS115 cells (Figure 5-3). In comparison, only about 40% of AOX was degraded in R19 cells. R19 cells expressing GFP-Atg9 was able to efficiently degrade AOX. A moderate rescue of R19 was observed when expressing atg9ΔN and atg9ΔQQHKA with about 50% AOX degraded. atg9ΔL3, atg9Δ489-502, atg9Δ579-668/ΔQQHKA and atg9ΔWEGKY failed to complement R19 as well, with no less than 30% AOX activity remaining. R19 cells expressing atg9Δ579-668

exhibited less AOX degradation than R19 itself. Interestingly, cells expressing the atg9Δ579-668/ΔQQHKA double mutant degraded AOX better than cells expressing atg9Δ579-668 alone. None of the atg9 mutants supported AOX degradation as seen in wild-type cells, implying that all the domains were essential for Atg9 function in glucose-induced micropexophagy.

We had also shown that Atg9 is required for nitrogen starvation-induced proteolysis (Chang *et al.*, 2005). Therefore, we then examined the ability of cells expressing these atg9 mutants to degrade endogenous protein during nitrogen starvation (Figure 5-4). The atg9 mutants were expressed in cells lacking functional Atg9 and harboring an arginine auxotrophy (WDY55) to permit amino acid starvation-induced proteolysis. When wild-type cells were starved for nitrogen and amino acids, the cellular protein degradation average rate was 0.4% per hour. Protein degradation of atg9 lacking cells on average was 0.05% per hour, an 8-fold lower rate than wild-type. Degradation in cells harboring full-length GFP-Atg9 was similar to that of the wild-type control. WDY55 cells expressing atg9 harboring mutations encompassing regions of the loop between the third and fourth transmembrane domains, atg9Δ489-502 and atg9ΔE491,4A, or atg9Δ579-668 poorly degraded endogenous proteins at 0.15% per hour. When atg9-W607A/Y611A or atg9ΔN were expressed protein degradation was only partially restored to almost 0.2% per hour. The data suggest that these mutants are not fully functional in autophagy induced by amino acid starvation.

Atg9ΔL3 and Atg9Δ579-668 Mutants Remain In The ER

We have shown previously that the loop #3 between transmembrane regions #3 and #4 was required for the exit of Atg9 out of the ER (Chang *et al.*, 2005; Schroder and Dunn, 2006). Because the minimal sequence necessary for atg9ΔL3 to be retained in the ER was not known, the homology of *P. pastoris, S. cerevisiae, D. melanogaster, C. elegans,* and *H. sapiens* was matched. The domain of the highest homology within atg9ΔL3 is the di-acidic YxDxE motif

(Schroder and Dunn, 2006). This sequence was first localized to the C-terminus of the VSV-G protein; the YKDAD motif is essential for the cystic fibrosis transmembrane conductance regulator to exit form the ER. The critical 6 amino acids located in the highest homology region were shown to be essential for CFTR from the ER, and this is localized to an accessible loop as in the homologous Atg9 sequence. A similar motif is also present in Kir2.1, a potassium channel membrane protein (Schroder and Dunn, 2006). To determine the significance of the di-acidic motif as compared to the larger atg9ΔL3 mutant, two mutations were made within the region of highest homology. atg9Δ489-502 obliterated the sequence altogether. Atg9ΔE491,4A changed the acidic glutamates at positions 491 and 494 to non-reactive alanines. These atg9 mutants were not functional for micropexophagy or autophagy (see above).

After finding that no variant of the atg9ΔL3 mutant is able to complement R19 cells by AOX assay, the cellular distribution of these atg9 mutants during glucose-induced micropexophagy was examined. DMM1 cells expressing GFP-Ppatg9ΔL3 was found at the ER surrounding the nucleus (Figure 5-5). In addition, the cellular location of GFP-Ppatg9Δ489-502 and GFP-Ppatg9ΔE491,4A was restricted to the ER near the cell surface and surrounding the nucleus (Figure 5-6). These cells showed the same fluorescence distribution as the R19 cells no matter which Ppatg9ΔL3 variant was expressed. Next, we examined the cellular location of GFP-atg9Δ579-668 expressed behind the GAPDH promoter. The GFP-atg9Δ579-668 was present at the peripheral and nuclear ER (Figure 5-7). Thus, in addition to the loop region between the third and fourth transmembrane domains, residues 579-668 of Atg9 appear to also be an ER exit motif.

To verify that the fluorescing region was indeed the ER which surrounds the nucleus in *P. pastoris* cells, R19 cells harbouring the ER-localizing mutations were fixed with DAPI and

observed by fluorescence microscopy (Figure 5-8). Each R19 strain expressing these GFP-tagged atg9 mutants exhibited the same morphology: the blue DAPI-stained nucleus was surrounded by GFP.

The preliminary trafficking of Atg9, a transmembrane protein, was never before defined. Hence, the finding that certain atg9 mutants remain in the ER is noteworthy. Moreover, there appear to be two distinct ER retention and/or exit motifs completely independent of one another.

Atg9ΔQQHKA Remains At The PC9

The QQHKA sequence at the C-terminus of Atg9 was revealed by a database inquiry to be a putative C-terminal ER exit motif. DMM1 cells expressing BFP-SKL and GFP-Ppatg9ΔQQHKA behind the GAPDH promoter were visualized during glucose-induced micropexophagy. GFP-Ppatg9ΔQQHKA localized to one or more punctate cytosolic structures of uniform size at the cell periphery (Figure 5-9). The GFP-atg9ΔQQHKA was not visualized at the PVS or the SM.

Since the localization of atg9ΔQQHKA appeared to be restricted to the PC9, we decided to further characterize this compartment by subcellular gradient fractionation (Figure 5-10). Under our gradient conditions, the ER marker pCPY and the mitochondrial marker CoxIV-GFP distributed between fractions 9-11, while the vacuole marker CPY and tER marker Sec13 migrated at fractions 3-5. Full-length GFP-Atg9 displayed a bimodal distribution peaking at fractions 7 and 11 in cells grown in methanol alone. Upon switching to glucose, GFP-Atg9 was peaked at fractions 4-6. During glucose adaptation, atg9ΔQQHKA localized broadly to fractions 7 through 13 with a peak at fraction 9. At this time, atg9Δ579-668 visualized by fluorescence to be at the ER, localized with the ER marker (fractions 9-11), but was also found at fractions 3 through 7. Based on this data, we suggest that the PC9 compartment distributed around fraction 9 lighter in density than the ER and mitochondria, but heavier than the tER and

vacuole. Upon glucose adaptation, GFP-Atg9 redistributed from a bimodal distribution to a lighter fraction, which may be the analogous to the PVS and/or SM.

Atg9-W607A/Y611A Fails To Localized To The Sequestering Membranes (SM) On The Vacuole

The WEGKY domain past the Atg9 last transmembrane domain present at amino acids 607-611 was revealed by database inquiry to be the motif shared by Pex14 and Pex5. Since this motif appears to be the same motif in Pex5 required for the interaction of Pex13 and Pex14, we decided to delete the WEGKY site. R19 cells expressing GFP-atg9-W607A/Y611A were examined by fluorescence microscopy (Figure 5-11). Upon glucose adaptation, the WEGKY mutant localized to the cytosolic PC9, the PVS near the base of the SM and occasionally at the PAS near the tips of the vacuolar arms but failed to traffic to the SM.

We also compared the molecular size of this mutant with normal GFP-Atg9 and the other mutants. Full-length form of GFP-Atg9 migrated as two bands; one at 130kDa, the predicted size, and a second at a slightly larger size of about 140kDa (Figure 5-12). Meanwhile, atg9-W607A/Y611A migrated as a single band at 130kDa. The slower migrating band was not observed. Upon comparison, the atg9ΔQQHKA mutant displayed a doublet; one at the predicted mass and a second unknown band migrating slightly larger.

Atg9ΔN Localizes To The Vacuole But Is Not Functional By AOX Assay

Previous work has shown that the N-terminus of ScAtg9 is vital for its interaction with ScAtg11 (He *et al.*, 2006; Chang and Huang, 2007). Furthermore, we have shown that Atg11 is needed for Atg9 transport to the PVS. The data presented in Figures 5-3 and 5-4 showed that the ΔN mutant was defective in both glucose-induced micropexophagy and starvation-induced proteolysis. DMM1 cells expressing GFP-PpAtg9ΔN were adapted from YNM to YND then examined by fluorescence microscopy. GFP-Atg9ΔN localized to the vacuole and SM (see

Chapter 3). Hence, an atg9 mutant lacking the N-terminus was able to transit to the SM. However, the presence of this mutant at the SM was not sufficient to support micropexophagy.

Sites Of Delay In Micropexophagy Caused By The Atg9 Mutants

We had observed that in cells lacking Vac8, a vacuolar membrane associated protein, micropexophagy was blocked at completion. That is, the SM completely surrounded the peroxisomes, but the peroxisomes were not degraded. However, when cells expressed *vac8* ΔARM4-6 or vac8 ΔARM5, SM nucleation from the vacuole was blocked (Fry *et al.*, 2006). Therefore, we decided to determine the sites of micropexophagy blockage in cells expressing the atg9 mutants. In atg9 null cells, the SM could be visualized around the peroxisomes, but the MIPA was not formed (Chang *et al.*, 2005). No cells expressing the mutant forms of atg9 exhibited blocks at nucleation or completion. Instead, cells harboring atg9 mutations exhibit vacuole and SM morphologies undergoing varying degrees of expansion based on the SM extensions around the peroxisomes. In atg9ΔN mutants, micropexophagy appeared blocked at early expansion (see Chapter 3), with atg9Δ579-668, atg9ΔL3, and atg9ΔQQHKA mutants blocked at early or late expansion (see Figure 5-5, 5-7, and 5-9), and finally atg9(W607A/Y611A) cells showing a block during late expansion (see Figure 5-11). These are differences are based on observations of the extents of sequestration by the vacuole and SM relative to the BFP-tagged peroxisomes. The effects of these mutants on MIPA assembly that occurs during late expansion has not yet been examined.

Discussion

In order to better characterize the molecular role of Atg9 in pexophagy, we have set out to define those amino acid motifs responsible for the trafficking and function of Atg9.

We have identified a number of motifs that are required for exiting the ER, the PC9, and the PVS. There exist two domains required for Atg9 to exit the ER (aa 489-502 specifically E491

and E494 and aa 579-668). The C-terminal QQHKA is necessary for Atg9 to exit the PC9, while W607 and Y611 are essential for Atg9 to become associated with the SM. None of these mutants is functional during glucose-induced micropexophagy or during starvation-induced proteolysis. Finally, the N-terminus is required for function, but not for trafficking of Atg9 to the SM. Our data demonstrates that the specific Atg9 domains are essential for its trafficking and function during micropexophagy. Furthermore, the association of Atg9 with the SM is critical for its function.

ER Exiting Motifs Of Atg9

Atg9ΔL3 remains in the ER. The minimal sequence required for cycling of Atg9 from the ER was narrowed down by sequential site-directed mutatgenesis to be the E491 and E494. These glutamates are the most highly conserved residues in this region. The importance of this motif to the early trafficking of Atg9 and its high homology emphasizes that the putative loop between the third and fourth transmembrane domains is cytosolic. The localization of GFP-atg9ΔQQHKA to the PC9 compartment indicates that the extreme end of the C-terminus is also cytosolic. The requirement for the N-terminus in interactions with ScAtg11 for ScAtg9 to localize to the PAS and the very early early expansion block for atg9ΔN mutants supports a cytosolic N-terminus model. Thus, both the putative N- and C-terminus appear cytosolic, and the predicted 5 or 6 transmembrane domains lends toward six transmembrane domains—an even number for both termini to be cytosolic. However, the ER exit motif just past the last transmembrane domain and the presence of the WXXXF/Y motif in the same area, both in the vicinity of the least predicted sixth transmembrane domain, argue against the existence of this sixth transmembrane region, unless the region is present somewhere else.

Our data also show that Atg9Δ579-668 fails to exit from the ER. Multiple regions of interest were found upon inspection of the deleted sequence, which is C-terminal of the last

putative transmembrane domain. The WEGKY pentapeptide motif itself was not considered to be the critical motif as point mutations within this sequence led to a phenotype other than ER localization. Within this region there exists a DxE export signal (a.a. 588-592, **D**P**E**V**S**, a.a. 606-608 **E**W**E**, a.a. 558-562 **D**FFR**E**F**S**) (Barlowe, 2003) is a di-acidic motif involved in recognition by Sec24 for incorporation into the COPII complex via Sec23-Sec24 complex interaction (Votsmeier and Gallwitz, 2001; Barlowe, 2003). The dihydrophobic FF/YY/LL/FY motif (a.a. 559-563 **FF**RE**F**) occurs in the cytoplasmic domains of the transmembrane cargo p24 family members as well as the ERGIC53/Emp47 and the Erv41/46 complexes and is thought to be required for their transport from the ER and throughout the cell (Sato, 2004). Interestingly, the most highly conserved region when comparing *P. pastoris* and *S. cerevisiae* are amino acids 600-624 which ends with a tyrosine at amino acid 624 and contains 2 other tyrosines about 5 amino acids apart in both directions. A series of these tyrosines composes the motif localized to the tail of the ERGIC53/Emp47 family and is thought to be important for these transmembrane proteins' transport from the ER (Sato, 2004). Thus, future studies are necessary to better define this domain.

These ER-exit motifs would likely function at the cytoplasmic surface of the ER possibly interacting with newly forming COPII vesicles. Evidence suggests that Sec24 has a major role in the recognition of cargo to be packaged into these vesicles. However, Sec23 and Sar1 have also been implicated in cargo recognition and transport of proteins out the ER (Sato and Nakano, 2007). Further studies are needed to identify those proteins that interact with these domains thereby promoting Atg9 exit from the ER.

PC9 Exiting Motif Of Atg9

The QQHKA domain present at the C-terminal tail of Atg9 is homologous to a KKXX-type ER retention motif. The KKXX C-terminal motif retains transmembrane proteins in the ER

and directs their retrograde trafficking from the *cis*-Golgi in yeast (Gaynor *et al.*, 1994). Disrupted KKXX motifs are transported to the vacuole and proteolytically cleaved by Pep4 (Gaynor *et al.*, 1994). In fact, when only one lysine is mutated to glutamine in Wbp1 (a protein required for N-linked glycosylation of proteins in the ER) it is transported to the vacuole (Gaynor *et al.*, 1994). However, atg9ΔQQHKA was able to exit the ER to reside at the PC9. During glucose-induced micropexophagy, atg9ΔQQHKA failed to exit the PC9 compartment. Thus, the dilysine requirement may be very rigid for this motif; a second alternative is that the QQHKA domain may not be sufficient alone for ER retention. Self-oligomerization enables proteins containing the KKXX domain such as p24 to exit the ER (Sato *et al.*, 2003). Differential binding mechanisms discriminate between ER-resident transmembrane proteins harbouring the KKXX domain and p24 proteins. Thus, even if Atg9 harbours a putative ER retrieval motif, its QQHKA domain could be superseded if Atg9 is present in a dimeric form.

The QQHKA domain is required for Atg9 to exit the PC9. Atg9 may be activated by or interact with another protein via this motif. We have shown that Vps15 and Atg11 are required for Atg9 to transit from the PC9 (Chang *et al.*, 2005). Vps15 is a subunit of the PI3K complex and appears to mediate SM nucleation and expansion in pexophagy. Atg11 mutants exhibit arrest during during SM expansion (Chang *et al.*, 2005). Atg11 interacts with Atg9, but at its N-terminus. No direct interaction has been shown to exist between Atg9 and Vps15. However, two proteins may act downstream of Vps15 to interact with the QQHKA domain of Atg9, thus explaining the requirement for Vps15 in early Atg9 trafficking. The serine/threonine kinase Vps15 activates the PI-3 kinase Vps34 which regulates PtdIns(3)P levels. The PtdIns(3)P binding proteins Atg18, Atg20, Atg21, Atg24 are known to be required for autophagy. Atg18 is required for a nucleation event and has no affect on Atg9 trafficking (Stromhaug *et al.*, 2001;

Chang *et al.*, 2005). Atg21 is required for the lipidation of Atg8 and thus the formation of the MIPA, a late expansion event (Stromhaug *et al.*, 2004). Atg24 is required for completion (Ano *et al.*, 2005). Little is known about Atg20 except that it forms a complex with Atg11 and Atg24 at the PAS. Atg20 contains a PX domain, a domain involved in protein sorting and membrane trafficking that interacts with PI3-P (Yorimitsu and Klionsky, 2005). Atg20 seems to be a good candidate responsible for the transmembrane protein Atg9's trafficking from the PC9. Further studies are needed to evaluate these possibilities.

PVS Exiting Motif of Atg9

The WEGKY motif is a WXXXY/F domain within Atg9. Starvation-induced macroautophagy in addition to glucose-induced micropexophagy have been shown to be defective in atg9-W607A/Y611A. atg9-W607A/Y611A localizes to the PC9, the PVS and the PAS but fails to associate with the SM during glucose-induced micropexophagy. Proteins sequester at the PVS prior to their assembly into the expanding SM and the PAS is thought to be an organization site for the expansion of the vacuolar membranes during MIPA formation (Dunn *et al.*, 2005).

The peroxisome membrane protein, Pex14, contains the WXXXY/F domain interacts with the seven WXXXY/F domains of Pex5 (peroxisome import receptor) (Saidowsky *et al.*, 2001). The N-terminus of Pex14 has been shown to be required for macropexophagy in *H. polymorpha*. Pex14 has also been shown to be the sole component of the peroxisomal translocon required for pexophagy (Zutphen *et al.*, 2007). The N-terminus of Pex14, a coiled-coil membrane protein, could bind to the WEGKY domain of Atg9. This action might be stabilized by interactions between the coiled-coil regions of Pex14 and Atg11. A second peroxisome membrane protein, Pex13, also interacts with the WXXXF/Y motifs of Pex5 (Otera *et al.*, 2002). However, Pex13 has been shown not to be required for pexophagy (Zutphen *et al.*, 2007).

Nevertheless, it is possible that Atg9 and Atg11 may interact with the Pex13/Pex14 complex thereby directing the movements of the SM around the peroxisomes.

We have observed that during glucose-induced micropexophagy GFP-Atg9 migrates as a doublet on Western blots. However, a doublet is not observed with atg9-W607A/Y611A. The slower migrating band would be consistent with a tyrosine phosphorylation within the WEGKY motif. Two likely protein tyrosine kinases are Yak1 and Kns1. Yak1 is involved in glucose signaling and Kns1 has been shown to interact with Atg1 (Hartley *et al.*, 1994; Ptacek *et al.*, 2005; Pratt *et al.*, 2007). Further studies are necessary to determine whether either of these proteins phosphorylate Atg9.

Functional Domain Of Atg9

During micropexophagy, Atg9ΔN properly trafficks to the sequestering membranes of the vacuole but pexophagy does not proceed. Thus, the deletion of the N-terminus is presumably required for Atg9 function in a late stage of micropexophagy. Thus, the interaction of Atg9 with another protein as mediated by the N-terminus would occur late in micropexophagy. The N-terminus of ScAtg9 has been shown to bind to the second and the first coiled-coil regions of ScAtg11 (He *et al.*, 2006; Chang and Huang, 2007). The PAS is essential for MIPA formation (Dunn *et al.*, 2005). Thus, the interaction of Atg11 with Atg9 may be critical for a late micropexophagic step.

Atg24 may also require Atg9 function for membrane fusion events during micropexophagy. Pexophagosomes do not fuse with the vacuole during micropexophagy in *atg24* cells (Ano *et al.*, 2005). An interaction between Atg9 and Atg24 mediated by Atg9's N-terminus could explain this defect—the action of the two proteins together may be required for the final step of vacuolar engulfment.

Summary

The appearance of the SM in cells harboring mutant Atg9 emphasizes that Atg9 is required for early and late expansion during micropexophagy. Furthermore, cells expressing mutant forms of Atg9 were defective in expansion, not nucleation or completion. Trafficking mutants of Atg9 did not support micropexophagy. These mutants failed to associate with the SM suggesting that Atg9 functions at the SM. We have also shown that there exists a domain within the N-terminus that is required for Atg9 function at the SM. The data demonstrate that the movements of Atg9 to the SM are essential for SM expansion.

Table 5-1: *Pichia pastoris* strains

Name	Genotype	Reference
GS115	*his4*	(Cregg *et al.*, 1985)
PPF1 (PPY12)	*arg4 his4*	(Yuan *et al.*, 1997)
SMD1163	*his4 pep4 prb1*	(Tuttle and Dunn, 1995)
DMM1	GS115::pDM1 (P_{AOX1}BFP-SKL, ZeocinR)	(Kim *et al.*, 2001)
R19	GS115 *atg9-1::*Zeocin	(Stromhaug *et al.*, 2001)
LAM2	PPF1 *atg9Δ*::ARG4	This study
WDY55	*arg4 his4 atg9-1::*ZeocinR	This study
WDY100	PPF1 *his4 arg4*::pWD26 (P_{GAPDH} RFP-ATG17, ARG4)	This study
TC10	R19 *his4*::pTC1 (P_{GAP} GFP-ATG9, HIS4)	(Chang *et al.*, 2005)
AJM22	GS115 *his4*::pPS69(P_{GAPDH} GFP/HA-ATG2, HIS4)	This study
AJM25	AJM22::pAJM6 (P_{GAPDH} mRFP-ATG9, ZeocinR)	This study
AJM26	GS115 *his4*::pAJM6 (P_{GAPDH} mRFP-ATG9, Zeocin)	(Chang *et al.*, 2005)
AJM32	AJM26 *his4*:: pPS64 (P_{GAPDH} GFP/HA-ATG11, HIS4)	(Chang *et al.*, 2005)
AJM33	AJM26 *his4*:: pPS55-G12 (P_{GAPDH} GFP/HA-ATG18, HIS4)	This study
ASK4	R19 *his4*::pGFP-G14(ΔL3) (P_{GAP} GFP-atg9ΔL3, HIS4)	This study
ASK5	R19 *his4*::pGFP-G14(ΔN) (P_{GAP} GFP-atg9ΔN, HIS4)	This study
ASK6	R19 *his4*::pGFP-G14(ΔC) (P_{GAP} GFP-atg9ΔC, HIS4)	This study
ASK7	DMM1 *his4*::pGFP-G14(ΔL3) (P_{GAP} GFP-atg9ΔL3, HIS4)	This study
ASK8	DMM1 *his4*::pGFP-G14(ΔN) (P_{GAP} GFP-atg9ΔN, HIS4)	This study
ASK9	DMM1 *his4*::pGFP-G14(ΔC) (P_{GAP} GFP-atg9ΔC, HIS4)	This study
LAM6	R19 *his4*::(P_{GAPDH} GFP-atg9 ΔQQHKA, HIS4)	This study
LAM7	R19 *his4*::(P_{GAPDH} GFP-atg9 Δ579-668, HIS4)	This study
LAM8	R19 *his4*::(P_{GAPDH} GFP-atg9 Δ579-668 / ΔQQHKA, HIS4)	This study
LAM9	DMM1 *his4*::(P_{GAPDH} GFP-atg9 ΔQQHKA, HIS4)	This study
LAM10	DMM1 *his4*::(P_{GAPDH} GFP-atg9 Δ579-668, HIS4)	This study
LAM11	DMM1 *his4*::(P_{GAPDH} GFP-atg9 Δ579-668 / ΔQQHKA, HIS4)	This study
LAM19	R19 *his4*::(P_{GAPDH} GFP-atg9 Δ489-502, HIS4)	This study
LAM20	DMM1 *his4*::(P_{GAPDH} GFP-atg9 Δ489-502, HIS4)	This study
LAM36	R19 *his4*::(P_{GAPDH} GFP-atg9 W607A/Y611A, HIS4)	This study
LAM51	R19 *his4*::(P_{GAPDH} GFP-atg9 EΔ491,4A, HIS4)	This study
LAM53	AJM26 *his4*::pWD24 (P_{GAPDH} GFP-ATG17, HIS4)	This study
LAM61	WDY100 *his4*::(P_{GAPDH} GFP-atg9 ΔQQHKA, HIS4)	This study
LAM62	WDY100 *his4*::(P_{GAPDH} GFP-atg9 W607A/Y611A, HIS4)	This study
LAM65	WDY55 *his4 arg4 atg9Δ*::pTC1 (P_{GAPDH} GFP-ATG9, HIS4)	This study
WDY75	AJM26 *his4*::pWD21 (P_{GAPDH} GFP-PpATG8, HIS4)	This study

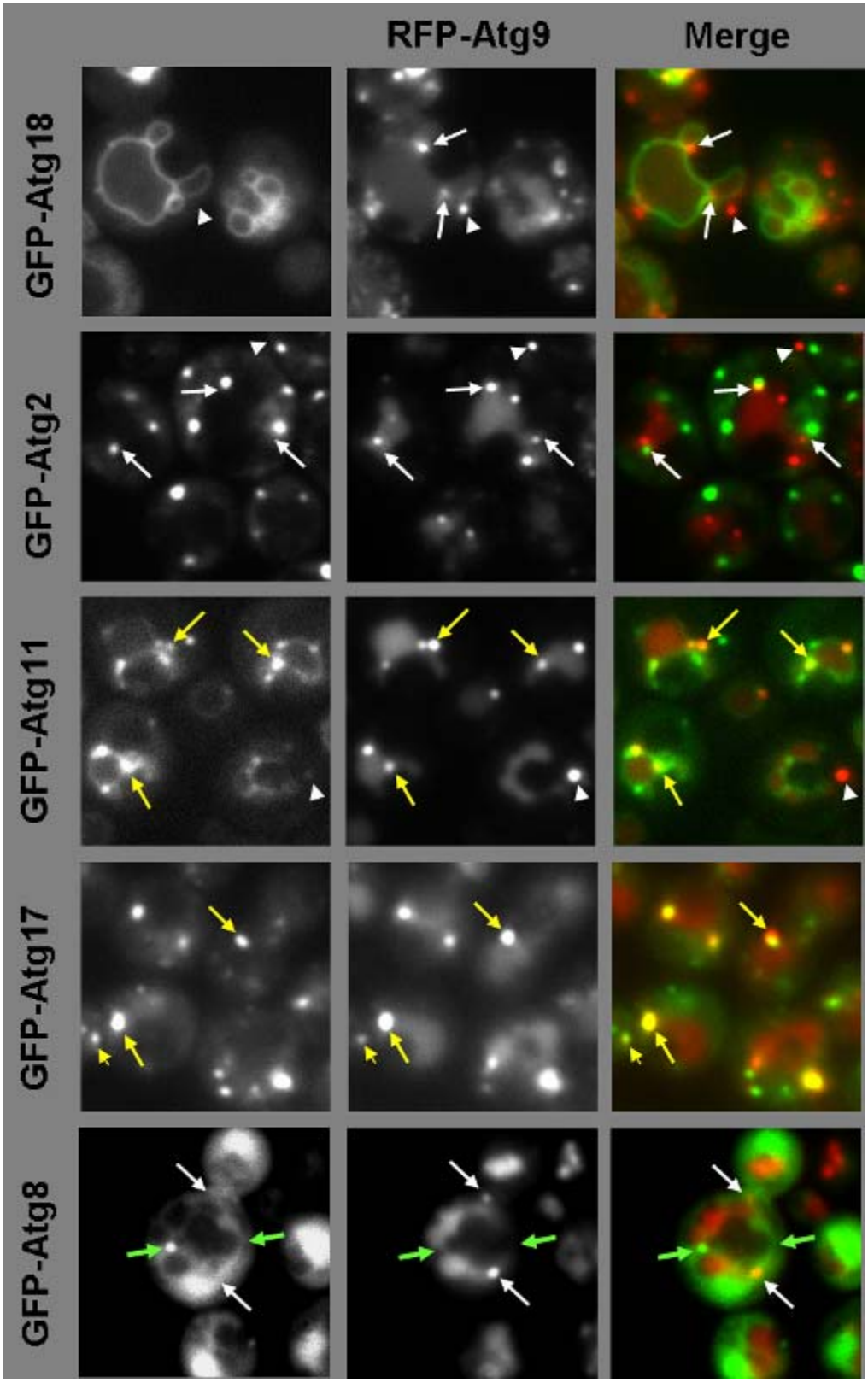

Figure 5-1. Localization of Atg9, Atg11 and Atg17 to the PVS. LAM25, LAM32, LAM33, LAM53, and WDY75 were grown in YNM, adapted to YND for 2 hours, and the Atg proteins

visualize by fluorescence microscopy. RFP-Atg9p is found at a peripheral compartment without Atg2 (white arrowhead), but with Atg17p (yellow arrowhead). RFP-Atg9p is also present at the PVS (white arrows) colocalized with Atg11p and Atg17p (yellow arrows). GFP-Atg8p is localized to the PAS and MIPA (green arrows).

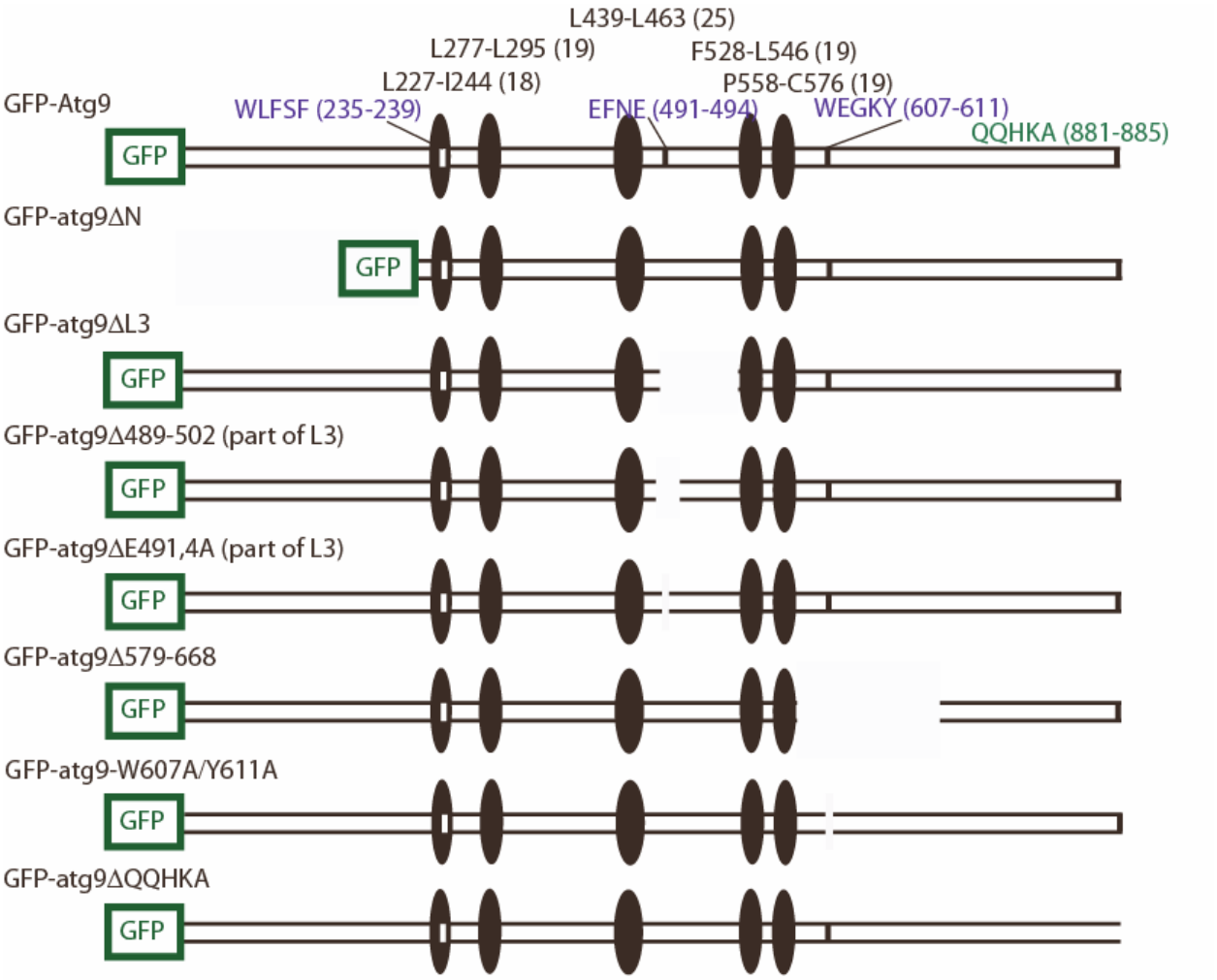

Figure 5-2. Linear structure of the PpAtg9 transmembrane protein and deletions performed by site-directed mutagenesis. Atg9 is an 885 amino acid long protein required for micropexophagy. The linear representation of Atg9 and its mutated regions are drawn to scale. GFP is N-terminally attached to Atg9. There exist 5-6 putative transmembrane (TM) domains. Five of putative TM domains are shown: L227-I244 (18 a.a.), L277-L295 (19 a.a.), L439-L463 (25 a.a.), F528-L546 (19 a.a.), and P558-C576 (19 a.a.), and are drawn to scale. Numerous motifs have been identified *in situ*. WLFSF (a.a. 235-239) and WEGKY (a.a. 607-611) are WXXXF/Y motifs shared with Pex5 and Pex14, although the WLFSF motif may be masked within the first transmembrane domain. The last 5 C-terminal amino acids are QQHKA (a.a. 881-885). Site-directed mutagenesis produced atg9ΔN, atg9ΔL3 (the region between the third and fourth transmembrane domain), atg9Δ489-502 (a highly conserved region of the region mutated in atg9ΔL3), atg9Δ579-668 (a conserved region after the last transmembrane domain), atg9-W607A/Y611A (the WXXXF/Y motif shared by Pex5 and Pex14), and atg9ΔQQHKA. GFP is attached to the most N-terminal region of each mutant.

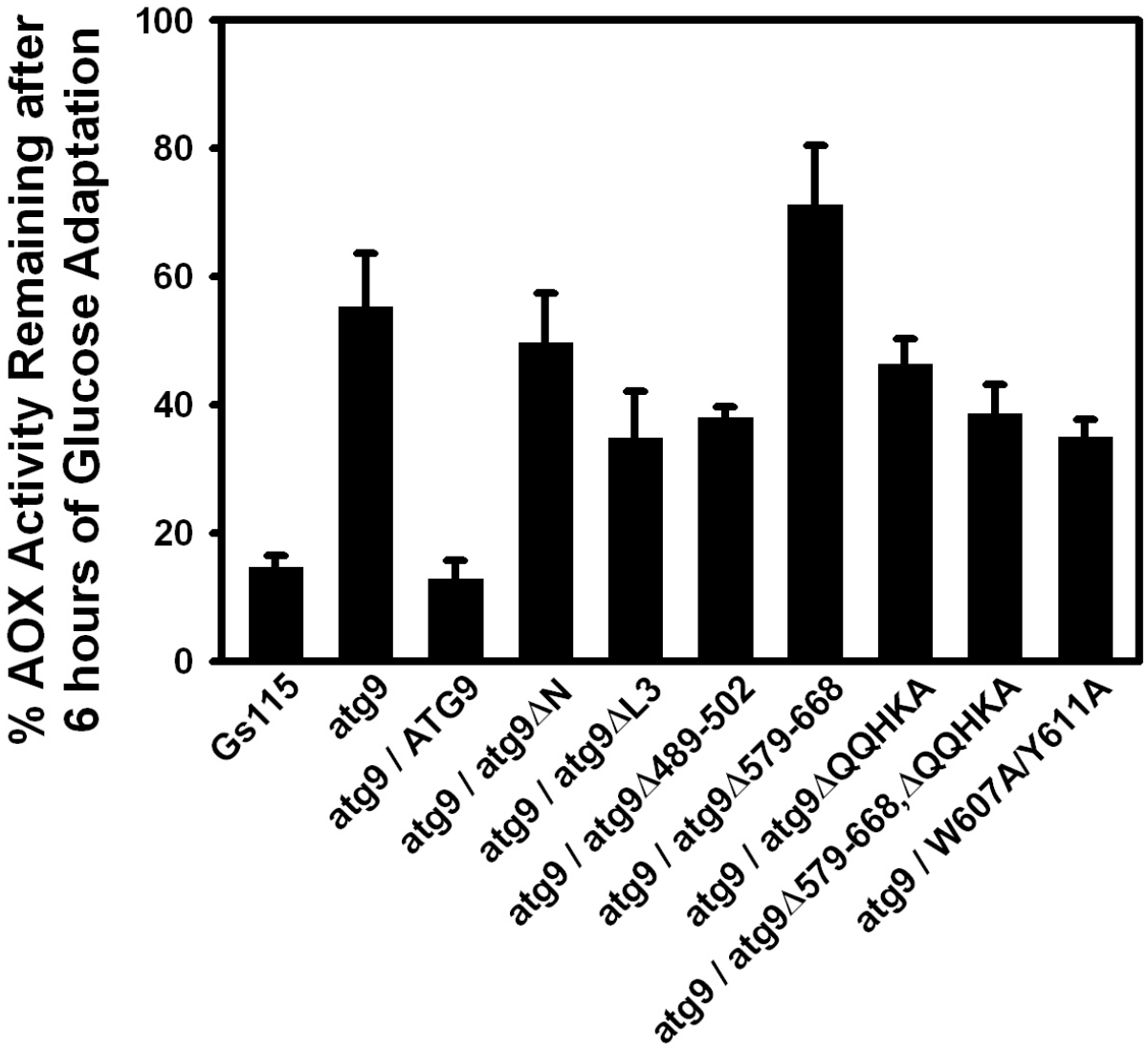

Figure 5-3. Atg9 mutants fail to support glucose-induced micropexophagy. Wild-type, *atg9* null mutants, and null mutants expressing mutant forms of *atg9* were grown in YNM and adapted to YND. AOX levels were measured at 0 and 6 hours post glucose adaptation. The values were expressed as the percentage of AOX activity remaining (average ± SEM).

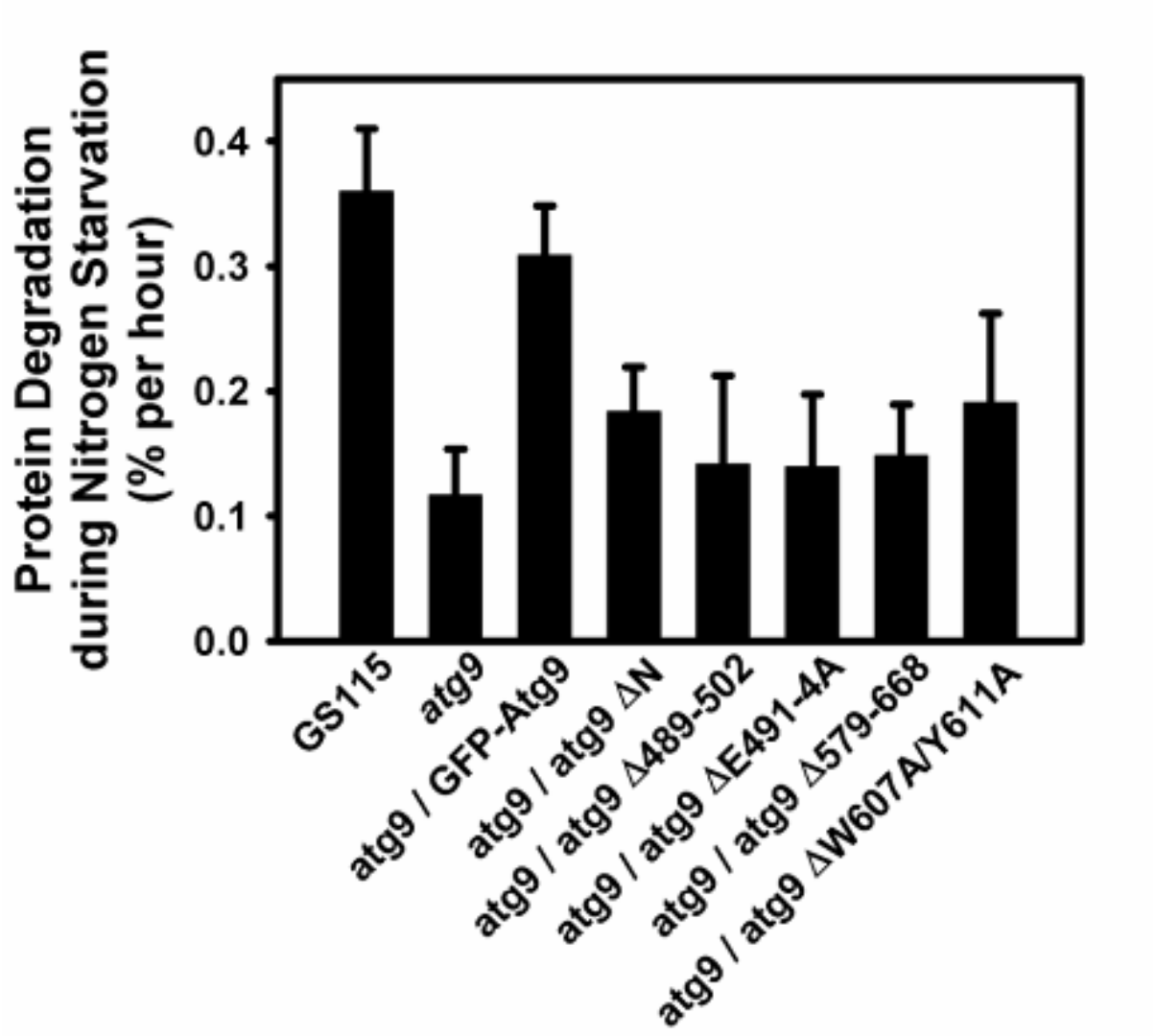

Figure 5-4. Protein degradation of Atg9 mutant cells during nitrogen starvation. Wild-type, *atg9* null mutants, and null mutants expressing mutant forms of *atg9* were grown in minimal medium with 14C-valine. After 18 hours, the cells were switched to nitrogen starvation medium and protein degradation measured as previously described in Materials and Methods.

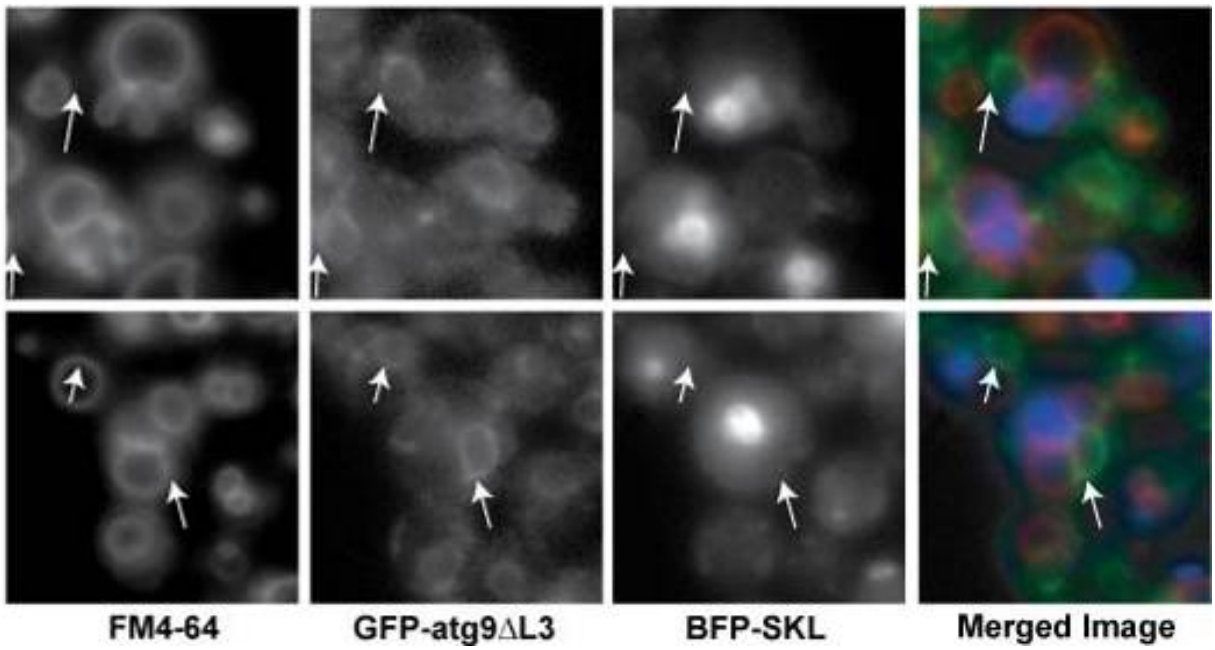

Figure 5-5. GFP-atg9ΔL3 remains in the ER during glucose-induced micropexophagy. DMM1 cells expressing BFP-SKL and GFP-atg9ΔL3 were grown in YNM in the presence of FM4-64. After 18 hours, the cells were adapted to YND for 2 hours and visualized by fluorescence microscopy. The GFP-atg9ΔL3 did not colocalize with the FM4-64 labeled vacuole or sequestering membranes that surrounded the BFP labeled peroxisomes. Instead, the GFP-atg9ΔL3 appeared at the cell periphery and around the nucleus (arrows).

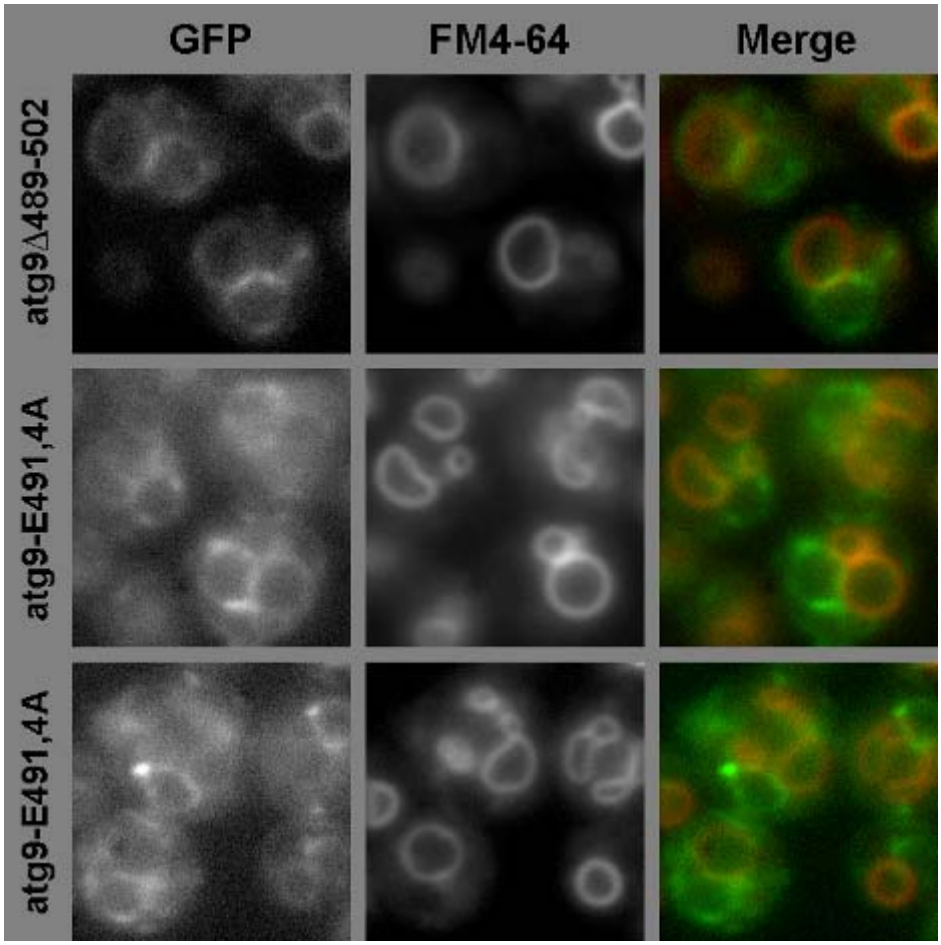

Figure 5-6. GFP-atg9Δ489-502 and GFP-atg9ΔE491,4A remain in the ER during glucose-induced micropexophagy. R19 cells expressing GFP-atg9Δ489-502 or GFP-atg9ΔE491,4A were grown in YNM in the presence of FM4-64. After 18 hours, the cells were adapted to YND for 2 hours and visualized by fluorescence microscopy. The GFP-atg9Δ489-502 or GFP-atg9ΔE491,4A did not colocalize with the FM4-64 labeled vacuole or sequestering membranes. Instead, the GFP-tagged proteins appeared at the cell periphery and around the nucleus.

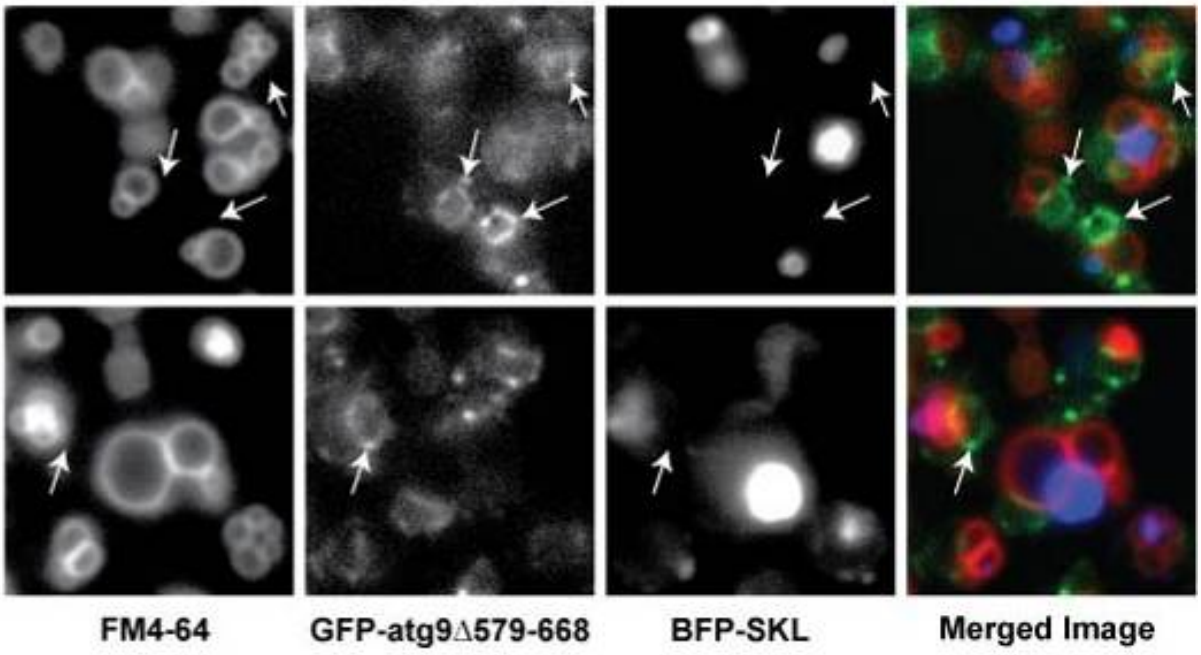

Figure 5-7. GFP-atg9Δ579-668 remains in the ER during glucose-induced micropexophagy. DMM1 cells expressing BFP-SKL and GFP-atg9Δ579-668 were grown in YNM in the presence of FM4-64. After 18 hours, the cells were adapted to YND for 2 hours and visualized by fluorescence microscopy. The GFP-atg9Δ579-668 did not colocalize with the FM4-64 labeled vacuole or sequestering membranes that surrounded the BFP labeled peroxisomes. Instead, the GFP-atg9Δ579-668 appeared at the nuclear membranes (arrows).

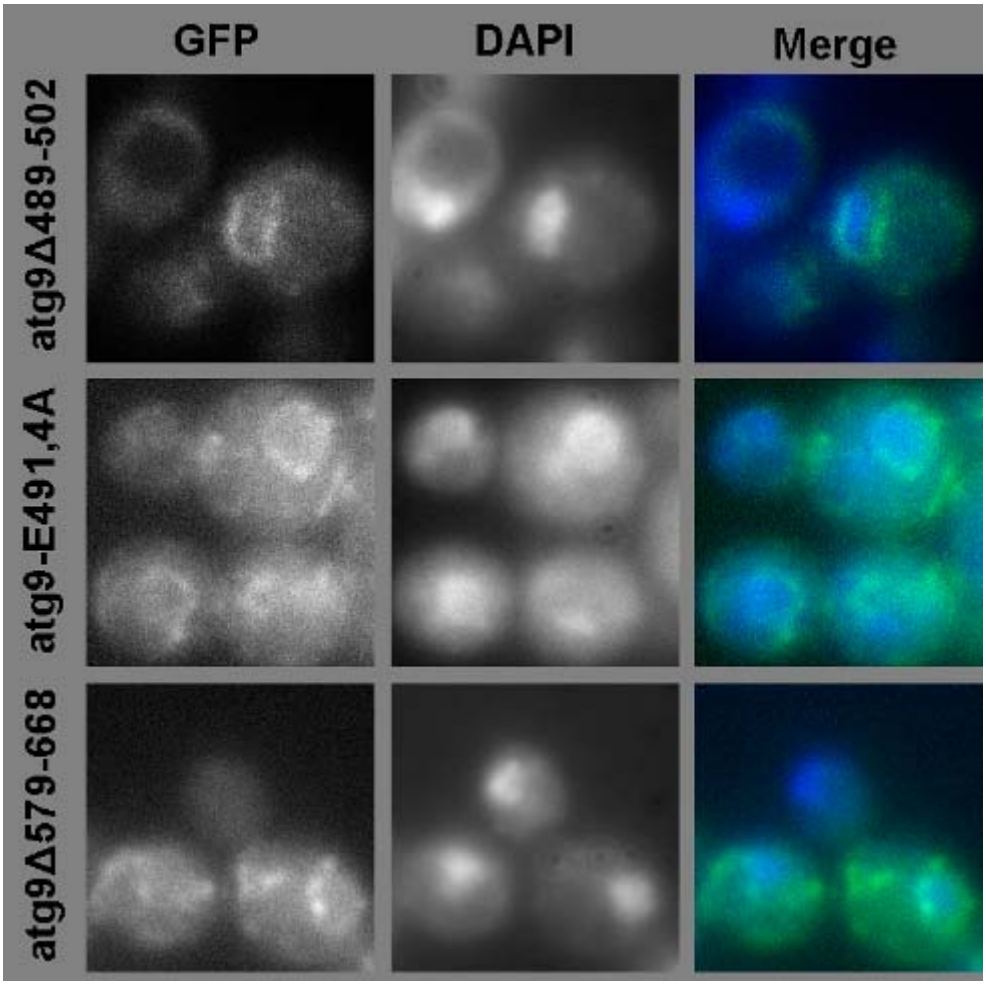

Figure 5-8. GFP-atg9Δ489-502, GFP-atg9ΔE491,4A, and GFP-atg9Δ579-668 localized to the nuclear membranes. To confirm that GFP-atg9Δ489-502, atg9ΔE491,4A, and atg9Δ579-668 all localize to the *P. pastoris* ER which surrounds the nucleus and not to another organelle, the nuclear DNA was stained with 4',6-diamidino-2-phenylindole (DAPI). R19 cells expressing GFP-atg9Δ489-502 or GFP-atg9ΔE491,4A or GFP-atg9Δ579-668 were grown in YNM in the presence. After 18 hours, the cells were adapted to YND for 2 hours and formaldehyde fixed. After staining the cells with DAPI, they were visualized by fluorescence microscopy. The GFP-tagged proteins were positioned at the nuclear membrane around the DAPI stained DNA.

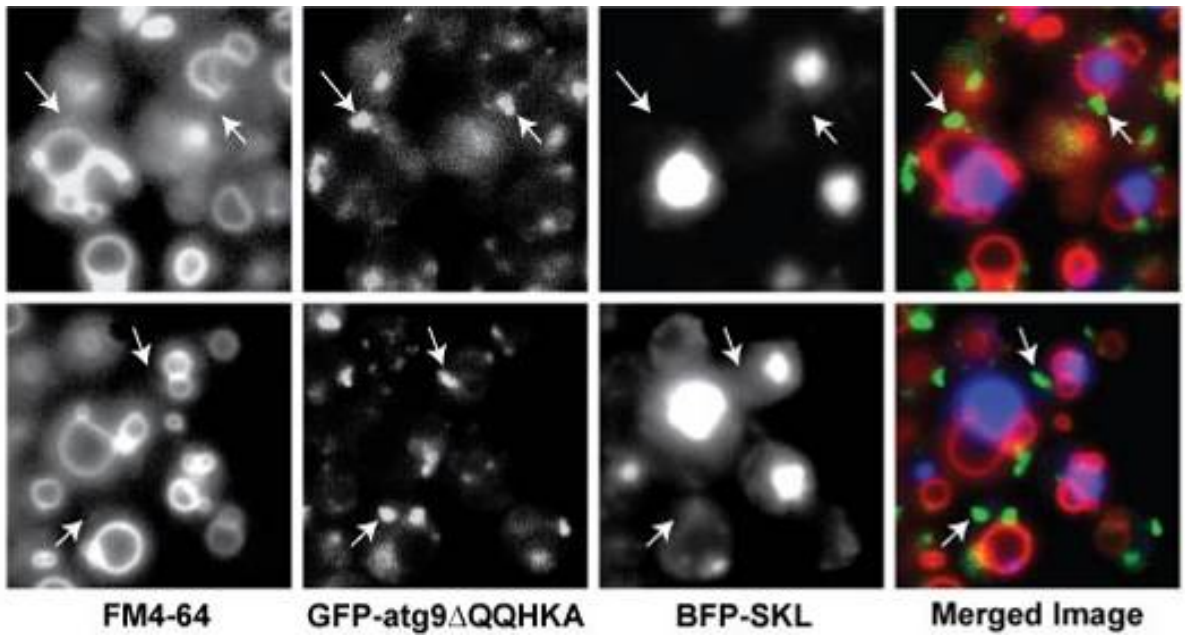

Figure 5-9. GFP-atg9ΔQQHKA remains at peripheral vesicles during glucose-induced micropexophagy. DMM1 cells expressing BFP-SKL and GFP-atg9ΔQQHKA were grown in YNM in the presence of FM4-64. After 18 hours, the cells were adapted to YND for 2 hours and visualized by fluorescence microscopy. The GFP-atg9ΔQQHKA did not colocalize with the FM4-64 labeled vacuole or sequestering membranes that surrounded the BFP labeled peroxisomes. Instead, the GFP-atg9ΔQQHKA localized to peripheral vesicles (arrows).

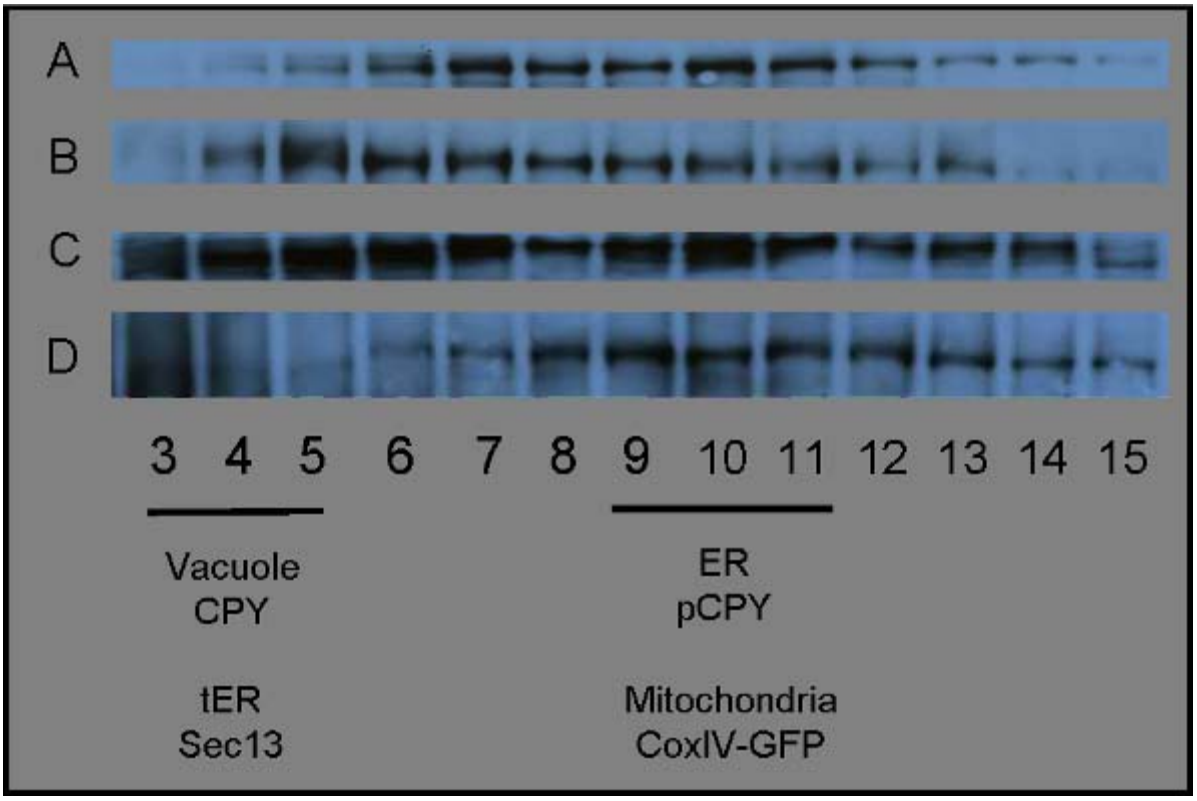

Figure 5-10. Distribution of Atg9 vesicles on sucrose gradients. TC10 were either grown in YNM for 18 hours (A) or adapted from YNM to YND for 4 hours (B). LAM7 was adapted from YNM to YND for 4 hours (C) and LAM6 was grown in YNM for 18 hours. The cells were spheroblasted, lysed, and the organelles sedimented at 100,000 xg. The pellet was resuspended and loaded onto a continuous sucrose gradient (15 – 55%). The gradient was centrifuged to equilibrium at 25k rpm for 15 hours. The ER marker pCPY and the mitochondrial marker CoxIV-GFP distribute around fractions 9-11. CPY which localizes to the vacuole and Sec13 which localizes to the transition endoplasmic reticulum (tER) distributed around fractions 4 and 5.

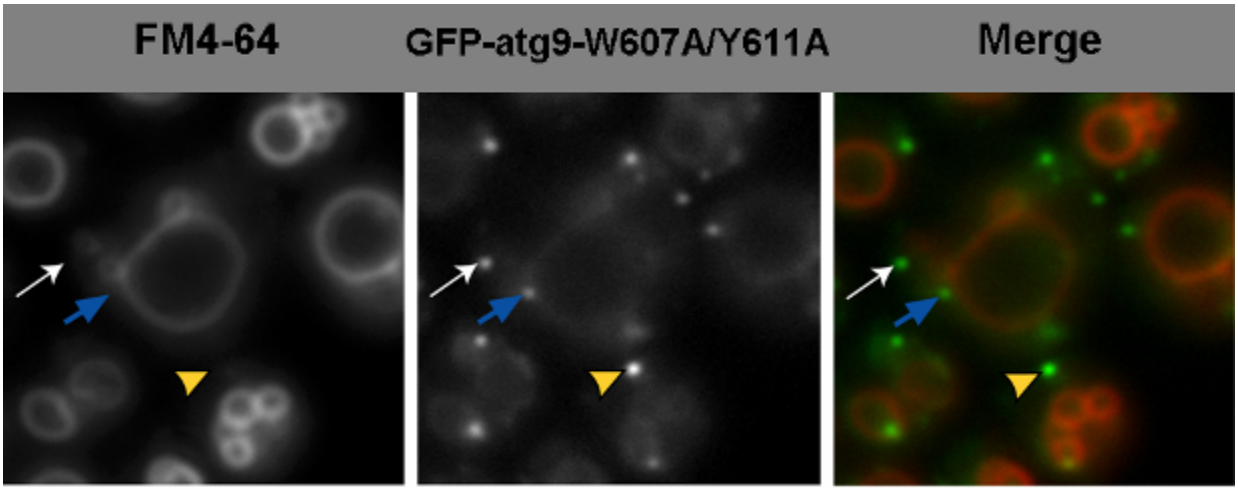

Figure 5-11. GFP-atg9(W607A/Y611A) fails to localize to the sequestering membranes (SM) during glucose-induced micropexophagy. R19 cells expressing GFP-atg9(W607A/Y611A) were grown in YNM in the presence of FM4-64. After 18 hours, the cells were adapted to YND for 2 hours and visualized by fluorescence microscopy. GFP-atg9(W607A/Y611A) localized to the PC9 (yellow arrowhead), PVS (blue arrow) and PAS (white arrow), but not the sequestering membranes or vacuole.

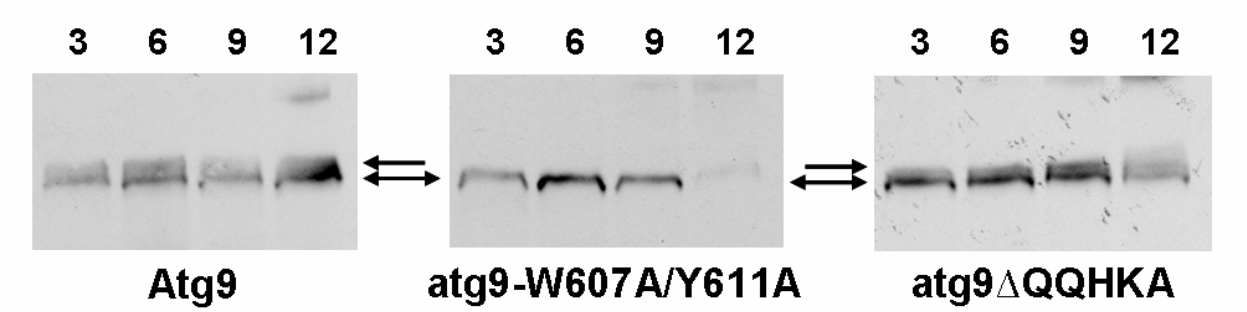

Figure 5-12. GFP-Atg9, not GFP-atg9(W607A/Y611A), migrates as a doublet on Westerns. At 3, 6, 9 and 12 hour post glucose adaptation, cells expressing GFP-Atg9, GFP-atg9(W607A/Y611A), or GFP-atg9ΔQQHKA, were lysed and the molecular sizes of the GFP-tagged proteins evaluated on Western blots. Both GFP-Atg9 and GFP-atg9ΔQQHKA migrated as a doublet: one band at 130kDa (arrow), the predicted size, and a second band at a slightly larger size of about 140kDa (asterisk). Meanwhile, atg9-W607A/Y611A migrated as a single band at 130kDa (arrow).

CHAPTER 6
SAR1P AND PEXOPHAGY

Introduction

Autophagy is a lysosomal degradation pathway meaning "self-eating." Autophagy can be subclassified based on substrate selectivity and mode of sequestration (for reviews see (Levine and Klionsky, 2004; Dunn *et al.*, 2005; Yorimitsu and Klionsky, 2005)). Nonselective micro- and macroautophagy can be stimulated by nitrogen and amino acid starvation. During microautophagy, sequestration occurs by invaginations of the lysosomal membrane. Sequestration of macromolecules and organelles into autophagosomes proceeds by macroautophagy. These autophagosomes eventually fuse with the lysosomes thereby delivering their cargo for degradation. The selective degradation of peroxisomes has been referred to as pexophagy. Micropexophagy is the sequestration of peroxisomes by the vacuole for degradation. When *Pichia pastoris* are subjected to glucose adaptation, clusters of peroxisomes are surrounded by finger-like protrusions originating from the vacuole. The peroxisome cluster is then incorporated into the vacuolar lumen where it is subsequently degraded. During adaptation from methanol to ethanol, individual peroxisomes are sequestered into autophagosomes and delivered to the vacuole for degradation. This process is called macropexophagy.

During glucose-induced micropexophagy, nucleation of the sequestering membranes proceeds from the vacuole. Membrane nucleation requires Atg18p[6], Vac8p and Vps15p(Stasyk *et al.*, 1999; Guan *et al.*, 2001; Fry *et al.*, 2006). Afterwards, the sequestering membranes expand to surround the peroxisomes. This expansion includes membranes from the vacuole and other undefined membranes. Membrane expansion requires Atg2p, Atg9p and Atg11p (Kim *et*

[6] We will conform to the ATG nomenclature. Unless stated by designations for other species, we refer to the P. pastoris homologs of the Sar1, Atg and Sec proteins in this paper.

al., 2001; Stromhaug *et al.*, 2001; Chang *et al.*, 2005). We have demonstrated that Atg9p, an integral membrane protein, traffics from a unique, peripheral compartment (PC9) [7] to perivacuolar structures (PVS) abutting the vacuole, and finally to the sequestering membranes. The movement of Atg9p to the sequestering membranes requires Atg2p and Atg11p. Mukaiyama, et al. have characterized the micropexophagic membrane apparatus (MIPA) required for expansion and completion events of micropexophagy (Mukaiyama *et al.*, 2004). The *de novo* assembly of the MIPA is positioned between expanding sequestering membranes. The assembly of the MIPA from a pre-autophagosome structure (PAS) requires Atg7p, Atg8p, and Atg9p (Mukaiyama *et al.*, 2004; Chang *et al.*, 2005). Atg8p, Atg9p and Atg17p localize to the PAS, with Atg8p also being found at the MIPA (Mukaiyama *et al.*, 2004; Chang *et al.*, 2005). Finally, completion of micropexophagy proceeds upon the fusion of MIPA with the adjacent sequestering membranes and incorporation of the peroxisomes into the vacuole for degradation. These fusion events require Vac8p and Atg24p (Ano *et al.*, 2005; Fry *et al.*, 2006; Oku *et al.*, 2006).

During ethanol-induced macropexophagy, peroxisomes are enwrapped by two or more membranes of unknown origin forming pexophagosomes (Dunn *et al.*, 2005). The molecular events responsible for the formation of the pexophagosome remain rather vague. These sequestering membranes contain Atg8p and Atg25p which arise from the PAS that contain a number of Atg proteins, including Atg8p, Atg9p and Atg17p (Chang *et al.*, 2005; Oku *et al.*, 2006). The completion of the pexophagosome requires Atg8p and Atg21p. The outer

[7] The abbreviations used are: AOX, alcohol oxidase; COPII, coat protein complex II; ER, endoplasmic reticulum; FM4-64, N-(triethlyammoniumpropyl)-4-(p-diethylaminophenylhexatrienyl) pyridinium dibromide; MIPA, micropexophagy-specific membrane apparatus; PAS, pre-autophagosome structure; PC2, Atg2, peripheral compartment; PC9, Atg9 peripheral compartment; PI4P, phosphatidylinositol 4'-monophosphate; PtdEtn, phosphatidylethanolamine; PVS, perivacuolar structure; SM, sequestering membranes; TCA, trichloroacetic acid; and v-SNARE, vesicle soluble NSF attachment receptor.

membrane of the pexophagosome then fuses with the vacuole delivering the peroxisomes for degradation. In addition to Atg25p at the pexophagosome, fusion requires Vam7p present at the vacuole and Atg24p present at the vertices and boundary regions of the fusion complex (Ano *et al.*, 2005; Monastyrska *et al.*, 2005; Stevens *et al.*, 2005). Within the vacuole, the inner membrane of the pexophagosome is ruptured by the lipase Atg15p and the released peroxisomes are rapidly degraded by proteinases (Teter *et al.*, 2001).

Recent data suggest that a number of molecular events of the secretory pathway may be shared by autophagy. For example, ScAtg8p interacts with the v-SNARE proteins Bet1p, Sec22p, and Nyv1p, which are required for endoplasmic reticulum (ER) to Golgi trafficking and vacuolar protein trafficking (Legesse-Miller *et al.*, 2000). In addition, studies have shown that a number of Sec proteins are required for autophagy, namely ScSec16p, ScSec17p, ScSec23p, ScSec24p, ScSec31p, ScSec12p, ScSec18p, and ScSec7p (Ishihara *et al.*, 2001; Hamasaki *et al.*, 2003; Reggiori *et al.*, 2004). The roles for ScSec16p, ScSec17p and ScSec23p have yet to be clearly defined (Ishihara *et al.*, 2001). ScSec12p facilitates the formation of the autophagic vacuole from the PAS (Reggiori *et al.*, 2004). When *sec24*^{ts} and *sec31*^{ts} mutants are exposed to nonpermissive temperatures, ScAtg8p is found at cytosolic structures, which are either multiple PAS forming autophagic vacuoles or autophagic vacuoles failing to fuse with the vacuole. Finally, ScSec18p and ScSec7p appear to be required for the fusion of the autophagic vacuole with the vacuole (Ishihara *et al.*, 2001; Reggiori *et al.*, 2004). Hence, a number of Sec proteins are indispensable for both protein secretion and autophagy.

Some of the secretory proteins required for autophagosome formation have a role in COPII-mediated trafficking (Ishihara *et al.*, 2001; Hamasaki *et al.*, 2003; Reggiori *et al.*, 2004). ScSec12p is a GDP/GTP transmembrane exchange factor which influences ScSar1p activity (for

review see (Sato and Nakano, 2007). ScSar1p, stimulated by the exchange of GTP for GDP, binds to the ER membrane. ScSec23p interacts with ScSec24p, which bind to ScSar1p. ScSec13p will bind to the ScSar1p-ScSec23p/ScSec24p coat protein complex promoting vesicular budding. Point mutations in ScSar1p inhibit COPII-dependent protein sorting (Ward *et al.*, 2001). The ScSar1pT39N mutant has a high affinity for GDP and blocks COPII vesicle formation from the ER. The ScSar1pH79G mutant is unable to hydrolyze GTP and prevents disassembly of COPII vesicle coats thereby inhibiting retrieval of proteins to the ER. The data suggest that COPII-dependent protein trafficking is essential for ongoing autophagy and may implicate the ER in the assembly of the autophagosomes (Ishihara *et al.*, 2001; Hamasaki *et al.*, 2003; Reggiori *et al.*, 2004).

Studies in *S. cerevisiae* have shown that the COPII complex of proteins is required for starvation-induced autophagy. However, the role of this protein complex in pexophagy has not been evaluated. In this study, we characterized the essential role of Sar1p in micro- and macropexophagy in *Pichia pastoris*. We demonstrated that when dominant-negative mutants, Sar1pT34N or Sar1pH79G, are expressed both micro- and macropexophagy are repressed. The nucleation and amplification of the sequestering membranes appeared to proceed normally during micropexophagy. However, the assembly of the MIPA was impaired when these Sar1p mutants were expressed. The failure of MIPA to form was not due to incorrect sorting of Atg2p, Atg9p, or Atg11p or an inactivation of Atg7p. However, the lipidation of Atg8p appeared to be altered. During micropexophagy, the pexophagosome failed to assemble when Sar1pT34N was expressed. To the contrary, the expression of Sar1pH79G did not appear to alter the formation of the pexophagosome, but disrupted its delivery of the peroxisomes to the vacuole. Our data

suggest that Sar1p is essential for the trafficking of ER proteins into and out of the sequestering membranes of micro- and macropexophagy.

Materials and Methods

Yeast Strains And Media

The yeast strains used in this study are listed in Table 1 and were routinely cultured at 30 °C in YPD (1% Bacto yeast extract, 2% Bacto peptone, and 2% dextrose). *P. pastoris* was grown in YNM (0.67% yeast nitrogen base, 0.4 mg/l biotin, and 0.5% methanol) to induce peroxisome biogenesis. The degradation of peroxisomes was induced when cells were transferred from YNM to YND (0.67% yeast nitrogen base, 0.4 mg/l biotin, and 2% glucose) or YNE (0.67% yeast nitrogen base, 0.4 mg/l biotin, and 0.5% ethanol). Nitrogen starvation medium, SD(-N), contained 0.17% yeast nitrogen base (without amino acids and NH_4SO_4) and 2% glucose. All media contained 2% agar when made as plates. Histidine and arginine were added at 40 μg/ml when needed. Vector amplification was done in *E. coli* (DH5α) cultured at 37 °C in LB (0.5% Bacto yeast extract, 1% Bacto tryptone, and 1% NaCl) with ampicillin (100 μg/ml). Zeocin was added at 25 μg/ml when culturing DH5α and 100 μg/ml when culturing *P. pastoris*.

Quantitative Assessment Of Alcohol Oxidase (AOX) Degradation

Cells were grown in 20 ml of YNM with methanol as sole carbon and energy source. At 40 hours, 0.4 g glucose was added with or without 0.1 mM copper sulfate. Aliquots (2 ml) of cells (8.0 OD_{600}) at 0 and 6 hours of glucose adaptation were pelleted and resuspended in 1 ml of 20 mM Tris pH 7.5 containing 50 mM NaCl, 1 mM EDTA, 1 mM PMSF, 1 μg/ml pepstatin A, and 0.5 μg/ml leupeptin. The cells were then lysed by vortexing in the presence of 0.5 ml glass beads (425-600 microns). The glass beads and cellular debris were removed by centrifugation

and AOX was measured by adding 50 µl of this extract to 3 ml of reaction mix containing 3.4 U/ml horseradish peroxidase and 0.53 mg/ml 2,2'-azino-bis(3-ethylbenz-thazoline-6-sulfonic acid) in 33 mM potassium phosphate buffer pH 7.5. The reaction was initiated by adding 10 µl methanol and terminated after 20 minutes by adding 200 µl of 4N HCl and the absorbance read at 410 nm.

Measurements of Protein Degradation

The degradation of cellular proteins during nitrogen starvation was performed as described previously (Tuttle and Dunn, 1995). Endogenous proteins were labeled with 1 µCi/ml ^{14}C-valine for 16 hours in 0.67% yeast nitrogen base, 2% glucose, 0.4 mg/l biotin, and 40 µg/ml histidine (if necessary). The cells were then washed and switched to SD(-N) with or without 0.1 mM copper sulfate and supplemented with 10 mM valine. Aliquots were removed at 2 - 24 hours of chase and trichloroacetic acid (TCA) was added to a final concentration of 20%. Acid soluble and insoluble radioactivity was separated by centrifugation and quantified by scintillation counting. The rates of protein degradation were calculated from the slopes of the linear plots of TCA-soluble radioactivity versus time of chase.

Western Blot Analysis

Cells were prepared for SDS-PAGE and Western blots as previously described (Chang *et al.*, 2005). The cells (2-3 OD_{600}) were pelleted, washed with water, and lysed in 150 µl of SDS sample buffer (67 mM Tris, pH 6.8, 2% SDS, 10% glycerol, 0.1% bromophenol blue, 1.5% DTT solution containing 4 mM PMSF, 4 mM pepstatin A, and 2 mM leupeptin) by vortexing with glass beads (425-600 micron diameter). Just prior to SDS-PAGE, the samples were incubated at 100 °C for 5 minutes and cell debris and glass beads were removed by centrifugation. Five to twenty microliters of sample were loaded onto 8%, 10% or 15% polyacrylamide gels. Upon

electrophoresis, the proteins were transferred to nitrocellulose using the Trans-Blot SD-Dry Transfer Cell (Bio-Rad Laboratories, Hercules, CA). The blots were blocked in 5% nonfat dried milk in PBS containing 0.1% Tween 20 (PBST) and incubated with the primary antibodies rabbit anti-AOX (Tuttle and Dunn, 1995), rabbit anti-HA (Covance, Emeryville, CA) or rabbit anti-GFP (Sigma, St. Louis, MO). The blots were then washed in PBST, and followed by incubation with secondary antibodies conjugated to HRP. After washing with PBST, the antibodies were detected using ECL (Amersham, Piscataway, NJ).

Construction of Conditional Expression Vectors

Expression vectors containing *sar1*(T34N) and *sar1*(H79G) behind the copper-inducible *CUP* promoter were constructed as follows. PpARG4 gene was amplified by PCR from pYM30 (kind gift of Dr Jim Cregg, Keck Graduate Institute) and inserted into the SspI and NdeI sites of pUC19. The resulting plasmid, pUC19-PpArg4, was amplified, cut with NdeI, blunt-ended with T4 DNA polymerase, and digested with EcoRI. The *S. cerevisiae CUP* promoter was excised from pCAJ3 vector with BamHI (blunt-ended with T4 DNA polymerase) and EcoRI, and then ligated into the pUC19-PpArg4. Next, the poly-A sequence from pIB2 was excised and inserted into the HindIII and AflII site yielding the pWD16 conditional expression vector. Finally, *sar1*(T34N) and *sar1*(H79G) kindly provided by Dr Ben Glick (University of Chicago) were amplified by PCR and inserted into the EcoRI and HindIII sites of pWD16. GFP-*ATG17* was constructed by inserting *ATG17* amplified by PCR from genomic DNA into the KpnI and XhoI sites of pPS55 following similar procedures used to construct expression vectors containing GFP-*ATG2*, GFP-*ATG8*, GFP-*ATG9*, GFP-*ATG11*, and GFP-*ATG18* (Guan *et al.*, 2001; Kim *et al.*, 2001; Stromhaug *et al.*, 2001; Chang *et al.*, 2005). RFP-HDEL was provided by Dr Ben Glick (University of Chicago) and pAJM6 (P_{GAPDH} mRFP-PpAtg9, ZeocinR) and pWD18 (P_{ATG7}

atg7-HA (C518S), *HIS4*) were constructed as previously described (Yuan *et al.*, 1999; Chang *et al.*, 2005).

Yeast Transformation

Cells grown overnight in YPD to a density of A_{600} = 1.0 were harvested and treated with 10 mM DTT in YPD containing 25 mM HEPES, pH 8, for 15 minutes at 30 °C. The cells were washed twice in ice-cold water and once in 1 M sorbitol and then resuspended in 1 M sorbitol. Cells (40 µl) were mixed with 0.2-1 µg of linearized vector and transferred to a 0.2 cm gap cuvette (Bio-Rad, Hercules, CA), and the DNA introduced by electroporation at 1.5 kV, 25 µF, 400 Ω (Gene Pulser, Bio-Rad Corp.). The cells transformed with vectors containing the *HIS4* gene were transferred to plates containing 0.67% yeast nitrogen base without amino acids, 2% glucose, 1 M sorbitol, 0.4 mg/l biotin, and 2% agar and incubated at 30 °C for 3 – 5 days before colonies appeared. For antibiotic selection, Zeocin was added to a final concentration of 100 µg/ml.

Fluorescence Microscopy

Cells expressing GFP and/or mRFP fusion proteins were grown in YNM for 20 hours. FM4-64 (Molecular Probes, Eugene, OR) was added to a final concentration of 20 ug/ml and cells incubated for 12 - 16 hours. Cells were then transferred to YND or YNE with or without 0.1 mM copper sulfate. After 2 - 4 hours, the cells were examined live using a Zeiss Axiophot fluorescence microscope. Image capture was done using a SPOT camera (Diagnostics Instruments, Inc., Sterling Heights, MI) interfaced with IP Lab software.

Electron Microscopy

Upon glucose or ethanol adaptation, cells were harvested by centrifugation, washed in water, and fixed with 1.5% $KMnO_4$ in veronal-acetate buffer (30 mM sodium acetate, 30 mM

sodium barbital, pH 7.6) for 20 minutes at room temperature (Veenhium *et al*., 1983). The samples were dehydrated by washing with increasing concentrations of ethanol followed by two washes with 100% propylene oxide. The cells were then infiltrated with a 50:50 mix of propylene oxide and POLY/BED 812 (Polysciences, Inc., Warrington, PA) for 16 hours at 4 °C and another 24 hours at 22 °C under vacuum. Afterwards, the cells were infiltrated with 100% POLY/BED with accelerator 2,4,6-Tri(dimethylaminomethyl)phenol (DMP-30, Polysciences, Inc.) for another 2 days at 22 °C under vacuum. The cells were pelleted and incubated at 60 °C for 2 days to complete the polymerization of the resin. The cell pellets were mounted on blocks, sectioned, and prepared for examination on a JEOL 100CX transmission electron microscope.

Results

Effects Of Dominant-Negative Mutants Of Sar1p On Autophagy And Pexophagy

ScSec12p, the guanine nucleotide exchange factor for the G-protein ScSar1p, has been shown to be required for autophagy in *S. cerevisiae* (Ishihara *et al.*, 2001; Hamasaki *et al.*, 2003; Reggiori *et al.*, 2004). Since Sar1p is essential for cell growth, the role of Sar1p in autophagy and pexophagy has been difficult to evaluate. To circumvent this technical problem, we have constructed dominant-negative forms of Sar1p whose expression is regulated by a copper-inducible *CUP1* promoter of *S. cerevisiae*. Sar1pT34N has a high affinity for GDP and blocks COPII vesicle formation. Sar1pH79G is defective in hydrolyzing GTP. In the absence of copper, the culture growth of WDY64 and WDY65 in minimal medium appeared normal (Fig. 6-10). However, when these cells were exposed to 0.1 mM copper sulfate to promote the synthesis of Sar1pT34N and Sar1pH79G, growth was rapidly and dramatically reduced (Fig. 6-10). The data suggest that we can tightly regulate the expression of these proteins with copper additions.

Using the aforementioned cells, we first examined whether the expression of these Sar1p mutants affected starvation-induced autophagy (Fig.6- 1A). The degradation of endogenous proteins in cells pre-labeled with ^{14}C-valine was measured in nitrogen-starved cells in the absence and presence of copper. Nitrogen starvation induces the nonselective delivery of cellular components to the vacuole by micro- and macroautophagy in yeast. We compared endogenous proteolysis in WT cells to cells expressing the Sar1p mutant proteins (Fig. 6-1A). We observed a 25% reduction of proteolysis in starved WT cells exposed to copper. This was compared to the over 60% reduction in starvation-induced proteolysis in cells whose expression of Sar1pT34N or Sar1pH79G had been induced with copper. The data show that Sar1p is required for starvation-induced macroautophagy.

Next, we examined the effects of the Sar1p mutant proteins on glucose-induced micropexophagy (Fig. 6-1B) and ethanol-induced macropexophagy (Fig. 6-1C). Cells were grown in methanol, adapted to glucose in the absence and presence of copper for 6 hours and the remaining AOX activity quantified. Less than 20% of the AOX remained in the WT cells regardless of the presence of copper. In the absence of copper, 80% of the AOX was degraded by the WDY64 and WDY65 cells. However, when these cells were incubated with copper, only 10% of the AOX was lost during glucose adaptation. Finally, cells were grown in methanol, adapted to ethanol in the absence and presence of copper for 0 - 24 hours and the remaining AOX detected by Western blotting. We observed that in the absence of copper AOX protein was almost completely degraded within 9 hours. However, when Sar1pT34N or Sar1pH79G was expressed, AOX protein remained for up to 24 hours. The data reveal that Sar1p is essential for both micro- and macropexophagy.

Suppression Of Glucose-Induced Micropexophagy By Dominant-Negative Mutants Of Sar1p Occurs At A Late Sequestration Event

We have shown that the expression of Sar1pT34N or Sar1pH79G dramatically inhibits the degradation of peroxisomes induced by glucose adaptation. We next examined whether these proteins inhibited the events of peroxisome sequestration and/or degradation. We first examined the morphology of those cells expressing Sar1pT34N and Sar1pH79G by electron microscopy. WDY64 and WDY65 were adapted from YNM to YND for 4h in the absence or presence of copper (Fig. 6-2). Without copper, the endoplasmic reticulum appeared as discontinuous sheets at the cell periphery and about the nucleus, while the Golgi apparatus was not easily observed. The morphological changes of these organelles when the Sar1p mutants were expressed were consistent with the known functions of Sar1p. For example, when Sar1pT34N, which inhibits ER budding, was expressed the ER was extended appearing as a continuous sheet at the cell periphery and throughout the cell. To the contrary, when cells expressed Sar1pH79G, which inhibits recycling from the Golgi apparatus back to the ER, the Golgi apparatus appeared as multiple cisternae. During glucose adaptation in cells not expressing the Sar1p mutants, peroxisomes were surrounded by the vacuole or within the vacuole (Fig. 6-2A and 6-2E). In cells expressing Sar1pT34N (Fig. 6-2B-D) or Sar1pH79G (Fig. 6-2F-H), the peroxisome clusters were situated outside the vacuole suggesting that Sar1p was required for delivery of the peroxisomes to the vacuole and not vacuolar degradation.

The events of micropexophagy include: signaling, sequestration, and degradation. The above data suggest that the Sar1p mutants were suppressing an event prior to degradation most likely sequestration. The engulfment of peroxisomes by sequestering membranes (SM) that arise from the vacuole proceeds via SM nucleation, expansion, and completion. These events can be visualized by observing the SM with FM4-64 staining incorporating peroxisomes expressing

BFP-SKL (Fig. 6-11). For these studies, we constructed cell lines expressing BFP-SKL behind the AOX promoter in cells expressing the Sar1p mutants. At 2h of glucose adaptation, cells were observed at all phases of micropexophagy. During nucleation, the sequestering membranes extend less than halfway around the peroxisomes. About 15% of the cells examined at 2h of glucose adaptation are at this stage. Expansion of the sequestering membranes can be observed in over half of the cells when the sequestering membranes extend 50 to 90% around the peroxisomes. The completion events are characterized by peroxisomes being completely surrounded by the sequestering membranes, but the membranes appear segmented and not completely fused. Over 30% of the cells examined were at this stage. Finally, the degradative stage was detected in 5% of the cells. This stage was characterized by a continuous ring of FM4-64 labeled membranes surrounding peroxisomes that were no longer clearly delineated due to degradation. The data suggest that the expansion and completion events are rate-limiting in micropexophagy. We observed 52% of the cells expressing Sar1pT34N at the expansion stage (Fig. 6-2C), 15% at completion (Fig. 6-2D), and 33% at degradation. In cells expressing Sar1pH79G, 23% of the cells were observed at nucleation, 48% at expansion (Fig. 6-2G), 20% at completion (Fig. 6-2H), and 9% at degradation. These results suggest that Sar1p was not required for nucleation by likely for the expansion and/or completion events and possibly degradation. Because peroxisomes were sometimes observed within the vacuole, it is possible that one or more vacuolar lipases or proteinases were missorted and not arriving at the vacuole.

Sar1p Is Essential For The Formation Of The MIPA

Our data suggest that Sar1p is critical for the expansion and/or completion phases of peroxisome sequestration during glucose-induced micropexophagy. Expansion of the sequestering membranes requires Atg2p, Atg9p, and Atg11p and the assembly of the MIPA, which requires Atg8p. Completion requires MIPA and other proteins including Vac8p and

Atg24p. During expansion, Atg9p traffics from a unique peripheral compartment (PC9) to become associated with the sequestering membranes. This trafficking requires Atg2p and Atg11p. Also at this time, Atg8p becomes associated with the newly assembled MIPA, which is positioned between the expanding sequestering membranes. Therefore, we decided to examine the effects of these Sar1p mutants on the trafficking of Atg2p, Atg9p, Atg11p, and Atg8p during glucose adaptation. Cell lines expressing Sar1pT34N or Sar1pH79G and GFP-Atg2p, GFP-Atg9p, GFP-Atg11p or GFP-Atg8p were constructed (see Table 1). The cells were adapted from YNM to YND in the absence and presence of copper sulfate and examined by fluorescence microscopy (Figs. 6-3 and 6-4).

We first examined the trafficking of Atg11p. During micropexophagy, Atg11p colocalizes with Atg9p at the perivacuolar structure (PVS) and SM and is required for the trafficking of Atg9p to the PVS (Chang *et al.*, 2005). In the absence of copper, Atg11p was found at the PVS, vacuole and SM at 2h of glucose adaptation. The distribution of Atg11p was unaltered when either Sar1pT34N or Sar1pH79G were expressed (Fig. 6-3). Next, we examined the distribution of GFP-Atg2p in cells. Upon glucose adaptation, Atg2p becomes associated with foci known as the Atg2p peripheral compartment (PC2). Its role in the expansion of the SM is not defined, but Atg2p is required for the transit of Atg9p to the SM. When LAM44 and LAM45 were adapted from YNM to YND in the absence of copper, Atg2p was found in the cytosol and at foci situated at the cell periphery and near the vacuole. When cells were adapted to glucose in the presence of copper, Atg2p was virtually absent from the cytosol and was instead observed in foci and larger irregularly shaped structures (Fig. 6-3, yellow arrows). These coalescing structures may represent an expansion of this peripheral compartment due to the

expression of the Sar1p mutants. The data suggest that the trafficking of Atg2p and Atg11p were not significantly influenced by Sar1p.

We have previously shown that during the membrane expansion events Atg9p transits from PC9, to the PVS, and finally to the SM (Chang *et al.*, 2005). Atg9p can also be observed occasionally colocalizing with Atg8p and Atg17p at the PAS. We next examined the effects of Sar1pT34N or Sar1pH79G on the cellular distribution of GFP-Atg9p during glucose adaptation. In the absence of copper, GFP-Atg9p was found at the PC9, PVS, and SM (Fig. 6-3). Atg9p was also present at the vacuole membrane. When copper was added, the distribution of GFP-Atg9p was not dramatically altered. In addition to the peripheral foci of the PC9 compartment (Fig. 6-3, white arrowhead), Atg9p was present at the PVS near the base of the sequestering arms (Fig. 6-3, white arrow), the PAS or MIPA nucleation site (Fig. 6-3, yellow arrowhead), and the SM.

We have reported that Atg2p and Atg9p localize to distinct peripheral compartments (Chang *et al.*, 2005). However, since Atg2p requires Atg9p for its localization, we suggest that these compartments may transiently interact. Based on our data, it is possible that Sar1p may influence the assembly of both PC2 and PC9 compartments. Indeed, the structure of the PC2 compartment was altered and there appeared to be more PC9 foci present in cells expressing the Sar1p mutants. Therefore, we next examined whether Atg2p and Atg9p colocalize in the presence of the Sar1p mutant proteins. We coexpressed RFP-Atg9p and GFP-Atg2p in WDY64 and WDY65 cell lines. In the absence or presence of copper, RFP-Atg9p was found within the lumens of the vacuole and SM (Fig. 6-3). We reported this observation previously and suggested that the lumenal RFP was the result of N-terminal proteolysis while Atg9p was at these membranes (Chang *et al.*, 2005). Furthermore, despite the expression of Sar1pT34N or Sar1pH79G, Atg9p did not colocalize with Atg2p (Fig. 6-3).

Finally, we examined the cellular distribution of GFP-Atg8p in glucose-adapted cells expressing the mutant forms of Sar1p (Fig. 6-4). Under normal conditions, Atg8p localizes to the PAS from which it transits to the newly assembled MIPA. At 2h of glucose adaptation without copper, GFP-Atg8p was present throughout the cytosol and localized specifically to one or two MIPA's situated between the adjoining sequestering membranes labeled with FM4-64 (Fig. 6-4, white arrows). When the expression of Sar1pT34N or Sar1pH79G is enhanced by copper, GFP-Atg8p was observed in multiple punctate (Fig. 6-4, white arrowheads) and flattened MIPA-like structures (Fig. 6-4, yellow arrows). However, these structures were not associated with the sequestering membranes, but randomly distributed throughout the cell. Our data suggest that in the presence of Sar1pT34N or Sar1pH79G, MIPA fails to assemble, thereby inhibiting the expansion and completion events.

We also noticed that the PAS, which normally appears as one or two foci, was structurally different when Sar1pT34N or Sar1pH79G were expressed. Therefore, we examined the cellular distribution of GFP-Atg17p, a structural component of the PAS not present at the MIPA (Fig. 6-12). During glucose adaptation in the absence of copper, GFP-Atg17p was found at one or two distinct foci juxtaposed to the vacuole or sequestering membranes. However, in the presence of copper, GFP-Atg17p was present in foci and larger diffuse structures of irregular shapes that were distant from the vacuole and SM. The data suggest that Sar1p may play a role in the maintenance of the PAS.

The Lipidation Of Atg8p During Glucose-Induced Micropexophagy Is Altered Upon Expression Of Dominant-Negative Sar1p Mutants

Based on GFP-Atg8p labeling, we have determined that the MIPA fails to assemble when either Sar1pT34N or Sar1pH79G are expressed. Atg8p not only localizes to the MIPA, but is essential for its formation. Upon proteolytic activation by Atg4p, the C-terminal glycine of

Atg8p becomes conjugated by a thio-ester linkage to cysteine 518 of Atg7p. Atg8p is then conjugated to phosphatidylethanolamine (PtdEtn) by the actions of Atg3p. We have previously shown that Atg7p-HA forms a DTT-sensitive thio-ester conjugate with a protein whose size we estimated at 25 kDa (Yuan *et al.*, 1999). When the active cysteine of Atg7p is mutated to a serine (Atg7pC518S-HA) this conjugation becomes DTT resistant. Therefore, when Atg7pC518S-HA is expressed in WT cells, we observe two protein bands at 70 kDa and 95 kDa (Fig. 6-5A). The upper band was not observed in cells lacking Atg8p suggesting that the 95 kDa band represented Atg7pC518S-HA conjugated by an ester linkage to Atg8p. In order to assess the effects of Sar1pT34N or Sar1pH79G on Atg7p activity, we expressed Atg7pC518S-HA in these mutants. These cells were grown in YNM and switched to YND for 3h and 6h with and without copper sulfate. Afterwards, the protein conjugate of Atg7p and Atg8p was visualized by Western blotting (Fig. 6-5A). In the absence and presence of copper, both unconjugated (70 kDa) and conjugated (95 kDa) forms of Atg7pC518S-HA were observed suggesting that Atg7p activity was not affected by either Sar1pT34N or Sar1pH79G.

We next examined the effects of Sar1pT34N or Sar1pH79G on the lipidation of Atg8p. This was done by examining the processing of Atg8p on Western blots given that the lipidated form of Atg8p migrates at a lower molecular mass on SDS-PAGE (Stromhaug *et al.*, 2004). Cells were grown in YNM and switched to YND with and without copper sulfate for 0 – 9h. At 0h, GFP-Atg8p migrated as a single band around 40 kDa (Fig. 6-5B). At 3 – 9h in the absence of copper, smaller forms of GFP-Atg8p began to appear with the lipidated form migrating at 35 kDa. When copper was present, the 35 kDa protein was virtually absent. The data suggest that the expression of Sar1pT34N or Sar1pH79G altered the lipidation of Atg8p.

Sar1p Is Required For Early And Late Events Of Macropexophagy

We have shown that Sar1pT34N and Sar1pH79G suppress the degradation of AOX during ethanol-induced macropexophagy. During macropexophagy, individual peroxisomes are engulfed by sequestering membranes that can be visualized by GFP-Atg8p. Like the MIPA, these membranes are presumed to be organized from the PAS (Dunn *et al.*, 2005). In cells not expressing Sar1pT34N and Sar1pH79G, GFP-Atg8p was present at the PAS (Fig. 6-6, yellow arrowheads), pexophagosomes (Fig. 6-6, white arrows), and within the vacuole (Fig. 6-6A). We next examined the effects of Sar1pT34N and Sar1pH79G on the assembly of pexophagosomes as visualized by GFP-Atg8p labeling (Fig. 6-6) and ultrastructural morphology (Fig. 6-7). When Sar1pT34N is expressed, peroxisomes were not sequestered within pexophagosomes or the vacuole, but observed in the cytosol. GFP-Atg8 localized to the PAS (Fig. 6-6, yellow arrowhead) and crescent-like structures (Fig. 6-7B), which may represent the nucleation of sequestering membranes that we observed near the peroxisomes (Fig. 6-7B, arrow). In cells expressing Sar1pH79G, we observed pexophagosomes with foci containing GFP-Atg8 (Fig. 6-6D, white arrows), but the diffuse vacuole labeling consistent with vacuolar fusion was absent. Ultrastructural analyses revealed that these pexophagic vacuoles were bound by multiple membranes (Fig. 6-7C, arrowheads). Furthermore, intact peroxisomes bound by a single membrane could be observed within the vacuole (Fig. 6-7D, arrowheads). RFP-Atg9p was found within the vacuole or localized to the vacuole surface and foci juxtaposed to the vacuole (Fig. 6-6A and 6-6C). This distribution was unaffected by the expression of either Sar1p mutant (Fig. 6-6B and 6-6D). RFP-Atg9 could be observed with some GFP-Atg8 foci at the pexophagosome (Fig. 6-7, white arrow). These observations combined with our biochemical data (Fig. 6-1) suggest that the pexophagosomes present in cells expressing Sar1pH79G may fuse poorly with the vacuole or are resistant to lytic enzymes of the vacuole. We have shown that

Sar1pT34N suppresses the formation of the pexophagosome, while the delivery of the peroxisome from the pexophagosome to the vacuole for degradation appears to be defective in cells expressing Sar1pH79G.

RFP-HDEL Localizes To Pexophagosomes When Sar1pH79G Is Expressed

These dominant-negative Sar1p mutants have been shown to effectively alter the trafficking of ER proteins in *S. cerevisiae* (Ward *et al.*, 2001). Since the ER has been implicated in the formation of autophagic vacuoles in mammalian cells (Dunn, 1990), we decided to examine the localization of RFP-HDEL during macropexophagy (Fig. 6-8). RFP-HDEL with its amino-terminal signal sequence and carboxy-terminal HDEL retrieval signal is targeted to the ER lumen by the receptor Erd2p which binds the HDEL sequence (Bevis *et al.*, 2002). Upon ethanol adaptation, RFP-HDEL was found exclusively at the ER located adjacent to the cell periphery and around the nucleus (Figs. 6-8 A and D). The distribution of RFP-HDEL was unaltered in ethanol-adapted cells expressing Sar1pT34N (Figs. 6-8 B and C). When Sar1pH79G is expressed during 2h of ethanol adaptation, we observed RFP-HDEL at the ER and engulfing individual peroxisomes (Fig. 6-8, arrows). At times longer than 3h, the RFP was observed within the vacuole (Fig. 6- 8, arrowheads). These pexophagosomes did not contain Sec7p, a protein of the Golgi apparatus (unpublished observations). The results suggest that components of the ER are observed with the pexophagosomes when ER recycling is inhibited by Sar1pH79G.

Discussion

Earlier reports have demonstrated that some Sec proteins are required for autophagy in *S. cerevisiae*. Three of these proteins, ScSec12p, ScSec23p, and ScSec24p, are essential for ScSar1p activity and trafficking of proteins out of and into the ER. We examined the role of Sar1p in the selective degradation of peroxisomes by pexophagy by tightly regulating the

expression of two dominant-negative mutants of Sar1p. Sar1pT34N has a high affinity for GDP and suppresses COPII-dependent protein exit from the ER. Sar1pH79G has a defective GTPase thereby inhibiting the recycling of proteins back to the ER. We have shown that this protein is essential for starvation-induced autophagy, glucose-induced micropexophagy, and ethanol-induced macropexophagy. How is it possible that Sar1p, which is essential for trafficking proteins between the ER and the Golgi, has such a far-reaching influence on micro- and macropexophagy? In this study, we attempted to address this question to define the roles of Sar1p in these diverse autophagic pathways.

Role of Sar1p in Micropexophagy

Our data suggest that the degradation of AOX is dramatically reduced when either Sar1pT34N or Sar1pH79G are expressed. The peroxisomes were observed almost completely engulfed by sequestering membranes outside the vacuole. This suggests that the blockage occurs at a late sequestration event (e.g., expansion and/or completion). Moreover, MIPA formation did not occur when either Sar1pT34N or Sar1pH79G were expressed. The MIPA is a crescent-shaped structure that joins the apposing sequestering membranes to initiate their fusion thereby completing expansion and completion events. This structure contains Atg8p and Atg26p and its formation requires a number of Atg proteins including Atg9p and Atg11p. Therefore, we examined the trafficking of Atg9p and Atg11p and showed that their trafficking to the sequestering membranes was unaffected by the Sar1p mutants.

The MIPA assembles from the PAS or nucleation complex, a structure that contains Atg8p and Atg17p (Oku *et al.*, 2006; Yamashita *et al.*, 2006). The formation of the MIPA is dependent upon the lipidation of Atg8p, which requires Atg4p, Atg7p, and Atg3p (Mukaiyama *et al.*, 2004). Our data suggest that the inability of cells expressing the Sar1p mutants to assemble the MIPA may be related to their inability to lipidate Atg8p (see Fig. 6-5B). Atg4p

proteolytically activates Atg8p. Atg7p forms a high-energy conjugate with Atg8p thereby delivering Atg8p to Atg3p for its conjugation to phosphatidylethanolamine. The data show that the formation of the high-energy conjugate with Atg7p proceeds normally when these Sar1p mutants are expressed (see Fig. 6-5A). Therefore, in inability to lipidate Atg8p may be related to an inactivation of Atg3p or a decrease in the availability of PtdEtn. The effects of Sar1p on Atg3p activity are unknown and remain to be examined. However, the availability of PtdEtn has been shown to be essential for the autophagic response (Nebauer *et al.*, 2007). Thus, the inability to form the MIPA may be related to lower levels or missorting of PtdEtn. The availability of PtdEtn was reduced in cells lacking ScVps4p or ScVps36p, proteins required for post-Golgi trafficking. The autophagy-like transport of cytosolic pAPI to the vacuole was inhibited in these mutants (Nebauer *et al.*, 2007). Meanwhile, ethanolamine rescued pAPI transport, suggesting that PtdEtn was a limiting factor. Furthermore, mutants defective in PtdEtn production show reduced ScAtg8p localization to the PAS and suppressed Cvt and autophagy pathways (Nebauer *et al.*, 2007). These effects were not due to reduced ScAtg8p levels, but to low levels of PtdEtn, suggesting that the availability of PtdEtn may be critical to the lipidation of Atg8p and assembly of the PAS. Psd2p, which synthesizes PtdEtn from phosphatidylserine, can interact with Sec28, a protein of the COPII complex (Schuldiner *et al.*, 2005). The trafficking of lipids out of the ER is thought to be mediated by both vesicular and non-vesicular traffic (Levine, 2004). However, the movements of PtdEtn to the cell surface were not affected by brefeldin A and thus, may not require Sar1p (Vance *et al.*, 1991). Nevertheless, the effects of Sar1p on the cellular levels of PtdEtn remain to be studied.

Atg26p is also required for MIPA formation. Phosphatidylinositol 4'-monophosphate (PI4P) transits from the ER to the PAS or nucleation complex thereby recruiting Atg26p by

interacting with its GRAM domain (Yamashita *et al.*, 2006). The sterol conversion of Atg26p is essential for the formation of the MIPA. It is possible that the trafficking of PI4P may be altered in cells expressing the Sar1p mutants. Indeed, Sar1p has been implicated in the exit of glycosylphosphatidylinositol (GPI) anchored GFP from the ER (Stephens and Pepperkok, 2004). However, we have no data to suggest that PI4P transport is influenced by Sar1p, and studies are currently ongoing.

In summary, the expression of Sar1pT34N or Sar1pH79G inhibits glucose-induced micropexophagy by suppressing the assembly of the MIPA. The most probable scenario is that Sar1p affects Atg8p lipidation and/or the trafficking of Atg26p which is essential to MIPA formation. The suppressed lipidation of Atg8 may be due to an inactivation of Atg3p or insufficient PtdEtn, while the movements of Atg26p require vesicular trafficking of PI4P from the ER to the PAS.

Role of Sar1p in Macropexophagy

The data from *sec* mutants provides circumstantial evidence that the autophagosome membranes may originate from the ER (Ishihara *et al.*, 2001; Hamasaki *et al.*, 2003; Reggiori *et al.*, 2004). In this study, we characterized the essential role of Sar1p in macropexophagy in *Pichia pastoris*. Ethanol-induced peroxisome degradation is suppressed when cells express either Sar1pT34N or Sar1pH79G (Fig. 6-1). However, these proteins inhibit different events of macropexophagy. We have shown that pexophagosomes do not form when Sar1pT34N is expressed. ScSec12p, a GDP/GTP exchange factor that influences ScSar1p activity, is also required for the formation of autophagic vacuoles in nitrogen-starved *S. cerevisiae* (Ishihara *et al.*, 2001; Reggiori *et al.*, 2004). *Brucella abortus* is an intracellular pathogen that infiltrates the autophagosome to replicate in vacuoles that contain the ER protein calnexin (Celli *et al.*, 2005). When HsSar1pT39N is expressed, this bacterium fails to replicate or localize with calnexin-

positive autophagic vacuoles, but instead is found in LAMP1-positive phagolysosomes (Celli *et al.*, 2005). These results substantiate our findings that HsSar1pT39N and its *P. pastoris* analogue Sar1pT34N suppresses autophagic vacuole formation. In the case of *B. abortus*, since the replication vacuole is not formed, this bacterium transits to the phagolysosome where it is killed and degraded. On the other hand, bacterial replication within calnexin-positive autophagic vacuoles was not altered by Sar1pH79G. This is consistent with our findings that Sar1pH79G does not affect formation of the pexophagosome.

Pexophagosomes with GFP-Atg8p at their delimiting membranes can be observed in cells expressing Sar1pH79G. Their morphology is consistent with fully formed pexophagosomes (see Fig. 6-7C). Meanwhile, profiles of pexophagosomes delimited by GFP-Atg8 can be occasionally observed within the vacuole (see Figs. 6-6C and 6-7D). The data suggest that Sar1pH79G may interrupt fusion of the pexophagosome with the vacuole and/or degradation of the pexophagosome within the vacuole. It is possible that the trafficking to the vacuole of the fusion machinery (Ypt7, Vti1, and Vam3) or the degradative lipases (Atg15) or proteinases (Pep4 and Prb1) may have been altered by Sar1pH79G (Levine and Klionsky, 2004). On the other hand, alterations in the membranes of the pexophagosome may interrupt fusion and lysis. Indeed, we have observed that the delimiting membranes of the pexophagosomes also contained RFP-HDEL, a marker for the ER membrane protein Erd2 (HDEL receptor), an ER membrane protein. At later times of macropexophagy, the RFP was found within the vacuole suggesting that there was some delivery of the pexophagosome to the vacuole. At no time in wild type cells did we observe RFP-HDEL delimiting the membranes of the pexophagosome or within the vacuole. These results are consistent with Sar1pH79G inhibiting retrograde trafficking of the RFP-HDEL and other ER components from the pexophagosome to the ER. The presence of

these ER components may ultimately suppress pexophagosome fusion with the vacuole and provide resistance to vacuolar lipases and proteinases. Thus, our data suggest that recycling of ER components from the pexophagosome is critical for delivery of the peroxisomes to the vacuole for degradation.

In summary, we propose that the movement of ER components into and out of the pexophagosome is influenced by Sar1p (Fig. 6-9). We have utilized dominant negative mutants of Sar1p that inhibit anterograde (Sar1pT34N) and retrograde (Sar1pH79G) movements of ER proteins. We have shown that anterograde movements of ER proteins to the pexophagosome are critical for its formation, while retrograde movements of ER proteins from the pexophagosome are essential for the delivery of the peroxisome to the vacuole.

Summary

We have utilized Sar1p mutants defective in anterograde (Sar1pT34N) and retrograde (Sar1pH79G) transport of ER proteins to demonstrate that Sar1p is essential for autophagy and pexophagy. These mutants suppress micropexophagy by inhibiting the formation of the MIPA and delivery of the peroxisomes to the vacuole. In regards to macropexophagy, inhibition of anterograde ER transport suppresses the formation of the pexophagosome. Meanwhile, inhibition of retrograde ER transport does not affect pexophagosome formation, but instead suppresses pexophagosome fusion with vacuole and/or degradation by the vacuolar enzymes. Our results demonstrate that protein sorting and vesicular movements directed by Sar1p are essential for micro- and macropexophagy.

Table6-1: *Pichia pastoris* strains

Name	Genotype	Reference
GS115	*his4*	(Cregg *et al.*, 1985)
PPF1	*arg4 his4*	(Yuan *et al.*, 1997)
DMM1	GS115::pDM1 (P_{AOX1}BFP-SKL, ZeocinR)	(Kim *et al.*, 2001)
AJM38	GS115 *his4*::pWD18 (P_{ATG7} *atg7*-HA (C518S), *HIS4*)	This study
WDY64	PPF1 *his4 arg4*::pWD16-Sar1(T34N) (P_{CUP} *sar1*(T34N), *ARG4*)	This study
WDY65	PPF1 *his4 arg4*::pWD16-Sar1(H79G) (P_{CUP} *sar1*(H79G), *ARG4*)	This study
WDY66	WDY64 *his4*::pWD21 (P_{GAPDH} GFP-*ATG8*, *HIS4*)	This study
WDY67	WDY65 *his4*:: pWD21 (P_{GAPDH} GFP-*ATG8*, *HIS4*)	This study
WDY70	DMM1 *his4*::pWD21 (P_{GAPDH} GFP-*ATG8*, *HIS4*)	This study
WDY111	SJCF257 *arg4 his4 atg8Δ*::pWD18(P_{ATG7} *atg7*-HA (C518S), *HIS4*)	This study
WDY120	LAM44 :: pAJM6 (P_{GAPDH} mRFP-*ATG9*, ZeocinR)	This study
WDY121	LAM45 :: pAJM6 (P_{GAPDH} mRFP-*ATG9*, ZeocinR)	This study
WDY122	WDY66 :: pAJM6 (P_{GAPDH} mRFP-*ATG9*, ZeocinR)	This study
WDY123	WDY67 :: pAJM6 (P_{GAPDH} mRFP-*ATG9*, ZeocinR)	This study
WDY126	WDY64 *his4*::pWD18(P_{ATG7} *atg7*-HA (C518S), *HIS4*)	This study
WDY127	WDY65 *his4*::pWD18(P_{ATG7} *atg7*-HA (C518S), *HIS4*)	This study
LAM13	DMM1 *his4*::pSar1(T34N) (P_{CUP} *sar1*(T34N), *HIS4*)	This study
LAM14	DMM1 *his4*::pSar1(H79G) (P_{CUP} *sar1*(H79G), *HIS4*)	This study
LAM40	WDY64 *his4*:: pTC1 (P_{GAPDH} GFP-*ATG9*, *HIS4*)	This study
LAM41	WDY65 *his4*:: pTC1 (P_{GAPDH} GFP-*ATG9*, *HIS4*)	This study
LAM42	WDY64 *his4*::pPS64 (P_{GAPDH} GFP/HA-*ATG11*, *HIS4*)	This study
LAM43	WDY65 *his4*::pPS64 (P_{GAPDH} GFP/HA-*ATG11*, *HIS4*)	This study
LAM44	WDY64 *his4*::pPS69 (P_{GAPDH} GFP-*ATG2*, *HIS4*)	This study
LAM45	WDY65 *his4*::pPS64 (P_{GAPDH} GFP-*ATG2*, *HIS4*)	This study
LAM46	WDY64 *his4*::pPS55-G12 (P_{GAPDH} GFP/HA-*ATG18*, *HIS4*)	This study
LAM47	WDY65 *his4*::pPS55-G12 (P_{GAPDH} GFP/HA-*ATG18*, *HIS4*)	This study
LAM54	WDY64 *his4*::pWD24 (P_{GAPDH} GFP-*ATG17*, *HIS4*)	This study
LAM55	WDY65 *his4*::pWD24 (P_{GAPDH} GFP-*ATG17*, *HIS4*)	This study
LAM63	WDY64 *his4*::pIB2-dsRED-HDEL (P_{GAPDH} dsRFP-HDEL, *HIS4*)	This study
LAM64	WDY65 *his4*::pIB2-dsRED-HDEL (P_{GAPDH} dsRFP-HDEL, *HIS4*)	This study

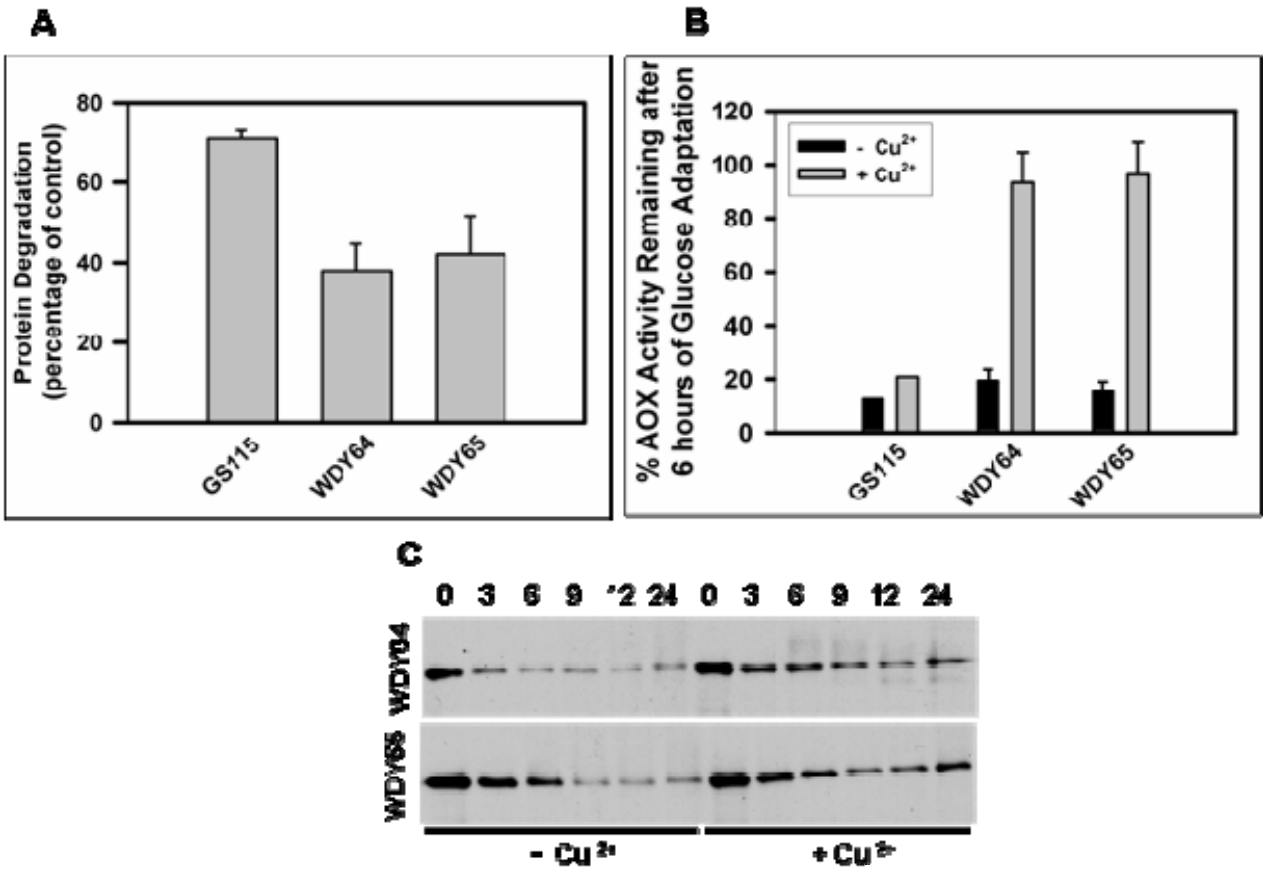

Figure 6-1. Sar1p is essential for autophagy and pexophagy. Autophagy (A), glucose-induced micropexophagy (B) and ethanol-induced macropexophagy (C) were evaluated in wild-type cells and cells expressing Sar1pT34N and Sar1pH79G. In panel A, endogenous proteins of GS115, WDY64, and WDY65 cells were labeled with ^{14}C-valine for 16 hours in YND. The cells were then washed and switched to SD-N medium (± $CuSO_4$) supplemented with 10 mM valine. Aliquots were removed at 2-24 hours of chase and precipitated with TCA. The rates of protein degradation based on the production of TCA-soluble radioactivity were expressed as a percentage relative to untreated controls. In panel B, GS115, WDY64, and WDY65 cells were grown in YNM and then switched to YND (± $CuSO_4$) at which time the loss of AOX activity was measured over 6h. The data represents the mean ± SD of 4-6 trials. In panel C, GS115, WDY64, and WDY65 cells were grown in YNM and then switched to YNE (± $CuSO_4$). At 0-24h samples were prepared for SDS-PAGE and the remaining AOX visualized by Western blotting. The data represents a representative blot of 3 different trials.

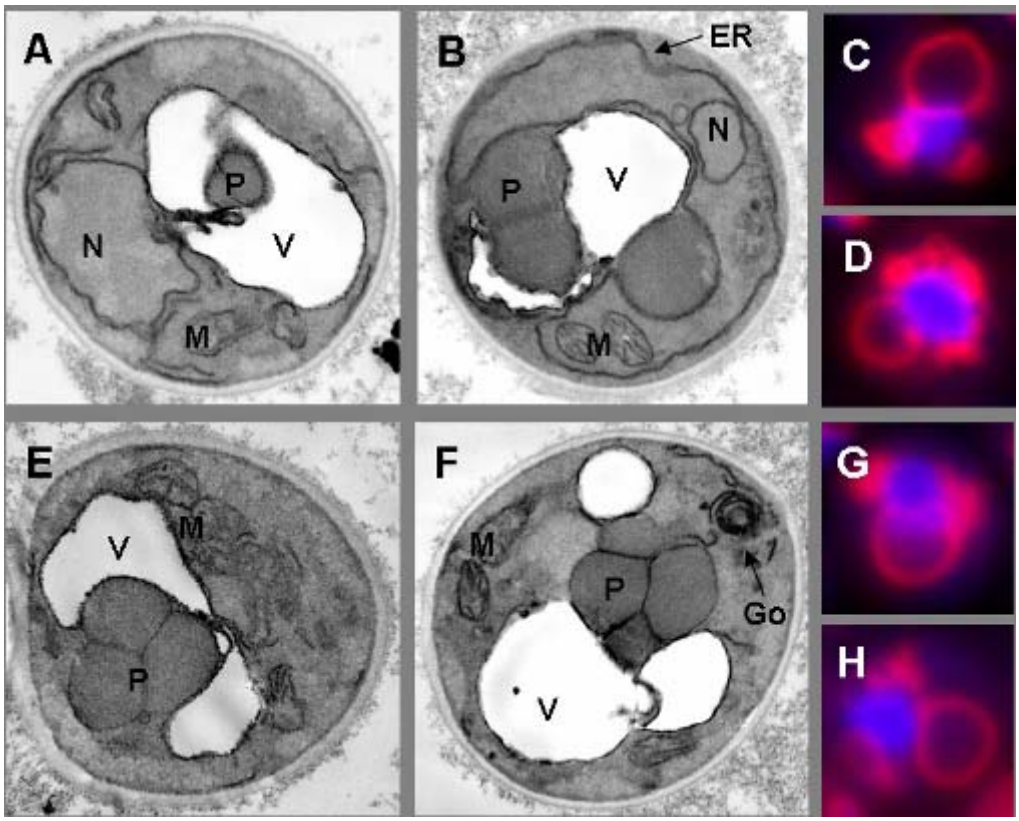

Figure 6-2. The expression of Sar1pT34N or Sar1pH79G suppresses a late sequestration event of micropexophagy. WDY64 (A, B), WDY65 (E and F), LAM13 (C, D), and LAM14 (G, H) were adapted from YNM to YND in the absence (A, E) and presence (B, C, D, F, G, H) of $CuSO_4$ for 2-3 hours. Cells were then fixed and prepared for viewing by electron microscopy (A, B, E, F) or viewed *in situ* by fluorescence microscopy (C, D, G, H). In cells not treated with $CuSO_4$, the peroxisomes (P) could be found within the vacuole (A) or surrounded by membranes derived from the vacuole (E). When cells expressed either Sar1pT34N (B) or Sar1pH79G, the peroxisomes were partially surrounded by the vacuole and sequestering membranes, but not observed within the vacuole. An extensive, ribbon-like endoplasmic reticulum (ER) was observed in cells expressing Sar1pT34N while a multilamellar Golgi (Go) apparatus was present with Sar1pH79G expression. By fluorescence microscopy, the vacuole and those sequestering membranes derived from the vacuole were observed by staining with FM4-64, and the peroxisomes were visualized by expressing BFP-SKL. In cells expressing either Sar1pT34N or Sar1pH79G, the peroxisomes were found to be almost completely surrounded by sequestering membranes. These membranes stained with FM4-64 and appeared as vesiculated extensions of the vacuole.

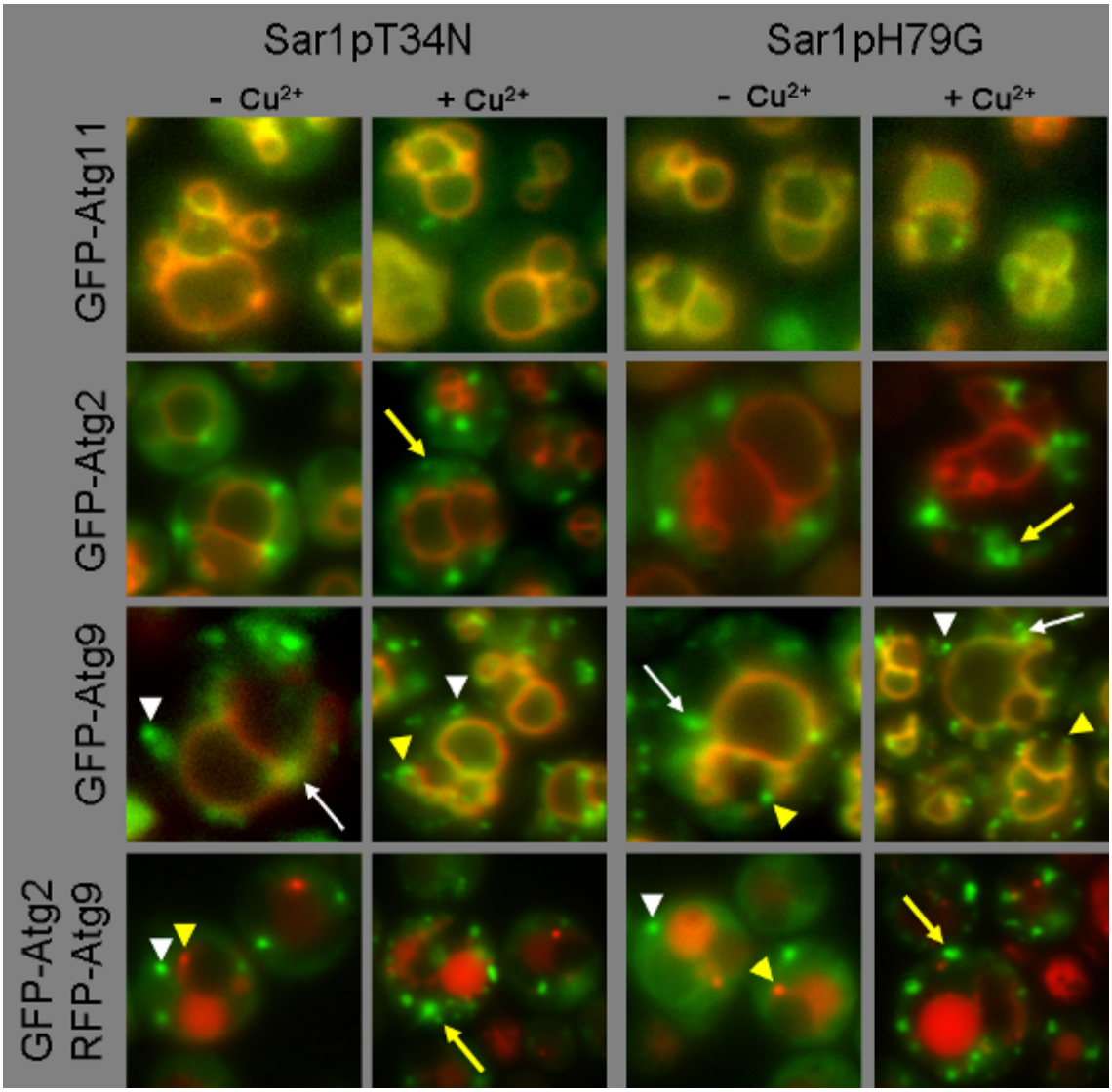

Figure 6-3. The trafficking of Atg11p, Atg2p and Atg9p during glucose-induced micropexophagy is not dependent upon Sar1p. WDY64 and WDY65 cells expressing GFP-Atg11p, GFP-Atg2p, GFP-Atg9p or GFP-Atg2p and RFP-Atg9p were adapted from YNM to YND in the absence and presence of $CuSO_4$. At 2h of glucose adaptation, the cells were visualized by fluorescence microscopy. The cellular localizations of Atg11p, Atg2p and Atg9p were unaltered in cells expressing Sar1pT34N or Sar1pH79G. GFP-Atg11p was present at the vacuole and sequestering membranes. GFP-Atg2p was visualized at peripheral foci. However, in the presence of the Sar1p mutants, these foci appeared to be greater in number and sometimes coalesced forming irregular structures (yellow arrows). GFP-Atg9p was observed at the vacuole and sequestering membranes labeled with FM4-64. Atg9p could also be visualized at perivacuolar structures (white arrows), peripheral foci (white arrowheads), and the PAS at the tips of the sequestering membranes (yellow arrowheads). The coalescing foci of Atg2p did not contain RFP-Atg9p.

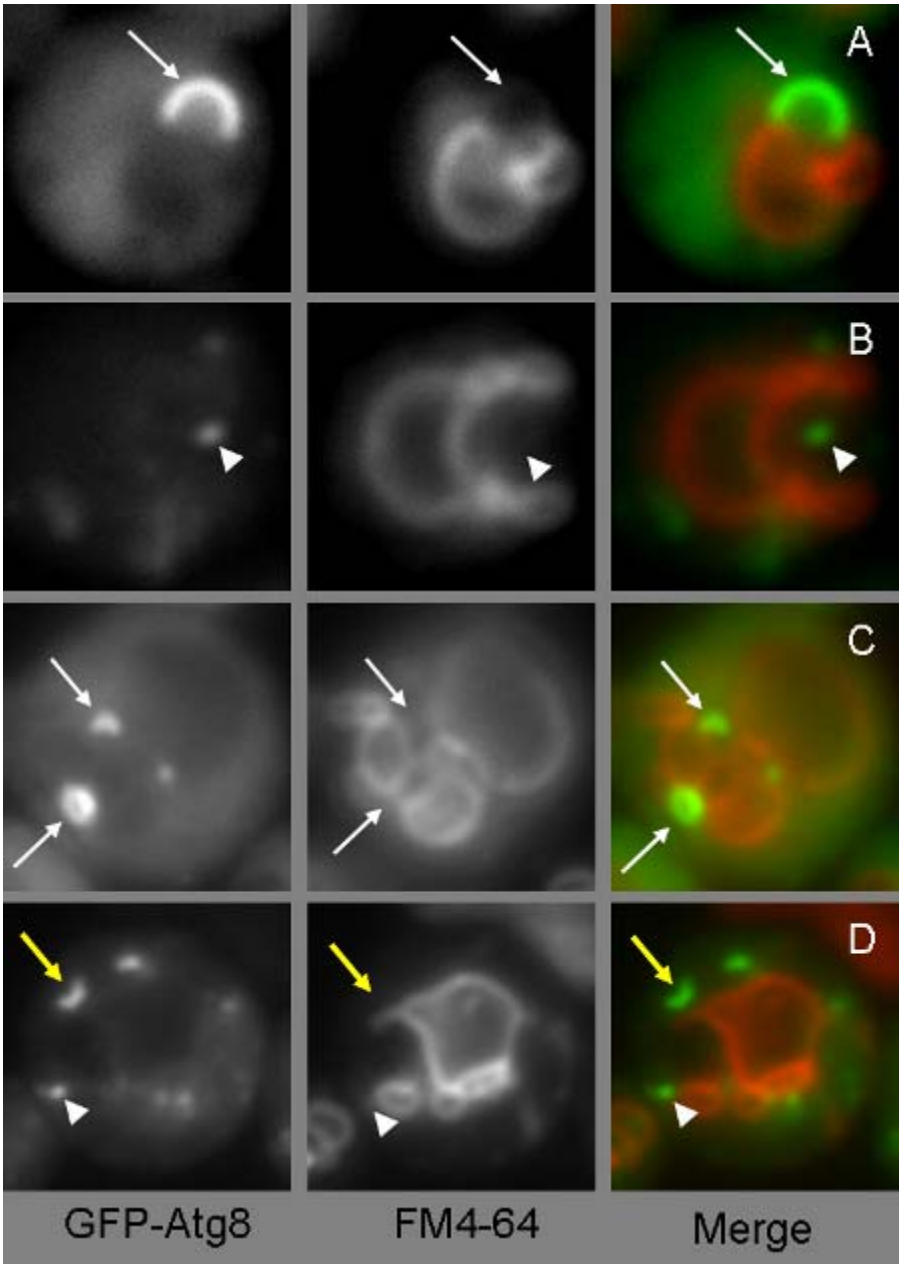

Figure 6-4. Sar1p is essential for the formation of the MIPA. WDY64 and WDY65 cell lines expressing GFP-Atg8 were adapted from YNM to YND in the absence and presence of CuSO4. At 2h of glucose adaptation, the cells were visualized by fluorescence microscopy. The vacuole and those sequestering membranes derived from the vacuole were observed by staining with FM4-64 while the MIPA was observed as a crescent-shaped structure labeled with GFP-Atg8 (arrows). In the absence of copper, the MIPA was found bridging the FM4-64 labeled membranes. However, when the expression of either Sar1pT34N or Sar1pH79G was induced with $CuSO_4$, GFP-Atg8p localized to one or more dots that appeared to be distributed throughout the cell (arrowheads). Occasionally, GFP-Atg8p could be found in a flattened MIPA-like structure, but not situated near sequestering membranes (yellow arrows).

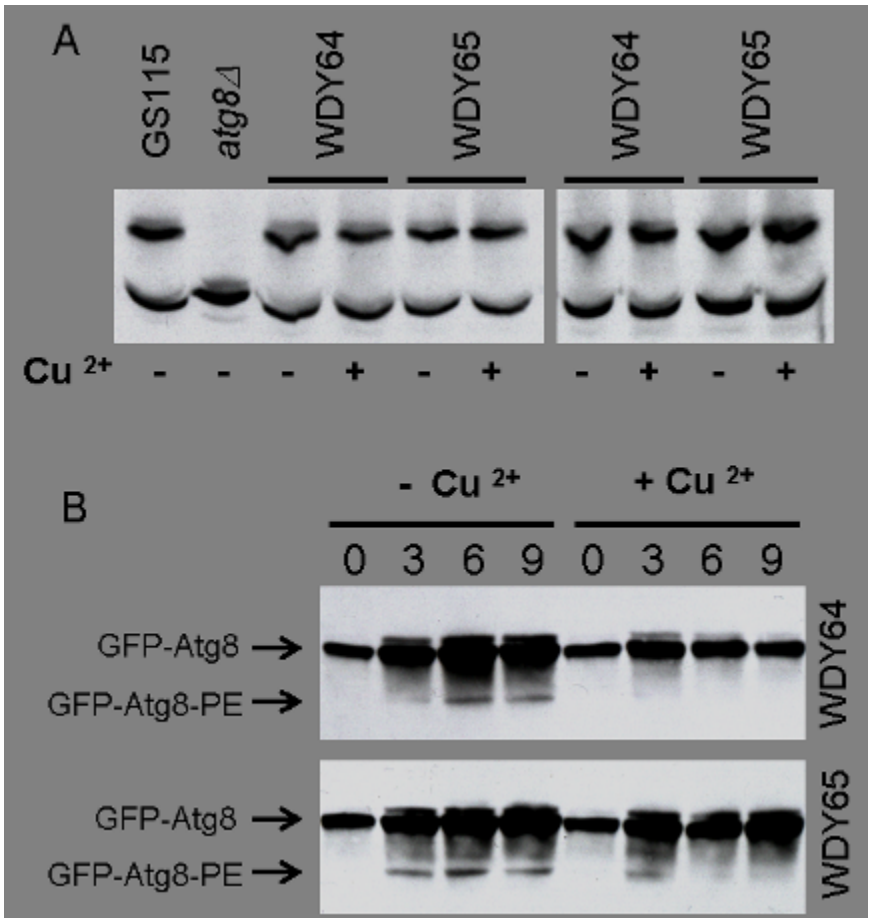

Figure 6-5. The effects of Sar1p on the lipidation of Atg8p. In panel A, Atg7pC518S-HA was expressed in GS115, SJCF257 (*atg8Δ*), WDY64 and WDY65 cells. The cells were adapted from YNM to YND in the absence and presence of $CuSO_4$ for 3h (left panel) and 6h (right panel). At that time, the cells were solubilized in SDS sample buffer, and the 75kDa Atg7p and 100kDa Atg7p protein-protein conjugate visualized by Western blotting. The protein-protein conjugates of Atg7pC518S were observed in wild-type cells and in cells expressing Sar1pT34N or Sar1pH79G, but not in cells lacking Atg8p. In panel B, WDY64 and WDY65 cells expressing GFP-Atg8p were adapted from YNM to YND in the absence and presence of $CuSO_4$ for 0-9h. The cells were then solubilized and the processing of Atg8p examined by Western blot. During glucose adaptation, a 38kDa form of GFP-Atg8p was observed at 3-6h. This protein was not present when Sar1pT34N or Sar1pH79G was expressed. The slower migration of this protein compared the GFP-Atg8p is consistent with the lipidated form of Atg8p.

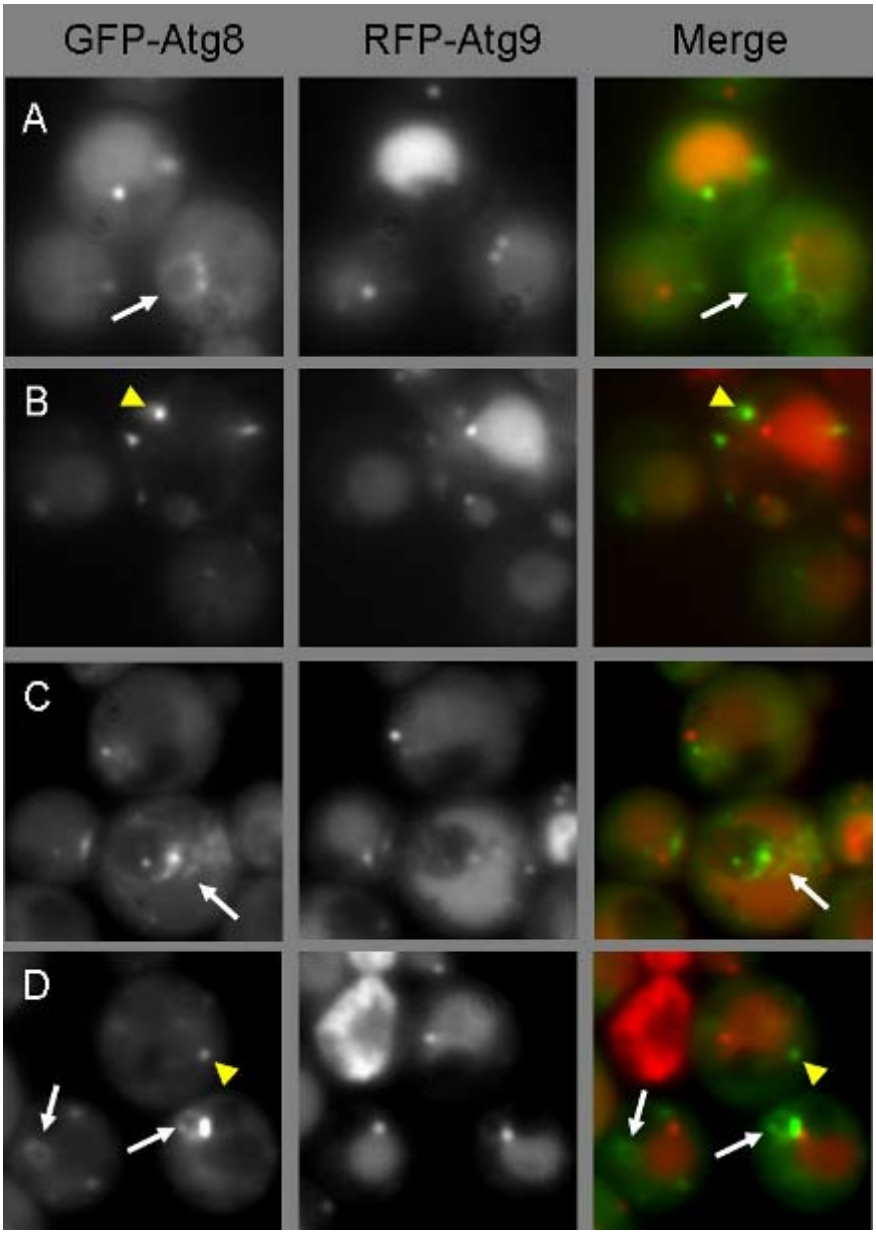

Figure 6-6. Effects of Sar1pT34N and Sar1pH79G on ethanol-induced macropexophagy. WDY64 (A and B) and WDY65 (C and D) cell lines expressing GFP-Atg8p and RFP-Atg9p were adapted from YNM to YNE in the absence (A and C) and presence (B and D) of CuSO4. At 2h of ethanol adaptation, the cells were visualized by fluorescence microscopy. In the absence of CuSO4, GFP-Atg8p was found at the PAS (yellow arrowheads) and pexophagosomes (white arrows). RFP-Atg9p was at foci juxtaposed to the vacuole or the pexophagosome. Colocalization of RFP-Atg9p and GFP-Atg8p at the PAS or pexophagosome was rare, but both proteins could be observed within the vacuole. When Sar1pT34N is expressed, GFP-Atg8p was found almost exclusively at foci presumed to be the PAS. GFP-Atg9p was observed within the vacuole and at perivacuolar foci that lacked GFP-Atg8p. To the contrary, when Sar1pH79G is expressed, GFP-Atg8p was found at the PAS and pexophagosome. GFP-Atg9p was visualized at perivacuolar foci and within the vacuole.

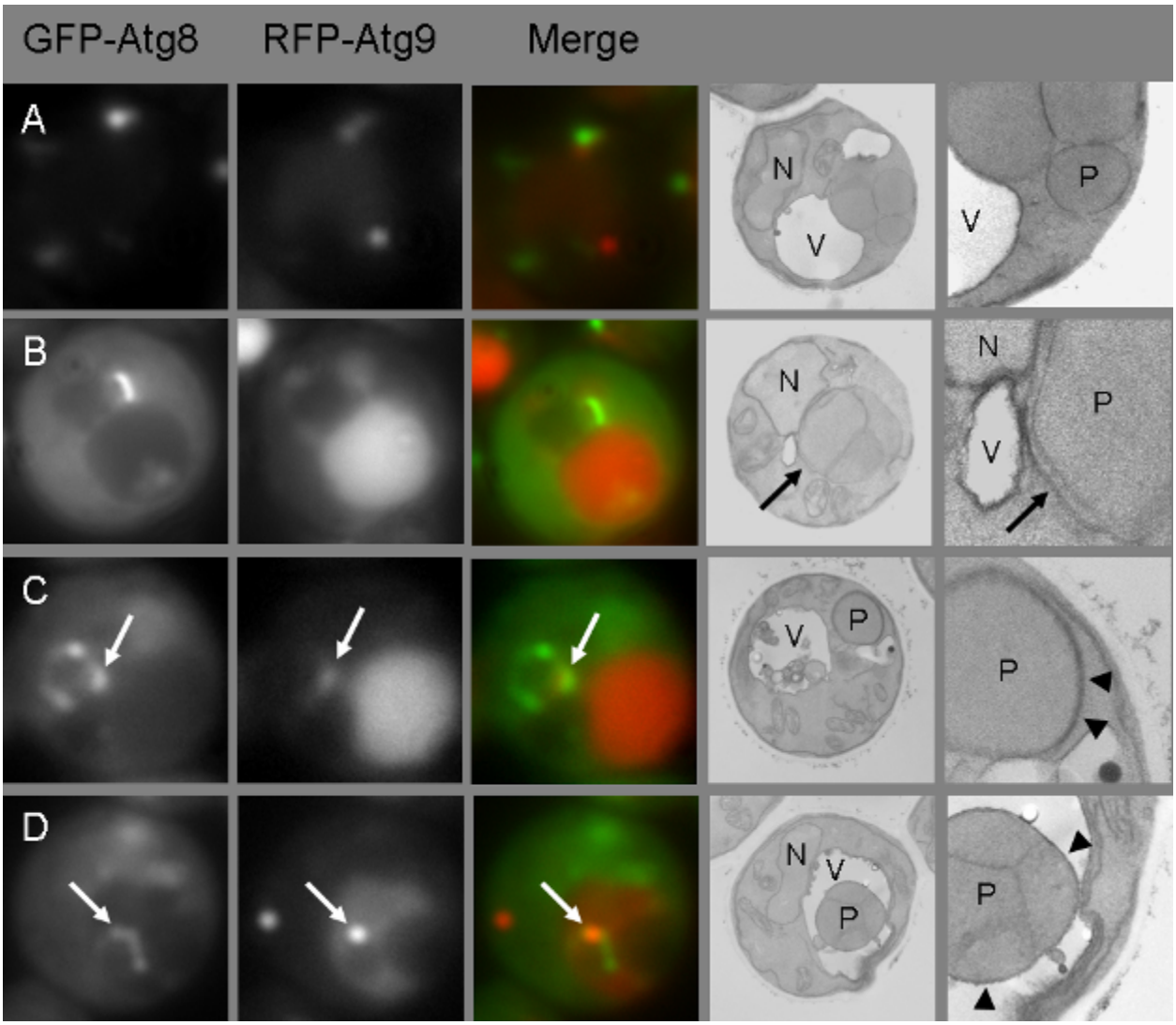

Figure 6-7. Sar1pT34N suppresses formation of the pexophagosome while Sar1pH79G suppresses delivery of the peroxisomes from the pexophagosome to the vacuole. WDY64 and WDY65 cell lines expressing GFP-Atg8p were adapted from YNM to YNE in the presence of copper sulfate. At 2h of ethanol adaptation, the cells were visualized by fluorescence microscopy or fixed and processed for electron microscopy. When Sar1pT34N was expressed, GFP-Atg8p was found at the PAS (A) and occasionally at crescent-shaped structures (B). Indeed, membranes were occasionally observed near peroxisomes, but not engulfing them (black arrow). Meanwhile, in cells expressing Sar1pH79G, pexophagosomes containing GFP-Atg8p were observed (C and D). Distinct foci containing GFP-Atg8p and RFP-Atg9p (white arrows) were observed at the pexophagosome. The pexophagosome bound by multiple membranes was visualized by electron microscopy (C, arrowheads). At times, we also observed remnants of GFP-Atg8p membranes and single membrane-bound undegraded peroxisomes within the vacuole (D, arrowheads). Trafficking of RFP-Atg9p to the vacuole was unaltered by the expression of either Sar1p mutant. N, nucleus; P, peroxisome; and V, vacuole.

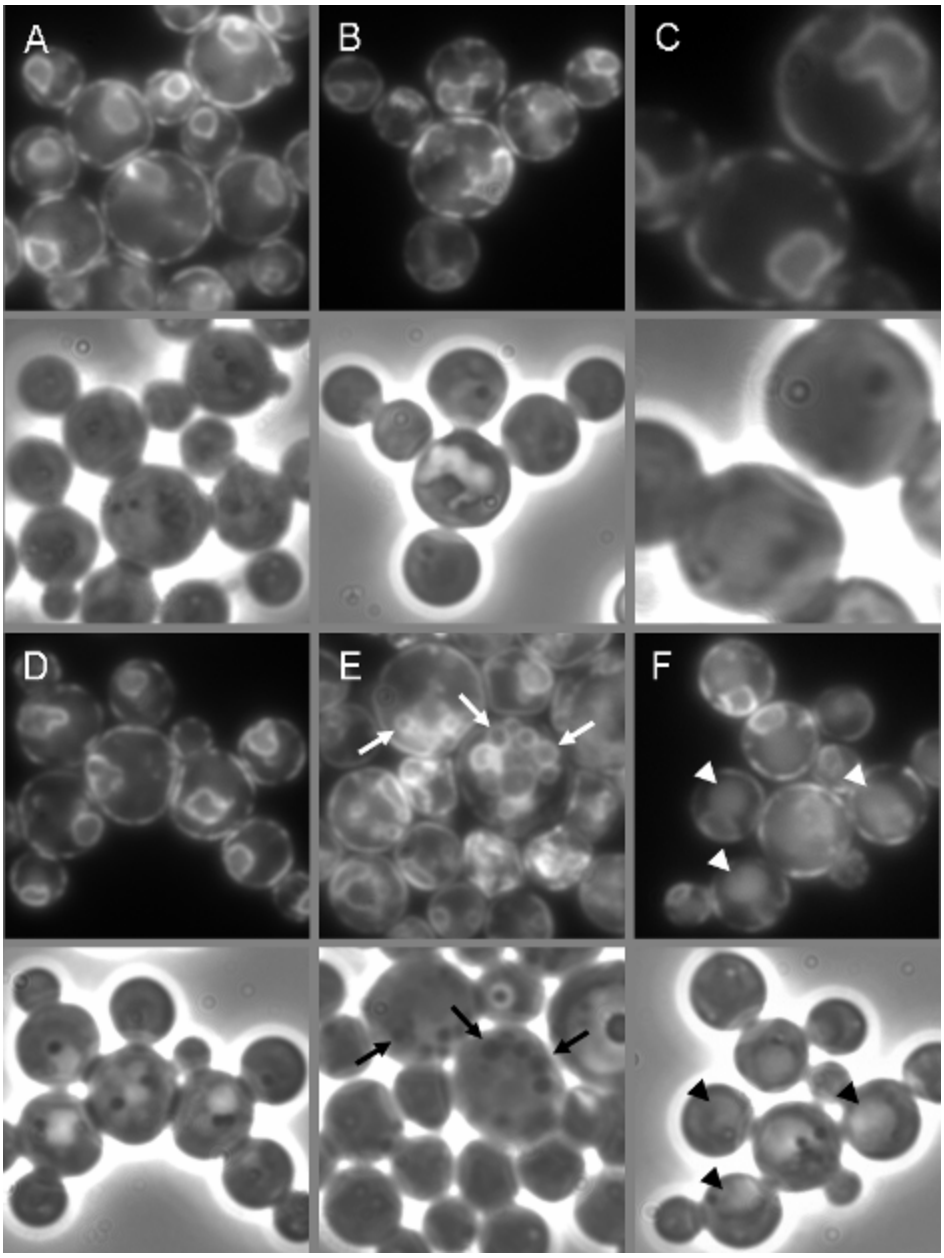

Figure 6-8. Components of the endoplasmic reticulum are present at the pexophagosome when cells express Sar1pH79G. WDY64 (A, B, and C) and WDY65 (D, E, and F) cell lines expressing RFP-HDEL were adapted from YNM to YNE in the absence (A and D) and presence (B, C, E, and F) of CuSO4. At 2h (A, B, D, and E) and 3h (C and F) of ethanol adaptation, the cells were visualized by fluorescence microscopy. RFP-HDEL was localized solely to the ER situated near the cell periphery and around the nucleus. This distribution was unaltered during macropexophagy (A and D). When Sar1pT34N was expressed, the cellular distribution of RFP-HDEL was restricted to the ER (B and C). However, at 2h of ethanol adaptation in the presence of Sar1pH79G, RFP-HDEL was visualized not only at the ER but also at vacuoles containing phase-dense peroxisomes (E, white arrows). At 3h, RFP-HDEL could be detected within the yeast vacuole (F, white arrowheads).

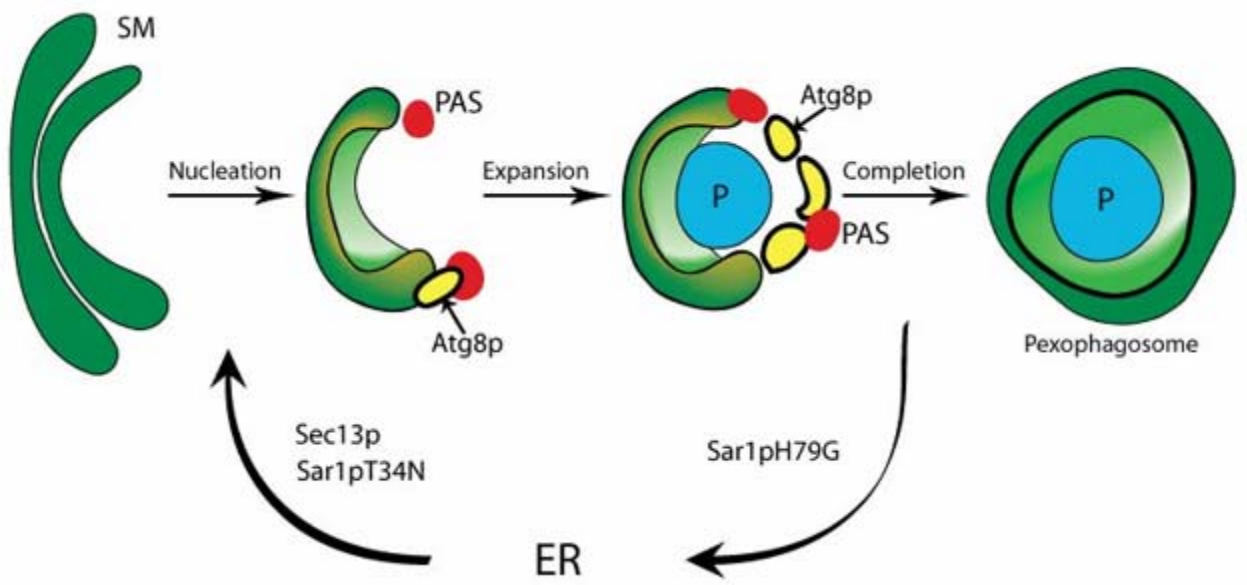

Figure 6-9. Model of the role of Sar1p in macropexophagy. During ethanol adaptation, peroxisomes (P) are engulfed by pexophagosomes that are assembled from sequestering membranes (SM) and expanded by the PAS with membranes containing Atg8p. Based on our data, we propose that Sar1p is required for the movements of ER proteins into and out of the pexophagosome. The pexophagosome assembles with the assistance of Sec13p and Sar1p delivery of ER proteins. The anterograde transport of ER proteins to the forming pexophagosome is inhibited by Sar1pT34N which is unable to exchange GTP for GDP. Once the pexophagosome is assembled, the ER proteins are recycled back to the ER with the aid of Sar1p. Retrograde transport of the ER proteins from the pexophagosome is inhibited by Sar1pH79G which is unable to hydrolyze GTP.

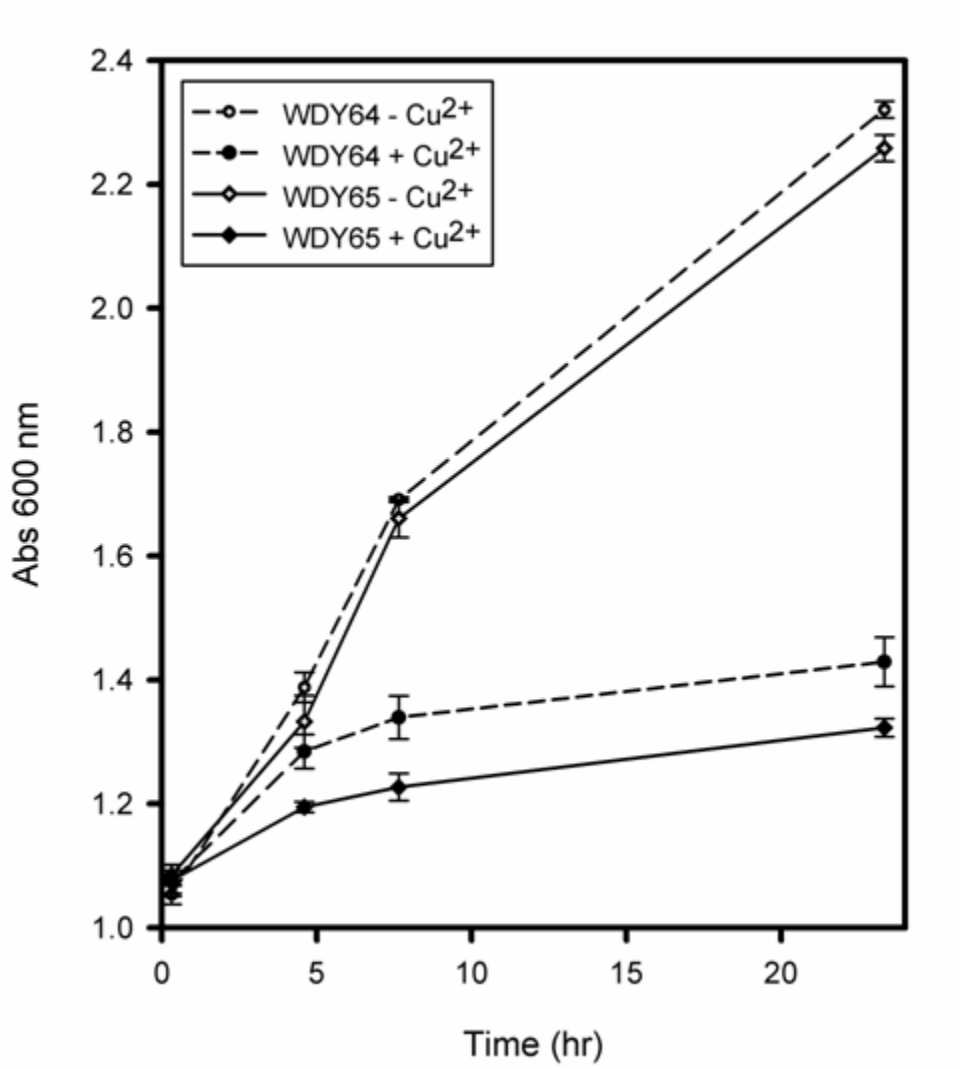

Figure 6-10. Effects of Sar1pT34N and Sar1pH79G on cell growth. Sar1pT34N and Sar1pH79G were grown in minimal medium for 24 hours in the absence or presence of $CuSO_4$ and growth of the culture assessed by measuring absorbance at 600nm. The effects of the Sar1p mutants on cell growth were minimal at five hours post copper induction. However, at longer times, growth was dramatically reduced compared to untreated cells.

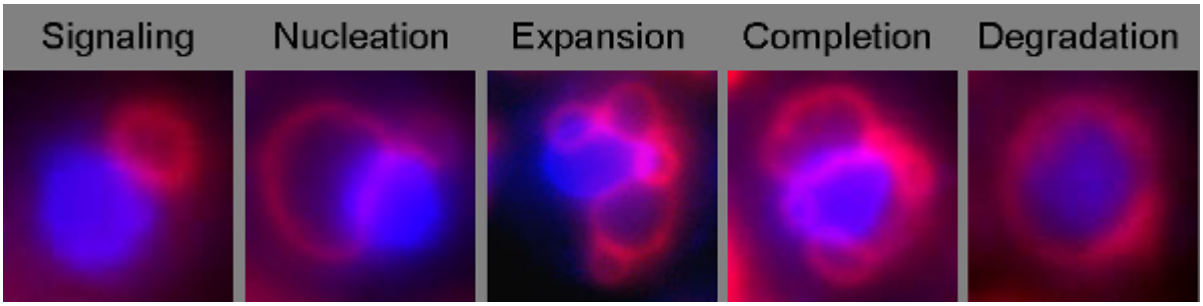

Figure 6-11. Stages of glucose-induced micropexophagy. Cells expressing BFP-SKL were adapted from YNM to YND for 2h. Cells at all stages of micropexophagy can be visualized by fluorescence microscopy. During YNM growth, the peroxisomes visualized by BFP-SKL were situated next to a round vacuole visualized by FM4-64. During nucleation, the sequestering membranes that arise from the vacuole only partially extend around the peroxisomes. The expansion stage was characterized by sequestering membranes extending 50 to 90% around the peroxisomes. The completion stage was characterized by peroxisomes fully surrounded by sequestering membranes that appear segmented and not fused. Finally, the degradative stage was characterized by continuous FM4-64 labeled membranes enclosing peroxisomes that were not clearly delineated.

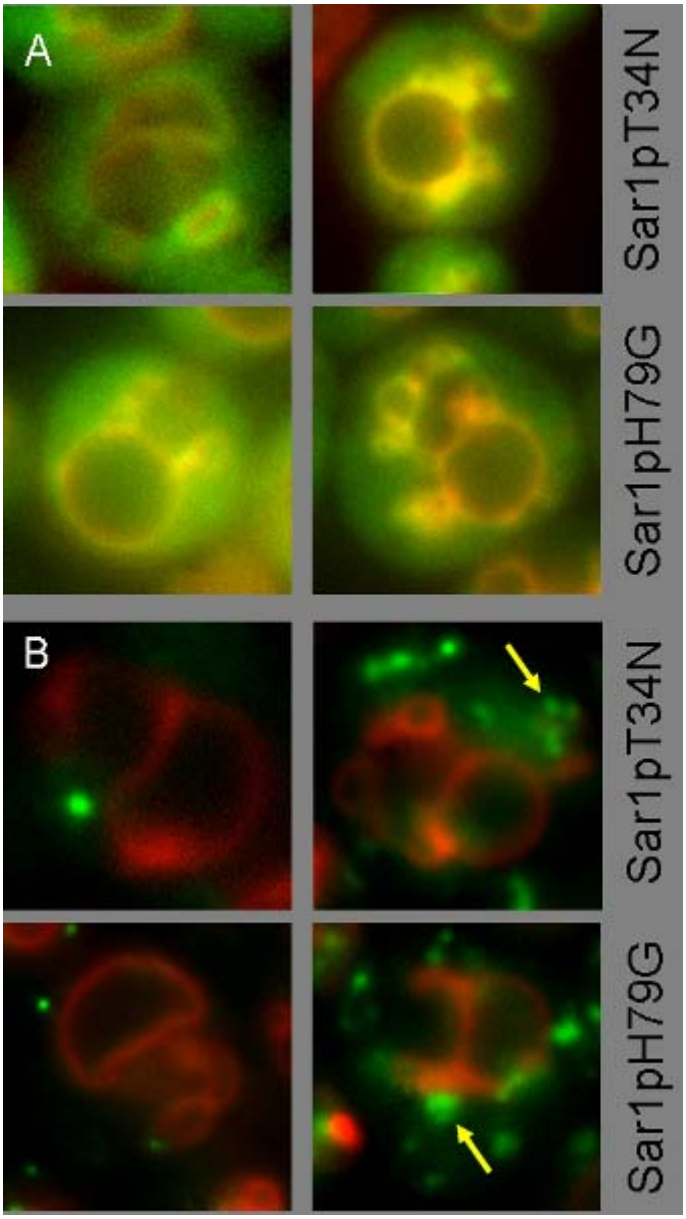

Figure 6-12. Cellular localization of Atg18p and Atg17p during glucose-induced micropexophagy in cells expressing Sar1pT34N or Sar1pH79G. WDY64 and WDY65 cells expressing GFP-Atg18p (A) or GFP-Atg17p (B) were adapted from YNM to YND (± CuSO4). At 2h of glucose adaptation, the cells were visualized by fluorescence microscopy. Regardless of the presence of the Sar1p mutants, GFP-Atg18p trafficked normally to the vacuole and sequestering membranes. In untreated cells, GFP-Atg17p was visualized at 1-3 foci (PAS) near the vacuole. In cells expressing Sar1pT34N or Sar1pH79G, GFP-Atg17p localized to multiple foci that at times appeared to coalesce (yellow arrows).

CHAPTER 7
CONCLUSION

These studies first explain how to procure a restriction enzyme-mediated integration mutant (REMI) (Chapter 2). Using this application, we have identified a number of ATG genes essential for pexophagy and autophagy.

In Chapter 3, I characterized one such gene, ATG9 that encodes an integral membrane protein with 5-6 transmembrane domains. At this time, Atg9 was the only known transmembrane protein required for pexophagy. We next evaluated the subcellular localization of Atg9 by tagging GFP to its N-terminus. In fed cells, I showed that Atg9 localized to a unique peripheral compartment (PC9) that did not contain protein markers for endoplasmic reticulum, transition ER, Golgi apparatus, or mitochondria. Upon glucose-induced micropexophagy, Atg9 was found at perivacuolar structures (PVS) situated at the base of the sequestering membranes (SM) that arose from the vacuole and at the SM. Because Atg9 was present in multiple compartments during pexophagy, my aim was to define its trafficking in the hopes of better understanding the assembly and expansion of the SM during pexophagy. I also showed that the trafficking of Atg9 to the PVS required Vps15 and Atg11. Movements of Atg9 from the PVS to the SM required Atg2 and Atg7. These studies were the first to demonstrate the movements of a membrane protein to the expanding sequestering membranes.

In Chapters 4 and 5, I set out to define the functional motifs within Atg9. Atg9 is present throughout all eukaryotes, and its homologous regions were examined by FASTA analysis. Atg9 membrane motifs of import were predicted by *in situ* analysis to increase the probability that my site-directed mutagenesis would be productive and efficient. Multiple motifs were shown to be important for Atg9 function and trafficking. I have shown that Atg9 has two domains required for ER exit (one of which is characterized by two glutamates), one di-lysine-like motif required

for PC9 exit, one motif necessary for its association with the SM and may associate with peroxisomal membrane proteins, and one domain not required for trafficking to the SM but is essential for Atg9 function. All of these motifs are required for Atg9 function during pexophagy and autophagy, suggesting that Atg9 functions at the SM.

In Chapter 5, I showed that Sar1p is essential for pexophagy and autophagy. Our expanding knowledge of the field of pexophagy has led to the pursuit of the role of the ER in pexophagy. Unfortunately, the very early events regulating pexophagy are poorly understood. Moreover, there has been considerable heated discussion concerning the origin of the pexophagic membranes. Whether the ER contributes to these membranes or the membranes are synthesized *de novo* has been a topic of heated debate for twenty years. Sar1 is the GTPase responsible for the generation of COPII vesicles. Thus, the study of dominant-negative Sar1 mutants in regards to the trafficking of Atg proteins appeared to be a straightforward approach to addressing pexophagic regulation and the formation of pexophagosomes. Sar1 appears to be the earliest post-translational protein factor influencing pexophagy. The finding that Sar1 is required for micropexophagic-specific membrane apparatus (MIPA) formation suggests a requirement for COPII trafficking in SM expansion and completion during micropexophagy. I also showed that cells expressing sar1T34N, which suppresses protein exit from the ER, cannot form autopexophagosomes. Meanwhile, cells expressing sar1pH79G, which inhibits retrograde transport back to the ER, do form autopexophagosomes. These autopexophagosomes contain an ER marker protein suggesting that sar1H79G inhibits the recycling of the ER proteins.

I am the first to characterize the roles of Atg9 and Sar1 in the expansion of the sequestering membranes during micropexophagy. These studies have provided new directions and molecular tools to examine these events during macropexophagy and autophagy.

LIST OF REFERENCES

Abeliovich, H., Zhang, C., Dunn, W.A., Jr., Shokat, K.M., and Klionsky, D.J. (2003). Chemical genetic analysis of Apg1 reveals a non-kinase role in the induction of autophagy. Mol. Biol. Cell 14, 477-490.

Ano, Y., Hattori, T., Oku, M., Mukaiyama, H., Baba, M., Ohsumi, Y., Kato, N., and Sakai, Y. (2005). A sorting nexin PpAtg24 regulates vacuolar membrane dynamics during pexophagy via binding to phosphatidylinositol-3-phosphate. Mol Biol Cell 16, 446-457.

Barlowe, C. (2002). Three-dimensional structure of a COPII prebudding complex. Dev Cell 3, 467-468.

Barlowe, C. (2003). Molecular recognition of cargo by the COPII complex: a most accommodating coat. Cell. 114, 395-397.

Barlowe, C. (2003). Signals for COPII-dependent export from the ER: what's the ticket out? Trends Cell Biol 13, 295-300.

Bevis, B.J., Hammond, A.T., Reinke, C.A., and Glick, B.S. (2002). De novo formation of transitional ER sites and Golgi structures in Pichia pastoris. Nat Cell Biol 4, 750-756.

Bevis, B.J., Hammond, A.T., Reinke, C.A., and Glick, B.S. (2002). De novo formation of transitional ER sites and Golgi structures in Pichia pastoris. Nat. Cell Biol. 4, 750-756.

Brown, D.H., Jr., Slobodkin, I.V., and Kumamoto, C.A. (1996). Stable transformation and regulated expression of an inducible reporter construct in Candida albicans using restriction enzyme-mediated integration. Mol Gen Genet 251, 75-80.

Brown, J.S., Aufauvre-Brown, A., and Holden, D.W. (1998). Insertional mutagenesis of Aspergillus fumigatus. Mol Gen Genet 259, 327-335.

Bryant, N.J., and Stevens, T.H. (1998). Vacuole biogenesis in Saccharomyces cerevisiae: protein transport pathways to the yeast vacuole. Microbiol Mol Biol Rev 62, 230-247.

Budovskaya, Y.V., Hama, H., DeWald, D.B., and Herman, P.K. (2002). The C terminus of the Vps34p phosphoinositide 3-kinase is necessary and sufficient for the interaction with the Vps15p protein kinase. J Biol Chem 277, 287-294.

Campbell, C.L., and Thorsness, P.E. (1998). Escape of mitochondrial DNA to the nucleus in yme1 yeast is mediated by vacuolar-dependent turnover of abnormal mitochondrial compartments. J. Cell Sci. 111 (Pt 16), 2455-2464.

Campbell, R.E., Tour, O., Palmer, A.E., Steinbach, P.A., Baird, G.S., Zacharias, D.A., and Tsien, R.Y. (2002). A monomeric red fluorescent protein. Proc. Natl. Acad. Sci. U S A 99, 7877-7882.

Celli, J., Salcedo, S.P., and Gorvel, J.P. (2005). Brucella coopts the small GTPase Sar1 for intracellular replication. Proc Natl Acad Sci U S A 102, 1673-1678.

Chang, C.Y., and Huang, W.P. (2007). Atg19 mediates a dual interaction cargo sorting mechanism in selective autophagy. Mol Biol Cell 18, 919-929.

Chang, T., Schroder, L.A., Thomson, J.M., Klocman, A.S., Tomasini, A.J., Stromhaug, P.E., and Dunn, W.A., Jr. (2005). PpATG9 encodes a novel membrane protein that traffics to vacuolar membranes, which sequester peroxisomes during pexophagy in Pichia pastoris. Mol Biol Cell 16, 4941-4953.

Cregg, J.M., Barringer, K.J., Hessler, A.Y., and Madden, K.R. (1985). Pichia pastoris as a host system for transformations. Mol Cell Biol 5, 3376-3385.

Cregg, J.M., Barringer, K.J., Hessler, A.Y., and Madden, K.R. (1985). Pichia pastoris as a host system for transformations. Mol. Cell. Biol. 5, 3376-3385.

Dietrich, L.E., Gurezka, R., Veit, M., and Ungermann, C. (2004). The SNARE Ykt6 mediates protein palmitoylation during an early stage of homotypic vacuole fusion. Embo J 23, 45-53.

Dunn, W.A., Jr. (1990). Studies on the mechanisms of autophagy: formation of the autophagic vacuole. J. Cell. Biol. 110, 1923-1933.

Dunn, W.A., Jr. (1994). Autophagy and related mechanisms of lysosome-mediated protein degradation. Trends Cell Biol. 4, 139-143.

Dunn, W.A., Jr., Cregg, J.M., Kiel, J.A., van der Klei, I.J., Oku, M., Sakai, Y., Sibirny, A.A., Stasyk, O.V., and Veenhuis, M. (2005). Pexophagy: the selective autophagy of peroxisomes. Autophagy 1, 75-83.

Fischer von Mollard, G., and Stevens, T.H. (1999). The Saccharomyces cerevisiae v-SNARE Vti1p is required for multiple membrane transport pathways to the vacuole. Mol Biol Cell 10, 1719-1732.

Fry, M.R., Thomson, J.M., Tomasini, A.J., and Dunn, W.A., Jr. (2006). Early and late molecular events of glucose-induced pexophagy in Pichia pastoris require Vac8. Autophagy 2, 280-288.

Gaynor, E.C., te Heesen, S., Graham, T.R., Aebi, M., and Emr, S.D. (1994). Signal-mediated retrieval of a membrane protein from the Golgi to the ER in yeast. J Cell Biol 127, 653-665.

Gimeno, R.E., Espenshade, P., and Kaiser, C.A. (1995). SED4 encodes a yeast endoplasmic reticulum protein that binds Sec16p and participates in vesicle formation. J Cell Biol 131, 325-338.

Granado, J.D., Kertesz-Chaloupkova, K., Aebi, M., and Kues, U. (1997). Restriction enzyme-mediated DNA integration in Coprinus cinereus. Mol Gen Genet 256, 28-36.

Guan, J., Stromhaug, P.E., George, M.D., Habibzadegah-Tari, P., Bevan, A., Dunn, W.A., Jr., and Klionsky, D.J. (2001). Cvt18/Gsa12 is required for cytoplasm-to-vacuole transport, pexophagy, and autophagy in Saccharomyces cerevisiae and Pichia pastoris. Mol Biol Cell 12, 3821-3838.

Habibzadegah-Tari, P., and Dunn, W.A., Jr. (2003). Glucose-induced pexophagy in Pichia pastoris. In: Autophagy, ed. D.J. Klionsky: Landes Bioscience.

Hamasaki, M., Noda, T., and Ohsumi, Y. (2003). The early secretory pathway contributes to autophagy in yeast. Cell Struct Funct 28, 49-54.

Hanada, K., Kumagai, K., Yasuda, S., Miura, Y., Kawano, M., Fukasawa, M., and Nishijima, M. (2003). Molecular machinery for non-vesicular trafficking of ceramide. Nature 426, 803-809.

Hanaoka, H., Noda, T., Shirano, Y., Kato, T., Hayashi, H., Shibata, D., Tabata, S., and Ohsumi, Y. (2002). Leaf senescence and starvation-induced chlorosis are accelerated by the disruption of an Arabidopsis autophagy gene. Plant Physiol. 129, 1181-1193.

Hartley, A.D., Ward, M.P., and Garrett, S. (1994). The Yak1 protein kinase of Saccharomyces cerevisiae moderates thermotolerance and inhibits growth by an Sch9 protein kinase-independent mechanism. Genetics 136, 465-474.

He, C., Song, H., Yorimitsu, T., Monastyrska, I., Yen, W.L., Legakis, J.E., and Klionsky, D.J. (2006). Recruitment of Atg9 to the preautophagosomal structure by Atg11 is essential for selective autophagy in budding yeast. J Cell Biol 175, 925-935.

Herman, P.K., Stack, J.H., and Emr, S.D. (1991b). A genetic and structural analysis of the yeast Vps15 protein kinase: evidence for a direct role of Vps15p in vacuolar protein delivery. Embo. J. 10, 4049-4060.

Herman, P.K., Stack, J.H., DeModena, J.A., and Emr, S.D. (1991a). A novel protein kinase homolog essential for protein sorting to the yeast lysosome-like vacuole. Cell. 64, 425-437.

Huang, W.P., and Klionsky, D.J. (2002). Autophagy in yeast: a review of the molecular machinery. Cell Struct. Funct. 27, 409-420.

Ishihara, N., Hamasaki, M., Yokota, S., Suzuki, K., Kamada, Y., Kihara, A., Yoshimori, T., Noda, T., and Ohsumi, Y. (2001). Autophagosome Requires Specific Early Sec Proteins for Its Formation and NSF/SNARE for Vacuolar Fusion. Mol Biol Cell 12, 3690-3702.

Kihara, A., Noda, T., Ishihara, N., and Ohsumi, Y. (2001). Two Distinct Vps34 Phosphatidylinositol 3-Kinase Complexes Function in Autophagy and Carboxypeptidase Y Sorting in Saccharomyces cerevisiae. J Cell Biol 152, 519-530.

Kim, J., Huang, W.P., Stromhaug, P.E., and Klionsky, D.J. (2002). Convergence of multiple autophagy and cytoplasm to vacuole targeting components to a perivacuolar membrane compartment prior to de novo vesicle formation. J Biol Chem 277, 763-773.

Kim, J., Huang, W.P., Strømhaug, P.E., and Klionsky, D.J. (2002). Convergence of multiple autophagy and cytoplasm to vacuole targeting components to a perivacuolar membrane compartment prior to de novo vesicle formation. J. Biol. Chem. 277, 763-773.

Kim, J., Kamada, Y., Stromhaug, P.E., Guan, J., Hefner-Gravink, A., Baba, M., Scott, S.V., Ohsumi, Y., Dunn, W.A., and Klionsky, D.J. (2001). Cvt9/gsa9 functions in sequestering selective cytosolic cargo destined for the vacuole. J Cell Biol 153, 381-396.

Klionsky, D.J. (2005). The molecular machinery of autophagy: unanswered questions. J. Cell Sci. 118, 7-18.

Klionsky, D.J., Cregg, J.M., Dunn, W.A., Jr., Emr, S.D., Sakai, Y., Sandoval, I.V., Sibirny, A., Subramani, S., Thumm, M., Veenhuis, M., and Ohsumi, Y. (2003). A unified nomenclature for yeast autophagy-related genes. Dev. Cell 5, 539-545.

Komduur, J.A., Veenhuis, M., and Kiel, J.A. (2003). The Hansenula polymorpha PDD7 gene is essential for macropexophagy and microautophagy. FEMS Yeast Res 3, 27-34.

Kuge, O., Dascher, C., Orci, L., Rowe, T., Amherdt, M., Plutner, H., Ravazzola, M., Tanigawa, G., Rothman, J.E., and Balch, W.E. (1994). Sar1 promotes vesicle budding from the endoplasmic reticulum but not Golgi compartments. J Cell Biol 125, 51-65.

Lang, T., Reiche, S., Straub, M., Bredschneider, M., and Thumm, M. (2000). Autophagy and the cvt pathway both depend on AUT9. J Bacteriol 182, 2125-2133.

Leao-Helder, A.N., Krikken, A.M., Gellissen, G., van der Klei, I.J., Veenhuis, M., and Kiel, J.A. (2004). Atg21p is essential for macropexophagy and microautophagy in the yeast Hansenula polymorpha. FEBS Lett 577, 491-495.

Leao-Helder, A.N., Krikken, A.M., van der Klei, I.J., Kiel, J.A., and Veenhuis, M. (2003). Transcriptional down-regulation of peroxisome numbers affects selective peroxisome degradation in Hansenula polymorpha. J Biol Chem 278, 40749-40756.

Legesse-Miller, A., Sagiv, Y., Glozman, R., and Elazar, Z. (2000). Aut7p, a soluble autophagic factor, participates in multiple membrane trafficking processes. J Biol Chem 275, 32966-32973.

Levine, B., and Klionsky, D.J. (2004). Development by self-digestion: molecular mechanisms and biological functions of autophagy. Dev. Cell 6, 463-477.

Levine, T. (2004). Short-range intracellular trafficking of small molecules across endoplasmic reticulum junctions. Trends Cell Biol 14, 483-490.

Linnemannstons, P., Voss, T., Hedden, P., Gaskin, P., and Tudzynski, B. (1999). Deletions in the gibberellin biosynthesis gene cluster of Gibberella fujikuroi by restriction enzyme-mediated integration and conventional transformation-mediated mutagenesis. Appl Environ Microbiol 65, 2558-2564.

Mari, M., and Reggiori, F. (2007). Atg9 trafficking in the yeast Saccharomyces cerevisiae. Autophagy 3, 145-148.

Monastyrska, I., Kiel, J.A., Krikken, A.M., Komduur, J.A., Veenhuis, M., and van der Klei, I.J. (2005). The Hansenula polymorpha ATG25 gene encodes a novel coiled-coil protein that is required for macropexophagy. Autophagy 1, 92-100.

Monastyrska, I., van der Heide, M., Krikken, A.M., Kiel, J.A., van der Klei, I.J., and Veenhuis, M. (2005). Atg8 is Essential for Macropexophagy in Hansenula polymorpha. Traffic 6, 66-74.

Mukaiyama, H., Baba, M., Osumi, M., Aoyagi, S., Kato, N., Ohsumi, Y., and Sakai, Y. (2004). Modification of a ubiquitin-like protein Paz2 conducted micropexophagy through formation of a novel membrane structure. Mol Biol Cell 15, 58-70.

Mukaiyama, H., Oku, M., Baba, M., Samizo, T., Hammond, A.T., Glick, B.S., Kato, N., and Sakai, Y. (2002). Paz2 and 13 other PAZ gene products regulate vacuolar engulfment of peroxisomes during micropexophagy. Genes Cells 7, 75-90.

Nebauer, R., Rosenberger, S., and Daum, G. (2007). Phosphatidylethanolamine, a limiting factor of autophagy in yeast strains bearing a defect in the carboxypeptidase Y pathway of vacuolar targeting. J Biol Chem 282, 16736-16743.

Nice, D.C., Sato, T.K., Strømhaug, P.E., Emr, S.D., and Klionsky, D.J. (2002). Cooperative binding of the cytoplasm to vacuole targeting pathway proteins, Cvt13 and Cvt20, to phosphatidylinositol 3-phosphate at the pre-autophagosomal structure is required for selective autophagy. J. Biol. Chem. 277, 30198-30207.

Noda, T., Kim, J., Huang, W.P., Baba, M., Tokunaga, C., Ohsumi, Y., and Klionsky, D.J. (2000). Apg9p/Cvt7p is an integral membrane protein required for transport vesicle formation in the Cvt and autophagy pathways. J Cell Biol 148, 465-480.

Noda, T., Kim, J., Huang, W.P., Baba, M., Tokunaga, C., Ohsumi, Y., and Klionsky, D.J. (2000). Apg9p/Cvt7p is an integral membrane protein required for transport vesicle formation in the Cvt and autophagy pathways. J. Cell Biol. 148, 465-480.

Oka, T., and Nakano, A. (1994). Inhibition of GTP hydrolysis by Sar1p causes accumulation of vesicles that are a functional intermediate of the ER-to-Golgi transport in yeast. J Cell Biol 124, 425-434.

Oku, M., Nishimura, T., Hattori, T., Ano, Y., Yamashita, S., and Sakai, Y. (2006). Role of Vac8 in formation of the vacuolar sequestering membrane during micropexophagy. Autophagy 2, 272-279.

Oku, M., Warnecke, D., Noda, T., Muller, F., Heinz, E., Mukaiyama, H., Kato, N., and Sakai, Y. (2003). Peroxisome degradation requires catalytically active sterol glucosyltransferase with a GRAM domain. Embo J 22, 3231-3241.

Panaretou, C., Domin, J., Cockcroft, S., and Waterfield, M.D. (1997). Characterization of p150, an adaptor protein for the human phosphatidylinositol (PtdIns) 3-kinase. Substrate presentation by phosphatidylinositol transfer protein to the p150.Ptdins 3-kinase complex. J Biol Chem 272, 2477-2485.

Pratt, Z.L., Drehman, B.J., Miller, M.E., and Johnston, S.D. (2007). Mutual interdependence of MSI1 (CAC3) and YAK1 in Saccharomyces cerevisiae. J Mol Biol 368, 30-43.

Ptacek, J., Devgan, G., Michaud, G., Zhu, H., Zhu, X., Fasolo, J., Guo, H., Jona, G., Breitkreutz, A., Sopko, R., McCartney, R.R., Schmidt, M.C., Rachidi, N., Lee, S.J., Mah, A.S., Meng, L., Stark, M.J., Stern, D.F., De Virgilio, C., Tyers, M., Andrews, B., Gerstein, M., Schweitzer, B., Predki, P.F., and Snyder, M. (2005). Global analysis of protein phosphorylation in yeast. Nature 438, 679-684.

Reggiori, F., Shintani, T., Nair, U., and Klionsky, D.J. (2005). Atg9 cycles between mitochondria and the pre-autophagosomal structure in yeasts. Autophagy 1, 101-109.

Reggiori, F., Tucker, K.A., Stromhaug, P.E., and Klionsky, D.J. (2004). The Atg1-Atg13 complex regulates Atg9 and Atg23 retrieval transport from the pre-autophagosomal structure. Dev Cell 6, 79-90.

Reggiori, F., Wang, C.W., Nair, U., Shintani, T., Abeliovich, H., and Klionsky, D.J. (2004). Early stages of the secretory pathway, but not endosomes, are required for Cvt vesicle and autophagosome assembly in Saccharomyces cerevisiae. Mol Biol Cell 15, 2189-2204.

Reggiori, F., Wang, C.W., Stromhaug, P.E., Shintani, T., and Klionsky, D.J. (2003). Vps51 is part of the yeast Vps fifty-three tethering complex essential for retrograde traffic from the early endosome and Cvt vesicle completion. J Biol Chem 278, 5009-5020.

Rohde, J., Dietrich, L., Langosch, D., and Ungermann, C. (2003). The transmembrane domain of Vam3 affects the composition of cis- and trans-SNARE complexes to promote homotypic vacuole fusion. J Biol Chem 278, 1656-1662.

Sakai, Y., Koller, A., Rangell, L.K., Keller, G.A., and Subramani, S. (1998). Peroxisome degradation by microautophagy in Pichia pastoris: identification of specific steps and morphological intermediates. J Cell Biol 141, 625-636.

Sato, K. (2004). COPII coat assembly and selective export from the endoplasmic reticulum. J Biochem (Tokyo) 136, 755-760.

Sato, K., and Nakano, A. (2007). Mechanisms of COPII vesicle formation and protein sorting. FEBS Lett 581, 2076-2082.

Sato, K., Sato, M., and Nakano, A. (2003). Rer1p, a retrieval receptor for ER membrane proteins, recognizes transmembrane domains in multiple modes. Mol Biol Cell 14, 3605-3616.

Sato, T., Yaegashi, K., Ishii, S., Hirano, T., Kajiwara, S., Shishido, K., and Enei, H. (1998). Transformation of the edible basidiomycete Lentinus edodes by restriction enzyme-mediated integration of plasmid DNA. Biosci Biotechnol Biochem 62, 2346-2350.

Schiestl, R.H., and Petes, T.D. (1991). Integration of DNA fragments by illegitimate recombination in Saccharomyces cerevisiae. Proc Natl Acad Sci U S A 88, 7585-7589.

Schroder, L.A., and Dunn, W.A., Jr. (2006). PpAtg9 trafficking during micropexophagy in Pichia pastoris. Autophagy 2, 52-54.

Schuldiner, M., Collins, S.R., Thompson, N.J., Denic, V., Bhamidipati, A., Punna, T., Ihmels, J., Andrews, B., Boone, C., Greenblatt, J.F., Weissman, J.S., and Krogan, N.J. (2005). Exploration of the function and organization of the yeast early secretory pathway through an epistatic miniarray profile. Cell. 123, 507-519.

Scott, S.V., Nice, D.C., 3rd, Nau, J.J., Weisman, L.S., Kamada, Y., Keizer-Gunnink, I., Funakoshi, T., Veenhuis, M., Ohsumi, Y., and Klionsky, D.J. (2000). Apg13p and Vac8p are part of a complex of phosphoproteins that are required for cytoplasm to vacuole targeting. J. Biol. Chem. 275, 25840-25849.

Sears, I.B., O'Connor, J., Rossanese, O.W., and Glick, B.S. (1998). A versatile set of vectors of constitutive and regulated gene expression in Pichia pastoris. Yeast 14, 783-790.

Shintani, T., Huang, W.P., Stromhaug, P.E., and Klionsky, D.J. (2002). Mechanism of cargo selection in the cytoplasm to vacuole targeting pathway. Dev Cell 3, 825-837.

Stack, J.H., DeWald, D.B., Takegawa, K., and Emr, S.D. (1995). Vesicle-mediated protein transport: regulatory interactions between the Vps15 protein kinase and the Vps34 PtdIns 3-kinase essential for protein sorting to the vacuole in yeast. J Cell Biol 129, 321-334.

Stasyk, O.V., van der Klei, I.J., Bellu, A.R., Shen, S., Kiel, J.A., Cregg, J.M., and Veenhuis, M. (1999). A Pichia pastoris VPS15 homologue is required in selective peroxisome autophagy. Curr Genet 36, 262-269.

Stasyk, O.V., van der Klei, I.J., Bellu, A.R., Shen, S., Kiel, J.A., Cregg, J.M., and Veenhuis, M. (1999). A Pichia pastoris VPS15 homologue is required in selective peroxisome autophagy. Curr Genet 36, 262-269.

Stephens, D.J., and Pepperkok, R. (2004). Differential effects of a GTP-restricted mutant of Sar1p on segregation of cargo during export from the endoplasmic reticulum. J Cell Sci 117, 3635-3644.

Stevens, P., Monastyrska, I., Leao-Helder, A.N., van der Klei, I.J., Veenhuis, M., and Kiel, J.A. (2005). Hansenula polymorpha Vam7p is required for macropexophagy. FEMS Yeast Res 5, 985-997.

Strømhaug, P.E., and Klionsky, D.J. (2001). Approaching the molecular mechanism of autophagy. Traffic 2, 524-531.

Stromhaug, P.E., Bevan, A., and Dunn, W.A., Jr. (2001). GSA11 encodes a unique 208-kDa protein required for pexophagy and autophagy in Pichia pastoris. J Biol Chem 276, 42422-42435.

Strømhaug, P.E., Reggiori, F., Guan, J., Wang, C.W., and Klionsky, D.J. (2004). Atg21 is a phosphoinositide binding protein required for efficient lipidation and localization of Atg8 during uptake of aminopeptidase I by selective autophagy. Mol Biol Cell 15, 3553-3566.

Stroud, W.J., Jiang, S., Jack, G., and Storrie, B. (2003). Persistence of Golgi matrix distribution exhibits the same dependence on Sar1p activity as a Golgi glycosyltransferase. Traffic 4, 631-641.

Suzuki, K., Kirisako, T., Kamada, Y., Mizushima, N., Noda, T., and Ohsumi, Y. (2001). The pre-autophagosomal structure organized by concerted functions of APG genes is essential for autophagosome formation. Embo J. 20, 5971-5981.

Teter, S.A., Eggerton, K.P., Scott, S.V., Kim, J., Fischer, A.M., and Klionsky, D.J. (2001). Degradation of lipid vesicles in the yeast vacuole requires function of Cvt17, a putative lipase. J Biol Chem 276, 2083-2087.

Tucker, K.A., Reggiori, F., Dunn, W.A., Jr., and Klionsky, D.J. (2003). Atg23 is essential for the Cvt pathway and efficient autophagy but not pexophagy. J. Biol. Chem. 278, 48445-48452.

Tuttle, D.L., and Dunn, W.A., Jr. (1995). Divergent modes of autophagy in the methylotrophic yeast Pichia pastoris. J. Cell Sci. 108, 25-35.

Tuttle, D.L., Lewin, A.S., and Dunn, W.A., Jr. (1993). Selective autophagy of peroxisomes in methylotrophic yeasts. Eur. J. Cell. Biol. 60, 283-290.

Van Der Wel, H., Morris, H.R., Panico, M., Paxton, T., North, S.J., Dell, A., Thomson, J.M., and West, C.M. (2001). A non-Golgi alpha1,2-fucosyltransferase that modifies Skp1 in the cytoplasm of Dictyostelium. J. Biol. Chem. 276, 33952-33963.

Van Dijk, R., Faber, K.N., Hammond, A.T., Glick, B.S., Veenhuis, M., and Kiel, J.A. (2001). Tagging Hansenula polymorpha genes by random integration of linear DNA fragments (RALF). Mol Genet Genomics 266, 646-656.

Vance, J.E., Aasman, E.J., and Szarka, R. (1991). Brefeldin A does not inhibit the movement of phosphatidylethanolamine from its sites for synthesis to the cell surface. J Biol Chem 266, 8241-8247.

Veenhuis, M., Douma, A., Harder, W., and Osumi, M. (1983). Degradation and turnover of peroxisomes in the yeast Hansenula polymorpha induced by selective inactivation of peroxisomal enzymes. Arch. Microbiol. 134, 193-203.

Votsmeier, C., and Gallwitz, D. (2001). An acidic sequence of a putative yeast Golgi membrane protein binds COPII and facilitates ER export. Embo J 20, 6742-6750.

Wang, C.W., and Klionsky, D.J. (2003). The molecular mechanism of autophagy. Mol. Med. 9, 65-76.

Wang, C.W., Kim, J., Huang, W.P., Abeliovich, H., Stromhaug, P.E., Dunn, W.A., Jr., and Klionsky, D.J. (2001). Apg2 is a novel protein required for the cytoplasm to vacuole targeting, autophagy, and pexophagy pathways. J. Biol. Chem. 276, 30442-30451.

Wang, X., Matteson, J., An, Y., Moyer, B., Yoo, J.S., Bannykh, S., Wilson, I.A., Riordan, J.R., and Balch, W.E. (2004). COPII-dependent export of cystic fibrosis transmembrane conductance regulator from the ER uses a di-acidic exit code. J Cell Biol 167, 65-74.

Wang, Y.X., Catlett, N.L., and Weisman, L.S. (1998). Vac8p, a vacuolar protein with armadillo repeats, functions in both vacuole inheritance and protein targeting from the cytoplasm to vacuole. J. Cell Biol. 140, 1063-1074.

Ward, T.H., Polishchuk, R.S., Caplan, S., Hirschberg, K., and Lippincott-Schwartz, J. (2001). Maintenance of Golgi structure and function depends on the integrity of ER export. J Cell Biol 155, 557-570.

Wohlgemuth, S.E., Julian, D., Akin, D.E., Fried, J., Toscano, K., Leeuwenburgh, C., and Dunn Jr, W.A. (2007). Autophagy in the Heart and Liver During Normal Aging and Calorie Restriction. Rejuvenation Res 10, 281-292.

Yamada, T., Carson, A.R., Caniggia, I., Umebayashi, K., Yoshimori, T., Nakabayashi, K., and Scherer, S.W. (2005). Endothelial Nitric-oxide Synthase Antisense (NOS3AS) Gene Encodes an Autophagy-related Protein (APG9-like2) Highly Expressed in Trophoblast. J. Biol. Chem. 280, 18283-18290.

Yamashita, S., Oku, M., Wasada, Y., Ano, Y., and Sakai, Y. (2006). PI4P-signaling pathway for the synthesis of a nascent membrane structure in selective autophagy. J Cell Biol 173, 709-717.

Yen, W.L., Legakis, J.E., Nair, U., and Klionsky, D.J. (2007). Atg27 Is Required for Autophagy-dependent Cycling of Atg9. Mol Biol Cell 18, 581-593.

Yorimitsu, T., and Klionsky, D.J. (2005). Atg11 Links Cargo to the Vesicle-forming Machinery in the Cytoplasm to Vacuole Targeting Pathway. Mol Biol Cell.

Yorimitsu, T., and Klionsky, D.J. (2005). Autophagy: molecular machinery for self-eating. Cell Death Differ 12 Suppl 2, 1542-1552.

Yuan, W., Strømhaug, P.E., and Dunn, W.A., Jr. (1999). Glucose-induced autophagy of peroxisomes in Pichia pastoris requires a unique E1-like protein. Mol. Biol. Cell 10, 1353-1366.

Yuan, W., Tuttle, D.L., Shi, Y.J., Ralph, G.S., and Dunn, W.A., Jr. (1997). Glucose-induced microautophagy in Pichia pastoris requires the alpha-subunit of phosphofructokinase. J. Cell Sci. 110, 1935-1945.

BIOGRAPHICAL SKETCH

Laura Aaron (Miller) Schroder graduated from Saint John Lutheran School in Ocala, FL in 1997. She earned an Associate in Arts from Central Florida Community College in Ocala, FL in 1999 and was inspired by Lowell Sanders, Ph.D. to pursue a Bachelor of Science in Chemistry from the University of South Florida in Tampa, FL. Laura's work in the laboratory of David J. Merkler, Ph.D. on glutathione as substrate for the enzyme peptidylglycine α-amidating monooxygenase cumulated in a poster at the American Society for Biochemistry and Molecular Biology conference and her first first-author paper. She was supported during this time with a summer research stipend from the Institute for Biomolecular Science during which she was mentored by Clark Craddock, Ph.D., J.D. Laura was also an undergraduate and 3 month postbaccaulaureate researcher in the lab of Denise R. Cooper, Ph.D. on PKC-βII alternative splicing. Laura began her graduate work in the Interdisciplinary Program in Biomedical Sciences, part of the College of Medicine at the University of Florida in 2001 August. Laura joined the lab of William A. Dunn, Jr. in 2002 December upon the recommendation of John Aris, Ph.D. and has authored three papers since then.

The test of a first-rate intelligence is the ability to hold two opposed ideas in mind at the same time, and still retain the ability to function.

- F. Scott Fitzgerald in *The Crack Up*